The Pathophysiological Role of MicroRNAs in Diabetic Cardiac Stem Cells

Nima Purvis

A thesis submitted for the degree of Doctor of Philosophy at the University of Otago, Dunedin, New Zealand.

November, 2018

ABSTRACT

Cardiac stem cells (CSCs) have been implicated as the most suitable source of stem cells for regenerating the diseased heart. However, diabetes is known to cause a progressive loss in the functional efficacy of CSCs. The mechanism behind this loss is unclear. MiRNAs are small, non-coding RNA molecules that regulate genes at the post-transcriptional level. In this study, I used a mouse model of type-2 diabetes to investigate if miRNAs are dysregulated in diabetic CSCs, and whether genetic manipulation of such miRNAs can provide novel insights into their pathophysiological role in improving the function of these cells in the diabetic condition.

Sca-1^{+} CSCs were isolated from type-2 diabetic (n=6) and non-diabetic (n=6) db/db mice. Among 598 miRNAs evaluated by an n-counter miRNA expression assay, the expression profiles of 16 miRNAs were significantly altered in the diabetic condition. Among these 16 miRNAs, miR-329 (1.7 ± 0.9 (P=0.01)), miR-376c (2.8 ± 0.8 (P=0.01)) and miR-495 (1.8 ± 0.6 (P=0.02)) were significantly upregulated while miR-30c (0.4 ± 0.1 (P=0.03)) was significantly downregulated in diabetic CSCs. These miRNAs are involved in cell proliferation and survival. Mass spectrometry analysis predicted pro-apoptotic VDAC1 as a direct target for miR-30c and cell cycle regulator CDK6 as the direct target for miR-329, -376c and -495. Western blot analyses confirmed a marked increase in VDAC1 expression (3.2 ± 0.6 (P=0.01)) and a significant decrease in CDK6 expression (0.7 ± 0.1 (P=0.04)) in the diabetic CSCs. Moreover, luciferase assays confirmed VDAC1 as the direct target for miR-30c. An overexpression of miR-30c in diabetic CSCs showed a marked reduction in VDAC1 (0.7 ± 0.1 (P=0.03)) and cleaved caspase-3 (0.6 ± 0.1 (P=0.04)) protein expression, as well as reduced caspase-3/7 activity (0.6 ± 0.1 (P<0.01)), suggesting that genetic manipulation of miRNAs could be beneficial in promoting CSC survival and function. Altogether, my results suggest that altered miR-30c expression may contribute to the reduced functional efficacy of CSCs in the diabetic heart by regulating apoptosis.

SELECTED PUBLICATIONS

Journal articles:

Purvis N, Bahn A and Katare R. (2015). The role of microRNA in cardiac stem cells. *Stem Cells International*. DOI: 10.1155, Article ID: 194894. Impact factor: 3.9.

Conference proceedings:

Purvis N, Bahn A and Katare R. (2018). International society for stem cell research. 'The pathophysiological role of microRNAs in diabetic cardiac stem cells. Poster presentation. Abstract No: 465359.

Katare R, Purvis N, Kumari S. (2018). Dysregulated microRNA-30c and -376c promotes functional disability of diabetic cardiac stem cells. *Circulation*, vol. 134, no. suppl_1, A18048. Abstract No: 18048.

Purvis N, Bahn A and Katare R. (2017). Stem cell society Singapore: Advances in cell therapy. 'The pathophysiological role of microRNAs in diabetic cardiac stem cells. Oral presentation.

Purvis N, Bahn A and Katare R. (2015). Australasian society for stem cell research. 'The pathophysiological role of microRNAs in diabetic cardiac stem cells. Poster presentation.

ACKNOWLEDGEMENTS

I would like to sincerely thank my primary supervisor, Associate Professor Rajesh Katare and my secondary supervisor, Dr. Andrew Bahn for their continual help and guidance throughout my work. Rajesh, thank you so much for your patience, expertise and motivation. I will always be gateful for what you taught me, both in research and in life. Andrew, thank you for your guidance and wisdom throughout the years. I will always be indebted to you as well. I would like to thank Professor Colin Brown and Professor Bryan Hyland for their understanding and encouragement at a difficult time in my life.

Thank you to the members of the Katare lab that helped and encouraged me when I needed it. Parul, thanks for your generosity and help with cell culture, flow cytometry and stem cell isolation. You were always smiling and happy to talk no matter what was going on around us. Sweta, you taught me so many things I can't even remember everything, and were always so nice to me, especially when I wasn't feeling the best. I will always be grateful for what you did for me, and hope to always be a part of your life. Shruti and Ingrid, thank you for always lending a hand and teaching me valuable techniques that contributed to me growing as a confident researcher. Midori, you were the first person that taught me the stem cell isolation procedure. You were so valuable not just for me, but for our whole lab. To Ramakanth who will always be my brother, and who also taught me flow cytometry techniques towards the end of my PhD. Torsten, thank you for teaching me the mass spectrometry protocol that basically turned my whole project around. Thank you to all my friends outside the lab who supported me when I needed to de-stress and for encouraging me to keep going, no matter what. And finally, thank you to the University of Otago and the Department of Physiology for funding my research and providing a doctoral scholarship.

Finally and most importantly, I would like to thank my parents (Martin and Maryam Purvis) for their love and support throughout my PhD. I will always love you.

TABLE OF CONTENTS

LIST OF FIGURES

LIST OF TABLES

ABBREVIATIONS

ALK5	Activin receptor-like kinase 5
ALK7	Activin receptor-like kinase 7
APC	Allophycocyanin
ASK1	Apoptosis signal-regulating kinase 1
Bcl-2	B-cell lymphoma 2
Bim	Critical apoptotic activator B-cell lymphoma 2 interacting mediator of cell death
BSA	Bovine serum albumin
Ca^{2+}	Calcium ions
CD105	Cluster of differentiation 105
CD34	Cluster of differentiation 34
CD90	Cluster of differentiation 90
CDC42	Cell division control protein 42
CDK6	Cyclin-dependent kinase 6
CID	Collision induced dissociation
CMPK1	Cytidine/Uridine monophosphate kinase 1
CPC	Cardiac progenitor cells
CSC	Cardiac stem cells
Ct	Cycle at threshold
CTGF	Connective tissue growth factor
CVD	Cardiovascular disease
D	Diabetic
D_{30c}	Diabetic CSC transfected with miR-30c precursor mimic
DCM	Diabetic cardiomyopathy
DGCR8	DiGeorge criticial region 8
DMEM/F12	Dulbecco's modified eagle medium supplemented with 10% Ham's F12 nutrient mixture
DNAJB4	DNAJ homolog subfamily B member 4
D_{scr}	Diabetic CSC transfected with scrambled mimic

EGR1	Early growth response protein 1
ESC	Embryonic stem cell
FACS	Fluorescence-activated cell sorting/ Flow cytometry
FASP	Filter-aided sample preparation
FFF	Field flow fractionation
FITC	Fluorescein isothiocyanate
FLuc	Firefly luciferase working solution
GCC2	Grip and coiled-coil domain-containing protein 2
GRB2	Growth factor receptor-bound protein 2
GSK3-β	Glycogen synthase kinase-3β
GUCY1B1	Guanylate cyclase soluble beta β1
GVHD	Acute graft vs host disease
HBSS	Hank's Balanced Salt Solution
HCD	High energy collision induced dissociation
HSC	Hematopoietic stem cells
IEF	Isoelectric focusing
iTRAQ	Isobaric tags for relative and absolute quantitation
JAK-STAT	Janus kinase-signal transducer and activator of transcription
KDM1A	Lysine-specific demethylase 1
Ki-67	Marker of proliferation Ki-67
KPNB1	Importin subunit β1
KRH	Krebs Ringer HEPES
Lin$^-$	lineage negative
MACS	Magnetic-activated cell sorting
MAPK	Mitogen-activated protein kinase
MBNL2	Muscleblind-like splicing regulator 2
MEF2C	Myocyte specific enhancer-2C
MI	Myocardial infarction
MiR-30a-e	MiR-30 family
MiRNA/miR	MicroRNA
MKK3	Mitogen-activated protein kinase kinase 3

MKK6	Mitogen-activated protein kinase kinase 6
mPTP	Mitochondrial permeability transition pore
mRNA	Messenger RNA
MS	Mass spectrometry
MS/MS	Tandem mass spectrometry
MSC	Mesenchymal stem cell
N.S.	No statistical significance
ND	Non-diabetic
ND_{30c}	Non-diabetic CSC transfected with miR-30c precursor mimic
ND_{scr}	Non-diabetic CSC transfected with scrambled mimic
NSC	Neural stem cells
OD	Optical density
P	P value
p21	Cyclin-dependent kinase inhibitor 1
p27	Cyclin-dependent kinase inhibitor 1B
p53	Tumor antigen p53
p130	Retinoblastoma-like protein 2
PAK1	Serine/threonine-protein kinase
PBS	Phosphate buffered saline
PCR	Polymerase chain reaction
PE-Cy7	Phycoerythrin–Cyanin 7
PI	Propidium Iodide
PI3K	Phosphoinositide 3-kinase
PI3K-AKT	Phosphoinositide 3-kinase-protein kinase B
Pim-1	Moloney murine leukemia virus-1
PIP3	Phosphatidylinositol-3,4,5-bisphosphate
PVDF	Polyvinylidene difluoride
q-PCR	Quantitative real-time PCR
R^2	Pearson correlation coefficient
RAA	Right atrial appendage
RIP1	Receptor interacting protein

RIPA	Radioimmunoprecipitation assay
RISC	RNA-induced silencing complex
RLuc	Renilla luciferase working solution
ROS	Reactive oxygen species
RT	Room temperature
R.T	Reverse transcription
SARNP	SAP domain-containing ribonucleoprotein
Sca-1	Stem cell antigen 1
SEM	Standard error of the mean
SEMA3A	Semaphoring 3A
SHAM	Placebo surgery
SPRED1	Sprouty-related EVH1 domain-containing protein 1
SWATH	Serial window acquisition of theoretical spectra
T2DM	Type-2 diabetes mellitus
TBS-T	Tris-buffered saline with tween 20
TEAB	Triethylammonium bicarbonate
Topo-2α	Topoisomerase-2α
TPT1	Translationally controlled tumor protein 1
U6	U6 small nuclear ribonucleoprotein
VDAC1	Voltage-dependent anion-selective channel 1
VEGF	Vascular endothelial growth factor
WB	Western blot
WNT	Wingless-type

CHAPTER 1: INTRODUCTION

The purpose of this thesis is to investigate the expression of microRNAs (miRNAs) in cardiac stem cells, as well as to demonstrate their pathophysiological role within these cells using a mouse model of type-2 diabetes mellitus (T2DM). In this section, a brief review of cardiovascular disease (CVD) will initially be described, followed by the current understanding of stem cells and their application as a viable treatment option for various diseases, including CVD. The characteristics of cardiac stem cells will then be discussed and compared to other stem cell subtypes in terms of their ability to promote cardiac repair and regenerate heart tissue. The effect of diabetes on cardiac stem cells will be highlighted as a limiting factor to their effectiveness as a therapeutic agent. The basic regulatory mechanisms associated with maintaining cardiac stem cell number and function will then be outlined. This will lead to the suggestion that manipulating the expression of molecular regulators such as miRNAs may be a better tool for maintaining the efficacy of cardiac stem cells, particularly for the purposes of reversing the deleterious effects of diabetes on these cells. Finally, the current understanding of miRNA will be described, as well as experimental evidences that have demonstrated their physiological and pathophysiological roles in cardiac stem cells, leading to the objectives and hypothesis of this study. I have previously published a review article that describes this background information in detail (Purvis *et al*., 2015).

1.1 Cardiovascular disease

1.1.1 Characterization and pathology

Cardiovascular disease (CVD) is currently the leading cause of death in the world for both men and women and is responsible for approximately 31% of deaths each year (WHO, 2018). This disease encompasses a number of pathological conditions that affects the heart and its

primary blood vessels. In its most common form, CVD can cause a build-up of fatty deposits inside arteries in a condition known as artherosclerosis. This can lead to harmful blood clots, which damage organs supplied by the affected artery due to a lack of oxygen (Stocker and Keaney, 2003). CVD is deadly, because aside from causing direct damage to the heart, it can also cause complications with other well-known diseases, such as diabetes mellitus. When confounded with T2DM, CVD can cause pathological changes to the myocardium. Studies have shown that regardless of previous history, T2DM dramatically increases the incidence of myocardial infarction (MI), characterized by the sustained ischemia and subsequent loss of cardiomyocytes (Mendis *et al*., 2010; Haffner *et al*., 1998).

Despite significant advances in the therapeutic treatment of CVD, the prevalence of heart failure continues to rise. A potential reason for this is that although CVD is traditionally treated by limiting scar formation or by preventing adverse remodelling, these methods do not account for the inevitable loss of cardiomyocytes that reduce cardiac function in CVD patients (Chiong *et al*., 2011; Zannad *et al*., 2009). It has become clear that this loss of cardiomyocytes can only be treated by replacing the damaged cells or regenerating the heart tissue. In recent years, stem cell therapies have been found to promote the regeneration of heart tissue and also improve cardiac function (Li *et al*., 2009; Caplan *et al*., 2006). This therefore indicates that the application of stem cells may be a novel option for the treatment of CVD.

1.2 Introduction to stem cells

1.2.1 Background, definition and general function

Stem cells have gained considerable amount of interest as a viable treatment option for patients with CVD, especially those resistant to conventional therapies (Segers and Lee, 2008). They can be defined as undifferentiated cell precursors that may give rise to different

cell types in the body (Li and Xie, 2005). These cells regularly function in a process known as self-renewal which involves a combination of proliferation and differentiation, ultimately leading to the production of multiple daughter cells with different cell fates (Kiger *et al*., 2001).

1.2.2 The specificity of different stem cell subsets

Stem cells are known to exist in a variety of different tissues where they each have a distinct phenotype. Accordingly, they can be separated into certain subsets and classified based on their tissue specificity. Among the most commonly researched stem cells are embryonic stem cells (ESCs), mesenchymal stem cells (MSCs) and hematopoietic stem cells (HSCs). These stem cells are typically identified based on specific antigenic markers, as detailed in Table 1.1. ESCs can be identified by targeting Oct4 and Nanog markers, while MSCs and HSCs can be identified by targeting Cluster of differentiation 105 (CD105) and Cluster of differentiation 90 (CD90), respectively (Rodrigues *et al*., 2017; Ullah *et al*., 2015; Matsuoka *et al*., 2001).

Table 1.1. Common antigenic markers of different stem cells

	ESCs	MSCs	HSCs
Common markers	Oct4, Nanog	CD105, CD90	CD34

ESCs are derived from the inner mass of the blastocyst and typically contribute to the formation of the embryo, which is known to undergo organogenesis in early development (Rippon and Bishop, 2004). ESCs are therefore pluripotent, meaning they have the ability to differentiate into many cells of the body (Rippon and Bishop, 2004). Interestingly, they also have beneficial implications in maintaining organ function, as studies have shown that ESCs

routinely differentiate into cell lines that promote the formation of new blood vessels (Caspi *et al*., 2007; Gepstein, 2002; Kehat *et al*., 2001). However, the clinical application of ESCs is often limited by pathological complications in the patient, leading to a greater demand for the use of alternative stem cells in stem cell therapy.

MSCs are a multipotent type of stem cell that are defined by their ability to adhere to plastic, as well as their high expression of certain antigenic markers (eg. CD90 and CD105). They are able to differentiate into ectodermal, mesodermal and endodermal cells based on their age (Ullah *et al*., 2015). Early forming MSCs have been shown to have a predisposition to differentiate into chondrocytes, adipocytes and osteocytes, while this differentiation potential declines at higher passages (Ullah *et al*., 2015). They can also be isolated more easily compared to other stem cell subtypes as they derived from many tissues including blood, placenta, heart, skeletal muscle, adipose tissue and bone marrow (Meirelles *et al*., 2006). MSCs are able to migrate towards damaged tissue and replace the dead cells through self-renewal (Ullah *et al*., 2015). However, it is difficult to generate adequate numbers of functional MSCs for therapeutic purposes. This is because these cells lose their capacity for differentiation very quickly over time as they are cultured *in vitro* (Ullah *et al*., 2015). MSCs also contribute to the formation of the microenvironment in the bone marrow, which indirectly enhances the development of HSCs.

HSCs are derived from the mesoderm and give rise to mature blood cells in a process known as hematopoiesis (Gunsilius *et al*., 2001). During this process, HSCs are able to differentiate into both myeloid and lymphoid blood cell lineages in the embryo, as well as in the adult. In adults, these cells are commonly found in the bone marrow, and commonly used for the restoration of bone marrow in patients with weakened immune systems, as well as those afflicted with malignant diseases that have undergone chemoradiotherapy (Congdon, 1957; Lorenz *et al*., 1951).

Resident stem cells have also been successfully isolated from a variety of tissues including bone marrow, peripheral blood, brain, liver and reproductive organs using validated isolation techniques (Asahara, 2000). Although they have a similar capacity for self-renewal as other types of stem cells, their growth potential and response to their microenvironment varies depending on the tissue source (Raveh-Amit *et al*., 2013). Resident stem cells are unique compared to other stem cell types in that they are tissue specific. They therefore hold great potential for stem cell therapy due to the possibility of stimulating differentiation of an *in vivo* population without the need for transplantation (Mimeault and Batra, 2008). However, there is an ongoing debate as to which type of stem cell is the best for tissue regeneration (Raveh-Amit *et al*., 2013).

1.2.3 Stem cell niche and microenvironment

Stem cells reside in anatomical locations called niches that are specialized to regulate their maintenance and repair. The niche creates a microenvironment that reduces both stem cell depletion and excessive proliferation (Scadden, 2006). It does this by receiving stimuli from other cells, as well as the extracellular matrix that activate or repress genes and transcriptional pathways. These interactions can augment the capacity of stem cells for self-renewal (Ferraro *et al*., 2010). The components of the niche are conserved even in the temporary absence of the stem cells which it is housing, allowing for the recruitment of exogenous stem cells to a pre-existing niche site. The primary components of the stem cell niche include stromal cells and extracellular matrix that provide scaffolding support and anchor the stem cell, as well as blood vessels that carry circulating stem cells into and out of the niche (Ferraro *et al*., 2010).

1.2.4 Brief history of stem cell research

The history of stem cell research has been complex, but rewarding. It is unclear when exactly the first stem cells were discovered. However, in 1978, Prindull and colleagues were reported to have identified a population of HSCs in human cord blood which were thought to be capable of forming colonies (Prindull *et al*., 1978). Shortly after this, Martin Evans was the first to identify pluripotent cells in mice blastocysts (Martin, 1981). These cells would later be known as ESCs, and this was the first time that stem cells were discovered in mice. Then in 1998, James Thompson successfully isolated human ESCs and maintained their growth *in vitro* in efforts to develop the first human ESC cell line (Thompson *et al*., 1998). Following the discovery of MSCs in 1999, researchers found that the proliferation and differentiation of adult mouse stem cells could be manipulated to generate different types of cells such as bone, cartilage, fat, tendon and muscle (Pittenger *et al*., 1999). These initial findings lead to the development of many programs investigating the role of stem cell therapies as potential treatments for conditions such as Parkinson's disease, muscular dystrophy, cancer and heart failure (Darabi *et al*., 2008; Wernig *et al*., 2008; Laflamme *et al*., 2007). Since then, ESCs have been found to successfully treat spinal cord injury (2010) and blindness (2012) (Stem cell timeline, 2015). This showed that by effectively harnessing their self-renewal capability, stem cells could thus be used as a tool for clinical applications.

1.2.5 Therapeutic application of stem cells

Stem cell therapy has been implicated as a viable treatment option for certain diseases, such as cancer and CVD (Goradel *et al*., 2017; Park *et al*., 2017). In addition, experimental evidences have strongly indicated the clinical use of stem cells in reversing the effects of neurodegeneration (Kim and Vellis, 2009). The transplantation of bone marrow has become the most widely used form of stem cell therapy to treat cancer (Karanes *et al*., 2008). It was

first introduced as a secondary treatment to attenuate the non-specific cytotoxic effects of conventional chemotherapy. This is due to the fact that bone marrow contains a pool of undifferentiated $CD34^+$ HSCs (Table 1.1) that can migrate to the damaged site after transplantation (Copelan, 2006). Through self-renewal, these stem cells are able to re-constitute many blood-forming and immune cells that are depleted in cancers such as leukemia and lymphoma, after chemotherapy (Copelan, 2006). However, this treatment has a major limitation, as it can cause acute graft versus host disease (GVHD) (Mielcarek *et al*., 2003). GVHD is a disease in which immune cells of the donor damage host epithelial cells after allogeneic transplantation. It occurs in 35-50% of all HSC transplant patients and may lead to abdominal pain and liver failure (Jacobsohn and Vogelsang, 2007).

The potential of stem cell-based therapies has also been researched in animal models of neurodegenerative diseases such as Parkinson's, Alzheimer's and Huntington's diseases (Kim and Vellis, 2009). Parkinson's disease is characterized by the depletion of dopaminergic neurons in the substantia nigra of the brain. Mouse embryonic and neural stem cells (NSCs) have been found to be capable of generating dopaminergic neurons after exposure to fibroblast growth factor 8 and sonic hedgehog proteins, indicating the potential of these stem cells in treating this disease (Lee *et al*, 2000; Kim *et al*., 2013). Moreover, the transplantation of NSCs in mice was found to attenuate the functional deficits in the central nervous system associated with Alzheimer's and Huntington's disease through neural cell replacement, neurotransmitter release, and production of neurotrophic factors (Kim and Vellis, 2009). In the case of Alzheimer's disease, NSC transplantation has been found to rescue spacial and memory learning deficits by elevating expression of brain-derived neurotrophic factor, which is known to increase synaptic density in the hippocampus (Blurton-Jones *et al*., 2009).

The bone marrow contains a high concentration of multipotent stem cells that can easily be acquired, and is therefore the most commonly used source of stem cells for clinical studies of heart failure. Bone marrow derived HSCs were the first adult stem cells discovered to

differentiate into cardiomyocytes after transplanting them into the infarcted hearts of mice (Leri *et al*., 2005). However, this effect has not yet been demonstrated in other animals (Leri *et al*., 2005; Murray *et al*., 2004; Balsam *et al*., 2004).

Similar to HSCs, MSCs and ESCs have also been shown to differentiate into cardiomyocytes *in vitro* (Caplan *et al*., 2006), as well as to a much lower concentration *in vivo* (Miyahara *et al*., 2006). They therefore can be introduced into the diseased heart to re-constitute dead cardiomyocytes. This was shown after MSCs were injected into a swine model of MI (Schuleri *et al*., 2009). The MSCs underwent cardiomyogenesis and were found to express cardiomyocyte-specific markers, indicating that they differentiated into cardiomyocytes. They also attenuated LV remodeling, thus reducing the size of the scar (Schuleri *et al*., 2009). Other models of ischamic cardiomyopathy have shown that the injection of MSCs improves cardiac function, increases angiogenesis and reduces myocardial fibrosis (Li *et al*., 2009; Liu *et al*., 2008; Nagaya *et al*., 2005).

ESCs as previously mentioned are pluripotent and therefore have the potential to completely regenerate the myocardium after a heart failure. They have been found to improve LV remodeling and systolic function after transplantation in rat models of MI (Caspi *et al*., 2007; Cai *et al*., 2007). The transplantation of mouse ESCs into an infarcted sheep myocardium has also been found to elicit differentiation into cardiomyocytes and improve LV function (Menard *et al*., 2005). Despite these evidences, ESCs pose several potential threats to patients due to their allogeneic nature. They have been found to cause immunological rejection, as well as the formation of teratomas in mice tissue. Therefore these risks bring about significant concerns towards the use of ESCs in a clinical setting, especially for the treatment of heart failure patients in which the immune system is already compromized.

Resident stem cells of the heart are now also being investigated for their ability to treat heart failure and improve cardiac function. Endogenous cardiac stem cells can be isolated and

expanded from the myocardium and epicardium of the heart (Bearzi *et al*., 2007). Although considerably less is known about the functions of these cells, there are strong indications that generating enough healthy cardiac stem cells to transplant back into patients with heart failure may be more beneficial than the use of other stem cell types. Our current understanding of the function of cardiac stem cells as well as its potential as a viable treatment option will therefore be explored in the next section.

1.3 Cardiac stem cells

1.3.1 Definition and general function

The heart was originally thought of as a terminally differentiated, post-mitotic organ until the discovery of a population of endogenously expressed cardiac stem cells (CSCs) that were capable of generating cardiomyocytes and coronary vessels (Santini *et al*., 2016). CSCs are known as a specialized stem cell type which can be used for the purposes of organ regeneration, and reside in specialized niches in the myocardium of the heart. The structure of the niches are specifically designed to support the survival of the cells within the myocardial tissue (Leri *et al*., 2014). They are able to differentiate into adult cardiomyocytes, smooth muscle cells and endothelial cells, and in doing so regulate the physiological turnover of cardiac cells in the body (Nadal-Ginard *et al*., 2014). A pool of resident CSCs are known to be expressed endogenously within the myocardium and epicardium of the heart. This pool can be activated in response to an ischemic event, inducing their migration to the site of injury (Liu *et al*., 2013).

1.3.2 CSCs as best source of stem cells for cardiac repair

Although stem cells from different origins have been used to repair damaged tissue in the past, recent studies have elicited an understanding that a specific stem cell subtype may confer a better regenerative response (Falanga, 2012). Compared to other stem cell subtypes, endogenous CSCs may therefore be a better option to regenerate heart tissue due to the fact that these cells are adapted to function in the specialized environment of the CSC niche. Moreover, unlike exogenous stem cells, CSCs are specifically programmed to differentiate into adult cardiomyocytes (Leri *et al*., 2005). Other stem cell types, such as bone marrow-derived cells and ESCs have been reported to be capable of cardiogenesis. However, the differentiated cells which they produce often die within a short period of time after transplantation, or have limited functionality compared to resident cardiomyocytes (Laflamme and Murry, 2011). It is therefore plausible to assume that the therapeutic application of CSCs would allow for a more efficient re-constitution of heart tissue, and thus functional recovery of the heart compared to stem cells from other sources in the body.

1.3.3 Selective markers for identification of CSCs

CSCs can be selectively identified based on the expression of surface antigenic markers. The earliest known marker for these cells is Mesp1, a transcription factor that regulates cardiovascular cell fate. In the presence of the Wnt inhibitor, Dkk1, Mesp1 was found to downregulate genes that promote pluripotency, while upregulating the cardiac transcription factors, Nkx2.5 and GATA4 (Cyganek *et al*., 2013; David *et al*., 2008). Other markers that have previously been used to identify CSCs include multidrug resistance protein 1 and stem cell growth factor receptor (c-kit) protein (Messina *et al*., 2004). However despite early indications of their beneficial use for this purpose, the lineage and functional properties of c-kit$^+$ cells has recently come under scrutiny. In the developing heart, c-kit$^+$ cells have been

found to primarily function as endothelial cells (Sultana *et al*., 2015). Moreover, it was reported that these cells retain their endothelial identity over time and undergo minimal differentiation into cardiomyocytes (Sultana *et al*., 2015; Berlo *et al*., 2014). This may indicate that c-kit is no longer suitable as a marker for CSCs.

Stem cell antigen 1 (Sca-1) is now being used as the primary marker for identifying CSCs in mice and is known to constitute 70% of the remaining cells in the mouse heart after depletion of cardiomyocytes (Matsuura *et al*., 2014; Valente *et al*., 2014). Importantly, cell populations with high expression of Sca-1 (Sca-1^{+}) have been shown to be inherently and functionally different to those with high expression of c-kit (Vicinanza *et al*., 2017). These Sca-1^{+} cells have also been shown to exhibit cardiac-specific and stemness characteristics such as a high proliferation capacity, which leads to an improvement in cardiac regeneration in mice (Li *et al*., 2017; Vicinanza *et al*., 2017). Moreover, these cells have a multipotent phenotype with the ability to differentiate into different cardiac cell lineages (Wang *et al*., 2014). These features suggest Sca-1 as an appropriate marker for identifying CSCs in mice. Antibodies specific for Sca-1 can thus be used to purify CSCs in a population of cardiac cells derived from mouse hearts. Nonetheless, the stem cell field is constantly evolving and new evidence provides new insights into the most suitable markers for these CSCs. It is evident that more research must be done to characterise the origin and functional nature of Sca-1 and other markers for these cells.

1.3.4 Experimental evidence for transplantation of CSCs in regenerating heart tissue

The therapeutic potential of CSCs is evident through the autologous transplantation of functional CSCs into the diseased heart (Purvis *et al*., 2015). This regenerative effect of CSCs involves two primary mechanisms: direct differentiation of the CSCs into cardiovascular cells or more commonly, secretion of paracrine factors which activate downstream regenerative

pathways (Nadal-Ginard *et al*., 2014). CSCs were initially found to exhibit this regenerative capability after autologous transplantation from healthy rat hearts into an infarcted myocardium (Zhang and Guo., 2018). Intramyocardial injection of CSCs promoted an increase in myocardial cell proliferation and improvements in exercise capacity, as well as a reduction in left ventricular end-diastolic volume in the rats with MI (Zhang and Guo., 2018). There was a significant increase in ejection fraction and myocardial proliferation, as well as a reduction in left-ventricular end-diastolic volume four weeks after transplantation into the left ventricle (Zhang and Guo, 2018).

Moreover, the migration rate of CSCs to the damaged site has been found to increase as early as one week following injection into the heart (Ling *et al*., 2017). CSC transplantation has also been shown to be effective at improving cardiac function in the human heart. The clinical relevance of this transplantation was shown by Makkar and colleagues who demonstrated that transplantation of cardiosphere-derived stem cells promotes cardiac regeneration, reduces scar tissue and improves heart contractility in human patients with MI (Makkar *et al*., 2012). Although these evidences suggest that CSC transplantation may be a useful method for replacing dead cardiomyocytes, diabetes mellitus poses a threat to the effectiveness of CSC therapy as it is known to enhance stem cell aging and death (Katare *et al*., 2013; Rota *et al*., 2006).

1.4 Diabetes mellitus

Diabetes mellitus is one of the most common non-communicable diseases in the world (WHO *et al*., 2018). It is characterized by an abnormal elevation in systemic glucose (hyperglycemia) due to either a deficiency in insulin production by the pancreas (type 1), or a reduced ability of cells to respond to the insulin that is produced (type 2) (Tripathi and Srivastava, 2006). T2DM is the more common of the two, accounting for over 90% of diabetic patients worldwide (Tripathi and Srivastava, 2006). In the heart, both type 1 and 2 diabetes mellitus

can causes abnormal alterations to the structure and function of the myocardium, manifesting in a condition called diabetic cardiomyopathy (DCM) (Boudina, 2010).

1.4.1 Diabetic cardiomyopathy

Unlike other diseases associated with CVD, DCM is caused by the development of diabetes, but is not confounded by coronary artery disease or hypertension (Boudina, 2010). DCM can limit the ability of the heart to pump blood by a number of mechanisms which include ventricular dilatation, myocyte hypertrophy, interstitial fibrosis and reduced systolic function of the left ventricle (Hayat *et al*., 2004). After evaluation of myocardial biopsies, apoptosis and necrosis has also been found to be elevated in diabetic subjects with heart failure, indicating that DCM also influences cell death (Hayat *et al*., 2004). Commonly used treatments for DCM include β-blockers, ACE inhibitors and $Ca2^{+}$ channel inhibitors which help to reverse the cardiac remodelling associated with the disease, therefore improving left ventricle function (Hayat *et al*., 2004). Recently stem cell-based therapies have also been used to treat DCM, indicating the potential application of CSC therapy for regeneration of the diseased heart (Segers and Lee, 2008).

1.4.2 Pathological effect of diabetes on CSCs

Diabetes is known to adversely affect CSC function by increasing the amount of oxidative stress within these cells. This phenomenon has been demonstrated by Rota and colleagues who found a substantial increase in the expression of oxidative stress markers, nitrotyrosine and deoxyguanosine in resident CSCs located in diabetic mice (Rota *et al*., 2006). The oxidative stress in turn produces elevated levels of reactive oxygen species (ROS) which is known to disrupt mitochondrial, caspase and mitogen-activated protein kinase pathways that regulate important biological processes within the cell, leading to apoptosis (cell death) (Glass

et al., 2010). This was also supported by Katare and colleagues, who demonstrated that Sca-1^+ cardiac progenitor cells (CPCs) isolated from the hearts of diabetic mice have reduced activity of key enzymes in the pentose phosphate pathway, glucose-6-phosphate and transketolase (Katare *et al*., 2013). The suppression of these enzymes lead to apoptosis of CPCs in the diabetic mice by increasing the expression of advanced glycation end-products and suppressing the pro-survival proviral integration site for moloney murine leukemia virus-1 (Pim-1)/B-cell lymphoma 2 (Bcl-2) signaling pathway (Katare *et al*., 2013). This may also explain why DCM can be characterized at the early stages of the disease by the downregulation of Pim-1 (Katare *et al*., 2011). Moreover, this finding correlated with a study showing that systemic delivery of Pim-1 into diabetic mice improved cardiac function and reduced cardiomyocyte apoptosis (Katare *et al*., 2011).

Diabetes also reduces the proliferative capacity of CSCs. This is due to the fact that the accumulation of oxidative stress in the cell promotes senescence, a cellular aging process characterized by a decline in cellular function where a cell ceases to replicate (Rota *et al*., 2006). Finally, diabetes was found to promote insulin-resistance in CPCs, and also dysregulate glucose metabolism by increasing the rate of glycolysis (Salabei *et al*., 2016). However, despite several studies demonstrating the harmful effects of diabetes on CSC number and function, the exact molecular mechanisms leading to the dysregulation of CSCs in the diabetic heart are still not fully understood. Nevertheless, certain regulatory molecules may prove beneficial in maintaining the functional viability of CSCs in the diabetic heart as they allow for the beneficial modulation of these cells. MiRNAs are one such molecule that has recently been investigated as a regulator for stem cell number and function. The appropriate application of miRNAs in a clinical setting may therefore regenerate damaged heart tissue in diabetic patients that require extensive tissue repair

1.5 MicroRNAs

1.5.1 Definition and statistics

MiRNAs are small (21-25 nucleotide), noncoding RNAs that are expressed in plants and animals and regulate gene expression at the posttranscriptional level (Wahid *et al*., 2010). They are differentially expressed in many different cell types in the body and are involved in a wide variety of cellular processes such as development, proliferation, differentiation and plasticity (Gangaraju and Lin, 2009). Thus far over 38,000 miRNAs have been characterized across all species. Each of these miRNAs has the potential to target hundreds of different genes (Count, M., 2018; Friedman *et al*., 2009). Moreover, 2200 miRNAs have been discovered in the human genome which can affect genes controlling important biological processes in the body (Hammond *et al*., 2015). Their differential expression has been shown to be useful in identifying diseases such as cancer, CVD and diabetes (Wang e*t al*., 2015). In this way, the miRNAs can act as biomarkers to predict the onset of a certain disease. However, there is still a limited understanding of the role of these miRNAs within stem cells.

1.5.2 Biogenesis pathway

MiRNAs are believed to derive from either genetic or intronic material during splicing but are both encompassed in the same biogenesis framework (Ruby, 2007). Those derived from genes are transcribed in the nucleus by RNA polymerases (II and III) into primary transcripts called pri-miRNAs (Winter, 2009). A microprocessor complex consisting of the Drosha enzyme and the RNA-binding protein, DiGeorge criticial region 8 (DGCR8) process the transcripts into precursor (pre-) miRNAs (Rawal, 2014). MiRNAs derived from introns bypass this Drosha-mediated processing and are directly converted into pre-miRNAs (Ruby, 2007). The pre-miRNAs are transported through a nuclear pore into the cytoplasm by an exportin-5 transporter protein, where they are further processed into a double-stranded mature miRNA

by the RNAse II enzyme, Dicer (Gangaraju and Lin, 2009). The mature miRNAs are unwound and incorporated along with argonaute proteins into an RNA-induced silencing complex (RISC). The RISC complex escorts the miRNA to conserved recognition sites on target messenger RNAs (mRNAs) which are either directly degraded by the miRNA or made dysfunctional through translational repression (Winter, 2009). These inhibitory pathways depend on complementary matching of the RISC complex to the target mRNA, which is mediated by associated argonaute proteins (Winter, 2009). The biogenesis pathway for miRNAs is described in Figure 1.1.

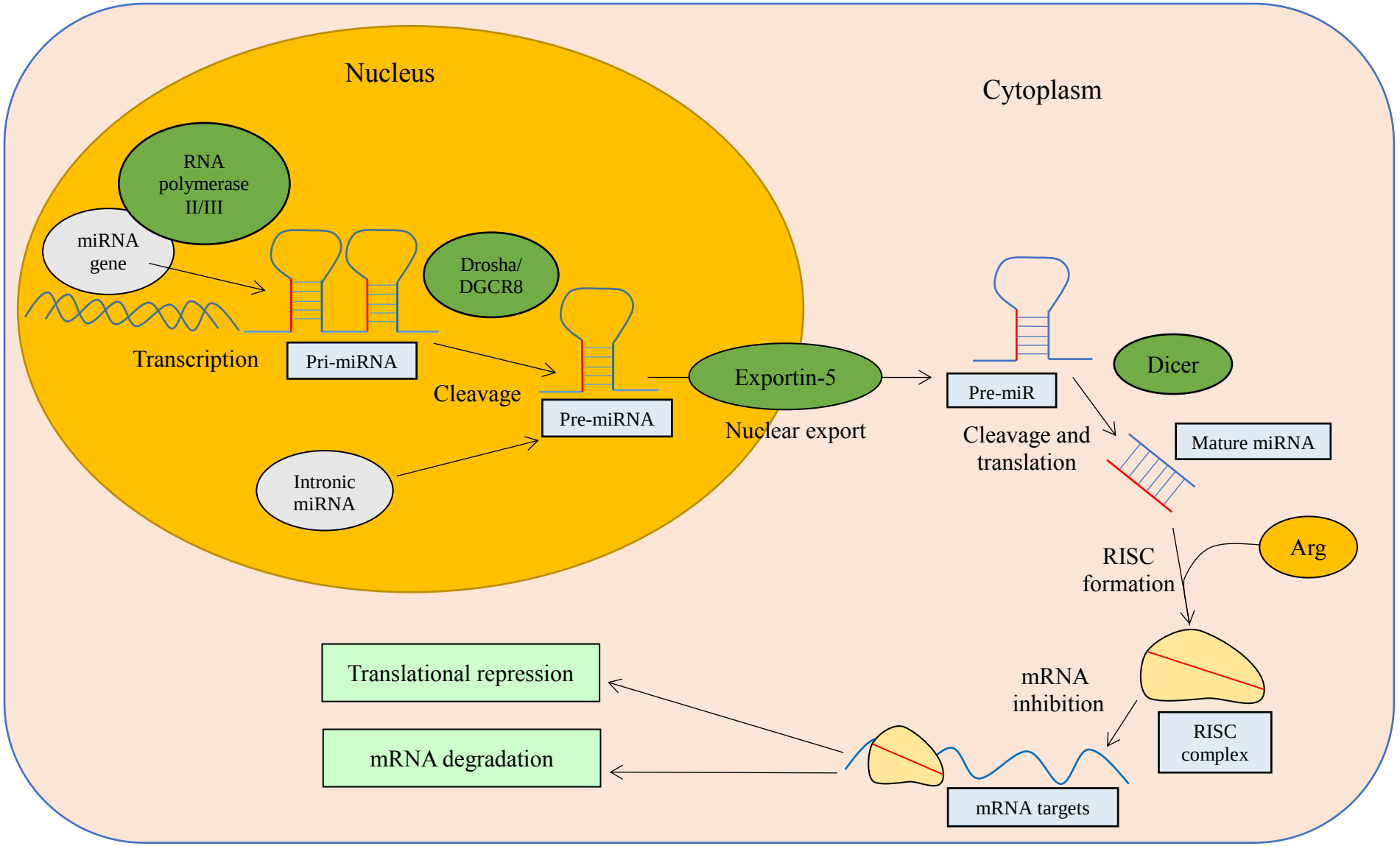

Figure 1.1. Schematic diagram depicting the biogenesis of microRNAs (miRNAs). The diagram outlines this process from the initial transcription of miRNA genes and processing of intronic miRNAs in the nucleus until its formation into double-stranded, mature miRNAs in the cytoplasm, and its eventual inhibition/repression of target mRNA. Arg = Argonaute proteins, RISC = RNA-induced silencing complex (Annotated from Purvis et al., 2015).

1.5.3 Physiological role in CSCs

Due to their ability to target a wide variety of different genes, miRNAs have the potential to have an impact on a number of biological functions. The physiological roles of these miRNAs have been documented in certain stem cell subtypes, however relatively little is known about their role in CSCs (Purvis *et al*., 2015).

1.5.3.1 MiRNAs regulate myocardial differentiation and proliferation of CSCs

MiR-1 and miR-133 are two of the most commonly investigated miRNAs within stem cells, and have been shown to be involved in regulating the differentiation of ESCs. Takaya and coauthors used trichostatin A and a histone deactylase inhibitor to induce myocardial differentiation in mouse ESCs. They found that the expression levels of miRNA-1 and miR-133 were reduced following this treatment, indicating that the ESCs successfully differentiated into CSCs. This outcome was also supported by a reduced expression of NKX2.5, a gene associated with cardiac differentiation (Takaya, 2009). Furthermore, the overexpression of miR-1 was found to inhibit CDK9 and HAND2 genes, which play roles in activating ventricular cardiomyocytes and activating cardiac-specific genes (Fig. 1.2) (Purvis *et al*., 2015; Takaya, 2009; Han *et al*., 2006). This suggests that miRNAs have the potential to regulate myocardial differentiation within stem cells by inhibiting the expression of cardiac-specific genes.

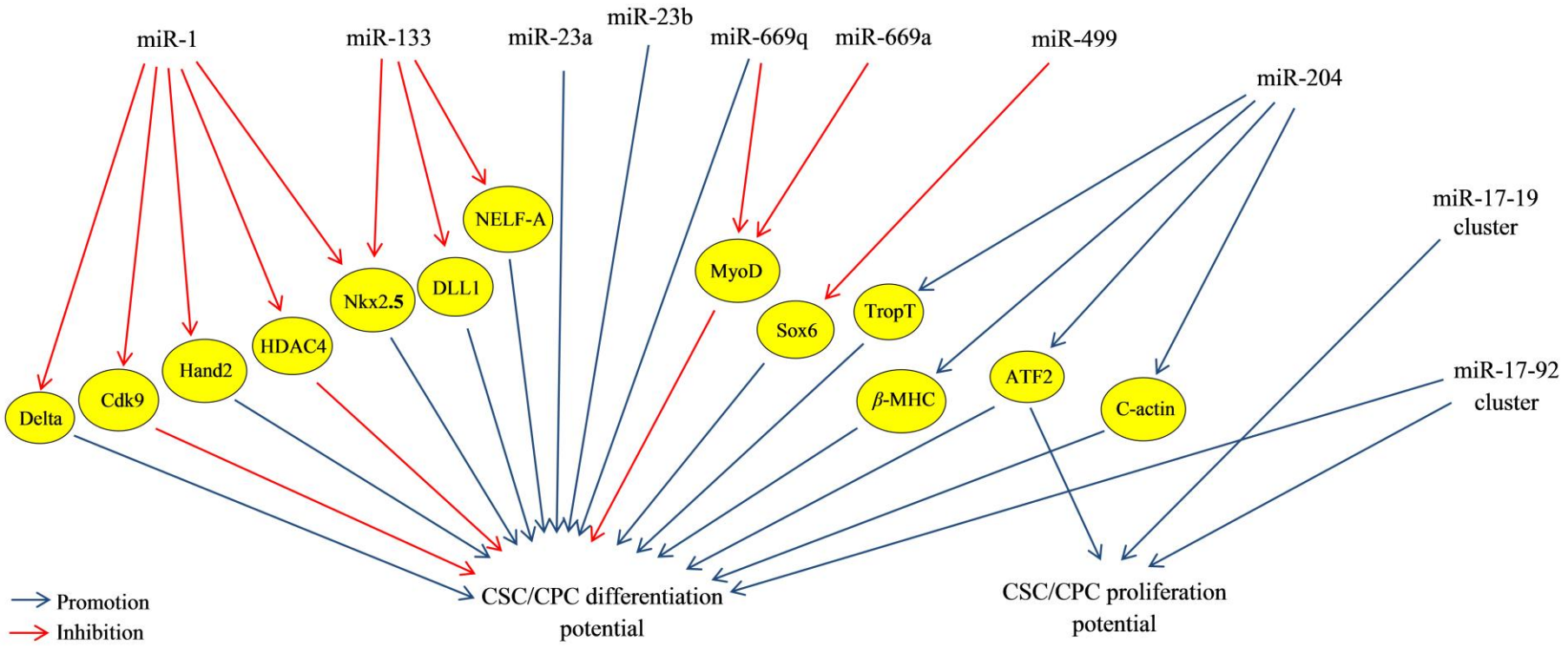

Figure 1.2. Summary diagram depicting the cellular interactions of various miRNA subtypes and clusters with regard to their role of regulating the differentiation and proliferation potentials of cardiac stem cells (CSCs) and progenitor cells (CPCs). These miRNAs target specific transcription factors and cardiac genes (yellow circles) and inhibit their protein expression, causing a downstream effect on stem cell differentiation and proliferation (promotion is indicated by blue arrows and inhibition is indicated by the red arrows) (Annotated from Purvis et al., 2015).

The ability of miRNAs to regulate of stem cell function has been found to be dependent on the nature of their molecular targets. For this reason, there has been a disparity in the literature concerning the functional roles of miRNAs on CSC proliferation and differentiation. An example of this is the interplay between miR-1 and miR-133 on DLL1, a transcription factor which promotes the expression of cardiac mesoderm genes and suppresses the expression of nonmesoderm genes. MiR-1 was found to increase the differentiation of CSCs by inhibiting DLL1, while miR-133 inhibited this process (Ivey *et al*., 2008). Another study found that cardiac-specific miRNAs, miR-1 and miR-499 were found to be important for CPC differentiation. MiR-1 was found to inhibit the HDAC4 gene, while miR-499 was found to inhibit SOX6 gene (Fig. 1.2) (Sluijter *et al*., 2010). These genes are transcription factors that promote the differentiation of CPCs, which was prevented after blocking the actions of miR-1 and miR-499 (Sluijter *et al*., 2010).

There has also been evidence to suggest that other less common miRNA subtypes such as miR-204 and miR-669 also have the potential to promote CSC and CPC differentiation. The inhibition of miR-204 was found to increase the proliferation of CPCs without affecting cell viability or apoptosis. This was further supported by a subsequent downregulation of cardiac-specific genes such as troponin TropT, β-MHC and C-actin (Fig. 1.2). Further bioinformatic analysis revealed that miR-204 targets ATF2, a transcription factor that elicited a similar increase in CPC proliferation after overexpressing it in these cells (Xiao, 2012). The roles of miR-669a and miR-669q were investigated in neonatal CPCs. When these miRNAs were overexpressed in mouse CPCs, there was a reduction in the differentiation potential of the cells due to a repression of MyoD gene; a promoter of muscle differentiation (Crippa *et al*., 2011).

1.5.3.2 MiRNAs promote angiogenic differentiation

Certain miRNAs have also been found to target genes that regulate angiogenesis in CPCs. The overexpression of miR-1 has been found to have pro-angiogenic effects such as vascular tube formation and migration of CPCs, thus promoting angiogenic differentiation. This pro-angiogenic potential of miR-1 was further demonstrated by inhibiting a negative regulator of apoptosis, sprouty-related EVH1 domain-containing protein 1 (SPRED1) (Mil *et al*., 2013). This role was also shown for miR-132 after discovering that the *in vivo* transplantation of saphenous vein derived cells, which readily secrete miR-132, into the infarcted myocardium of mice, resulted in the activation and vascular differentiation of endogenous CSCs (Katare *et al*., 2011).

1.5.4 Pathophysiological role in CSCs

Despite their ability to regulate physiological processes within the body, miRNAs can also have pathological consequences to the regular functioning of biological systems. This is generally attributed to the ability of such miRNAs to non-specifically target many different genes with a wide variety of functions (Purvis *et al*., 2015). In doing so, miRNAs can cause the unwanted activation of signaling pathways leading to cell death and disease.

There is evidence to suggest that miRNAs may have a pathophysiological role in CSCs associated with apoptosis and necrotic cell death. In one study, CPCs were found to inhibit the critical apoptotic activator B-cell lymphoma 2 interacting mediator of cell death (Bim) after treatment with a miRNA cocktail consisting of miR-21, -24, and -221, leading to the enhanced survival of the progenitor cells. Furthermore, a marked improvement in the engraftment and survival of these cells was observed following the *in vivo* transplantation of the cocktail-treated cells into an infarcted myocardium (Hu *et al*., 2011).

Unlike the programmed form of cell death (apoptosis), necrosis is a premature form which results from enzymatic self-digestion and usually occurs in injured cells or dying tissue (Majno and Joris, 1995). Certain miRNAs have also been discovered to regulate the necrotic cell death of CSCs. For instance, CSCs that were exposed to oxidative stress and treated with a miR-155 precursor mimic, were found to target receptor interacting protein (RIP1), a protein required for the activation of necrotic death signaling pathways (Liu *et al*., 2011). Apoptosis and necrotic cell death are major contributors for the reduction in stem cell number after transplantation in patients with chronic morbidities such as diabetes (Moore *et al*., 2014; Katare *et al*., 2011). This may indicate the therapeutic use of such miRNAs that regulate these functions by improving the efficacy of stem cell therapy.

1.5.5 Therapeutic use of miRNAs in CSCs

Their well-documented capacity to regulate CSC function suggests that miRNAs may have the potential to have a positive impact on CVD. Although the evidence for this is limited, studies have supported the inclusion of certain miRNAs in CSC-based therapies. For instance, certain CSC-derived miRNAs such as miR-378 have been found to regulate genes that contribute to MI. The inhibition of miR-378 was found to improve the viability of Sca-1^{+} CSCs by enhancing the expression of connective tissue growth factor (CTGF), a promoter of cardiac tissue scarring and fibrosis (Kim *et al*., 2013; Shi-Wen *et al*., 2008). This indicates that the inhibition of miR-378 could improve CSC number and function in the ischemic heart, a notion that was further supported in the same study after finding that electrical stimulation of the CSCs led to a reduction in miR-378 expression and therefore cytoprotection against the effects of CTGF (Shi-Wen *et al*., 2008).

In contrast, other miRNAs such as miR-499 seem to regulate genes that protect the heart against CVDs by enhancing the self-renewal capabilities of CSCs into functional cardiomyocytes. MiR-499 translocates across gap junctions from cardiomyocytes onto structurally coupled CSCs in a cell-dependent manner, favouring their differentiation into adult cardiomyocytes by repressing the target genes, Sox6 and regulator of differentiation 1 (Hosoda *et al*., 2011). This accounts for substantially higher expression levels of miR-499 in the differentiated cells compared to barely detectable levels in CSCs. Moreover, in vivo transplantation of CSCs expressing miR-499 into infarcted rat hearts promoted a more effective functional and structural recovery of the damaged heart compared to CSCs devoid of miR-499, indicating the beneifical role of miR-499 in improving cardiac function (Hosoda *et al*., 2011).

The positive impact of certain miRNAs on CSC function suggests that these miRNAs may have the potential to counteract the harmful effects of diabetes on these cells. To understand this further, the expression of different miRNAs can be compared between diabetic and non-diabetic CSCs to determine which miRNAs are altered in the diabetic condition. This altered expression can then be correlated with a potential pathophysiological role for these miRNAs within the CSCs. This role can be demonstrating by manipulating the expression of the miRNAs within the diabetic CSCs and observing how the altered miRNA expression effects CSC number and function in the diabetic condition.

1.6 Objectives and hypothesis

The first objective of this project was to determine whether diabetes effects the expression of miRNAs within mouse and human CSCs. The outcome of this led to the second objective which was to demonstrate the pathophysiological role of the differentially expressed miRNAs in the diabetic CSCs.

I hypothesized that certain miRNAs would exhibit a significant change in their level of expression in diabetic CSCs compared to non-diabetic CSCs in db/db mice, and that this effect of diabetes on miRNA expression could be translated to human CSCs. Furthermore, I hypothesized that genetic manipulation of these differentially expressed miRNAs would provide novel insights into their pathophysiological roles in diabetic CSCs.

CHAPTER 2: GENERAL METHODOLOGY

This chapter outlines the general methodology for the procedures and techniques that were most frequently used throughout this project. This includes the initial isolation of CSCs from mouse heart tissue, as well as downstream experiments such as flow cytometry, RNA extraction, q-PCR, protein extraction and western blot analysis. Although subsequent chapters of this thesis are more specialized, they also contain elements of these general techniques and are therefore referenced in this Chapter accordingly.

2.1 Animal information

The db/db mouse is an inbred mouse strain (C57BLKS/J) that is a useful animal model for T2DM (Burke *et al*., 2017). These mice develop an obese phenotype that predisposes them to diabetes at an early age due to a mutation in the leptin receptor gene (db) that regulates body fat (Mao *et al*., 2006; Chen *et al*., 1996). The diabetic db/db mice are extremely obese in appearance and can therefore be easily differentiated from the leaner non-diabetic mice. They also have been documented to develop other symptoms that mimic diabetes in humans such as hyperinsulinemia and hyperglycemia from six weeks of age (Burke *et al*., 2017; Kobayashi *et al*., 2000).

The Katare laboratory holds a colony of db/db mice at the Hercus-Taieri Resource Unit in the University of Otago. These mice were transported as required for the extraction of heart tissue and eventual isolation of CSCs. The use of these mice was approved by the Animal Ethics Committee of the University of Otago (Reference No: 25/12). The mice were 8-10 weeks old at the time of tissue collection and were either diabetic or non-diabetic, reflected by an obese or lean appearance, respectively. Hyperglycemia was confirmed in all diabetic mice by measuring an increased glucose concentration in their urine. All animals were age and gender-

matched and their hearts were collected and pooled together (4 hearts per sample) comprising the first set of diabetic (n=6) and non-diabetic CSC samples (n=6) that were analysed in Chapter 4.

2.2 General plan for mouse CSC study

Here, I will describe the plan (depicted in Fig. 2.1) used to fulfil the objectives of my study. After obtaining the mice, the CSCs were isolated and cultured *in vitro*. The CSCs were then purified before extracting total RNA and protein. The total RNA was used for a Nanostring expression profiling microarray, as well as for a q-PCR experiment that was subsequently performed for validation of Nanostring analysis data (described in Chapter 4, sections 4.2.1 and 4.2.3). Next, total protein was used for western blotting analysis to confirm the target genes for the dysregulated miRNAs (described in Chapter 5, section 5.2.3). Validating the dysregulation of the miRNAs in the diabetic CSCs will indicate the effect of diabetes on miRNA expression, thus answering the first objective of the study. The second objective will be answered by performing functional experiments (described in Chapter 6, sections 6.2.3 and 6.2.4) on the dysregulated miRNAs to determine their role in the diabetic CSCs.

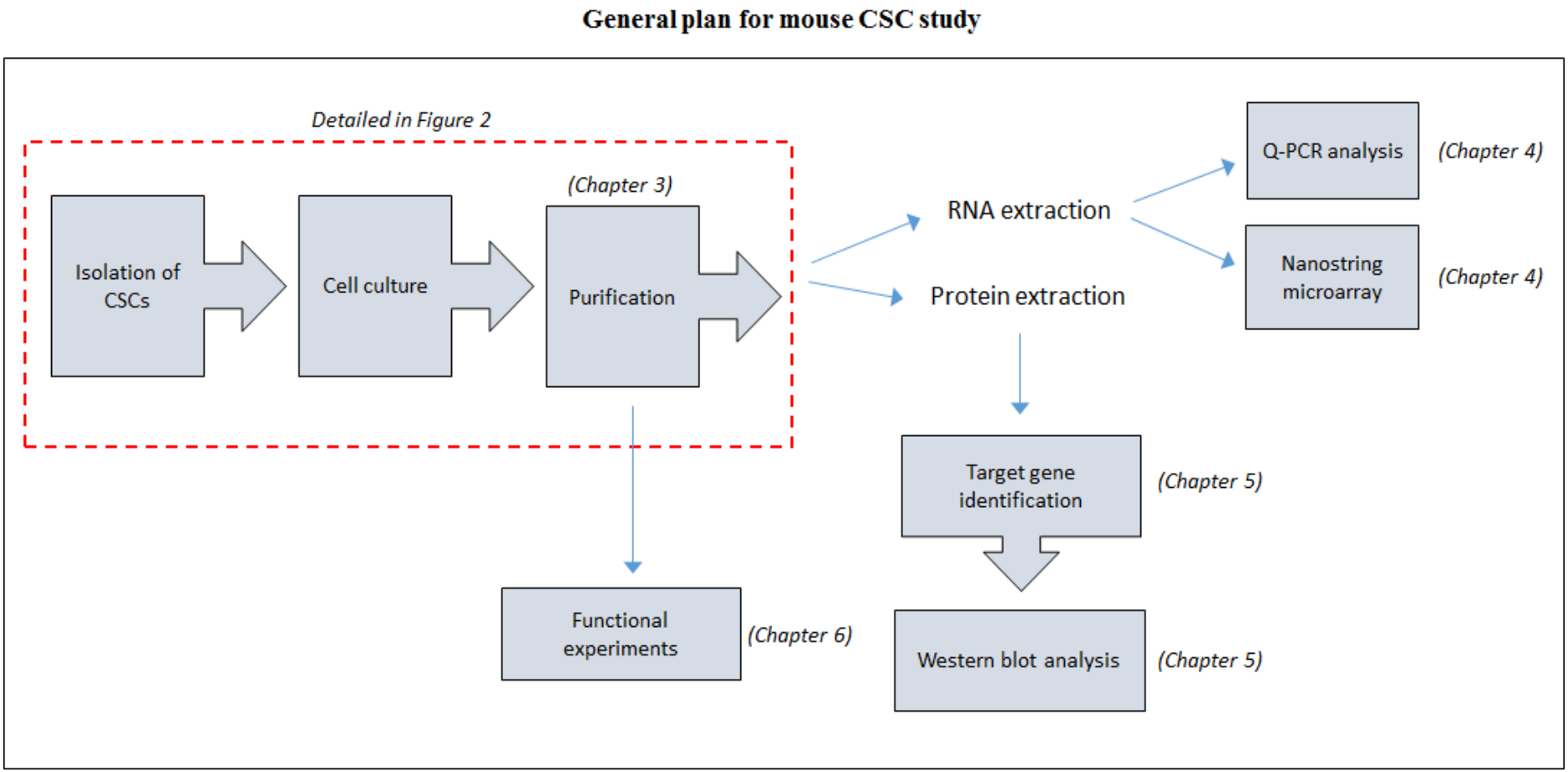

Figure 2.1. Schematic flow chart outlining the general plan used for the mouse CSC study. The chart describes the isolation of CSCs to the extraction of total RNA and total protein, which were then processed in chapters 4, 5 and 6. Details of the plan used for culturing the CSCs is depicted in Figure 2.2. The extracted RNA was used for a Nanostring expression profiling microarray and q-PCR analysis. The extracted protein was used for target gene identification and western blot analysis. Functional experiments were also performed using the purified CSCs.

2.3 Culturing CSCs

2.3.1 Initial cardiac cell isolation protocol

A culture of CSCs was initially established using 24 diabetic and 24 non-diabetic age and gender-matched db/db mice. Based on previous data from the Katare lab and previous indications from other studies, these hearts were pooled to generate a sufficient number of CSCs for downstream experiments (Carlson *et al*., 2011). Each sample thus consisted of a pool of 4 mouse hearts, allowing for the comparative analysis of 6 diabetic and 6 non-diabetic CSC samples. The hearts were extracted from the mice and placed in sterile Hank's Balanced Salt Solution (HBSS) isolation buffer (Table A1.1 in Appendix 1) on ice. This buffer maintains cellular pH and osmotic balance and provides essential inorganic ions. Previous publications from the Katare lab and others have shown that collagenase is optimal for isolating CSCs, while destroying other cell types in mouse heart tissue (Katare *et al*., 2013; Messina *et al*., 2004). A collagenase solution consisting of 30 mL sterile HBSS and 2% collagenase type II and IV (Worthington, USA, Table A1.1 in Appendix 1) was therefore prepared and incubated at 37°C for 20 minutes. The mouse hearts were placed in a 10 cm dish and the adipose tissue was removed. The hearts were then washed with sterile HBSS and chopped into smaller fragments using surgical scissors. These fragments were pipetted into a 15 mL tube and the supernatant was aspirated. The fragments were further washed using sterile HBSS, and then placed in a T75 flask in which 15 mL of the pre-incubated collagenase solution was added.

Collagenase is a protease which dissociates peptide bonds found in collagen and was thus used for digestion of the heart tissue. The heart tissue was digested at 37°C for 70 minutes on a cell shaker. The supernatant was collected in a new 50 mL tube on ice and 15 mL of the collagenase solution was pipetted onto the heart tissue in the T75 flask. The heart tissue was mechanically digested by strong, repetitive pipetting (x15), and the supernatant was again

collected in the 50 mL tube on ice. The cell suspension was then centrifuged at 1400 rpm for 5 minutes. After aspirating the supernatant and re-suspending the cell pellet, 1 mL of Dulbecco's modified eagle medium supplemented with 10% Ham's F12 nutrient mixture (DMEM/F12, ThermoFisher, USA) growth medium was pipetted into the suspension. The media was also supplemented with 1% antibiotic-antimycotic (100X) (Thermo Fisher, New Zealand) to prevent contamination. The cell suspension for each sample was transferred into T25 flasks, supplemented with 4 mL growth media and incubated at 37°C for 60 minutes. The media in the flask was then aspirated and replaced with 5 mL of fresh media and incubated at 37°C for 24 hours. From this time-point, the media was replaced every 2-3 days to remove cellular debris and maintain maximum confluency.

The final samples that were obtained consisted of a population of non-specific cardiac cells that were presumed to contain a subset of CSCs. This cardiac cell population was initially grown within T25 flasks and passaged four times before being purified, as described in Chapter 3, section 3.2.3.

2.3.2 Protocol used to achieve sufficient cell numbers

The isolated cardiac cells were cultured and ultimately purified to obtain a pure CSC population. The cells were grown in either T25 or T75 cell culture flasks and incubated at 37°C after being suspended in DMEM/F12 growth media (ThermoFisher, USA). Cells were monitored and passaged when they reached 80% confluency. The CSCs were grown as a primary cell culture. It was therefore important to have a clear plan of the steps involved in culturing CSCs in order to obtain appropriate cell numbers and ensure experiments are completed in a timely manner. For this reason, a schematic diagram was constructed outlining the different stages of CSC passaging from the initial isolation from mouse heart tissue to processing by RNA and protein extraction, as shown in Figure 2.2. The details of these steps

including passaging techniques, freezing cells and the purification procedure will be described in Chapter 3.

Freshly isolated cardiac cells (P0) were initially plated in a single T25 flask. After seven days of culture to reach confluency, the cells were passaged to two T25 flasks at P1. These two flasks were cultured for four days until confluent, at which point one flask was further passaged to three T25 flasks at P2, while cells from the remaining flask were frozen to retain a stock of cells at P1. Two of the T25 flasks at P2 were scaled up to two corresponding T75 flasks at P3, while cells from the remaining T25 flask were frozen to retain a stock of cells at P2. The cells in the T75 flasks at P3 were grown for seven days until confluent and then purified using the MACS purification procedure (Chapter 3, section 3.2.1). Cells from the remaining T25 flask were frozen at P3 (Fig. 2.2).

The proportion of CSCs after purification was greatly reduced compared to the original total cell population; therefore the CSCs were plated into two T25 flasks at P4. The CSCs in each T25 flask were subsequently scaled up to a T75 flask at P5 after culturing them for seven days. An additional seven days of culturing allowed for the passaging of confluent T75 flasks to P6 (Fig. 2.2). These cells were then used for downstream experiments.

Cell Culture plan for CSCs

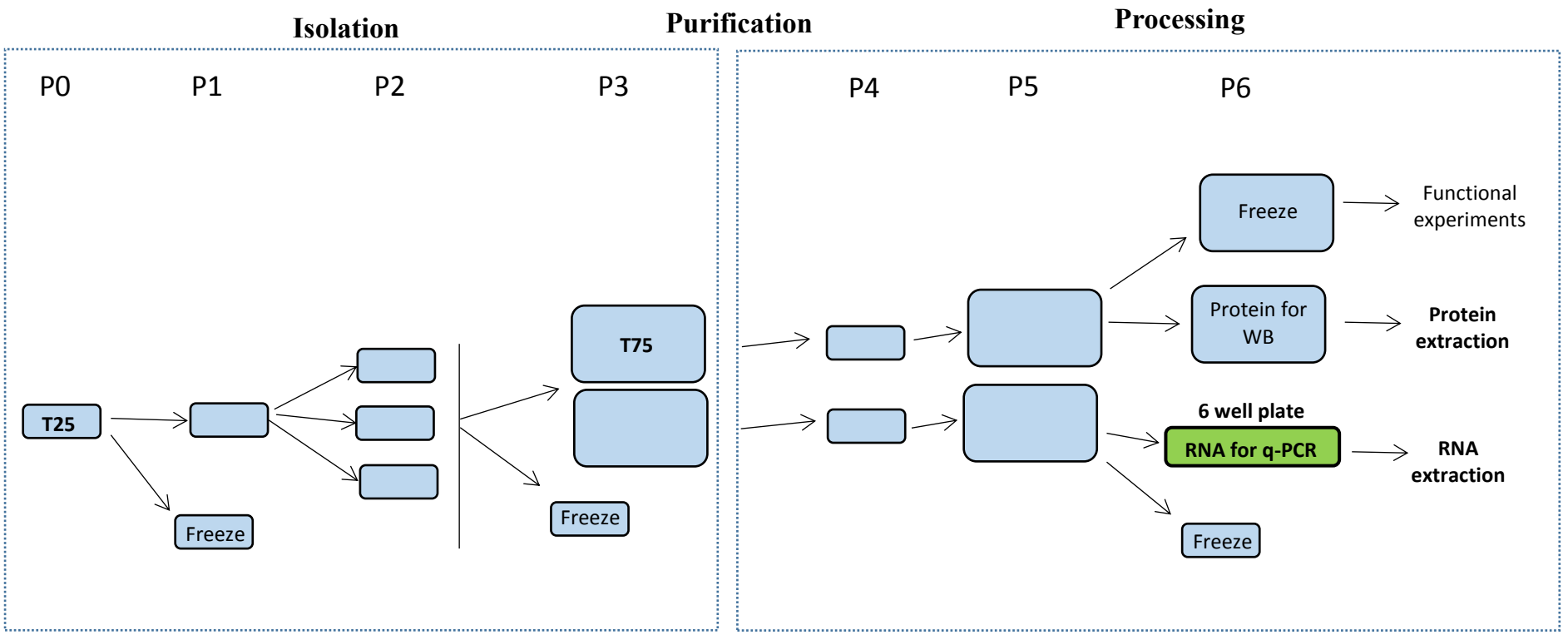

Figure 2.2. Schematic diagram outlining the cell culture experiments used within this study. This covers the initial isolation and purification of CSCs from mouse heart tissue to their eventual processing by RNA and protein extraction. The CSCs were processed at P6 by extracting protein for western blot analysis (WB) and extracting RNA for q-PCR. A proportion of cells were frozen at passage 1, 2, 3, and 6 in order to retain a stock for future use. This diagram shows the stages of culturing for one sample (non-diabetic/diabetic), however multiple diabetic (n=5) and non-diabetic (n=5) samples were cultured concurrently. T25 flasks are represented as small, blue rectangles, while T75 flasks are represented by larger, blue rectangles, and 6-well plates are represented by longer, green rectangle.

2.4 Flow cytometry

Flow cytometry (FACS) was used to confirm the purity of the isolated CSCs from both mouse (Chapter 3, section 3.3.3) and human heart tissue (Chapter 7, section 7.3.2). The general procedure involves staining the cells with fluorophore-conjugated antibodies and analysing the expression of CSC surface markers.

2.4.1 Staining of cells

The CSCs in each sample were first trypsinized and counted using a hemocytometer. The CSC samples were then aliquoted to achieve the desired concentration (1×10^6 cells/mL) for each reaction. The samples were centrifuged at 1400 rpm for 5 minutes and re-suspended in 1 mL of freshly prepared FACS buffer (Table A1.1 in Appendix 1). The 50 µL suspensions containing 5×10^4 cells were pipetted into polystyrene tubes (BD Biosciences, USA) along with 50 µL of a fluorophore-conjugated antibody solution (2.5 µL of antibody in 47.5 µL FACS buffer) and incubated in the dark for 30 minutes at 4°C. The monoclonal anti-mouse, Sca-1 antibody (Miltenyl Biotenic, Germany) was used to identify the mouse CSCs (Chapter 3, section 3.2.1), while the monoclonal anti-human CD105, CD90 and Cluster of differentiation 34 (CD34) antibodies (eBiosciences, USA, Table A1.2 in Appendix 1) were used to identify the human CSCs (Chapter 7, section 7.2.3). Unstained/negative controls containing 50 µL of FACS buffer without cells were also included for each sample and subjected to the same incubation conditions. At the end of the incubation period, the tubes containing cells were washed twice with 2 mL of FACS buffer and then centrifuged at 1400 rpm for 5 minutes at 4°C. The cell pellets were then re-suspended in 300 µL of FACS buffer.

2.4.2 Staining of compensation controls

In FACS, the fluorescence from more than one fluorophore may be detected in the same channel of the flow cytometer if their emission spectra overlap. Fluorescence compensation can be used to remove this spill-over of fluorescence (Schwartz *et al*., 1998). The AbC anti-mouse and anti-human bead kits (Thermo Fischer Scientific, USA) were used for compensation of mouse and human samples, respectively. This kit includes AbC capture beads that bind to mouse immunoglobulin, as well as negative beads that have no binding capacity. Binding of the two bead components with a fluorophore-conjugated antibody elicits a reaction whereby two distinct populations (positive and negative) of beads are created. This can be used to set the compensation parameters of the stained cells. The bead solutions were initially prepared by adding 2 drops of the AbC capture beads to separate tubes and then directly adding 2.5 µL of each respective conjugated antibody. The tubes containing beads were incubated in the dark for 15 minutes at RT, then washed twice with 3 mL of phosphate buffered saline (PBS) and centrifuged at 1400 rpm for 5 minutes at 4°C. The design for these tubes, as well as the fluorophores used is outlined in Table A2.1 and Table A2.2, respectively in Appendix 2.

After the incubation period, the AbC capture bead pellets were re-suspended in 300 µL of PBS along with 2 drops of the negative capture beads (used as an unstained compensation control). Dead cells were also prepared as a positive compensation control for the PI channel. The cells in this sample were killed after incubation at -80°C for 24 hours. Just before analysing the samples, a 10 µL volume of 1 mg/mL Propidium Iodide (PI) (Life Technologies, USA) was added to the stained cell and bead samples, as well as the dead cell sample. PI is a dye that stains dead cells (Cummings *et al*., 2012).

2.4.3 Data acquisition

The Gallios flow cytometer (Beckman Counter Inc, USA) was used for data acquisition. At least 10,000 events within the gate of interest were acquired by the flow cytometer for each sample to ensure reliability of the data. The compensation parameters and flow cytometer voltages were set up to minimise spill over of samples in adjacent channels. Once the data was acquired for each sample, FlowJo 10.0 software (TreeStar, USA) was used for the analysis. The FSA (forward scatter area) and FSW (for scatter width) of the cell distribution was visualized and subjected to doublet discrimination. The compensation matrix was then created by gating the negative populations of cells in the channel containing the unstained sample. This involved identifying and excluding the population of dead cells from the PI channel. Fluorophore controls showed a similar spread of data as the unstained cells, indicating that the unstained samples could be used as controls for selecting positive cells for a particular marker. This compensation matrix was therefore applied to all positively stained cell samples to determine the proportion (%) of the respective markers in the CSCs (eg. Sca-1 in Chapter 3, or CD105 in Chapter 7).

2.5 RNA extraction

Total RNA was extracted from diabetic and non-diabetic CSCs at different stages of the project using the established Qiagen protocol that has previously been used in the Katare laboratory (Rawal *et al*., 2016; Katare *et al*., 2011). The volumes of reagents used from the Qiagen RNA extraction kit (Qiagen, USA) depended on the size of the culture dish (Table 2.1).

Table 2.1. Volumes of Qiagen reagents based on culture dish size					
Culture dish	Surface area (per plate)	Qiagen lysis buffer	Chloroform	Isopropoanol	Ethanol (75%)
6-well plate	$9cm^2$	900 µL	180 µL	450 µL	900 µL
12-well plate	$4cm^2$	400 µL	80 µL	200 µL	400 µL

At the end of the experimental period, the media within each well was aspirated and the cells were washed using 1 mL of sterilized PBS. Next, Qiagen lysis buffer was added to the cells, which were subsequently incubated for 5 minutes at room temperature (RT). A cell scraper was used to manually detach and simultaneously lyse the cells in the flask. The resulting lysate was transferred to a fresh RNAse-free 1.5 mL collection tube to which chloroform was added and shaken vigorously for 15 seconds. This allows the chloroform to separate the RNA from protein and other cellular debris. Tubes were then centrifuged at 12,500 rpm for 15 minutes at 4°C. The clear upper aqueous phase containing RNA was transferred to a new Eppendorf tube taking care not to disturb the protein precipitate (Coombs *et al.*, 1999).

Next, a volume of 100% ethanol equivalent to 1.5 fold of the initial lysis buffer was added to the Eppendorf tube and mixed by pipetting. This allows the RNA to be precipitated from the clear aqueous phase. Up to 700 µL of the aqueous phase was immediately transferred to an RNeasy Mini spin column fitted with a 2 mL collection tube and centrifuged at 10,000 rpm for 15 seconds at RT. This step was repeated until all the aqueous phase was passed through the column. After discarding the flow through in the collection tube, the RNA was washed with 700 µL of RWT buffer once and 500 µL of RPE buffer twice. Each time the column was centrifuged at 10,000 rpm for 15 seconds at RT and the flow through discarded. After the final wash, the column was placed in a new collection tube and centrifuged at full speed for 1 minute to prevent any carry-over of RPE buffer. Finally, the column was placed in a 1.5 mL RNAse free collection tube, and RNA was eluted by addition of 30 µL of nuclease-free dH_2O by centrifuging at 10,000 rpm for 1 minute. The RNA from each sample was quantified using

a Nanodrop spectrophotometer (ThermoScientific, USA) and the purity (260/280 absorbance) was also measured. A representative example of these measurements is shown below on RNA samples extracted from five diabetic and five non-diabetic mouse CSCs (Table 2.2).

Table 2.2. RNA concentration and purity

RNA sample	Concentration (ng/μL)	260nm absorbance	280nm absorbance	260/280 (purity)
Non-diabetic #1	52.70	0.067	0.034	1.971
Non-diabetic #2	154.33	0.189	0.093	2.032
Non-diabetic #3	52.45	0.064	0.033	1.939
Non-diabetic #4	42.45	0.053	0.026	2.039
Non-diabetic #5	64.80	0.081	0.041	1.976
Diabetic #1	33.30	0.040	0.021	1.905
Diabetic #2	101.60	0.127	0.062	2.048
Diabetic #3	101.80	0.126	0.064	1.969
Diabetic #4	170.45	0.218	0.106	2.057
Diabetic #5	32.88	0.040	0.021	1.905

2.6 q-PCR protocol and analysis

The quantitative real-time PCR (q-PCR) is a commonly used procedure for determining molecular changes at the genetic level (Hugget *et al*., 2005). It was used in this project to determine changes in the expression levels of the miRNAs between diabetic and non-diabetic CSCs. The general protocol that was used for this technique is described below.

2.6.1 Reverse transcription (R.T)

Reverse transcription of total RNA to complementary DNA (cDNA) was initially performed using miRNA-specific R.T primers. As described in the standardized ThermoFisher protocol, 20 ng of total RNA is required for each q-PCR reaction. Samples with high RNA concentrations (>40 ng/µL) were diluted (1:10) to obtain working solutions of RNA. The RNA volumes were prepared in 0.2 mL PCR tubes and diluted with nuclease-free dH_2O up to a volume of 5 µL. A master mix containing components of the TaqMan assay kit (ThermoFisher Scientific, USA) was prepared as indicated in Table 2.3. A 7 µL volume of R.T master mix and 3 µL of a miRNA-specific R.T primer (5X dilution) (ThermoFisher Scientific, USA) were added to the RNA samples, giving a total volume of 15 µL for each tube (Table 2.3). The samples were then incubated in a thermal cycler under the conditions described in Table 2.4A to synthesise cDNA.

Table 2.3. Solutions required for R.T samples		
Component		**For 1 reaction (µL)**
RNA sample		5
RT master mix reagents	dNTPS (100mM)	0.15
	Multiscribe reverse transcriptase	1
	Reverse transcription buffer (10X dilution)	1.5
	RNase inhibitor	0.19
	Nuclease-free dH_2O	4.16
miRNA-specific R.T primers (5X dilution)		3
Total volume		15

Table 2.4. Incubation settings for reverse transcription and PCR reaction			
A. Reverse transcription			
	Incubation temperature	Incubation time	No. of Cycles
Step 1	16 °C	30 mins	1
Step 2	42 °C	30 mins	1
Step 3	85 °C	5 mins	1
B. PCR			
	Incubation temperature	Incubation time	No. of Cycles
Step 1	95 °C	10 mins	1
Step 2	95 °C	15 sec	40
	60 °C	1 min	

2.6.2 Polymerase chain reaction (PCR)

Next, the cDNA products corresponding to each RNA sample were amplified with the PCR reaction. After pipetting 1 µL of each cDNA sample into a 96-well PCR plate in triplicate, 6.25 µL of a PCR premix solution (Takara, Japan) was added to each well, along with 4.75 µL of nuclease-free dH_2O. This was followed by adding 0.5 µL of a miRNA-specific TM primer (20 X dilution) (ThermoFisher Scientific, USA), giving a total volume of 12.5 µL for each well (Table 2.5). Negative controls were also prepared alongside the experimental samples in order to test for the quality of the cDNA products and TM primers. The cDNA samples were then amplified by incubation in a PCR machine (ThermoFisher Scientific, USA) under the conditions described in Table 2.4B.

Table 2.5. Solutions required for PCR samples

Component	**For 1 reaction (µL)**
R.T-reaction	1
PCR premix	6.25
Nuclease-free dH_2O	4.75
miRNA-specific TM primer (20X dilution)	0.5
Total volume	12.5

2.6.3 Data analysis

In order to determine the relative fold changes of each target miRNA, the raw q-PCR data was analysed using cycle at threshold (Ct) values as a measure of expression (Schmittgen and Livak, 2008). Ct values are defined as the number of PCR cycles at which a set fluorescence threshold is achieved. The data was analysed by first calculating the mean of the three replicate Ct values for each RNA sample. A ΔCt was then calculated for each target miRNA

by subtracting the mean Ct of the endogenous control, U6 small nuclear ribonucleoprotein (U6) from the mean Ct of the target miRNAs in each sample. Finally, a ΔΔCt was determined for each miRNA by subtracting the mean ΔCt of the non-diabetic samples from the mean ΔCt of both non-diabetic and diabetic samples. The ΔΔCt values were used to calculate the relative fold changes for the diabetic and non-diabetic CSC-derived RNA samples using the following formula:

$$\textbf{Fold change} = (\mathbf{2})^{-\mathbf{\Delta\Delta Ct}}$$

Mean fold changes were determined for all target miRNAs in each sample and a two-tailed unpaired t-test was performed to determine the statistical significance ($P<0.05$) for the differences in expression of each target miRNA between diabetic and non-diabetic CSC-derived miRNA samples. The standard error was also calculated for each reaction to account for data variability.

2.7 Protein extraction and quantification

2.7.1 Protein extraction

Total protein was extracted to conduct western blot analysis. For this, CSCs were trypsinized and centrifuged to form a pellet in 1.5 mL centrifuge tubes on ice. The cell pellet was re-suspended in 1 mL of the radioimmunoprecipitation assay (RIPA) lysis buffer, which was supplemented with protease inhibitors to prevent protein degradation during the extraction process. Cells were lysed by repeat-pipetting and aggressive syringing with a 1 mL syringe fitted with a 30G needle. The RIPA lysis buffer was prepared (Table A1.1 in Appendix 1) at a pH of 7.4, then incubated for 20 minutes at RT, and centrifuged at 14000 rpm for 30 minutes at RT to allow for protein separation from the other cellular components. The resulting protein supernatant was collected and stored at -80°C.

2.7.2 Bradford assay for protein quantification

A Bradford colorimetric assay (Sapan *et al*., 1999) was used to determine protein concentration in this study. A serial dilution of 0 – 2 mg/mL was made using bovine serum albumin (BSA), as shown in Table 2.6.

Table 2.6. Serial dilutions for Bradford assay

BSA concentration (mg/mL)	BSA volume from 2 mg/mL stock (µL)	Volume of Bradford reagent (µL)
0	0	1000
0.4	20	980
0.7	35	965
1.0	50	950
1.3	65	935
2.0	100	900

The Bradford reagent contains a Coomassie dye that binds to the protein causing a progressive colour change in the solution from brown to blue depending on the protein concentration (Sapan *et al*., 1999). Thus, the serial dilutions were observed as a progressive colour gradient from brown to blue for 0 – 2 mg/mL of BSA. A 1 µL volume of each protein suspension was then diluted in 999 µL of Bradford reagent. Finally, 100 µL of the solution containing BSA and protein dilutions were pipetted in triplicate in wells of a clear 96-well plate. The optical density of each well was measured in a spectrophotometer at a 595 nm wavelength. After subtracting the mean optical densities (OD) of the negative control (0 mg/mL of BSA) from that of the BSA and protein, a reference standard curve graph was constructed using Graphpad Prism software (Fig. A3 in Appendix 3). The gradient and thus effectiveness of the standard curve was determined from the R-squared statistical measure of linear regression. This indicates the proportion of variance between different concentrations of BSA and the resulting optical densities, and is evaluated between 0 and 1.0. An R-squared value of 1.0 indicates that no

variance exists between the variables. The protein concentrations in each sample were then calculated using the formula:

$$x = \frac{OD - b}{a}$$

Where: x = concentration, OD = optical density, a = slope of graph, and b = Y-intercept

2.8 Western blot protocol and analysis

Western blot analyses were used as to determine the link between specific miRNAs and their target genes. The aim of this was to demonstrate the functional role for the changes in the expression of miRNAs in the diabetic CSCs.

2.8.1 SDS-PAGE gel electrophoresis

The total protein was denatured by incubation at 95°C for 5 minutes after dilution with 2X loading buffer (Table A1.1 in Appendix 1) containing 30% mercaptoethanol at a 1:1 dilution. Thirty micrograms of total protein and 6 µL of Precision Plus Kaleidoscope Protein Standard (Bio-Rad, NZ) were loaded on a 12% SDS-PAGE gel (Table A1.1 in Appendix 1). Gel electrophoresis was run at 100V for 20 minutes, and then 150V for approximately 60 minutes to separate the proteins based on size and charge. The gel was run until the protein samples reached the end of the resolving gel.

2.8.2 Protein transfer

The protein was then transferred from the gel to a polyvinylidene difluoride (PVDF) membrane pre-soaked in methanol using a transfer sandwich cassette. The cassette consisted of two pieces of fibrous pad, two pieces of filter paper, and a PVDF membrane, arranged as shown in Figure 2.3.

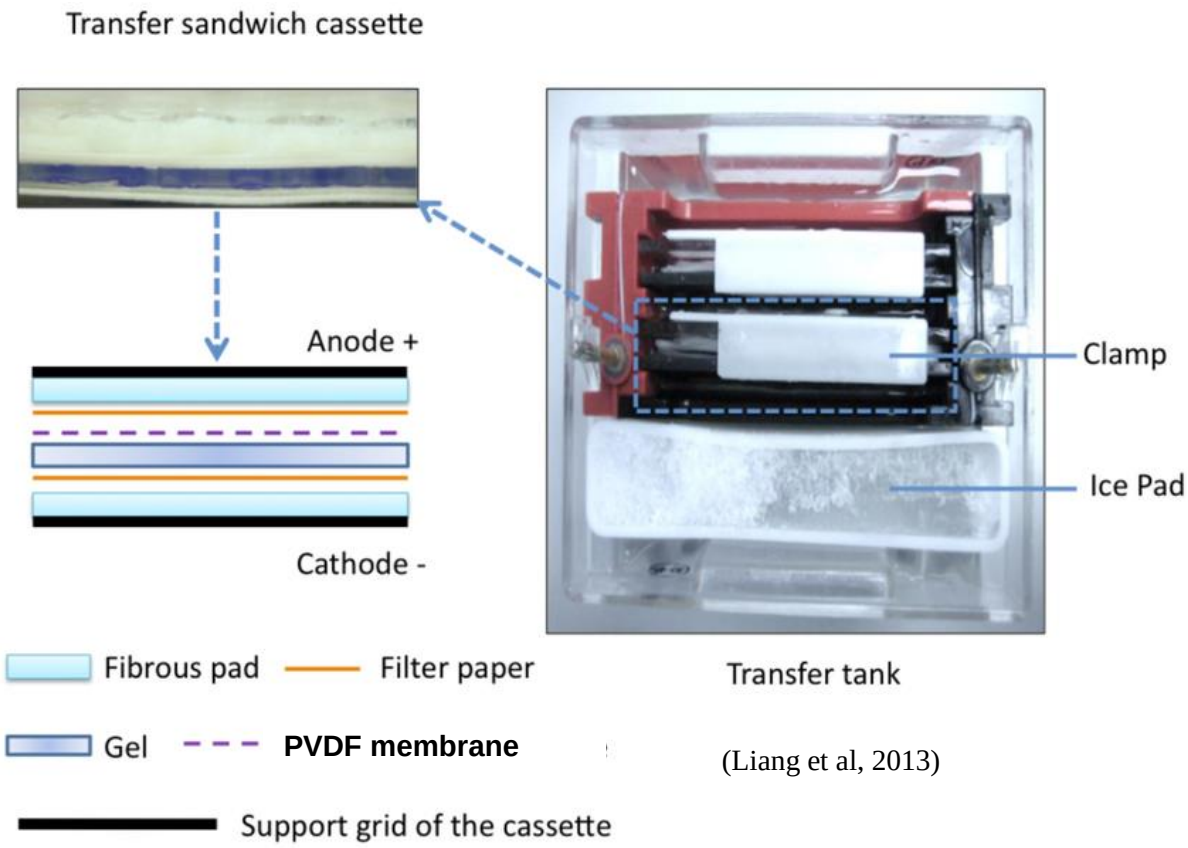

(Liang et al, 2013)

Figure 2.3. Diagram depicting the transfer sandwich cassette that was used in the western blot procedure after gel electrophoresis. This allows for the transfer of protein from the SDS-PAGE gel (dark blue rectangle) to the PVDF membrane (dotted line) as the current travels from the cathode to the anode. Diagram adapted from Liang et al., 2013.

The membrane was initially cut according to the size of the gel and then activated by soaking in 100% methanol for 30 seconds, followed by incubation in transfer buffer for 3 minutes. The transfer sandwich was assembled by first placing a fibrous pad onto the cathode side of the cassette, followed by filter paper and then the gel (Liang *et al*., 2013). The membrane was then carefully placed over the gel and smoothed out with a roller to remove air bubbles between the gel and the membrane. The second filter paper was then placed on the membrane followed by the second fibrous pad, and then clamped shut. The sandwich was then placed into the cassette which was topped up with 1 L of transfer buffer. Transfer was done at 90V at 4°C for 90 minutes. In order to confirm whether the proteins have been successfully transferred onto the membrane, a Ponceau stain was performed. The membrane was soaked in red Ponceau reagent for 1 minute with gentle shaking, then soaked in dH_2O until the reagent was washed away. The protein bands in each lane could be visualized on the membrane after taking an image using a Syngene PXi gel imaging system (Atkinson, USA) (Fig. A4 in Appendix 4).

2.8.3 Blocking and probing with the antibody

After washing the membrane three times in Tris-buffered saline with tween 20 (TBS-T) (Table A1.1 in Appendix 1) for 10 minutes each, the membranes were incubated with 5% BSA in 10 mL of TBS-T for 60 minutes at RT with gentle shaking to block the binding of detection antibody to non-specific proteins. This is followed by probing the membrane with primary antibody which was diluted in 10 mL of blocking buffer according to the manufacturer's protocol. The membrane was incubated for 18 hours at 4°C with gentle shaking. After this incubation period the primary antibody was collected and stored (at -20°C) for re-use. The membrane was then washed three times in TBS-T for 10 minutes each with gentle shaking. A secondary antibody that is specifically reactive to the rabbit/mouse host

species of the primary antibody was then prepared at a dilution of 1:3,000 in blocking buffer and added to the membrane. The membrane was incubated at RT for 60 minutes, then washed three times in TBS-T for 10 minutes each.

2.8.4 Detection of chemiluminescent signals

After the final wash, the membrane was blotted dry to remove excess washing buffer and placed on a clear plastic film on the Syngene PXi gel imaging tray. Two West Pico ECL reagents: SuperSignal solution and Peroxide solution (Thermo Fischer Scientific, USA) were prepared at a 1:1 dilution to detect the chemiluminescent signals (Imaizumi *et al*., 2002). A 1 mL volume of this mixture was applied onto the membrane to completely cover it. The tray was closed to incubate the membrane in the dark for 5 minutes at RT to allow for the reaction of peroxidase with luminol substrate. The membrane was then sealed in the plastic film and correctly positioned in the Syngene machine. Chemiluminescent images were captured using the software for later analysis (shown in Chapter 4, section 4.3 and Chapter 6, section 6.3) using the ImageJ program. The density of each protein band could be determined by inverting the colour scheme, and then using a function of ImageJ to calculate the area of the band. The relative proportion of a specific protein on the membrane could therefore be calculated by dividing the density of the specific protein by the density of a reference (housekeeping) gene (eg. β-actin). The membrane was then either further processed by adding a second primary antibody (for a reference or other specific gene), or dried by dipping the membrane in 100% methanol for 15 seconds, then left to dry between paper towels overnight.

2.9 Statistical methodology

In this project, I have used a number of statistical measures to demonstrate both the reliability and variance in the data. A two-tailed unpaired t-test was used to determine whether changes

in miRNA or gene expression between diabetic and non-diabetic groups were statistically significant ($P<0.05$). The standard error of the mean was calculated for each data set by taking the square root of the standard deviation divided by the sample size. These standard errors are depicted as error bars on the histograms in the following chapters. The sample sizes and number of biological repeats for each experiment were determined from previous literature in the field (Galimov *et al*., 2016; Hu *et al*., 2014).

A one-way ANOVA was also included in experiments which were repeated three times. This was used to determine the variance between repetitions in each data subset where the same samples were used. An 'F' value was calculated for each subset and compared to a statistical 'Fcrit' value. If the F value is larger than the Fcrit, the null hypothesis which states that there is no significant difference between each repetition can be rejected (Ardelean, 2017). These values can thus be used as a measure of consistency between the repetitions of each experiment. Finally, the Kruskal Wallis H test was implemented as a non-parametric statistical measure of consistency in experiments with low (n=3) sample numbers. This test similarly determines if the null hypothesis is rejected by comparing the calculated 'H' value to the statistical 'Hcrit' value. If the H value exceeds the Hcrit value, there is a significant difference in the repetitions of the corresponding data set (Macfarland and Yates, 2016).

CHAPTER 3: ESTABLISHING A CULTURE OF PURIFIED MOUSE CSCS

3.1 Introduction

In this chapter, I will discuss the theory and techniques involved in establishing a culture of CSCs from mouse heart tissue. The results of this Chapter are particularly important in terms of the overall project as many downstream experiments were heavily dependent on the purity and viability of the CSCs that were obtained. I will start by outlining the aims and objectives of this section, followed by the background information necessary for understanding the growth and purification of CSCs. I will then describe the methodology associated with establishing a CSC culture, as well as a brief discussion on the qualitative and quantitative data that was obtained during this process.

3.1.1 Aims and Objectives

The aim of this section of the project was to establish a culture of purified CSCs from diabetic and non-diabetic db/db mouse heart tissue.

3.1.2 The principle of cell culture

Cell culture is a technique that is commonly used to grow cells in a controlled, artificial environment (*in vitro*) while simulating the *in vivo* physiological conditions of the cell. *In vitro* cell culture is one of the most valuable methods to investigate the biological functions of mammalian cells (Oyeleye *et al*., 2016). These cells can be obtained from a variety of tissues using a method designed for cell digestion and disaggregation (Oyeleye *et al*., 2016). There

are several methods of culturing mammalian cells *in vitro* depending on their normal physiological growth conditions. The method that I used in this study involves culturing an adherent monolayer of cells in a flask that can be serially monitored using light microscopy. The proliferation capacity of these cells is maintained by supplementing them with growth media containing nutrients and growth factors (Gospodarowicz and Moran, 1976).

This type of cell culture has also been used to investigate the self-renewing capabilities of stem cells. MSCs and ESCs have routinely been grown as adherent monolayers, which can then be differentiated into more specialized cells such as chondrocytes, osteocytes, adipocytes and cardiomyocytes by adding a differentiation medium (Almalki and Agrawal, 2016; Yamamoto *et al*., 2003). I used this approach in my study to culture CSCs and investigate their self-renewing capabilities in the diabetic condition.

3.1.3 Passaging CSCs *in vitro*

After their initial isolation from organs or tissue, stem cells are commonly plated into suitable flasks or containers in preparation for culturing. An advantage of culturing stem cells compared to other cell types is that they have a higher proliferation potential, resulting in a faster and more efficient growth curve. In this case, a small number of isolated CSCs can be grown and expanded to yield an exponentially greater number of these cells over time, indicating that a relatively smaller amount of heart tissue is required as a starting point. However, this can also pose problems for the viability of the cells:

Due to their high capacity for proliferation, the number of stem cells increases dramatically over just a few days by spreading out across the surface of the flask. For this reason, the cells soon exhaust the available surface area and become overcrowded or ‘confluent’. This has several negative implications with regards to cell viability as the high confluency reduces the capacity of the cells for proliferation, and also may lead to cell death (Brezden and Rauth *et*

al., 1996). Passaging is a technique that is used to increase the available surface area used by the cells which acts to sustain their growth over longer periods of culture (Masters and Stacey, 2007). In my project, passaging was extremely important for promoting the expansion of the CSCs *in vitro* whereby the cells were either scaled up to a larger flask, or divided into multiple same-sized flasks to maintain cell growth.

3.1.4 Purification of CSCs

A population of non-specific cardiac cells can easily be obtained from the chemical digestion of heart tissue. However, in order to isolate the CSCs from other material within this cardiac cell population, they must be separated by a process called 'purification'.

There are a variety of different techniques that can be used for purifying CSCs. Field flow fractionation (FFF) is one common purification method which utilizes gravitational forces to separate stem cells based on their size and morphology (Roda *et al*., 2009). However, although this method is efficient, it is not specific because stem cells are not easily differentiated based on size. Affinity-based purification methods such as fluorescence-activated cell sorting (FACS) overcome these limitations by using specific antibodies that bind to stem cell surface markers (Zhu and Murthy, 2014). In FACS, the antibodies are tagged with fluorescent dyes to sort the cells in a suspension based on fluorescence and light scattering. However, a disadvantage of this technique is that it requires expensive equipment and produces a low cell yield (10^7 cells) (Putnam *et al*., 2003).

Molecular tagging with magnetic beads is another affinity-based method commonly used for stem cell purification. Magnetic-activated cell sorting (MACS) is highly specific and produces a greater cell yield (10^{11} cells) compared to other purification methods (González-González *et al*., 2011; Thiel *et al*., 1998). It utilises a variety of specific antigenic markers that are expressed on the surface of stem cells which can be targeted using magnetically labelled

antibodies. MACS has also be used to purify CSCs and CPCs, and will therefore be used to purify CSCs in my study (Vicinanza *et al*., 2017; Xiao *et al*., 2016).

Sca-1 (Stem cell antigen-1) is a well-known murine antigen that is expressed on the surface of mouse CSCs as well as other stem cell subtypes in mouse tissue (Wang *et al*., 2014; Wang *et al*., 2009). It was originally only used as a marker for MSCs and HSCs, however in 2003 a population of Sca-1^+ cells was also found in the myocardium of adult mice (Oh *et al*., 2003). These Sca-1^+ cells were unique as they were negative for other stem cell markers such as CD45, CD34 and c-kit (Oh *et al*., 2003). They were also reported to exhibit similar telomerase activity to that observed in the newborn heart, suggesting they have stem cell-like properties. Moreover, there was no telomerase activity detected from Sca-1^- cells in the same population (Oh *et al*., 2003). The Sca-1^+ cells were also found to migrate towards an infarcted mouse myocardium following intravenous administration (Liu *et al*., 2013). This finding in combination with the observed ability of these cells to fuse to the injured myocardium and differentiate into healthy cardiomyocytes, suggested that Sca-1 could be considered as a suitable marker for the identification and purification of functional CSCs derived from mouse heart tissue (Liu *et al*., 2013; Oh *et al*., 2003).

3.1.5 Cryopreservation of CSCs

As with all stem cells, CSCs can be exposed to contaminants causing unexpected cell death and also attain senescence after several passages (Hu *et al*., 2014). In order to retain a stock of freshly isolated CSCs over a long period of time, cryopreservation can be used. This involves the suspension of CSCs in a cryoprotectant solution followed by immediate exposure to extremely low temperatures to freeze the cells. The cryoprotectant maintains the structural and functional properties of the cell while limiting any enzymatic and chemical reactions that may cause damage due to the freezing conditions (Bakhach, 2009). As such, this method can

be used to store CSCs in either liquid nitrogen (-196 °C) or temperatures exceeding -80 °C for up to 2 years (Hosoda *et al*., 2017). It has also been shown to preserve the proliferative capacity, cardiac differentiation and angiogenic capabilities of the CSCs after re-initiating growth of the cells from at least one month of exposure at -80 °C (Jackson *et al*., 2017). In this project, certain experiments were performed on the same samples at different time points and therefore cryopreservation at -80 °C was routinely used to retain a stock of each purified CSC sample for future experiments.

3.2 Methods

3.2.1 MACS purification protocol

After isolating the CSCs from mouse heart tissue (using the protocol outlined in Chapter 2, section 2.3.1), the CSCs were purified using MACS (Miltenyi Biotec) (Fig. 3.1). This technique initially involves immunolabeling the cells with the Sca-1 antibody, followed by the application of magnetically labelled microbeads. This magnetic labelling allows for the retention of Sca-1^+ cells after passing the total cell population through a magnetic field.

3.2.1.1 Magnetic labelling

A volume of approximately 5 mL per sample of DMEM/F12 media was stored at 4 °C for 30 minutes prior to starting the experiment. Non-specific cardiac cells from each diabetic (n=6) and non-diabetic (n=6) sample were then pelleted as described in Chapter 2, section 2.3.1. The pellets from each sample were re-suspended with 1 mL of the pre-cold DMEM/F12. The number of cells from each sample were counted using a hemocytometer (Table A5 in Appendix 5). The cells were then transferred into 2 mL microcentrifuge tubes (1×10^7 cells/tube) and centrifuged at 1400 rpm for 10 minutes. The supernatant was aspirated from

each sample and the cells were re-suspended with 90 µL of the pre-cold DMEM/F12 (10^7 cells/90 µL).

A volume of 10 µL/ 10^7 cells containing 30 µg anti-Sca-1-FITC (Miltenyi Biotec, Australia) was added to each sample, mixed well, and incubated at 4 °C for 10 minutes. The cells were then washed by adding 1 mL of pre-cold DMEM/F12 directly into the tubes and centrifuged at 1400 rpm for 10 minutes. The supernatant was aspirated from each tube and the cells were re-suspended with 80 µL of the pre-cold DMEM/F12 (10^7 cells/80 µL). A volume of 20 µL/ 10^7 cells of anti-FITC microbeads (Miltenyi Biotec, Australia) was added to each sample, mixed well, and incubated at 4 °C for 15 minutes. The cells were then washed again by adding 1 mL of pre-cold DMEM/F12 media, and centrifuged at 1400 rpm for 10 minutes. After the supernatant was aspirated, the cells labelled with the Sca-1 antibody were re-suspended in 500 µL of pre-warmed DMEM/F12. In preparation for magnetic separation, an MS column was placed in the magnetic field of a MiniMACS separator.

3.2.1.2 Magnetic separation

The MS column within the magnetic field was initially washed with 500 µL of pre-warmed DMEM/F12 such that the media passes into a 15 mL tube positioned below the MACS separator, as shown in Figure 3.1. The 15 mL tube was then discarded and replaced with another 15 mL tube. A cell suspension was then added to the column followed by 500 µL of DMEM/F12. The flow-through solution collected contains cells which are negative for Sca-1. The MS column was removed from the MACS separator within the magnetic field and placed within a new 15 mL tube. A 1 mL volume of DMEM/F12 was added to the column and a plunger from a syringe was used to immediately flush out the fraction of cells that are magnetically labelled and positive for Sca-1. The magnetic separation procedure was repeated for each sample which were then centrifuged at 1400 rpm for 10 minutes. The samples were

then added to 4 mL of DMEM/F12 media and plated in a fresh T25 flask and incubated at 37 °C for 24 hours.

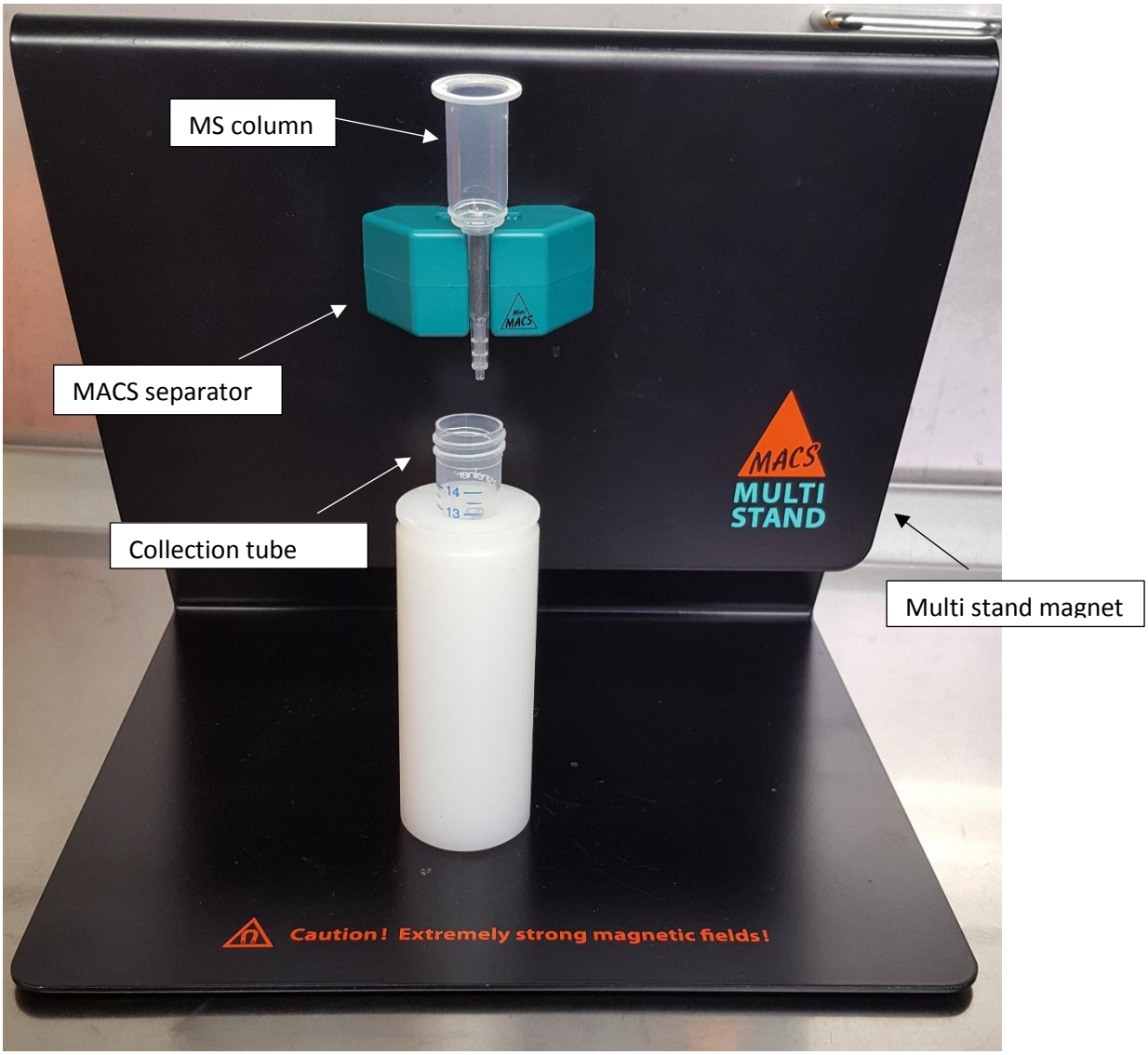

Figure 3.1. Magnetic activated cell sorting apparatus. The MS column is shown placed within the MACS separator (green), with a 15 mL collection tube directly below. The MACS separator is within the magnetic field formed from its association with the multi stand magnet (black).

3.2.2 Flow cytometry protocol

In order to confirm that the purified cells are Sca-1^+ CSCs, FACS was performed for the detection of the Sca-1 marker using diabetic and non-diabetic samples. Cells were prepared for FACS as described in Chapter 2, section 2.4. The tubes that were prepared consisted of one unstained sample, one dead sample (stained with 3µM PI), two experimental samples containing live CSCs (one diabetic, one non-diabetic), and one sample containing fluoresceinisothiocyanate (FITC)-conjugated CD40 beads. The FITC beads were used as a control to account for spill-over of the fluorescent signal between flow cytometer channels. Monoclonal anti-mouse, FITC-conjugated Sca-1 (10 µL of 30 µg anti-Sca-1-FITC/10^7 cells, Miltenyl Biotenic, Germany, Table 1.2A in Appendix 1) was used as the primary antibody for the CSCs. The samples were processed by the flow cytometer and analysed according to the protocol outlined in Chapter 2, section 2.4.3.

3.2.3 Passaging CSCs

Following purification, the CSCs were passaged in order to maintain optimal growth of the cells for long periods of time. This technique was frequently used to transfer the cells into a larger flask to provide greater surface area for optimal growth; or 'split' to create duplicate samples, as outlined in Chapter 2, section 2.3. The old media was aspirated from the T25 flask and the cells were washed with 2.5 mL of pre-warmed phosphate-buffered saline (PBS). After aspirating the PBS solution from the flask, 2.5 mL of the TrypLE dissociation reagent was pipetted into the flask. The flask was gently rocked so as to completely cover the cell layer with the dissociation reagent. The flask was then incubated at 37 °C for 3 minutes, then gently tapped to dissociate the remaining cells which were confirmed by observing them under a light microscope. When ≥ 90% of the cells were detached, 5 mL of pre-warmed DMEM/F12 media was added to the flask and dispersed over the cell layer surface several times. If ≤ 90%

of the cells were detached, the flask was re-incubated for 1-2 minutes until dissociation was observed. The cell suspension was then transferred to a 15 mL tube and centrifuged at 1400 rpm for 5 minutes. The cell pellet was then re-suspended in 1 mL of media and either pipetted into a larger flask or split at a ratio of 1:2 into same-sized flasks, along with the appropriate volume of media. A 1:2 split ratio has been documented in other studies to allow for optimal CSC growth (Monsanto *et al*., 2017).

3.2.4 Freezing CSCs

The isolation and expansion of CSCs *in vitro* consumes a substantial amount of time and resources. Therefore, in order to save time for future experiments and avoid the isolation process, it is imperative to have a stock of extra CSCs at each passage number. The CSCs corresponding to each sample can be frozen at -80 °C and be thawed and re-initiated when needed. The CSCs were frozen by suspending them in a MSC freezing medium (Millipore, Darmstadt, Germany). After the samples were pelleted, 1 mL of freezing medium was used to freeze one T25 confluent flask. The freezing medium was mixed gently within a cryogenic tube, and incubated at -20 °C for 1 hour. It was then transferred to a -80 °C storage container to ensure viability for up to 2 years.

When required for further experiments, the cells were thawed by placing the cryogenic tubes directly into a 37 °C water bath for 2-3 minutes or until the ice melted. The cells were then slowly pipetted into individual 15 mL tubes containing 9 mL of pre-warmed DMEM/F12 and centrifuging at 1400 rpm for 5 minutes. The pellet was then re-suspended in 1 mL of pre-warmed DMEM/F12 and incubated at 37 °C for 24 hours. The DMEM/F12 media was then replaced and the sample observed carefully under the microscope to ensure the cells are attached and start to proliferate.

3.3 Results

3.3.1 Morphology of cells after initial isolation

Immediately following isolation, these cells were observed as a dense monolayer of suspended cells and debris (Fig. 3.2A). After 24 hours of incubation at 37°C, the majority of the debris was washed away with DMEM/F12 media, leaving a small proportion of spherical cardiac cells which attached to the bottom of the flask (Fig. 3.2B).

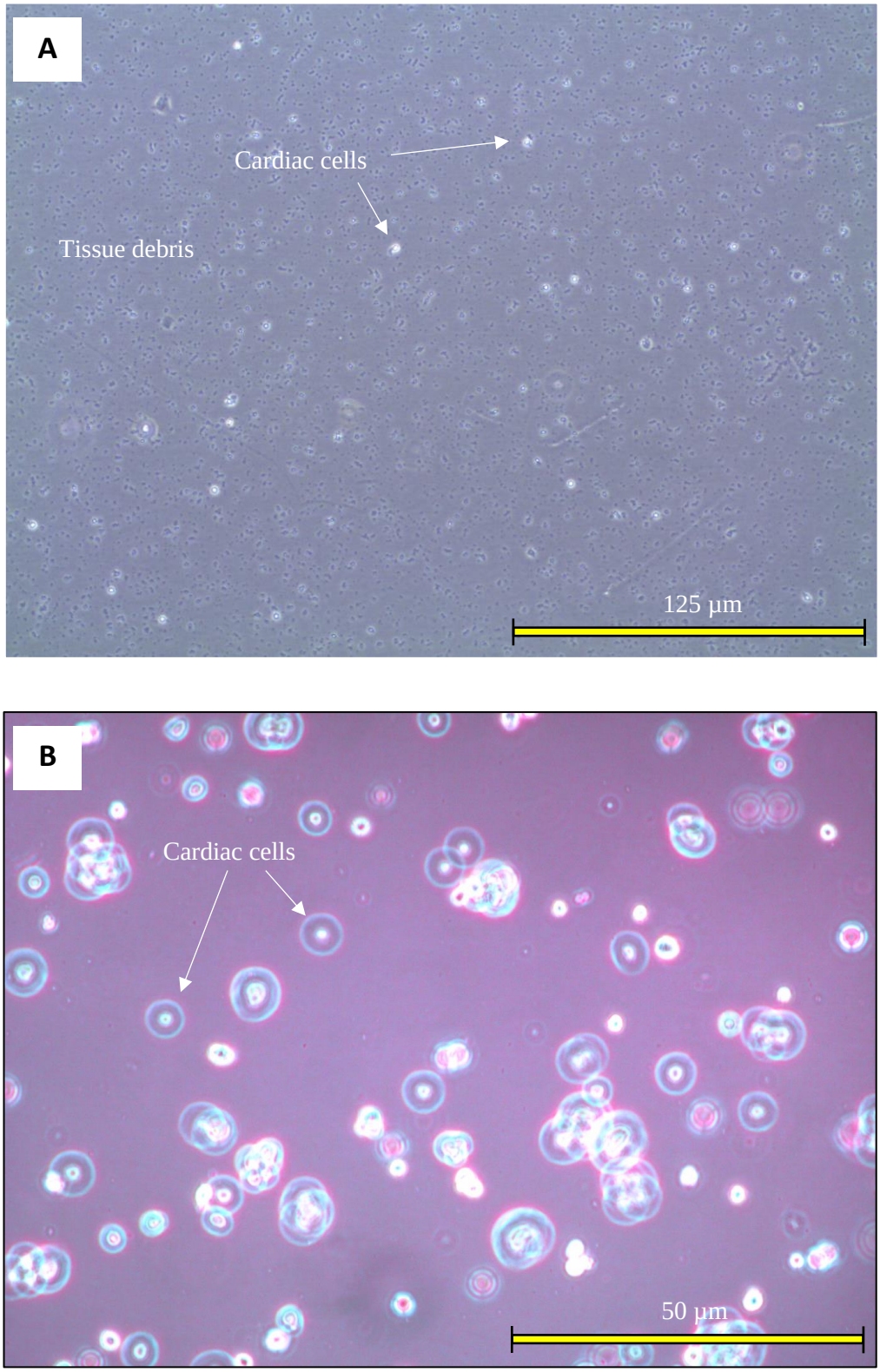

Figure 3.2. Phase contrast images taken from observing early cardiac cells under a light microscope. The cells are shown immediately after isolation from diabetic mouse heart tissue and subsequent plating into a T25 flask. They are initially observed as a dense monolayer of cardiac cells and tissue debris (A, Scale bar = 125 µm, 4x magnification), but soon form a spherical shape after incubation (B, Scale bar = 50 µm, 10x magnification), before attaching to the flask and branching out into their normal morphology.

Further replenishment of the cells with fresh growth media following another 24 hour incubation washed away any dead, floating cells while simultaneously providing fresh nutrients for those that survived. Within the next 48 hours, the cells appeared to stretch out into an elongated, spindle shape with multiple branches extending across the surface of the flask. Similar to MSCs, the CSCs contained large nuclei that were bright and reflective under a light microscope (Fig. 3.3) (Potdar and Sutar, 2010).

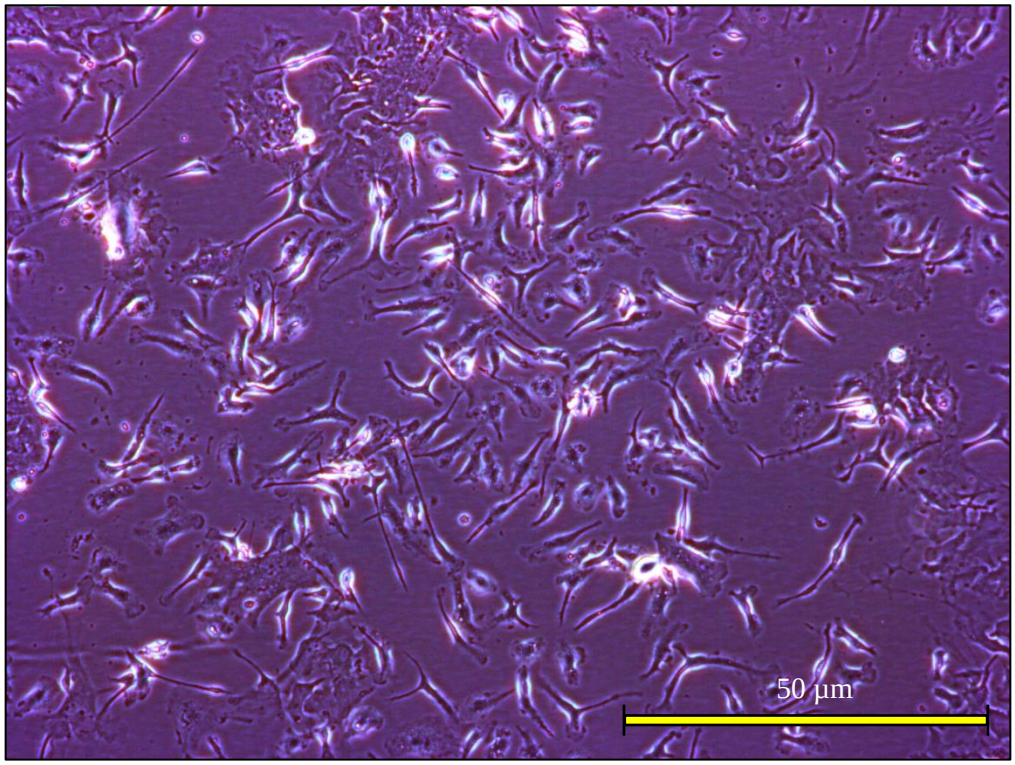

Figure 3.3. Phase contrast image taken from observing cardiac cells under a light microscope. The cells are shown at six days after their initial isolation from diabetic mouse heart tissue. Cell morphology shifts from a spherical shape to an elongated, spindle shape as cells branch out and proliferate across the surface of the flask (Scale bar = 50 µm, 10x magnification).

The morphology of the cells resembled a mesenchymal phenotype and there were no apparent morphological differences between cells derived from non-diabetic and diabetic origins. As the cells branched out and grew larger, they simultaneously proliferated through cell division, thus gradually becoming confluent. They also started to interconnect with branches of neighbouring cells, which seemingly acted to accelerate their proliferation (Fig. 3.3). Approximately one week after their initial isolation, cells became 80-90% confluent, during which they were trypsinized and plated into two further T25 flasks to accommodate their rapidly increasing cell number.

3.3.2 Morphology of Sca-1$^+$ CSCs after MACS purification

Following the purification of the CSCs by MACS, the number of CSCs were quantified for each sample. The total number of cells was markedly reduced by 4-5 fold following purification by magnetic sorting. The Sca-1$^+$ CSCs that were plated into new flasks were similar in morphology to the previously observed cardiac cells after 24 hours of incubation (Fig. 3.4A). Morphologically, the Sca-1$^+$ CSCs had a greater cross-sectional area (Fig. 3.4B) after one week of culture when compared to the cell population before purification (Fig. 3.3).

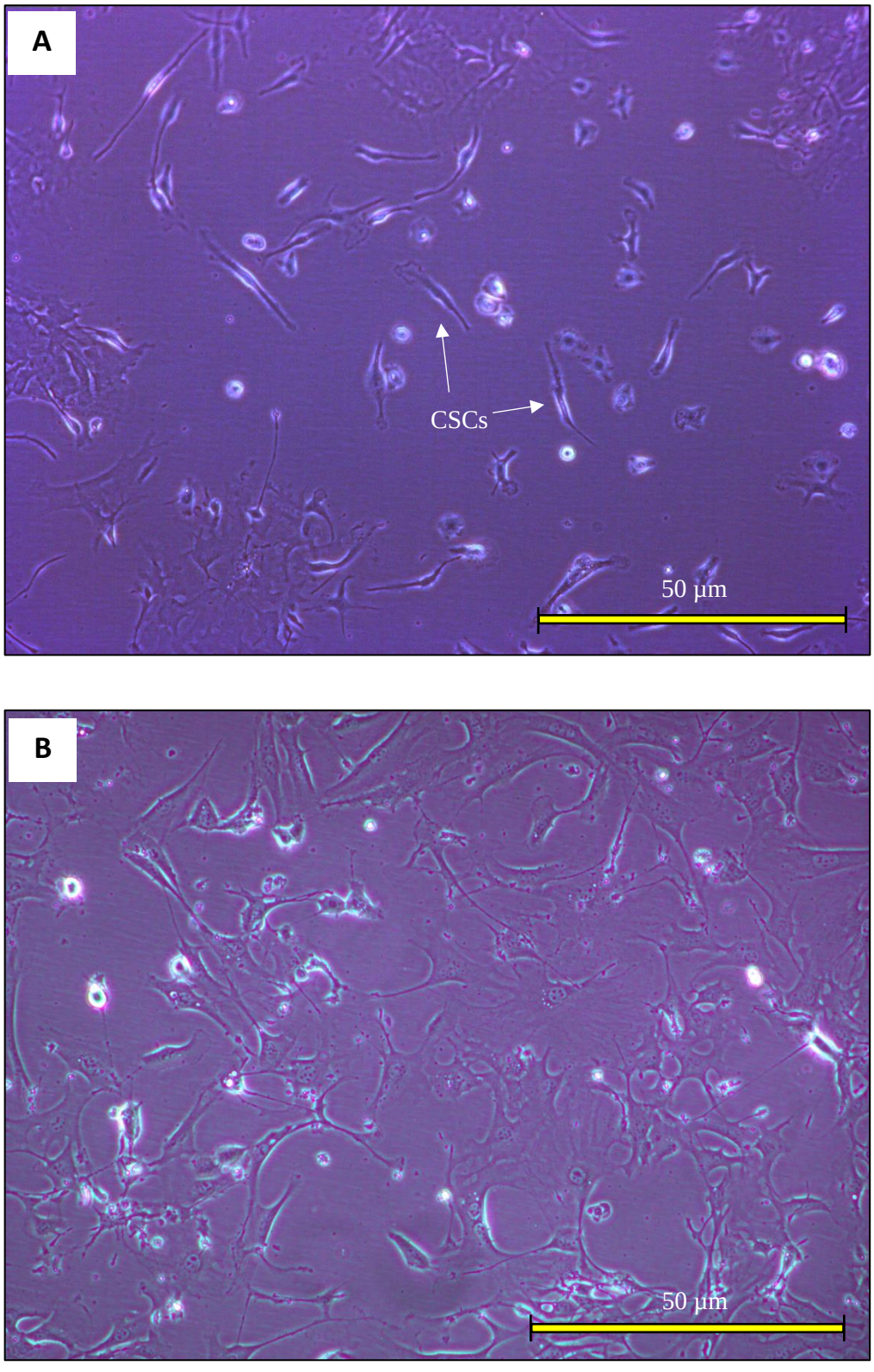

Figure 3.4. Phase contrast images taken from observing purified CSCs under a light microscope. The cells were isolated from diabetic heart tissue and are shown at 24 hours (A) and one week after MACS purification (B) (Scale bar = 50 µm, 10x magnification).

The CSCs were grown in DMEM/F12 culture media and incubated at 37 °C for approximately 10 days following purification until the cells became 80-90% confluent (Fig. 3.5). At this stage the CSCs could be further processed for functional studies by extracting the RNA or protein, or alternatively cryopreserved and stored at -80 °C.

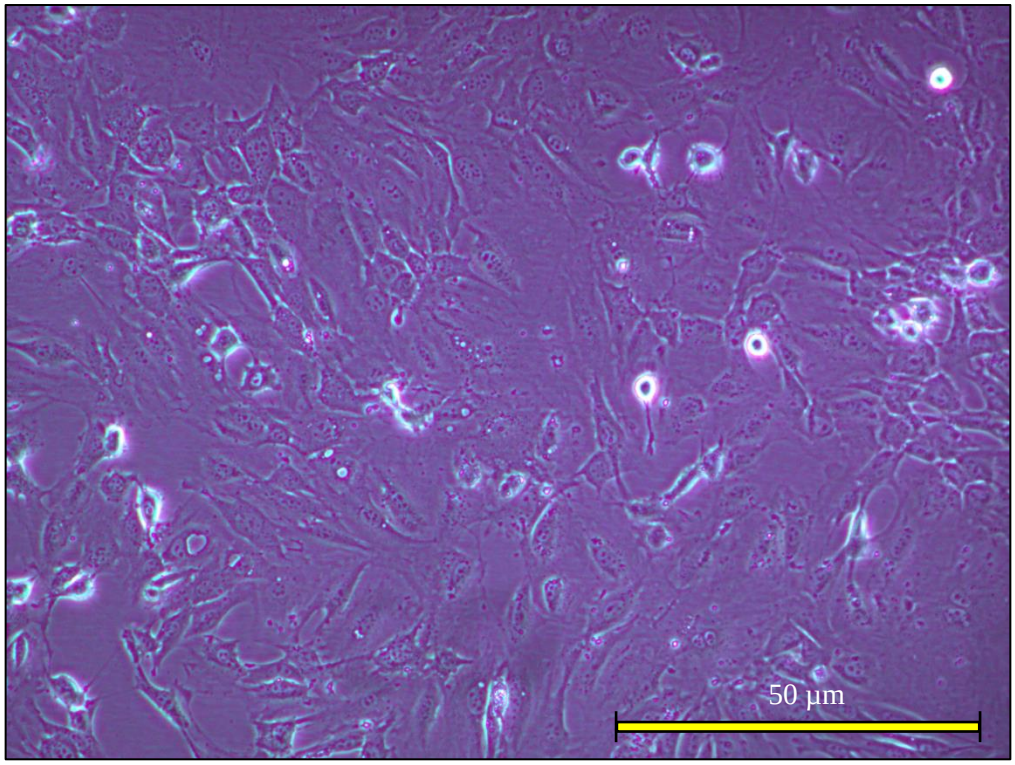

Figure 3.5. Phase contrast image taken from observing purified CSCs under a light microscope. The cells were isolated from diabetic heart tissue and are shown at 10 days after MACS purification. The cells are shown at 80% confluence which is an appropriate level for processing/freezing (Scale bar = 50 µm, 10x magnification).

3.3.3 Flow cytometry of Sca-1$^+$ CSC samples

The Katare laboratory has consistently measured the purity of Sca-1$^+$ CSCs purified using the MACS technique (Katare *et al*., 2013). However, to confirm this myself I performed FACS on one diabetic and one non-diabetic CSC sample. Around 20,000 cells were measured in each sample. The percentages of live cells were consistent among both non-diabetic (98%, Fig. 3.6A) and diabetic (97%, Fig. 3.6A). More than 80% of the cells expressed Sca-1 in both CSC samples. A representative FACS quantification histogram depicting the proportion of live Sca-1$^+$ cells within the non-diabetic CSC sample is shown below (Fig. 3.6B).

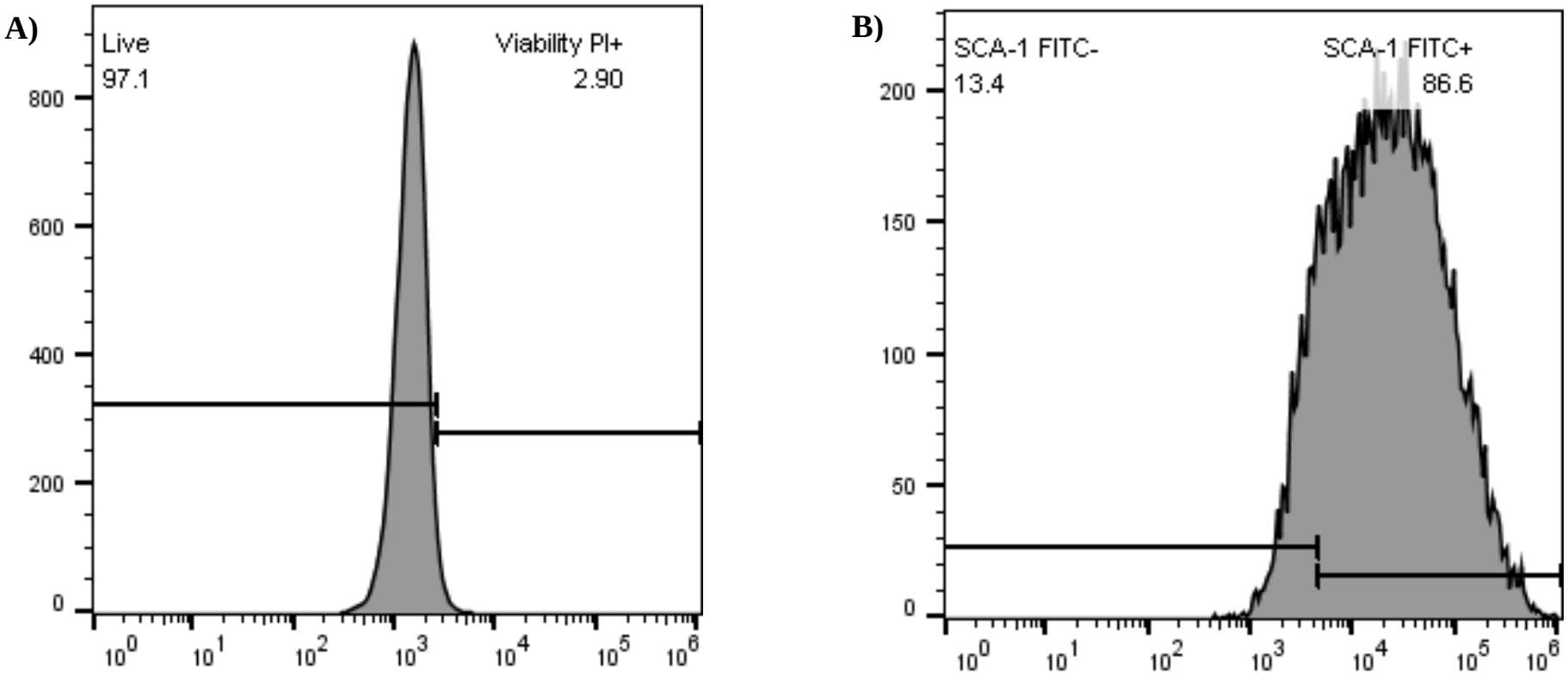

Figure 3.6. Data taken from the FACS analysis of a non-diabetic CSC sample after MACS purification. The proportion of live and dead cells in the sample is shown on the left (A). Dead cells are positive for PI and are thus shown on the graph as PI^+ cells. The proportion of $Sca\text{-}1^+$ (SCA-1 FITC+) and $Sca\text{-}1^-$ cells (SCA-1 FITC-) within the cell population is also shown on the right (B).

3.4 Discussion

Establishing a culture of viable CSCs was vital as it provided a framework for downstream experiments in order to investigate their expression and functional characteristics in the diabetic condition. After isolating the CSCs from both diabetic and non-diabetic db/db mice, the morphology, purity and growth conditions of the CSCs were confirmed by comparing the results to other studies as described below.

3.4.1 Qualitative results of the CSCs

All diabetic and non-diabetic CSCs exhibited a morphology that was similar to the MSC profile. This was supported by studies reporting the resemblance of heart-derived Sca-1^+ progenitor cells to a mesenchymal phenotype (Oh *et al*., 2004; Valente *et al*., 2014). These cells are also notably distinct from the HSC or endothelial progenitor cell profile commonly found in Sca-1^- cells derived from the heart (Oh *et al*., 2004; Valente *et al*., 2014). Furthermore, MSCs derived from bone marrow and adipose tissue are known to form a homogenous population of elongated spindle-shaped cells with an abundant cytoplasm and large nuclei after passage 3 (Li *et al*., 2015). This characterisation was also consistent with the CSCs observed in this study after passage 1, suggesting the isolated cells possess stem cell-like features. There were no observable morphological differences between diabetic and non-diabetic CSCs, however a detailed ultrastructural analysis was not performed. Thus far, there is no known evidence for diabetes affecting the morphology of CSCs.

3.4.2 Growth rate of the CSCs

There was no change in the growth of the CSCs for the first 9-10 passages. However, in subsequent passages there was a noticeable decline in growth rate which was assumed to be attributed to cell senescence. This may be due to dysfunctional telomeres or genotoxic stresses that promote DNA damage, thus causing irreversible arrest of the cell cycle (Takai *et al*., 2003; Rodier *et al*., 2009). Senescent cells are also known to have a large, flat morphology which resembled the CSCs in my study above passage 10 (Fig. A6 in Appendix 6) (Rodier *et al*., 2011). As the CSCs have a similar phenotypic profile to MSCs, it is plausible that they undergo the same loss of cell division that is associated with senescence after long periods of cell culture (Turinetto *et al*., 2016). Interestingly, the diabetic CSCs did not exhibit any difference in growth rate or growth pattern and were comparable to the non-diabetic CSCs. This finding contrasts with another study reporting the production of ROS in diabetic CPCs, leading to telomeric shortening and irreversible growth arrest (senescence) (Rota *et al*., 2006). However, there were disparities in the type of diabetes as Rota *et al*. used type-1 diabetic mice, whereas I used T2DM mice in my study. This is supported by the fact that the apoptotic effect of ROS can vary depending on the age of the animal (Tasat *et al*., 2003). Nevertheless, there is very limited evidence for the effect of ROS on CPCs and CSCs *in vitro*.

3.4.3 Purity of the CSCs

Within the context of this project, stem cell purity can be defined as a measure of the total proportion of stem cells within a population that contain a high expression of specific and well-recognized antigenic markers (Yuan *et al*., 2011). As previously mentioned, Sca-1 is known as a marker for the identification CSCs and was thus used to measure the purity of

these cells. The proportion of Sca-1$^+$ cells were considerably high in both the diabetic and non-diabetic sample.

Despite there being no quantifiable threshold for Sca-1 as a measure of CSC purity, studies have indicated that there is a correlation between Sca-1 expression and the CSC phenotype. CSC colonies that are isolated from mouse heart tissue containing a high proportion of Sca-1 (91%) exhibit functional properties that are consistent with the heart-derived stem cells originally identified by Takamiya and coauthors (Takamiya *et al*., 2011). Pure Sca-1$^+$ CSCs were able to attenuate the size of infarcted heart tissue, while preserving ventricular function and capillary density after transplantation in a mouse model of MI (Takamiya *et al*., 2011). These CSCs were also found to directly differentiate into cardiomyocytes, as well as expressing other pluripotent stem cell markers such as Nanog and telomerase reverse transcriptase (Takamiya *et al*., 2011). To further support this correlation, CSC colonies with significantly lower levels of Sca-1 (17%) isolated from the same hearts exhibit a substantially reduced differentiation potential compared to those with greater Sca-1 expression (Takamiya *et al*., 2011). These evidences, along with the increased expression of Sca-1$^+$ cells in the FACS analysis suggests that the CSC population was pure.

In this chapter I have shown how the Sca-1$^+$ mouse CSCs were isolated from diabetic and non-diabetic mice, and purified. I have also outlined the culturing methods used to generate sufficient numbers of CSCs for downstream experiments. In the following chapter, I will address the first objective of my project by demonstrating how diabetes may alter miRNA expression in mouse CSCs.

CHAPTER 4: DIFFERENTIAL REGULATION OF MIRNAS IN DIABETIC MOUSE CSCs

4.1 Introduction

This chapter will focus on demonstrating the differential effects of diabetes on miRNA expression in the CSCs isolated from diabetic mice. I will first describe the objective, followed by a brief background outlining the theory and rationale of the techniques that were used. I will then outline the methodology and results of these experiments, followed by a brief discussion of the observed data and its relevance with literature in the field.

4.1.1 Aims and Objectives

The primary aim for this chapter is to identify whether diabetes causes dysregulation of miRNAs derived from mouse CSCs. The second aim is to validate this altered miRNA expression through q-PCR and western blot analysis.

4.1.2 Diabetes causes dysregulation of miRNAs

Diabetes has been demonstrated to cause altered miRNA expression throughout the body in both mice and humans (Assmann *et al*., 2017; Shantikumar *et al*., 2012). This differential expression has been reported in various tissues including skeletal muscle, liver, adipose tissue and cardiomyocytes (Fomison-Nurse *et al*., 2018; Rawal *et al*., 2017; Shantikumar *et al*., 2012). Zampetaki and coauthors identified the abnormal expression of thirteen miRNA subtypes in the plasma collected from 80 diabetic individuals compared to healthy volunteers over a 10 year observation period (Zampetaki *et al*., 2010). While the mechanism behind this

effect is poorly understood, certain studies have shown that the elevated glucose and hypoxia associated with diabetes may alter important proteins that are involved in miRNA synthesis (Rahimi *et al*., 2014).

To my knowledge, it is not known whether diabetes also affects miRNA expression within the CSCs. Therefore, in this section of the project, I aim to determine the differential expression pattern of miRNAs in the diabetic CSCs. The outcome of this objective is important as it provides implications towards the pathophysiological roles of miRNAs in regulating CSC function.

4.1.3 Nanostring microarray can measure differential miRNA expression in diabetic CSCs

Expression profiling has been suggested to determine the level at which the miRNAs are expressed, indicating whether a patient is likely to have a disease (Liu *et al*., 2008). This technique has also been extensively performed in stem cell research to determine the effect of miRNAs on their biological function. Microarrays are a common method for expression profiling that can be used to determine changes in DNA and RNA expression (Govindarajan *et al*., 2012). A genetic microarray consists of a collection of microscopic spots that are attached to a glass slide or chip containing target DNA fragments. Fluorescent markers attached to specific DNA probes are hybridized to the target DNA fragments through complementary sequence binding. A computer can then record the fluorescence emitted from the DNA fragments after passing the slide through a laser beam which can be used to determine gene expression. This process is sensitive and specific for the simultaneous identification of multiple DNA fragments, and can be used to determine differences in the expression levels of mRNA/miRNA and protein between healthy and disease states (Govindarajan *et al*., 2012).

In this project, a Nanostring microarray was used to determine whether there is a difference in the expression profile of miRNAs in diabetic CSCs. The primary advantage of the Nanostring microarray is that while most conventional microarrays have a relative measurement of DNA that represents mRNA or miRNA expression, the Nanostring microarray measures the absolute quantity of the DNA in the cell or tissue extract. This allows for more reliable and accurate data, which is crucial as the Nanostring microarray forms the backbone of this project and therefore influences important downstream results.

4.2 Methods

4.2.1 Nanostring microarray

Six diabetic and six non-diabetic CSC samples (isolated from 24 diabetic and 24 non-diabetic db/db mice, respectively) were used for the Nanostring microarray. For each sample, four mouse hearts were pooled together (n=6 samples in both diabetic and non-diabetic) to generate a sufficient number of CSCs that could be grown and passaged *in vitro*. After purifying the Sca-1 positive CSCs using the MACS protocol (Chapter 3, section 3.2.1), total RNA was extracted (detail protocol in Chapter 2, section 2.5) and sent to Nanostring Technologies (Life Sciences, Seattle, U.S.A.). An ncounter mouse miRNA expression assay kit was used to isolate the miRNAs from the total RNA in each sample through ligation with specific, corresponding oligonucleotide tags. For each sample, 100ng of total RNA was added to the miRNA-tag ligation reaction and then diluted to a 1:10 concentration to produce 10ng of RNA for the miRNA-tag sample.

These miR-tag samples were then hybridized with 598 random miRNA-specific DNA probes. Each probe was arranged in pairs, consisting of a reporter probe, which emits fluorescence; and a capture probe, which immobilizes the miRNAs for data collection (Fig. 4.1A). Specific miRNA-probe complexes were formed as a result of the hybridization and immobilized on a 12 sample nCounter cartridge. Excess probes were removed from the complexes and a GEN2

digital analyzer (Fig. 4.1B) was then used to image the fluorescent miRNA-probes, quantify the number of miRNAs in each sample and group them according to their relative expression pattern (Fig. 4.1C). A set of six positive control probes were also included in the reaction which had consistent expression across all RNA samples, except one diabetic sample (Fig. 4.2). This was determined from a Pearson correlation coefficient (R^2) of above 0.95. The one diabetic sample with a low R^2 value indicated an inhibition of miRNA-tag ligation and was therefore excluded from the data analysis.

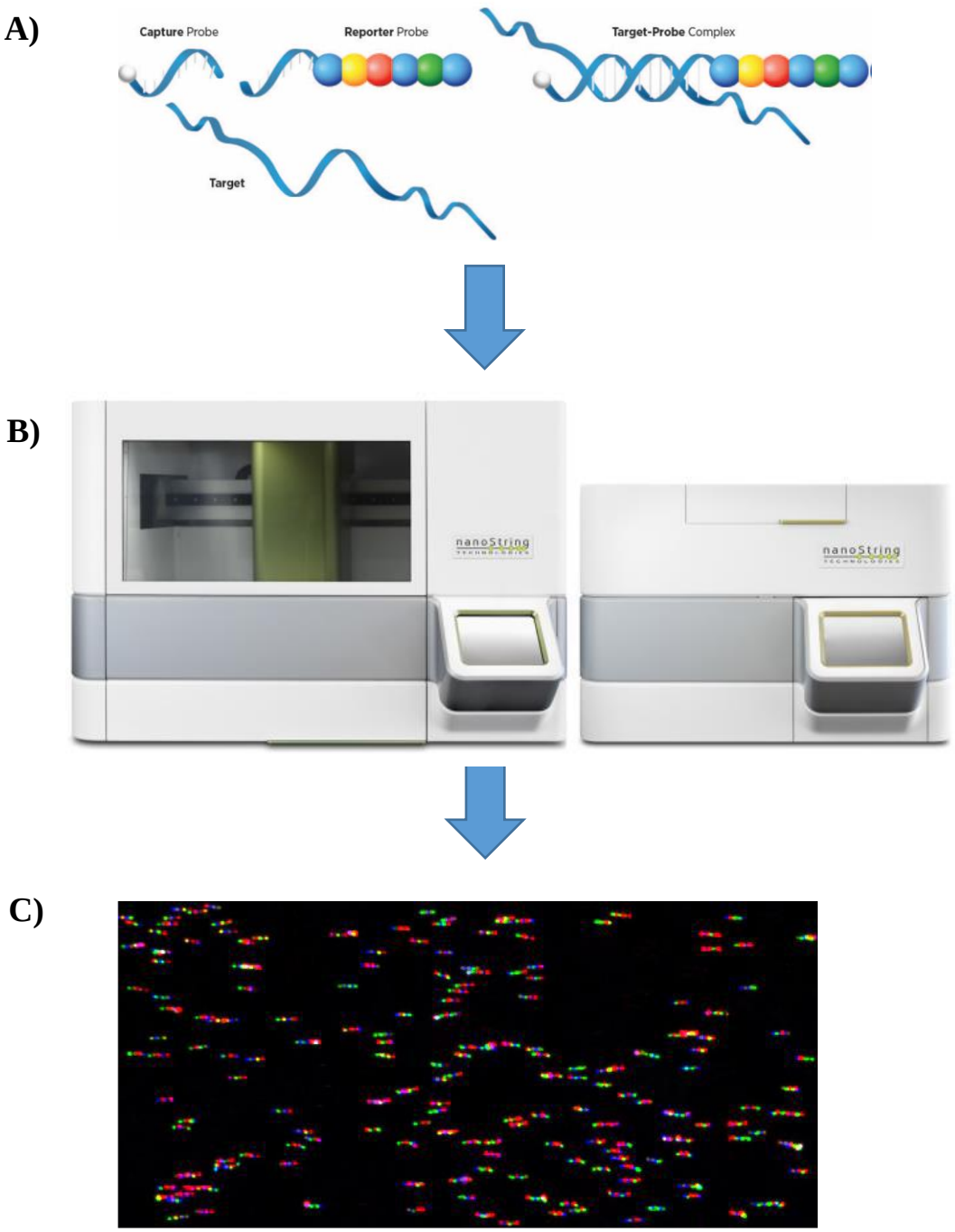

Figure 4.1. The primary steps involved in the Nanostring microarray reaction starting with hybridization of the miRNAs to reporter and capture DNA probes (A). The colour-coded fluorescent reporter probe is used to identify complementary miRNAs upon binding to the capture probe. The capture probe binds to and immobilizes the miRNAs before imaging. The samples are then imaged and quantified using the GEN2 digital analyzer (B), and the fluorescent bands corresponding to different miRNAs are grouped according to their expression pattern (C).

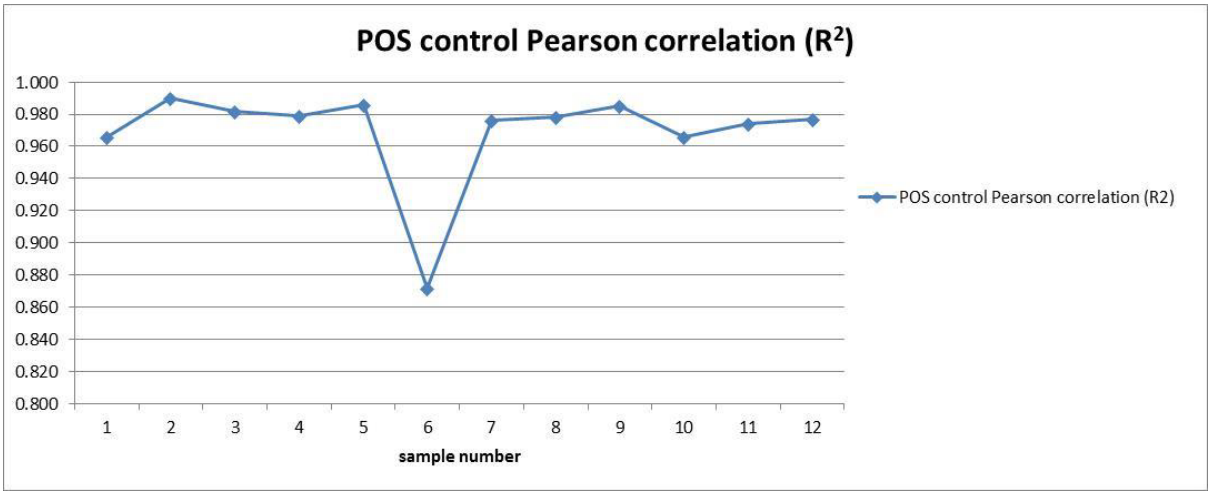

Figure 4.2. Graph indicating the Pearson Correlation Coefficients (R^2) that were calculated for positive control samples in the normalization phase of data collection across all RNA samples in the Nanostring microarray. Samples 1-6 are total RNA extracted from diabetic CSCs, while Samples 7-12 are total RNA extracted from non-diabetic CSCs. One diabetic RNA sample was excluded from data analysis due to a low R^2 value.

4.2.2 Bioinformatic analysis

4.2.2.1 Predicted effect of differentially regulated miRNAs on CSC function

To confirm the reliability of the differentially regulated miRNAs within the CSCs, the function of the miRNAs must also be considered. As such, the alterations in miRNA expression that were demonstrated by the Nanostring analysis must also be validated by measuring the expression of corresponding 'target' genes. To do this, the miRPath bioinformatic tool (DIANA TOOLS (Vlachos *et al*., 2012)) was initially used to identify which of the differentially regulated miRNAs are associated with self-renewal/proliferation, the main function of CSCs. Seven miRNAs that were shown to either promote or inhibit cell proliferation by targeting genes within these signaling pathways were therefore selected for molecular validation by q-PCR (Chapter 4, section 4.2.3).

4.2.2.2 Identification of target genes

MiRNA-target prediction databases are presently the most common method for the identification of miRNA target genes. These databases were therefore used to identify targets for the most substantially and significantly altered miRNAs among those validated by q-PCR. Four separate prediction databases (microT-CDS (Paraskevopoulou *et al*., 2013), miRDB (Wong and Wang, 2015), microRNA.org (Betel *et al*., 2008) and TargetScan (Agarwal *et al*., 2015)) were used to identify common target genes for the candidate miRNAs. The selected targets were validated by performing western blot analyses (Chapter 4. section 4.2.4) to determine the total protein expression of these genes within the diabetic and non-diabetic CSCs.

4.2.3 q-PCR of candidate miRNAs

A quantitative real-time PCR (q-PCR) was used to demonstrate the reliability of the dysregulated miRNAs from the Nanostring microarray. q-PCRs can measure the relative differences in DNA and RNA expression at the molecular level (Morey *et al*., 2006). The changes in miRNA expression that were observed in the Nanostring analysis were validated by real-time PCR analysis for the top seven miRNAs (six upregulated, one downregulated). Following the protocol in Chapter 2 (section 2.2.6), total RNA from 10 CSC samples (five diabetic, five non-diabetic) that were previously sent to Nanostring Technologies were reverse transcribed to cDNA using stem loop primers specific to the candidate miRNAs. I previously demonstrated that 20 ng of miRNA was sufficient for the reverse transcription of RNA into cDNA, and thus this amount was used to calculate the appropriate volume of RNA sample for each reverse transcription reaction (Rawal *et al*., 2017). The PCR reaction was performed in triplicate and repeated twice to obtain a more reliable outcome for the expression of miRNAs within the CSCs, as well as to identify any technical errors in the procedure. The q-PCR data

was analysed by using the cycle at threshold (Ct) quantification method as described in Chapter 2, section 2.6.3. This analysis was used to determine molecular fold changes for each miRNA subtype within the diabetic and non-diabetic CSCs.

4.2.4 Western blot analysis

Bioinformatic analysis predicted two common target genes (GSK3-β and MEF2C) for the four most significantly altered miRNAs (*detailed in the results below*). Western blot analysis was performed to determine whether the expression of these genes in the diabetic CSCs correlated with the altered expression profiles of the corresponding miRNAs. Total protein was extracted from four diabetic and four non-diabetic CSCs and probed for Mouse monoclonal anti-GSK3-β (NovusBio, 1:1000) and Mouse monoclonal anti-MEF2C (NovusBio, 1:1000) against the GSK3-β and MEF2C genes, respectively using the western blot protocol detailed in Chapter 2, section 2.7.

4.3 Results

4.3.1 Diabetes induces dysregulation of miRNAs in CSCs

Raw data was obtained from the Nanostring microarray for 598 miRNA subtypes in the diabetic and non-diabetic CSCs. To provide a reference for comparative analysis, the raw expression values of the miRNAs in the diabetic CSCs were further normalized to those in non-diabetic CSCs. For this, the mean of the non-diabetic expression values of each sample was first calculated. Fold changes for each miRNA subtype were then calculated by dividing the miRNA expression value in each diabetic sample by the mean miRNA expression value in the non-diabetic samples. The mean fold change for each miRNA subtype was calculated and a two-tailed t-test was performed to determine the statistical significance of these fold changes (Table

4.1). MiRNAs were selected on the basis of significant fold change ($P<0.05$) in the diabetic CSCs compared to non-diabetic CSCs. Among the 598 miRNAs tested, 16 miRNAs (as listed in Table 4.1), showed significant dysregulation in the diabetic CSCs. Among the 16 miRNAs, 14 were significantly upregulated, while 2 were significantly downregulated in the diabetic CSCs.

Table 4.1. MiRNAs with significant fold changes in diabetic and non-diabetic CSCs				
miRNA subtype	**Expression in non-diabetic CSCs**	**Expression in diabetic CSCs**	**Fold change in diabetic CSCs**	**P value**
miR-382	1.46 ± 0.57	2.40 ± 0.17	1.64 ± 0.59	0.001
miR-376c	1.40 ± 0.39	3.90 ± 0.68	2.79 ± 0.78	0.005
miR-329	1.97 ± 0.81	3.39 ± 0.61	1.72 ± 0.87	0.010
miR-1983	1.20 ± 0.26	2.29 ± 0.35	1.91 ± 0.44	0.012
miR-495	1.26 ± 0.27	2.32 ± 0.35	1.84 ± 0.60	0.016
miR-28	1.09 ± 0.16	1.74 ± 0.21	1.60 ± 0.44	0.022
miR-30c	1.16 ± 0.25	0.46 ± 0.08	0.40 ± 0.26	0.025
miR-99b	1.03 ± 0.09	1.33 ± 0.10	1.29 ± 0.14	0.026
miR-125b	1.13 ± 0.19	1.56 ± 0.11	1.38 ± 0.22	0.029
miR-19a	1.31 ± 0.29	2.02 ± 0.30	1.54 ± 0.42	0.036
miR-106b	1.10 ± 0.17	0.60 ± 0.07	0.55 ± 0.18	0.037
miR-125a	1.31 ± 0.35	1.63 ± 0.12	1.24 ± 0.37	0.037
miR-126	2.17 ± 0.86	4.83 ± 1.49	2.23 ± 1.72	0.041
miR-804	1.03 ± 0.09	1.32 ± 0.11	1.28 ± 0.14	0.043
miR-365	1.05 ± 0.10	1.39 ± 0.11	1.32 ± 0.15	0.045
miR-132	1.07 ± 0.14	1.88 ± 0.35	1.76 ± 0.38	0.045

4.3.2 Dysregulated miRNAs were predicted to regulate CSC function

Analysis using the miRPath bioinformatic tool showed that 7 out of the 16 significantly altered miRNAs were predicted to regulate signaling pathways associated with proliferation and self-renewal, including the wingless-type (WNT), vascular endothelial growth factor (VEGF), hedgehog, janus kinase-signal transducer and activator of transcription (JAK-STAT), focal adhesion and phosphoinositide 3-kinase-protein kinase B (PI3K-AKT) pathways. Within these pathways miR-329, -495, -376c, -19a, -365 and -804 were predicted to inhibit cell proliferation, while miR-30c was the only miRNA that was predicted to promote cell proliferation (Table 4.2). Interestingly, the effect of these miRNAs on proliferation correlated with their altered expression profiles in the diabetic CSCs. Among the seven miRNAs analysed, those that were predicted to inhibit proliferation (miR-376, -329, -495, -19a, -804 and -365) were upregulated (Tables 4.1 and 4.2), while the only miRNA that was predicted to promote proliferation (miR-30c) was downregulated in the diabetic CSCs (Tables 4.1 and 4.2). Since proliferation and self-renewal are the major functions of all stem cells (including CSCs), this data suggested that seven miRNAs could regulate CSC function. These seven miRNAs were therefore chosen for further validation by performing q-PCR analysis.

Table 4.2. Predicted effect of miRNAs on cell proliferation		
Signaling pathway	**miRNAs promoting cell proliferation**	**miRNAs inhibiting cell proliferation**
WNT		miR-376c
VEGF		miR-329, -495, -19a
Hedgehog	miR-30c	miR-376c, -19a, -365
JAK-STAT		miR-329, -495, -19a, -365
Focal adhesion	miR-30c	miR-365, miR-804
PI3K-AKT	miR-30c	miR-376c, miR-365
T2DM		miR-329, -495, -19a

4.3.3 q-PCR analysis partially validated the Nanostring data

Out of the seven miRNAs analysed, only four (miR-495 (16.39 ± 1.81 vs 1.14 ± 0.17, $P<0.001$), -329 (12.85 ± 2.28 vs 1.52 ± 0.49, $P<0.001$), -376c (13.01 ± 2.61 vs 2.30 ± 1.01, $P=0.002$) and -30c (0.29 ± 0.05 vs 1.07 ± 0.12, $P=0.006$)) replicated the changes observed in the Nanostring analysis (Fig. 4.3).

In contrast, miR-365 (1.41 ± 0.11 vs 1.42 ± 0.49, diabetic vs non-diabetic, $P=0.99$), miR-19a (1.67 ± 0.51 vs 1.25 ± 0.26, diabetic vs non-diabetic, $P=0.47$) and miR-804 (1.24 ± 0.24 vs 1.24 ± 0.28, diabetic vs non-diabetic, $P=0.99$) showed no statistical difference in expression pattern in the diabetic CSCs compared to the non-diabetic CSCs (Fig. 4.3).

Although it was originally considered to be more specific than other microarrays, the Nanostring microarray produced false-positive results. Furthermore, the miRNAs which were known regulators of CSC proliferation and differentiation (miR-1, -133, -378, -499, -204, and

-669) were not among the significantly changed miRNAs in the study. This indicates the necessity to validate this Nanostring data using q-PCR and western blot analysis. With their dysregulated expression partially validated by q-PCR, miR-329, -376c, -495 and -30c were thus chosen as candidate miRNAs for western blot analysis. However, specific gene targets first had to be identified by bioinformatic analysis.

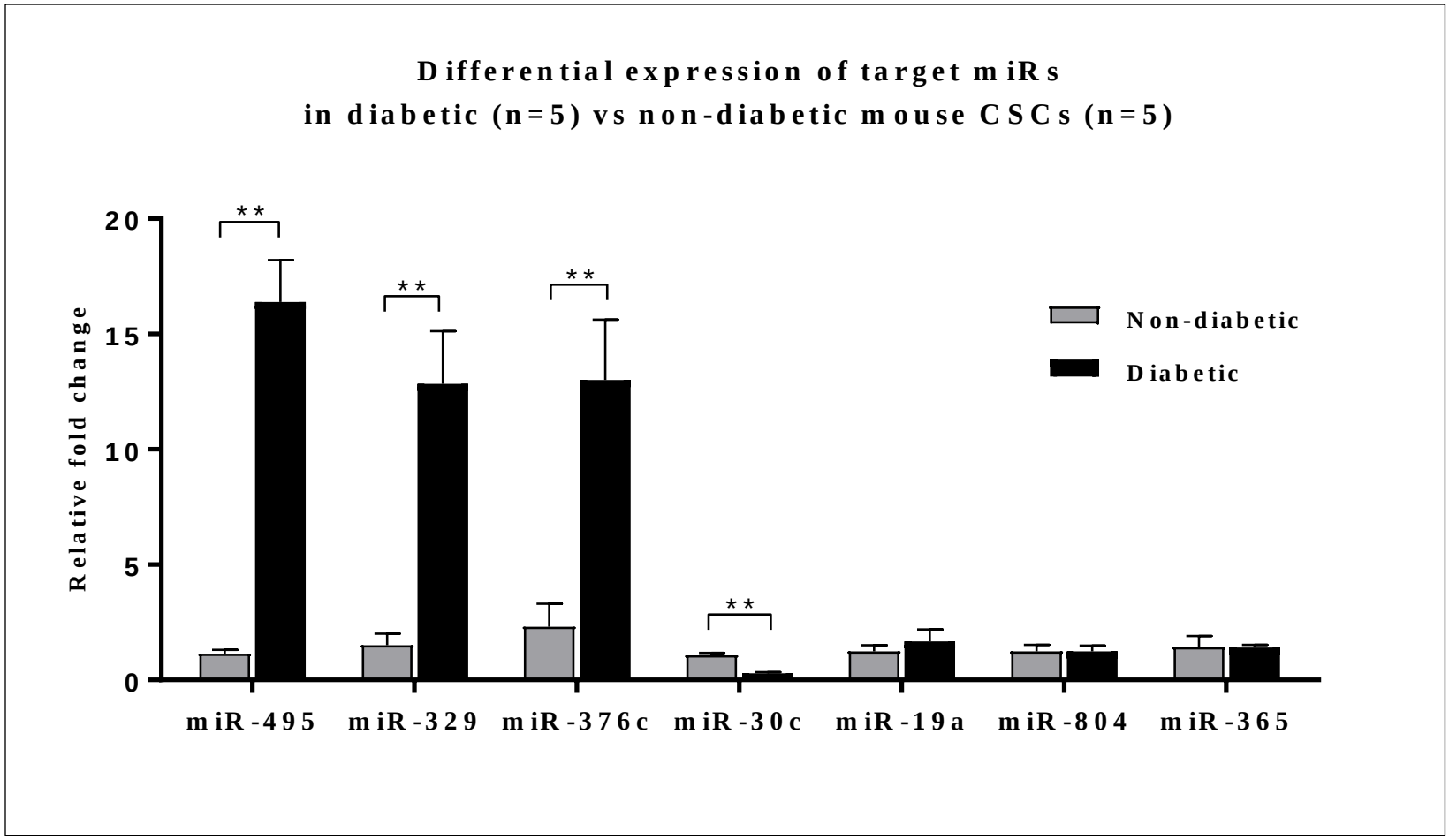

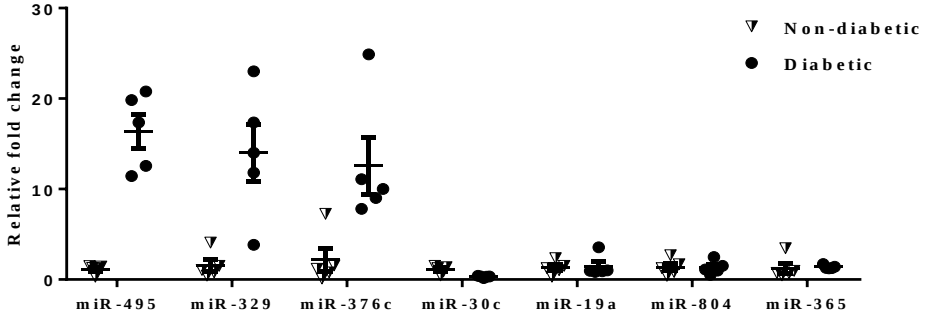

Figure 4.3. Quantitative q-PCR bar graph and scatter plot depicting significantly altered miRNAs from Nanostring microarray within non-diabetic (n=5) and diabetic CSCs (n=5). MiRNAs -495, -329, -376c and -30c were significantly regulated in the diabetic CSCs. Data are means ± SEM. A two-tailed t-test was performed to determine significant data (** = P<0.01).

4.3.4 GSK3-β and MEF2C predicted as common targets for four selected miRNAs

Four online bioinformatic prediction tools (microT-CDS, miRDB, microRNA.org, TargetScan) were used to predict gene targets for the four candidate miRNAs validated by q-PCR. These bioinformatic analyses provide an indication of genes that may potentially acts as targets for the miRNAs across all cell types, however experimental validation is required to confirm them as targets within the CSCs. Across all four miRNA-target prediction databases, the glycogen synthase kinase-3β (GSK3-β) and myocyte specific enhancer-2C (MEF2C) genes were identified as the most frequent targets of miR-329, -376c, -495 and -30c. GSK3-β was predicted as a target for all four miRNAs, while MEF2C was predicted as a target for miR-329, -376c and -495 (Table 4.3). They were therefore chosen as appropriate gene targets for a functional validation study using western blot analysis.

Table 4.3. Genes across four miRNA-target prediction databases

Target gene	microT-CDS	miRDB	microRNA.org	TargetScan
GSK3-β	miR-329, miR-495	miR-495, miR-30c	miR-376c, miR-495	miR-329, miR-376c, miR-495, miR-30c
MEF2C	miR-329, miR-376c, miR-495	miR-329, miR-376c, miR-495	miR-329, miR-495	miR-329, miR-376c, miR-495

Furthermore, using miRPath, GSK3-β and MEF2C were also predicted to regulate signaling pathways associated with cell proliferation. Two of the prominent signaling pathways that are involved with promoting cell proliferation are the PI3K-AKT and mitogen-activated protein kinase (MAPK) signaling pathways; both of which were found to contain GSK3-β and MEF2C. The MAPK pathway showed significant results (P=0.02) for the expression of the

four candidate miRNAs. The following diagrams depict the predicted interactions of the miRNAs on both the genes in regulating cell proliferation. GSK3-β acts as a target for miR-329, -376c, -495 and -30c within the PI3K-AKT signaling pathway (Fig. 4.4A), while MEF2C was found to act as a target for miR-329. -495 and -376c within the MAPK signaling pathway (Fig. 4.4B). Both signaling pathways also suggested that GSK3-β and MEF2C may increase proliferation by promoting the cell cycle.

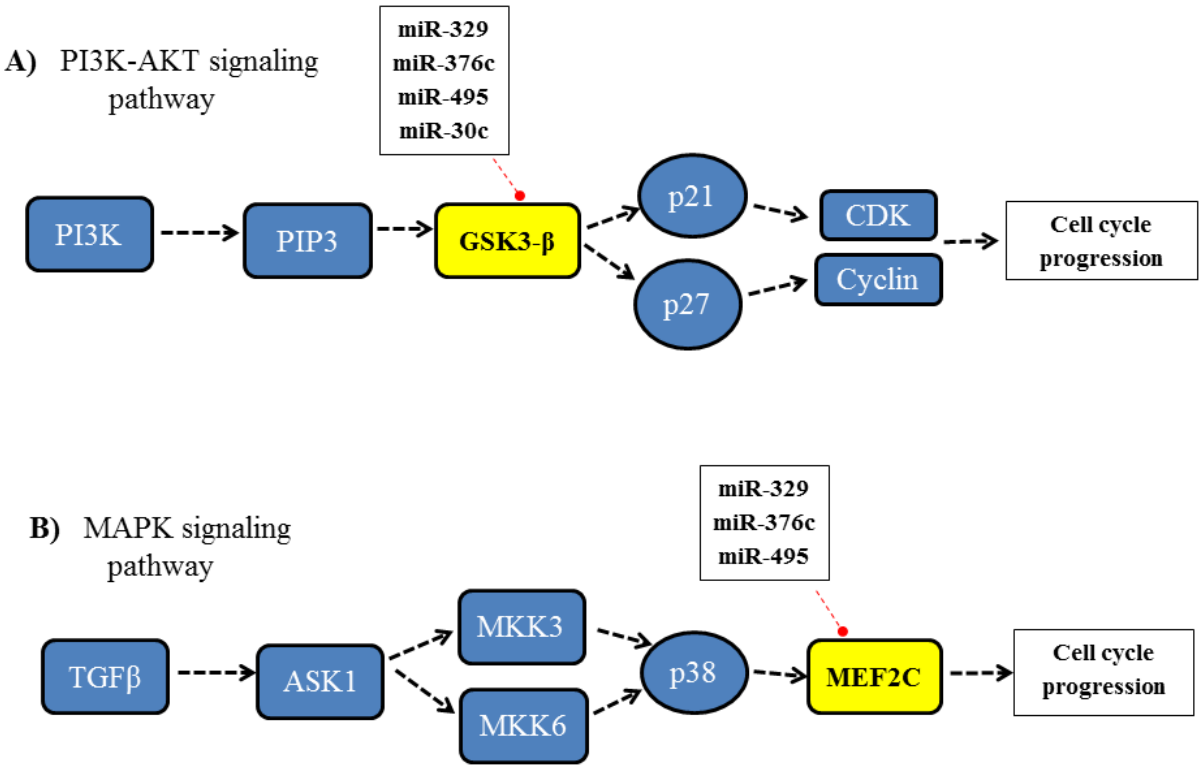

Figure 4.4. As depicted in the miRPath bioinformatic tool, the PI3K-AKT (A) and MAPK (B) signaling pathways lead to cell cycle progression (cell proliferation). In the PI3K-AKT signaling pathway, phosphoinositide 3-kinase (PI3K) activates phosphatidylinositol-3,4,5-bisphosphate (PIP3), which increases the expression of the tumor-suppressors, cyclin-dependent kinase inhibitor 1 (p21) and cyclin-dependent kinase inhibitor 1B (p27). This leads to the activation of cyclins and cyclin-dependent kinases, which promote the cell cycle. In MAPK signaling, transforming growth factor β (TGFβ) activates apoptosis signal-regulating kinase 1 (ASK1), which leads to the activation of the dual enzymes, mitogen-activated protein kinase kinase 3 (MKK3) and mitogen-activated protein kinase kinase 6 (MKK6). This increases the expression of the tumor suppressor, p38, which activates the cell cycle promoter, MEF2C. The four candidate miRNAs (miR-329, -376c, -495 and -30c) were found to target one or both of the two target genes (GSK3-β, MEF2C) within these pathways. The GSK3-β and MEF2C genes are highlighted in yellow within each pathway. The black, dashed arrow indicates stimulation, while the red dotted line indicates miRNA inhibition.

4.3.4 GSK3-β and MEF2C protein expression did not change in diabetic CSCs

An inversely proportionate difference in the protein expression of GSK3-β and MEF2C in the diabetic CSCs could functionally validate the change in expression of miRNAs -329, -376c, -495 and -30c that were observed in the Nanostring microarray and q-PCR data. However, despite being predicted as suitable targets by four miRNA-target prediction databases, western blot analyses showed no change in the expression pattern of both GSK3-β and MEF2C in the diabetic CSCs (Fig. 4.5). This outcome revealed that, at least for the purposes of this study, the method of predicting target genes for miRNAs by using miRNA-target prediction databases was not reliable.

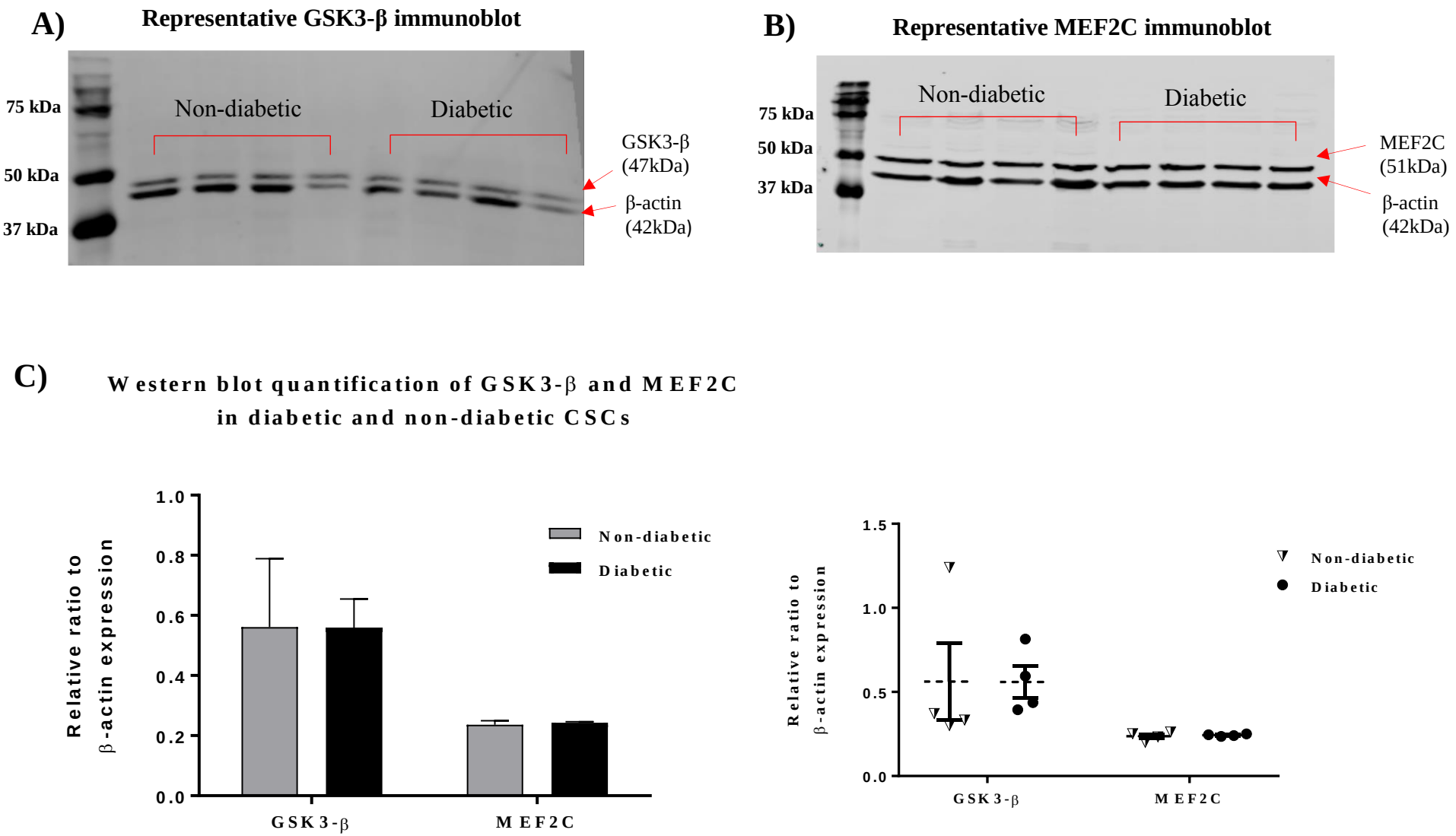

Figure 4.5. Representative immunoblots and western blot quantification data (bar graph and scatter plot) (C) of GSK3-β (47kDa) (A) and MEF2C (51kDa) (B) target gene expression in diabetic (n=4) and non-diabetic CSCs (n=4). β-actin (42kDa) was used as an endogenous control for each gene. Data are means ± SEM. A two-tailed t-test was performed to determine significant data ($P<0.05$).

4.4 Discussion

4.4.1 Summary of results

In this Chapter, I have shown for the first time that diabetes induces dysregulation of miRNA expression in CSCs. This was demonstrated using the Nanostring microarray which showed that 16 out of 598 miRNAs investigated exhibit significantly altered expression profiles in the diabetic CSCs. With the aid of bioinformatic tools to correlate the altered expression of these miRNAs with the main function of CSCs (self-renewal and proliferation), 7 of the 16 miRNAs were found to be predicted to target genes that led to this outcome. Among those that were predicted to regulate CSC function, the q-PCR validated only four miRNAs (miR-329, -376c, -495 and -30c). Bioinformatic analysis predicted GSK3-β and MEF2C as suitable common targets for the four validated miRNAs. However, western blot analysis did not show any changes in both GSK3-β and MEF2C expression in the diabetic CSCs, suggesting the paucity of the prediction software in my experimental setup.

4.4.2 Nanostring microarray and q-PCR experiments

The Nanostring microarray has several advantages compared to other more conventional microarrays. It is extremely specific due to the inclusion of unique oligonucleotide tags, as well as a pair of reporter and capture probes that bind to each miRNA in the reaction. After hybridisation with the probes, the miRNAs are labelled with a colour-code to increase the likelihood of detection (Malkov *et al*., 2009). Another advantage is that the Nanostring microarray measures miRNA expression without the need for amplification, unlike in traditional microarray analysis. This eliminates enzymatic bias that occurs in other microarrays when amplifying DNA (Geiss *et al*., 2008). Furthermore, it contains a more reliable quantification procedure in that the absolute number of each specific miRNA is counted, providing a more accurate dataset compared to those derived from methods where miRNAs are

expressed as a relative amount (Llorens *et al*., 2013). This aspect is especially important in my study because it is concerned with determining differences in absolute expression of miRNAs between two different conditions.

Despite these advantages, among the seven miRNAs chosen, only four (miR-329, -376c, -495 and -30c) were replicated to exhibit similar expression differences by q-PCR analysis. Although the fold changes between nanostring analysis and q-PCR were not similar, the trend in the significantly altered miRNAs was the same. It is also noteworthy that nanostring analysis counts the absolute miRNA levels, whereas q-PCR counts the relative change in the miRNA expression levels. Hence it is not surprising that the fold changes look different. Therefore, although the reproducibility of the Nanostring microarray has been praised over other techniques (Veldman-Jones *et al*., 2015), my study has revealed that the Nanostring data must be validated by other means to produce the most reliable results. The three miRNAs (miR-19a, -804 and -365) that could not be validated using this method may reflect the unforeseen inaccuracy of the Nanostring microarray, although limitations of the 95% confidence of the two-tailed t-test may have also contributed. Nevertheless, the four miRNAs (-495, -376c, -329 and -30c) that were validated by q-PCR were regarded as reliable due to their highly statistically significant differential expression that matched with their original Nanostring expression profiles in the diabetic CSCs.

4.4.3 Candidate miRNAs on stem cell function and the diabetic heart

While the roles of the differentially expressed miRNAs (-329, -376c, -495 and -30c) have been well established in various forms of cancer (Kang *et al*., 2016; Yang *et al*., 2014), only minimal evidence is available for their role in multipotent stem cells. MiR-495 and miR-329 have been demonstrated to regulate the differentiation of human MSCs and ESCs (Li *et al*., 2017; Cha *et al*., 2016; Lee *et al*., 2014, Yang *et al*., 2013), while miR-376c and miR-30c have been shown

to regulate the differentiation of mouse and human NSCs (Sun *et al*., 2016; Liu *et al*., 2014). To my knowledge there is no evidence for the role of these miRNAs in CSCs. However, their predicted effect on cell proliferation (Table 3) can be compared to other studies that have investigated their self-renewing capabilities in various cell lines (Sun *et al*., 2016; Jin *et al*., 2013; Xiao *et al*., 2013). Furthermore, the pathophysiological roles of these miRNAs can be further understood by determining whether their differential expression in the diabetic CSCs (Table 2) correlates with their impact on the diabetic heart.

4.4.3.1 MiR-30c

Among the candidate miRNAs, miR-30c is the only miRNA that is known to be highly expressed in the heart (Cheng *et al*., 2007). It is also associated with DCM as demonstrated by Raut and colleagues, who showed that miR-30c binds to and targets cell division control protein 42 (CDC42), p21-activated kinase 1 (PAK1) and cell tumor antigen p53 in cardiomyocytes of diabetic rats (Raut *et al*., 2016; Raut *et al*., 2015). These genes have been found to promote myocardial fibrosis and hypertrophy, and therefore lead to cardiac dysfunction (Ye *et al*., 2013; Care *et al*., 2007). This suggests that miR-30c is beneficial in preserving cardiac function during diabetes, correlating with the downregulated expression of this miRNA in the diabetic CSCs (Table 2).

MiR-30c was also the only candidate miRNA that was predicted to promote cell proliferation (Table 3). The effect of miR-30c on proliferation is antagonistic in cancerous conditions with various studies showing miR-30c to reduce proliferation in cancer cell lines (Jia *et al*., 2011; Irani and Hussain, 2015). However, in non-cancerous cells such as NSCs, Sun and colleagues demonstrated that miR-30c overexpression promotes proliferation by reducing the expression of semaphoring 3A (SEMA3A), a protein involved in promoting neurogenesis (Sun *et al*., 2016). In the heart, Liu *et al*. showed that miR-30c overexpression promotes myocardial cell

proliferation by inhibiting the transcription factor, GLI2 within the Hedgehog signaling pathway (Liu *et al*., 2016). Notably, this was also one of the signaling pathways in which miR-30c was predicted to promote proliferation using the bioinformatic analysis (Table 3). This therefore supports the predicted effect of miR-30c on the proliferation of CSCs.

4.4.3.2 MiR-329

MiR-329 was upregulated in the diabetic CSCs (Table 2). This is supported by studies that have demonstrated a pathological role for miR-329 in the diabetic heart. Wang and colleagues demonstrated that miR-329 overexpression in mouse endothelial cells inhibits the expression of CD146, a promoter of cell proliferation and angiogenesis (Wang *et al*., 2013). This was further supported by Welton *et al*., who showed that knocking down miR-329 increases arterial endothelial cell proliferation, as well as neovascularization and blood flow recovery after femoral artery ligation in a model of critical limb ischemia (Welton *et al*., 2014).

Bioinformatic analyses predicted that miR-329 inhibits cell proliferation (Table 3). Evidence for this has been demonstrated by a study from Yang and colleagues who showed that miR-329 can inhibit the proliferation of neuroblastoma cells by targeting lysine-specific demethylase 1 (KDM1A) (Yang *et al*., 2014). In addition, using glioma cells, Xiao and colleagues identified the transcription factor, E2F1 as the direct target for miR-329. E2F1 is a promoter of the AKT signaling pathway, which is a known activator of the cell cycle (Xiao *et al*., 2013). Growth factor receptor-bound protein 2 (GRB2) was also identified as another direct target for miR-329 in pancreatic cancer cells. The overexpression of GRB2 reduces the anti-proliferative and apoptotic effects of miR-329 in these cells (Wang *et al*., 2016). These studies therefore support the predicted role of miR-329 in inhibiting cell proliferation.

4.4.3.3 MiR-495

The role of miR-495 in the diabetic heart is unclear, as studies have shown conflicting evidence as to whether this miRNA is beneficial or pathological to cardiac function. Therefore, there is no conclusive evidence to support the upregulation of miR-495 that was observed in the diabetic CSCs (Table 2). One study found that miR-495 knock-down increases endothelial cell proliferation, as well as neovascularization and blood flow recovery in mice with ischemia (Welton *et al*., 2014). Conversely, Clark and Naya demonstrated that miR-495 overexpression promotes the proliferation of rat cardiomyocytes by targeting the transcriptional coactivator and cell cycle inhibitor, CITED2 (Clark and Naya, 2015). One reason for this differential effect may be that the role of miR-495 in the heart is species-dependent as the studies showed it to be beneficial in the mouse heart, but pathological in the rat heart.

Bioinformatic analyses also predicted miR-495 to inhibit cell proliferation (Table 3). This is supported by a study from Chen and colleagues who found that miR-495 overexpression, as well as knock-down of the miR-495 target gene, CDK6, causes cell cycle arrest and inhibition of cell proliferation in glioblastoma multiform cells (Chen *et al*., 2013). In another study, Chu and colleagues showed that miR-495 inhibits the proliferation of lung cancer cells by targeting metastasis-associated protein 3 (MTA3) (Chu *et al*., 2013). However, because miR-495 has mostly been studied in cancer cell lines, it is unclear whether this anti-proliferative effect can be translated from cancer tissue to healthy tissue. MiR-495 is also known to inhibit stem cell differentiation. In particular, this role has been identified by inhibiting the target genes, DNMT3A methyltransferase and SOX9 transcription factor in mouse ESCs and MSCs, respectively (Lee *et al*., 2014; Yang *et al*., 2013).

4.4.3.4 MiR-376c

Compared to the other candidate miRNAs, considerably less information is known about the role of miR-376c in the diabetic heart. The predicted effect of miR-376c inhibiting cell proliferation was also not supported by the literature. On the contrary, certain studies have indicated that miR-376c promotes proliferation. Fu and colleagues showed that miR-376c overexpression increases the proliferation of trophoblasts by targeting activin receptor-like kinase 5 (ALK5) and activin receptor-like kinase 7 (ALK7) receptors (Fu *et al*., 2013). In contrast, Jin and colleagues showed that miR-376c overexpression inhibited cell proliferation and invasion in osteosarcoma cells (Jin *et al*., 2013). However, as with other miRNAs, miR-376c has differential effects on non-cancerous cells as shown by Kureel and colleagues, who showed that miR-376c overexpression inhibited the differentiation of osteoblasts (Kureel *et al*., 2018). Based on this, my study has provided the first evidence that diabetes increases the expression of miR-376c in CSCs.

4.4.4 Predicted target gene expression in diabetic CSCs

Bioinformatic analysis predicted GSK3-β and MEF2C as suitable targets for the candidate miRNAs. Both GSK3-β and MEF2C have been demonstrated to regulate the proliferation, differentiation and survival of stem cell subtypes (Esfandiari *et al*., 2012; Li *et al*., 2008). However, western blot analyses showed no change in total protein expression of these genes between diabetic and non-diabetic CSCs (Fig. 4.5). These results differed from several other studies which indicate that the expression profiles of GSK3-β and MEF2C are altered in diabetic mice and rats (Feng *et al*., 2008; Eldar-Finkelman *et al*., 1999).

One explanation for these results is that the expression of these genes are tissue-specific in the diabetic condition. This tissue-specificity has been indicated by a reduction in GSK3-β expression in human skeletal muscle, but no change in expression in adipocytes after

troglitazone treatment (Ciaraldi *et al*., 2006). It was also supported by Patel and colleagues who demonstrated that GSK3-β knock-down in mice led to a greater improvement in glucose tolerance and insulin signaling in skeletal muscle compared to other tissues such as the liver (Patel *et al*., 2008). GSK3-β primarily acts by inactivating glycogen synthase, an enzyme that limits the effects of diabetes by converting glucose to glycogen (Saltiel, 2001). The extent to which GSK3-β regulates glucose metabolism may therefore reflect its differential expression in other tissues.

Despite being a common method for target identification, recent analysis of the miRNA-target prediction software has revealed that this method relies on a computational prediction and therefore may not always produce experimentally validated results (Witkos *et al*., 2011). It is noteworthy that the prediction software is primarily used as a starting tool for further analysis. Nevertheless, this may indicate that in order to validate the change in expression of the candidate miRNAs, another form of validation must be designed that is specific for the experimental samples used in this study. In the following chapter, I will argue that due to the complexity of the protein interactions and variability in growth conditions of the CSCs *in vitro*, the researcher must identify certain target genes within their own experimental CSC samples rather than relying on prediction software (bioinformatic tools).

CHAPTER 5: IDENTIFICATION AND VALIDATION OF MIRNA TARGETS

5.1 Introduction

In Chapter 4, the western blot analysis of GSK3β and MEF2C failed to show any change in expression in the diabetic CSCs, despite being predicted as miRNA targets in multiple protein databases. It also indicated that the bioinformatic prediction software may not be as reliable as once thought, and a more accurate technique for miRNA target identification was required. In this Chapter, mass spectrometry was used as a tool for the identification of miRNA target genes. Once appropriate target genes have been selected, they can be confirmed as direct miRNA targets by luciferase assays. If these techniques proved to be successful, western blot analysis could then be repeated for the new miRNA target genes in diabetic and non-diabetic CSCs. This in turn would address the first objective of the project. Evidence for the advantages of these techniques will first be described, followed by the corresponding protocols that were performed. The data will then be analysed and compared to the relevant literature.

5.1.1 Aims and Objectives

The primary aim of this chapter was to identify the direct target genes for the miRNAs which showed altered expression in the diabetic CSCs in order to validate the functional efficacy of the altered miRNAs. The second aim was to validate the expression of these genes in the diabetic CSCs by performing western blot analysis.

5.1.2 Conventional techniques for identifying miRNA targets

Due to the fact that the primary function of miRNAs is to regulate gene expression, appropriate target genes must first be identified in order to functionally validate the changes observed in the diabetic CSCs. There are a number of existing techniques that have been used for this purpose. Gene expression analysis has been applied by correlating the differential expression of miRNAs with subsequent target mRNA degradation after transfection in cell lines (Lim *et al*., 2005). Alternatively, RISC components such as argonaute proteins can be tagged with an epitope and co-immunoprecipitated along with target mRNA in cells by using an antibody against the epitope. The precipitates can then be analysed by a microarray to identify miRNA targets (Beitzinger *et al*., 2007).

The most common method for identifying miRNA targets is through the use of bioinformatic tools and target-based prediction software. Although there have been advances in the accuracy of computational algorithms within these databases, there are still a high number of false positives resulting from inaccurate sequence matching (Oh *et al*., 2017; Oliveira *et al*., 2017; Pinzón *et al*., 2017; Min and Yoon, 2010). Evidence for this limitation was notably found in my study (Chapter 4, section 4.3.5) where the GSK3β and MEF2C genes, that were predicted to be direct targets for the dysregulated miRNAs in diabetic CSCs, showed no change in total protein expression. Quantitative proteomics is a biochemical approach towards miRNA target identification that is recently gaining a lot of interest due to its high sensitivity and effectiveness. This method relies on mass spectrometry to assess and quantify peptides in an experimental sample, and then correlate the results with advanced sequencing databases (Ma *et al*., 2015).

5.1.3 Mass spectrometry

Mass spectrometry (MS) is a technique that measures the chemical compositions of substances by ionization. The ions can be sorted and separated according to their mass and charge by a mass spectrometer. MS has been routinely used to characterise molecules by determining their mass, isotopic signature or chemical structure (Biemann, 1963). It can also be applied towards the characterisation of proteins of interest whereby the proteins are enzymatically digested into peptides and then fractionated into ions (Wysocki *et al*., 2005; Trauger *et al*., 2002). The isobaric tags for relative and absolute quantitation (iTRAQ) method can be used to label the resulting peptides and quantify them based on the signal intensities of the fractionated ions. These signal intensities correspond to the relative abundance of a peptide in a sample population (Wiese *et al*., 2007). Peptide mass fingerprinting can then be used to identify an unknown protein in the sample by correlating the mass-to-charge ratios of the ions with protein databases that contain sequencing information (James *et al*., 1993).

Recent evidence for the use of this technique for the characterization and identification of miRNA target genes is very convincing (Ma *et al*., 2015). For this reason, I used MS in my study to determine the appropriate target genes for the differentially regulated miRNAs in the diabetic CSCs.

5.1.4 Luciferase for validating miRNA targets

The genes identified from mass spectrometry must then be confirmed as direct targets by performing a luciferase assay. This assay is commonly used to study gene expression in mammalian cells at the transcriptional level. Each luciferase assay contains a specific oxidative luciferase enzyme that enables the emission of light from the organisms that express them. For instance, the firefly luciferase assay utilizes a specific luciferase enzyme in fireflies to convert luciferin into oxyluciferin. The energy released by this reaction (shown below)

comes in the form of light, and is proportional to the amount of luciferase in the assay (Nguyen *et al*., 1988).

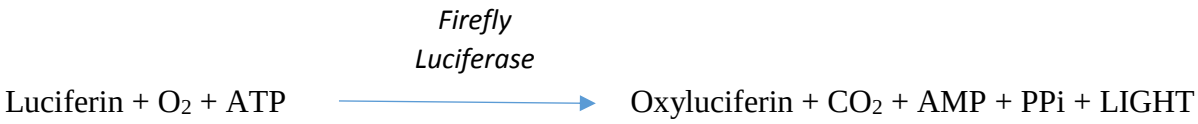

The assay can be used in conjunction with MS for identifying target genes. The regulatory (3') region of the specific, identified gene is cloned in an expression vector (plasmid) downstream to a luciferase gene and introduced into cells. When the cell is lysed, the luciferase enzyme is exposed to oxygen. The luciferin substrate can then be added to the cell to produce light (luminescence) which can be measured using a luminometer. The luminescence produced is proportional to the expression of the gene of interest that was cloned with luciferase (Nguyen *et al*., 1988). As such, I utilized a firefly luciferase reporter assay in my project to determine the expression of a predicted target gene of one of the differentially regulated miRNAs.

The identification of miRNA targets is vital for confirming the differential expression of the candidate miRNAs (-495, -376, -329 and -30c) that were partially validated by q-PCR. Contrary to my previous attempts involving the use of prediction software, here I used a more specific proteomic technique (MS) to predict the target genes for the differentially regulated candidate miRNAs.

5.2 Methods

5.2.1 Mass spectrometry (MS) protocol

5.2.1.1 Sample preparation

I performed the sample preparation for MS with help from Dr. Torsten Kleffman (Department of Biochemistry, University of Otago). Total protein was initially extracted from diabetic (n=5) and non-diabetic CSC samples (n=5) and quantified by performing a Bradford assay (Chapter 2). The normal recipe for RIPA lysis buffer was modified for MS, in which the SDS was used at a lower concentration (0.02% for MS compared to 0.1% in the regular RIPA buffer) and Triton was excluded to limit the amount of detergent in the protein suspensions. The total protein samples were processed by a filter-aided sample preparation (FASP, Wiśniewski *et al*., 2009). The procedure for this was modified for compatibility with downstream iTRAQ labelling. The protein samples were loaded into 0.5 mL ultrafiltration units (10 kDa cut-off) and buffer-exchanged into 8 M urea in 0.25 M triethylammonium bicarbonate (TEAB). The samples were then washed and purified by centrifuging three times at 14,000 x g at 20 °C for 15 minutes each, reducing the volume of the samples down to 20 µL each time. The washing step reduces the presence of detergents and nucleic acids in the samples that can produce excessive background signal in the mass spectrometer. The protein concentration was measured in aliquots of each sample by performing a Bradford assay (Chapter 2, section 2.7.2). The proteins in each sample were then digested into smaller peptides by adding trypsin (1 µg trypsin / 20 µg of protein) on-filter for 24 hours at 37 °C. An additional aliquot of trypsin was added to each sample and incubated for 4 hours at 37 °C, before transferring the filter content of each sample into new tubes. The peptides were labelled with iTRAQ reagents (8plex iTRAQ kit, Sigma-Aldrich, Germany) and pooled according to the manufacturer's instructions.

Peptides of the pooled iTRAQ labelled samples were subjected to off-gel isoelectric focusing (IEF) using an Agilent OFFGEL Fractionator (Agilent Technologies). Isoelectric focusing separates the peptides in each sample by subjecting them to an electric field along a pH gradient. As the peptides migrate from the anode to the cathode, they eventually stop when they lose their charge. This separates the peptides into stationary bands called 'fractions' (Gundry *et al*., 2010). The samples in this project were fractionated into 24 fractions along a pH gradient (pH 4-10) according to the manufacturer's instructions. The fractions were concentrated using a centrifugal vacuum concentrator and analysed in duplicates by nanoflow liquid chromatography-coupled LTQ Orbitrap tandem mass spectrometry (Tripletof 6600). The nanoflow liquid chromatography ionises the peptides into a small heated capillary within an electric field to produce charged droplets. The ions can then be characterized according to their mass-to-charge ratio (MS/MS spectra) by the mass spectrometer (Gundry *et al*., 2010).

During the nanoflow liquid chromatography, half of each fraction was loaded onto a trap column and separated on a packed emitter tip column through an acetonitrile gradient (5-35%) in aqueous 0.2% formic acid for 45 minutes, followed by an increase to 99% over 10 minutes. The mass spectrometer was operated in MS mode at 60,000 resolution (400 m/z) and eight data-dependent MS/MS scans were performed on the ions. The first four scans were performed as collision induced dissociation (CID) scans on the strongest four precursors for peptide identification. CID allows for fragmentation of the ions by colliding them with neutral molecules (eg. nitrogen) (Parcher *et al*., 2018). The next four scans were performed as high energy collision induced dissociation (HCD) scans of the same four precursors for reporter ion quantification. The fragmented ions were thus detected and quantified in the mass spectrometer, constituting the raw MS data.

5.2.1.2 Peptide mass fingerprinting using SWATH acquisition

The MS data was analysed by peptide mass fingerprinting in order to identify differentially regulated miRNA targets. The SWATH (Serial window acquisition of theoretical spectra) acquisition containing Peakview 2.0 and MarkerView 1.2 analyses software (SCIEX, Australia) was used for this purpose. The MS/MS spectra of 2000 randomly selected peptides were imported into PeakView and converted into SWATH files containing specific peptide tags. PeakView expresses the MS/MS spectra of each peptide as 'peaks' based on the intensity of their mass-to-charge ratio. The data was then imported to MarkerView which displays the quantified peaks in a scatter plot. The principal component analysis function was used to calculate a logarithmic (Log_{10}) fold change signifying the relative difference in the MS/MS spectra of each peptide in the diabetic and non-diabetic samples. This data could then be sorted based on statistical significance by performing a two-tailed t-test on the MS/MS spectra of each peptide. Peptides were only selected if they exhibited a Log fold change within a selected range ($-0.3 < x < 0.3$) as well as a P value below 0.05. The MS/MS spectral data of each selected peptide could then be converted into peptide sequences by importing their SWATH peptide tags into FASTA software (EMBL-EBI, UK). The sequence of each peptide was then searched in the National Centre for Biotechnology Information database (ncbi.nlm.nih.gov/proteins) to determine the entire genome sequence of the corresponding gene. The identities of these genes were verified by importing the genome sequences into the STRING database. In this way, a list of genes were identified in the original experimental samples that were either significantly upregulated or significantly downregulated in the diabetic CSCs.

5.2.1.3 Correlating results to bioinformatic tools and literature

The identified genes were searched in five well known bioinformatic databases (TargetScan, miRanda, RNA22, microRNA.org and miRDB) to determine which have been predicted as targets for the differentially regulated candidate miRNAs (miR-329, -376c, -495 and -30c). Two target genes, voltage-dependent anion-selective channel 1 (VDAC1) and cyclin-dependent kinase 6 (CDK6) were finally selected based on two criteria:

1. The magnitude of the fold change of a corresponding peptide determined from mass spectrometry analysis
2. The number of bioinformatic databases that have predicted the genes as targets for the differentially regulated miRNAs

5.2.2 Luciferase assay protocol

A luciferase assay was performed to determine whether the VDAC1 gene identified from MS analysis is a direct target for miR-30c. VDAC1 is a 31 kDa protein that forms a channel through the outer mitochondrial and plasma membranes. The channel at the outer mitochondrial membrane allows for the entry and exit of small hydrophilic molecules into the mitochondria, while the channel in the plasma membrane allows for the diffusion of substances that regulate cell volume (Baumgarner *et al*., 2009; Baker *et al*., 2004).

Plasmids containing a 3'UTR region of the VDAC1 and CDK6 genes were first transformed into and extracted from bacteria, and then quantified using a Nanodrop Spectrophotometer. The 3'UTR region of CDK6 was included as a negative control due to the fact that it was not a predicted target for miR-30c. Next, one non-diabetic CSC sample was cultured in T25 flasks at P8. Once confluent, the cells were counted using a hemocytometer and seeded into 16 wells of a white 96-well plate (1×10^4 cells / well) at P9. The cells were then incubated for 24 hours

at 37 °C. The CSCs in each well were co-transfected with either miR-30c or scrambled mimic as well as either of the 3'UTR plasmids of each gene in quadruplicate, according to Table 5.1. The miR-30c/scrambled mimic were added to each well at a concentration of 10 µM, while the 3'UTR plasmids were added at a concentration of 250 nM along with the standard dilution of RNAiMAX lipofectamine reagent for a 96-well plate (Table 5.1).

Table 5.1. Volumes and concentrations of reagents for luciferase assay

Reagents	Concentration per well	Volume per well (µL)
Lipofectamine RNAiMAX reagent		1.50
DMEM/F12 media for lipofectamine dilution		25
Renilla control 3'UTR plasmid	775 ng/µL	0.32
VDAC1 3'UTR plasmid	704 ng/µL	0.36
CDK6 3'UTR plasmid	519 ng/µL	0.48
MiR-30c/scrambled mimic	10 mol/L	0.50
DMEM/F12 media for mimic dilution		25

The miR-30c precursor (sequence in Appendix 7) or scrambled mimic was first diluted by adding 0.5 µL of the mimic to 25 µL of serum-deprived DMEM/F12 media. A 1.5 µL volume of lipofectamine reagent was also diluted in 25 µL of serum-deprived DMEM/F12 media and added to the diluted miR-30c/scrambled mimic. The mixture was then incubated for 5 minutes at RT, and then added to each corresponding well of the 96-well plate. The 3'UTR plasmids consisting of the VDAC1, CDK6 or Renilla control was subsequently added to the wells at a volume of 1.5 µL before incubating the plate for 48 hours at 37 °C.

The Luc-Pair Duo-Luciferase assay kit (GeneCopoeia, USA) was then used to perform the luciferase assay. The kit contains two luciferin substrates (Luc Sub I and II) which are oxidized by the firefly luciferase enzyme. The 96-well plate containing the CSCs was allowed to equilibrate to RT and the growth media was aspirated. Twenty microlitres of 10-times diluted luciferase lysis buffer was added to each well. The plate was then incubated on an

orbital shaker for 15 minutes to mix the solution. FLuc (Firefly) and RLuc (Renilla) working solutions were prepared by adding 10 µL of Luc Sub I and II (100X) to 1 mL of Luc Buffer I and II, respectively. The solutions were then mixed well by inverting the tubes and then incubated in the dark for 5 minutes at RT. After the incubation period, 100 µL of FLuc solution was added to each well of the 96-well plate and mixed by pipetting up and down using a multi-channel pipette. The tubes were then incubated in the dark for 5 minutes at RT and luminescence was measured using a luminometer. After recording the luminescence values, 100 µL of RLuc solution was added to each well. The solution was mixed by pipetting and incubated in the dark for 5 minutes at RT, luminescence was measured as described above. The ratio of luminescence emitted from the Firefly and Renilla luciferase enzymes in the CSCs transfected with either miR-30c or scrambled mimic was then calculated from which a fold change was determined for the expression of the 3'UTR of VDAC1 and CDK6. A two tailed t-test was performed to determine the significance of these fold changes.

5.2.3 Western blot analysis protocol for identifying target genes

Once the target genes were identified, western blot analysis was performed for functional validation at the protein level. Western blots were performed as described in Chapter 2, section 2.8. Following the transfer of proteins, membranes were incubated with a mouse, monoclonal anti-CDK6 antibody (1:1000, Cell Signaling Technology, U.S.A, 40kDa, Table A1.2 in Appendix 1) and a rabbit, polyclonal anti-VDAC1 antibody (1:1000, abcam, Australia, 31kDa, Table A1.2 in Appendix 1). Goat, anti-mouse or mouse, anti-rabbit antibody (1:3000, ThermoFisher, USA, Table A1.2 in Appendix 1) were subsequently used as secondary antibodies for anti-CDK6 and anti-VDAC1, respectively. A rabbit, polyclonal anti-α-tubulin antibody (1:1000, abcam, Australia, 50kDa, Table A1.2 in Appendix 1) was also used to identify the α-tubulin gene, which was used as a loading control. Western blots were

repeated three independent times for each antibody, and quantified by densitometry using ImageJ software (NIH, USA).

5.3 Results

5.3.1 Target proteins were identified by Mass Spectrometry

Among the 2000 peptides evaluated by mass spectrometry, there were 435 (22%) that were significantly dysregulated in diabetic CSCs. Among these, 197 peptides (45%) were significantly upregulated and 238 peptides (55%) were significantly downregulated in the diabetic CSCs.

From this list, the 16 most significantly upregulated (fold change > 1.5 in diabetic CSCs) and 16 most significantly downregulated (fold change < 0.8 in diabetic CSCs) peptides were selected for bioinformatic analysis. Bioinformatic analysis was used to determine which of these peptides constitute appropriate miRNA targets. In this analysis, five miRNA-target prediction databases (TargetScan, RNA22, miRanda, microRNA.org, miRDB) were searched to determine which of the 32 significantly dysregulated peptides were likely to bind to the candidate miRNAs (miR-329, -495 and -376c and -30c). The results revealed that 10 significantly dysregulated peptides (8 downregulated, 2 upregulated) constituted proteins that were predicted as targets for the candidate miRNAs (Table 5.2).

Table 5.2. Significantly differentially expressed MS peptides as miRNA targets			
Target proteins	Fold change (diabetic vs non- diabetic CSCs)	Candidate miRNAs predicted	Number of databases
Downregulated			
KPNB1	0.39 (P<0.001)	miR-376c	1 (TargetScan)
CDK6	0.44 (P<0.0001)	miR-329 miR-495 miR-376c	2 (miRDB, RNA22) 3 (TargetScan, miRDB, miRanda) 1 (TargetScan)
GCC2	0.54 (P<0.001)	miR-329 miR-495 miR-376c	1 (TargetScan) 1 (TargetScan) 1 (TargetScan)
SARNP	0.60 (P<0.01)	miR-329 miR-376c	1 (TargetScan) 1 (TargetScan)
GUCY1B1	0.63 (P=0.01)	miR-329 miR-495	1 (TargetScan) 2 (TargetScan, miRanda)
DNAJB4	0.68 (P=0.04)	miR-329 miR-30c	2 (TargetScan, miRanda) 2 (miRanda, microRNA.org)
TPT1	0.75 (P<0.001)	miR-329 miR-495	1 (TargetScan) 1 (TargetScan)
CMPK1	0.78 (P<0.0001)	miR-495 miR-376c	2 (TargetScan, miRanda) 1 (TargetScan)
Upregulated			
MBNL2	1.69 (P=0.02)	miR-495 miR-30c	1 (miRanda) 1 (miRDB)
VDAC1	1.67 (P<0.01)	miR-30c	2 (RNA22, microRNA.org)

Table 5.2. Table describing the significantly altered target proteins from the MS analysis. The target proteins are separated based on whether they are upregulated or downregulated in the diabetic CSCs. Significance was determined by a two-tailed t-test. Bioinformatic miR-target prediction databases were used to identify the target proteins that are predicted to be regulated by the candidate miRNAs. A larger group of dysregulated MS peptides are shown in Appendix 11. KPNB1 = Importin subunit β1, CDK6 = Cyclin-dependent kinase 6, GCC2 = Grip and coiled-coil domain-containing protein 2, SARNP = SAP domain-containing ribonucleoprotein, GUCY1B1 = Guanylate cyclase soluble β1, DNAJB4 = DnaJ homolog subfamily B member 4, TPT1 = Translationally controlled tumor protein 1, CMPK1 = Cytidine/Uridine monophosphate kinase 1, MBNL2 = Muscleblind-like splicing regulator 2, VDAC1 = Voltage-dependent anion-selective channel 1.

Two of these proteins (CDK6 and VDAC1) were selected for western blot analysis using two criteria:

1. The number of databases that identified an association between miRNA and protein
2. The correlation between the differential expression of the miRNAs and protein in diabetic CSCs

The cell cycle promoter, CDK6 was predicted to be a target for miR-329, -495 and -376c in four databases combined (miRDB, RNA22, miRanda and TargetScan). Out of all peptides analysed, this was the most number of databases where a peptide was identified as a predicted target for the candidate miRNAs. The downregulation of CDK6 in the diabetic CSCs (fold change of 0.44 ± 0.12) also correlated with the upregulation of miR-329, -495 and -376c in the original Nanostring microarray (Chapter 4, section 4.3.1). This protein was therefore selected as the most appropriate target for validating the altered expression profiles of miR-329, -495 and -376c in the diabetic and non-diabetic CSCs.

VDAC1 was predicted to be a target for miR-30c in two databases (RNA22 and microRNA.org). In addition, the upregulated expression of VDAC1 in the diabetic CSCs (fold change of 1.67 ± 0.11) also correlated with the downregulated expression of miR-30c in the original Nanostring microarray. VDAC1 was also the only significantly upregulated peptide that was predicted to be the sole target for miR-30c. For these reasons, VDAC1 was selected as the most appropriate target for validating the altered expression profile of miR-30c in the diabetic and non-diabetic CSCs.

Among the 2000 randomly selected peptides assessed by mass spectrometry, those corresponding to the CDK6 and VDAC1 genes were also among the most substantially and significantly ($P<0.05$) altered in the diabetic CSCs. The significantly altered expression profiles of CDK6 and VDAC1 are summarized in Table 5.3, along with the relevant bioinformatic databases that were used to predict miRNA-target association.

Table 5.3. Target genes chosen using mass spectrometry from those significantly regulated in diabetic CSCs			
Target gene	miRNAs predicted	Bioinformatic databases	Fold change in diabetic CSCs (vs non-diabetic CSCs)
CDK6	miR-329 miR-495 miR-376c	miRDB, RNA22, miRanda, TargetScan	**0.44** ± 0.12 (P<0.001)
VDAC1	miR-30c	RNA22, microRNA.org	**1.67** ± 0.11 (P=0.006)

The characteristics of CDK6 and its relation to stem cell function are well documented (Laurenti *et al*., 2015; Scheicher *et al*., 2015), however not much is known about the functional consequences of VDAC1 dysregulation in CSCs. Furthermore, the role of miR-30c is not well defined in CSCs. For these reasons, VDAC1 was selected for a luciferase assay to confirm this protein as a direct target for miR-30c, before examining the role of miR-30c in diabetic CSCs by performing functional experiments.

5.3.2 Luciferase assay confirmed VDAC1 as the direct target of miR-30c

The luciferase assay was performed to confirm if VDAC1 is a direct target for miR-30c as indicated by the MS data. Mean expression data was calculated for 3'UTR of VDAC1 in the CSCs transfected with miR-30c and scrambled mimic which was expressed as a percentage of the VDAC1 expression in the scrambled control after normalisation. As shown in Figure 5.1, transfecting cells with the miR-30c precursor mimic significantly reduced the luminescence of the VDAC1 3'UTR (0.62 ± 0.18, $P < 0.01$). This supports the MS data and bioinformatic analysis and provides the first evidence that VDAC1 is a 'direct' target for miR-30c. The inclusion of the CDK6 3'UTR as a negative control showed a non-significant increase (1.34 ±

0.36, P = 0.54) in the expression of the 3'UTR of CDK6 in the CSC transfected with the miR-30c precursor mimic further validating my technique and results as CDK6 is not a predicted target for miR-30c.

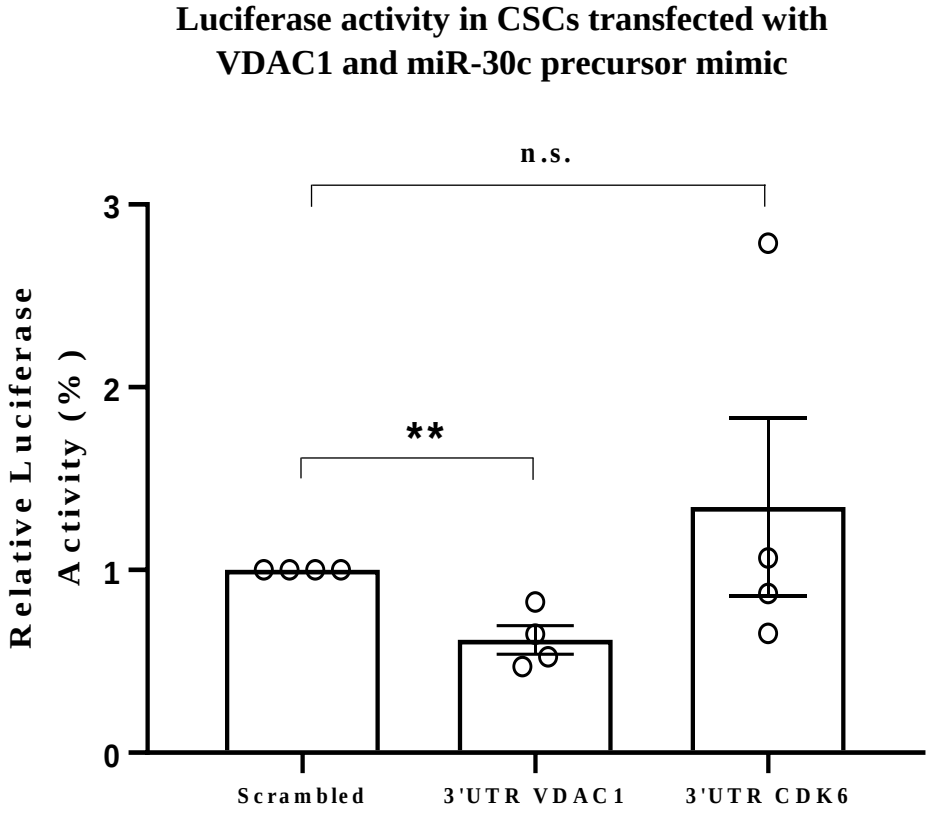

Figure 5.1. Quantitative data showing reduced luciferase activity of Luc-VDAC1-3'UTR construct (0.62 ± 0.18, n=3, P<0.01) compared to scrambled (control) in a non-diabetic CSC co-transfected with 10μM miR-30c precursor mimic and VDAC1 plasmid. The Luc-CDK6-3'UTR was used as a negative control. Data are means ± SEM. Significance (** = P<0.01) is illustrated by a two-tailed t-test. n.s. = not significant.

5.3.3 Western blot analysis validated VDAC1 and CDK6 as functional targets of the candidate miRNAs

To functionally validate the expression of VDAC1 and CDK6 proteins in the diabetic CSCs, western blots were performed (Fig. A8.1 in Appendix 8). A two-tailed unpaired t-test showed a significant downregulation of CDK6 protein expression in diabetic CSCs (0.73 ± 0.10, n=4, P = 0.04) compared to in non-diabetic CSCs (1.00 ± 0.17, n=4) (Fig. 5.2A). A one-way ANOVA also showed no significant difference between repetitions in either non-diabetic (P > 0.05, F = 1.46 x 10^{-12}, Fcrit = 3.49) or diabetic groups (P > 0.05, F = 0.63, Fcrit = 3.49). This therefore provides evidence to suggest a functional validation for the upregulated expression profiles of the miRNAs (miR-329, -376c and -495) in the Nanostring microarray. A two-tailed unpaired t-test also showed a significant upregulation of VDAC1 protein expression in the diabetic CSCs (3.16 ± 0.58, n=4, P < 0.01) compared to the non-diabetic CSCs (1.00 ± 0.22) (Fig. 5.2B), thereby suggesting a functional validation for the downregulated expression of miR-30c in the diabetic CSCs. Similarly, the one-way ANOVA showed no significant difference between repetitions in either non-diabetic (P > 0.05, F = 5.5 x 10^{-16}, Fcrit = 4.26) or diabetic groups (P > 0.05, F = 1.97, Fcrit = 4.26).

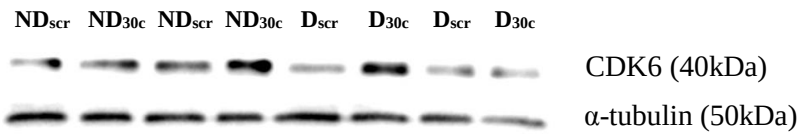

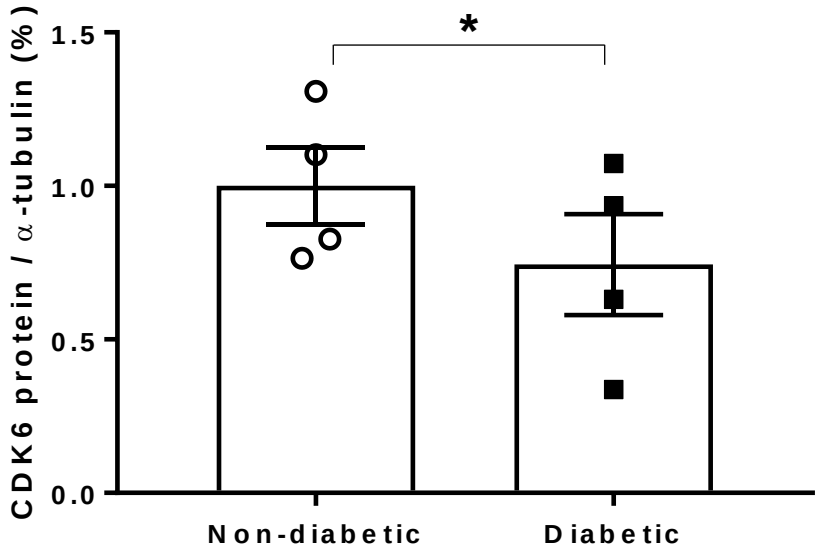

Figure 5.2A. Representative immunoblot and quantitative data showing the significant downregulation of CDK6 in diabetic CSCs vs non-diabetic CSCs (0.73 ± 0.10 vs 1.00 ± 0.17, n=4, P<0.05, repeated three times). Data measured as percentage of CDK6 protein compared to α-tubulin endogenous control. Data are means ± SEM. Significance (* = P<0.05) was determined from a two-tailed t-test.

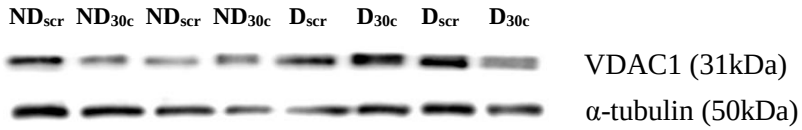

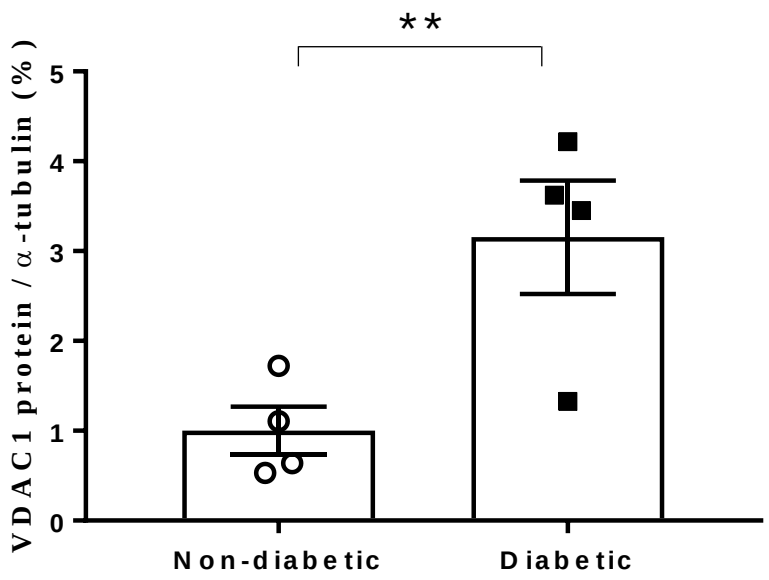

Figure 5.2B. Representative immunoblot and quantitative data showing the significant upregulation of VDAC1 in diabetic vs non-diabetic CSCs (3.16 ± 0.58 vs 1.00 ± 0.22, n=4, P<0.01, repeated three times). Data measured as percentage of VDAC1 protein compared to alpha tubulin endogenous control. Data are means ± SEM. Significance (** = P<0.01) was determined from a two-tailed t-test.

5.4 Discussion

5.4.1 Summary of results

In this chapter, mass spectrometry predicted CDK6 as a common target protein for miR-329, -376c, -495, while VDAC1 was predicted as a direct target protein for miR-30c. VDAC1 was subsequently confirmed as a direct target for miR-30c using the luciferase assay. The results of the assay showed that there was a significant reduction in the expression of the 3'UTR construct of VDAC1 in CSCs transfected with the miR-30c precursor mimic compared to the scrambled control. Western blot analyses showed that CDK6 was significantly downregulated in diabetic CSCs, correlating with the upregulated Nanostring profiles of miR-329, -376c and -495. Conversely, western blots showed VDAC1 to be significantly upregulated in the diabetic CSCs, correlating with the downregulated Nanostring profile of miR-30c. These western blot analyses therefore validated the dysregulated expression of the candidate miRNAs in the Nanostring microarray and q-PCR. To my knowledge, this is the first evidence to show that VDAC1 is the direct target for miR-30c.

5.4.2 Mass spectrometry analysis

Among the peptides that were found to be dysregulated in the diabetic CSCs by mass spectrometry, 22% were significantly altered ($P<0.05$). This was slightly higher than the percentages of significant peptides (12% and 14%) found in other studies using mass spectrometry for target miRNA identification (Ou *et al*., 2014; Bargaje *et al*., 2012). As mentioned in the results, CDK6 and VDAC1 were determined to be the most suitable target genes for the candidate miRNAs. The altered expression profiles of both CDK6 and VDAC1 in the diabetic CSCs correlated with the expression patterns of the candidate miRNAs that were predicted to target each gene (Chapter 5, section 5.3.1). This suggested that CDK6 and VDAC1 total protein may exhibit a similar expression pattern in the diabetic CSCs compared

to their respective mass spectrometry profiles. Interestingly, GSK3-β and MEF2C genes which were originally predicted as targets for the miRNAs by bioinformatic analyses, were not among the peptides identified by mass spectrometry.

5.4.3 Known functional roles of VDAC1 and CDK6

In the mitochondria, VDAC1 is a component of the permeability pore complex (PTP) that is responsible for the release of mitochondrial products such as cytochrome C which triggers apoptotic cell death (Baumgartner *et al*., 2009). In this process, apoptotic proteins specifically interact with VDAC1, causing oligomerization and subsequent opening of the channel (Abu-Hamad *et al*., 2009). VDAC1 also allows for the diffusion of calcium ions into the mitochondria, which causes calcium overload and an accumulation of ROS, leading to apoptosis through caspase activation (Chen *et al*., 2009). VDAC1 is also known to regulate mitochondrial membrane potential, depending on the open/closed conformation of the channel. The channel has a closed conformation at membrane potentials above 30 mV and is cation-selective, while it is anion-selective at lower membrane potentials (Rostovtseva *et al*., 2006). Evidently, a primary function of VDAC1 is to promote apoptosis (Abu-Hamad *et al*., 2009; Shoshan-Barmatz *et al*., 2009). Functional assays and additional western blots were performed in the next chapter (Chapter 6, section 6.3.2, 6.3.3 and 6.3.4) to demonstrate the pro-apoptotic effect of VDAC1.

CDK6 is a 40 kDa serine threonine kinase that is involved in stimulating the G1/S phase of the cell cycle by binding to and activating the cell cycle-dependent genes, cyclin D1, 2 and 3 (Meyerson and Harlow, 1994). It therefore mainly acts to promote cell proliferation by stimulating cell cycle progression. CDK6 is generally located in the nuclei of proliferating cells, but has also been found in the cytoplasm (Mahony *et al*., 1998). Another study has suggested that CDK6 may also contain an intrinsic quality control function in terms of the life

cycle of the cell. Moreover, overexpression of CDK6 can lead to the accumulation of the apoptotic proteins, p53 and retinoblastoma-like protein 2 (p130) and increased sensitivity to UV-irradiation. This suggests that CDK6 may trigger a negative feedback mechanism to limit the proliferation of damaged or dysfunctional cells (Nagasawa *et al*., 2001).

5.4.4 Specific miRNAs regulate VDAC1 and CDK6

There is no known literature thus far describing the existence of VDAC1 or CDK6 within the CSCs. Nevertheless, studies have shown that these genes are regulated by miRNAs in other cell types. For instance, in a mouse model of Parkinson's disease, miR-7 was found to prevent the release of cytochrome C from the PTP by binding to and inhibiting VDAC1. This led to the generation of ROS and subsequent apoptosis of the mouse primary neurons. It also implicated a neuroprotective role for miR-7 in Parkinson's disease in which mitochondrial dysfunction is a known contributor (Chaudhuri *et al*., 2016). Similarly, miR-29a improved neuronal cell survival in mice through the inhibition of VDAC1. This correlated with the development of ataxia in the same mice following miR-29a knockdown through upregulation of VDAC1 (Roshan *et al*., 2014).

There has been evidence that miRNAs target CDK6 to regulate cell proliferation. Wu and colleagues showed that miR-129 reduced proliferation through the direct inhibition of CDK6 in lung epithelial derived cells in mice (Wu *et al*., 2010). In another study, Sun and colleagues showed that miR-34a inhibits CDK6 in an adenocarcinomic human epithelial cell line and suggested that this could prevent tumour metastasis through the targeted inhibition of CDK6 (Sun *et al*., 2008). MiR-34a is of particular relevance to my study as it has been found to be activated in the diabetic heart, as well as in diabetic CPCs (Fomison-Nurse *et al*., 2018). Interestingly, among the dysregulated miRNAs in my study, only miR-495 has been demonstrated to inhibit the growth of gliomas by downregulating CDK6 in human brain

tissue (Chen *et al*., 2013). Although there may be different growth conditions involved in cancerous tissue, this finding provides an insight into the functional role of miR-495 in preventing cell proliferation, as well as supporting my mass spectrometry and western blot results.

CDK6 has also been found to regulate the proliferation of HSCs. Scheicher and colleagues demonstrated that CDK6 is essential for the suppression of early growth response protein 1 (EGR1), a transcriptional activator of HSCs (Scheicher *et al*., 2015). EGR1 was also found to be highly expressed in quiescent, as well as CDK6 knock-out cells (Min *et al*., 2008). This indicates that high levels of CDK6 in HSCs promotes proliferation by downregulating EGR1. CDK6 has been shown to have binding sites for miR-183 in tumour cell lines, thus indicating that miR-183 may regulate HSC proliferation, if it targets CDK6 within these cells (Kim *et al*., 2017).

5.4.5 Effect of diabetes on VDAC1 and CDK6 expression and function

The effect of diabetes on VDAC1 and CDK6 function in mouse CSCs remains unclear. However, few evidence suggest that diabetes can alter the expression of both proteins in other cell types. Coronary endothelial cells isolated from diabetic mice showed an upregulation of VDAC1 compared to those isolated from non-diabetic mice (Sasaki *et al*., 2012). Furthermore, hyperglycemia has been shown to increase VDAC1 expression in pancreatic β-cells (Ahmed *et al*., 2010). This correlates with my observation of VDAC1 upregulation in diabetic mouse CSCs. There is relatively less understood about the association between diabetes and CDK6 expression. Kushner and coauthors discovered that the knockdown of cyclin D2, an activator for CDK6, caused glucose intolerance in mice which then progressed to diabetes (Kushner *et al*., 2005). This indicates lower levels of CDK6 expression in the diabetic mice, which was supported in my study by the reduced expression of CDK6 in the

diabetoic mouse CSCs. Based on these findings, the next aim of my project was therefore to investigate the functional role for the target proteins in the diabetic heart and their effect on the candidate miRNAs. Western blot analyses showed that the expression of VDAC1 was more significantly and substantially altered compared to the expression of CDK6 in the diabetic CSCs. In addition, there are no published studies describing the roles of miR-30c in mouse CSCs. Furthermore, VDAC1 is a pro-apoptotic gene, and it is known that diabetes promotes intracellular pathways that lead to apoptosis (Krijnen *et al*., 2009). This motivated me to focus on conducting a more detailed examination of the functional effect of miR-30c and its target protein, VDAC1. Therefore, functional assays were performed in the next Chapter to determine the roles of miR-30c in mouse CSCs, as well as to provide evidence for the effect of diabetes on miR-30c function.

CHAPTER 6: FUNCTIONAL STUDIES TO DETERMINE THE ROLE OF MIR-30C IN DIABETIC CSCS

6.1 Introduction

I previously showed that miR-30c expression was significantly downregulated in diabetic mouse CSCs (Chapter 4, section 4.3.1) and confirmed VDAC1 as the direct target for miR-30c (Chapter 5, section 5.3.2). However, it is important to understand the functional importance of miR-30c downregulation in diabetic CSCs. In this Chapter, I will therefore answer the second objective of my PhD project by outlining the procedures and techniques that were performed to understand the function of miR-30c in CSCs. The experiments performed in this chapter will also address the significance of VDAC1 as a direct target for miR-30c and its association with the pathophysiological role of miR-30c. I will provide a brief overview of the rationale and methodology for the functional assays, followed by a discussion of my findings and how it can be used to answer my objective.

6.1.1 Aims and objectives

The first aim of this chapter is to confirm that miR-30c directly alters the expression of VDAC1 within diabetic and non-diabetic CSCs. The second aim is to determine the pathophysiological role of miR-30c by performing functional studies on both diabetic and non-diabetic CSCs.

6.1.2 Structure and functions of miR-30c

MiR-30c is one of the five members of the highly conserved miR-30 family (miR-30a-e) that share 85% sequence similarity. It is derived from the miR-30c-1 and miR-30c-2 genes that originate from intronic sequences in both humans and mice (Li *et al*., 2007). Despite being discovered as early as 2002 (Lagos-Quintana *et al*., 2002), there is only a limited amount of information available on the functional role of miR-30c. As with a number of other miRNAs, miR-30c has been implicated to play a role as a tumour suppressor due to its ability to target genes involved with promoting uncontrolled proliferation and invasion. It has also been found to be downregulated in cancerous tissue compared to non-cancerous tissue. Furthermore, the growth of an oncogene promoting cell line was found to be reduced after transfection with a miR-30c precursor mimic compared to those transfected with a scrambled mimic (Tanic *et al*., 2012). This indicates that miR-30c may indirectly reduce tumorogenesis by limiting the proliferation of cancerous cells.

MiR-30c has also been indicated to have a role in lipid metabolism. It was observed to be significantly upregulated during cellular adipogenesis and also promote adipogenesis after overexpression in adipose-derived stem cells (Karbiener *et al*., 2011). In mice, overexpression of miR-30c also reduces hyperlipidemia by inhibiting apolipoprotein B, which transports lipids and cholesterol to various tissues in the body. Hyperlipidemia is a major risk factor for atherosclerosis, which indicates miR-30c may be protective against heart disease. This notion was further strengthened after smaller atherosclerotic plaques were observed in mice expressing miR-30c (Soh *et al*., 2013).

6.1.3 Role of miR-30c in cardiovascular disease

MiR-30c has been shown to be highly expressed in cardiac tissue and cardiomyocytes (Soh *et al*., 2013; Duisters *et al*., 2009). Moreover, it has been found to be downregulated in mouse cardiac tissue after pathological cardiac remodelling following MI and ischemia/reperfusion (Gambacciani *et al*., 2013; Duisters *et al*., 2009). This downregulation was associated with an increased expression of connective tissue growth factor (CTGF), which has been demonstrated to increase in cardiac fibrosis and heart failure (Gambacciani *et al*., 2013). However, the protective role of miR-30c in preventing cardiac dysfunction has not yet been replicated in *in vivo* studies.

As discussed earlier (Chapter 1, section 1.1.2), diabetes may lead to the development of DCM which is commonly associated with diastolic dysfunction and cardiac hypertrophy in the absence of hypertension or coronary artery disease. MiR-30c has been found to mediate the effects of DCM by inhibiting the cardiac hypertrophy promoter genes, cell division control protein 42 (CDC42) and serine/threonine-protein kinase (PAK1) in cardiomyocytes of diabetic rats (Raut *et al*., 2015). Furthermore, miR-30c overexpression reduced the expression of the tumor protein p53 (p53) and cyclin-dependent kinase inhibitor 1 (p21) genes in high glucose-treated rat cardiomyocytes, as well as in cardiac tissue samples taken from the autopsies of diabetic patients. These genes are known to cause cardiomyocyte apoptosis and cell cycle arrest, which can then lead to compensatory hypertrophy in the remaining viable cardiomyocytes (Raut *et al*., 2016; Letonja and Petrovič, 2014; Fiordaliso *et al*., 2001). This suggests that overexpression of miR-30c can reduce the pro-hypertrophic effects of DCM, indicating that it may be beneficial for the treatment of DCM.

6.1.4 Rationale for determining role of miR-30c in diabetic CSCs

Although miR-30c has been characterized in a number of different tissues including the heart, there is a limited understanding of its function in stem/progenitor cells. My study has identified a downregulation of miR-30c in diabetic mouse CSCs, as well as confirming VDAC1 as the direct target of miR-30c. VDAC1 is generally known to promote apoptosis; however this function has never been documented within CSCs. This chapter will therefore determine the functional implications of miR-30c in regulating the apoptosis of CSCs through the inhibition of VDAC1. In an effort to uncover novel insights of this role, miR-30c was overexpressed in the diabetic and non-diabetic CSCs and western blot analyses were subsequently performed to determine the expression of VDAC1. Moreover, a caspase and proliferation assay were performed on the transfected CSCs to determine the direct effect of miR-30c on apoptosis and cell proliferation, respectively. The results of these experiments will not only further verify miR-30c as an inhibitor of VDAC1, but also shed light on a pathophysiological role for miR-30c in CSCs. This may lead to a better understanding as to why diabetes causes a reduced expression of miR-30c in the CSCs.

6.2 Methods:

6.2.1 Re-initiating CSCs for functional experiments

In preparation for the functional experiments described in this chapter, four diabetic and four non-diabetic CSC samples were thawed and re-initiated at P6 in T25 flasks. After scaling up to T75 flasks at P7, each CSC sample was plated into two T25 flasks as well as three wells of a 12-well plate at P8. During this process, the CSCs were lysed, pelleted and then counted using a hemocytometer (Appendix 5). The CSCs were then seeded into the T25 flasks at 1 x 10^6 cells per flask, and seeded into the 12-well plates at 1 x 10^5 cells per well. The CSCs in the T25 flasks were grown for the purposes of extracting transfected protein for western blot

analyses. Moreover, the CSCs in the 12-well plates were grown for the purposes of extracting transfected RNA for q-PCR analyses. CSCs were incubated at 37 °C until 70% confluent before transfection.

6.2.2 Transfecting CSCs with miR-30c precursor mimic

Transfection is the process of introducing purified nucleic acids into eukaryotic cells. It can be used in preparation for functional assays by introducing precursor mimics associated with the simulated expression of a specific miRNA (Chen *et al*., 2006). For this reason, diabetic and non-diabetic CSCs were transfected with a precursor mimic for miR-30c to simulate miR-30c overexpression within these cells.

Diabetic (n=4) and non-diabetic CSCs (n=4) grown in T25 flasks and 12-well plates were initially transfected with 10 μM of either miR-30c precursor mimic or scrambled sequence (control) following the standardized RNAiMAX transfection procedure (Life Technologies, USA). The reagent volumes were customized for each transfection experiment depending on the number of CSCs required for the corresponding functional assays (Table A9 in Appendix 9). To obtain the appropriate concentrations for optimal transfection of each well, 180 uL of the lipofectamine RNAiMAX reagent (Life technologies, USA) and 60 uL of the miR-30c precursor mimic (Thermofisher, USA) were diluted in 3.5 mL serum-free DMEM/F12 media. The reagents were mixed together at a 1:1 ratio and incubated for 5 minutes at RT. A 150 uL volume of diluted miR-30c precursor mimic/lipofectamine mixture was added to each well of the 12-well plate containing the diabetic and non-diabetic mouse CSCs. Similarly, 650 uL of the diluted miR-30c precursor mimic/lipofectamine mixture was added to each T25 flask. The transfected cells were then incubated at 37 °C for 72 hours before being analysed.

The transfectional efficiency of these cells was also measured by q-PCR analysis. Total RNA was first extracted from each CSC sample and quantified as described in Chapter 2, section

2.5. The concentrations and purity of these total RNA samples are described in Table A3.1 in Appendix 3. The q-PCR data was analysed using the $^{\Delta\Delta}$Ct method and samples were normalized to a U6 endogenous control. Fold changes were then calculated to determine the difference in miR-30c expression in total RNA derived from miR-30c-transfected CSCs compared to the scrambled controls. These fold changes were normalized to scrambled controls for both diabetic and non-diabetic samples to show the difference in miR-30c expression. A two-tailed t-test was also performed to determine the statistical significance ($P < 0.01$) of the fold changes in each condition.

6.2.3 Western blot analyses for VDAC1 and cleaved caspase-3 in transfected diabetic CSCs

A western blot analyses of VDAC1 was previously performed in Chapter 5, section 5.3.3 to validate the downregulated Nanostring expression profile of miR-30c in the diabetic CSCs. In this chapter, diabetic and non-diabetic mouse CSCs were overexpressed with miR-30c and western blot analyses were performed to confirm the direct inhibitory effect of miR-30c on the VDAC1 protein. Total protein was extracted from the T25 flasks containing diabetic (n=4) and non-diabetic CSCs (n=4) transfected with miR-30c precursor or scrambled control. The protein samples were quantified (concentrations described in Table A3.2 in Appendix 3) and western blot analyses were performed and analysed using the general protocol described in Chapter 2, section 2.8. The rabbit, polyclonal anti-VDAC1 (abcam, Australia) and rabbit, polyclonal anti-α-tubulin (abcam, Australia) were used as primary antibodies for the VDAC1 and α-tubulin antigens, respectively. The mouse anti-rabbit IgG (Sigma-Aldrich, NZ) was used as the secondary antibody. In this chapter, α-tubulin (50kDa) was used as an endogenous control instead of β-actin as used in the earlier chapter due to technical difficulties with the new β-actin antibody. The blots were repeated three independent times and the relative

expression of VDAC1 (31kDa) was determined for all samples by calculating the mean VDAC1/α-tubulin ratio. The data was expressed as a fold change by normalising the mean VDAC1 expression in miR-30c-transfected samples to the scrambled controls. The statistical significance ($P < 0.05$) of the data was then determined by a two-tailed unpaired t-test. A one-way ANOVA was also performed to determine the consistency of the results between repetitions.

Next, to determine the anti-apoptotic effect of miR-30c through repression of VDAC1, western blots were performed to measure the level of apoptotic marker cleaved caspase-3 (19kDa). A rabbit, polyclonal anti-Cleaved caspase-3 (Cell Signaling Technology, USA) and rabbit, polyclonal anti-α-tubulin (abcam, Australia) were used as primary antibodies for the Cleaved caspase-3 and α-tubulin antigens, respectively. The mouse anti-rabbit IgG (Sigma-Aldrich, NZ) was used again as the secondary antibody. The blots were repeated three times and α-tubulin was used as the endogenous control. The data was expressed as a fold change by normalising the mean cleaved caspase-3 expression in miR-30c-transfected samples to the scrambled controls.

6.2.4 Caspase 3/7 assay protocol

A caspase 3/7 assay was performed using the total protein extracted from the miR-30c or scrambled control transfected diabetic and non-diabetic CSCs (n=4 each). This assay allows for the detection of caspase-3 and -7 activity which is directly proportional to the amount of apoptosis within the cells (O'brien *et al*., 2005). A caspase-Glo 3/7 reagent (Promega, USA) was prepared by adding the Caspase-Glo 3/7 buffer to the Caspase-Glo 3/7 substrate and mixing well as outlined in the standardized protocol (Promega, 2018). The extracted total protein samples were quantified and added to a white, transparent 96-well plate at a concentration of 100 µg per well. The Caspase-Glo reagent was then added at a 1:1 ratio to

the volume of protein in each well and mixed with pipetting. Wells with RIPA (lysis) buffer alone were used as a blank measurement. The plate was then incubated in the dark at RT for 1 hour to allow for cell lysis and caspase cleavage. The luminescence of each well was finally measured using a luminometer to determine the caspase 3/7 activity. This caspase assay was repeated three times, and mean percentage fold changes were calculated from the relative differences in caspase activity in the diabetic and non-diabetic CSCs transfected with either miR-30c or scrambled control. A two-tailed t-test was then performed to determine the statistical significance ($P < 0.05$) of the fold changes. A one-way ANOVA was also performed to determine the consistency of the results between repetitions.

6.2.5 q-PCR for proliferation markers

Finally, to determine whether miR-30c enhances the proliferation capacity of the CSCs, a q-PCR was performed to determine the mRNA expression levels of common proliferation markers, Ki-67 and Topoisomerase-2α (Topo-2α). Both Ki-67 and Topo-2α are known to be highly expressed in all active phases (G1, S, and G2) of the cell cycle and for this reason were chosen as suitable markers for the purposes of this study (Ladsetin *et al*., 2010; Holden, 1999).

Forward and reverse (3' and 5') Taqman primers for Ki-67 and Topo-2α (Sigma-Aldrich, NZ) (Sequences in Appendix 7) were incorporated in the standard q-PCR procedure described in Chapter 2, section 2.6. Ribosomal protein L13A (Rpl-13a) was also used as an endogenous control due to its high level of expression in genes derived from mouse cardiac tissue (Everaert *et al*., 2011). The mRNA expression of these genes were thus determined from the total RNA derived from non-diabetic (n=4) and diabetic CSC samples (n=4). The q-PCR was repeated twice and mean fold changes of Ki-67 and Topo-2α were calculated across all

samples. The statistical significance ($P < 0.05$) of the data was then determined by a two-tailed t-test.

6.3 Results

6.3.1 Diabetic CSCs can be successfully transfected with miR-30c precursor mimic

After transfecting the diabetic and non-diabetic CSCs with the miR-30c and scrambled controls, the transfection efficiency was determined by performing q-PCR analysis. The q-PCR data showed that there was a significant and substantial increase in the expression of miR-30c in both diabetic (fold change of 1809, n=4, $P < 0.01$) and non-diabetic CSCs (fold change of 2332, n=4, $P < 0.01$) transfected with the miR-30c precursor mimic compared to the scrambled control for each condition (Fig. 6.1). There was also a reduction in miR-30c expression between diabetic and non-diabetic CSCs transfected with scrambled mimic (fold change of 0.71, n=4, $P < 0.01$). These results indicate that the transfection procedure was successful and that the concentration of miR-30c precursor mimic used (10 μM) is appropriate to elicit the overexpression of miR-30c in the CSCs. There was also a reduced expression of miR-30c in transfected diabetic CSCs compared to transfected non-diabetic CSCs, however this was not statistically significant ($P > 0.05$).

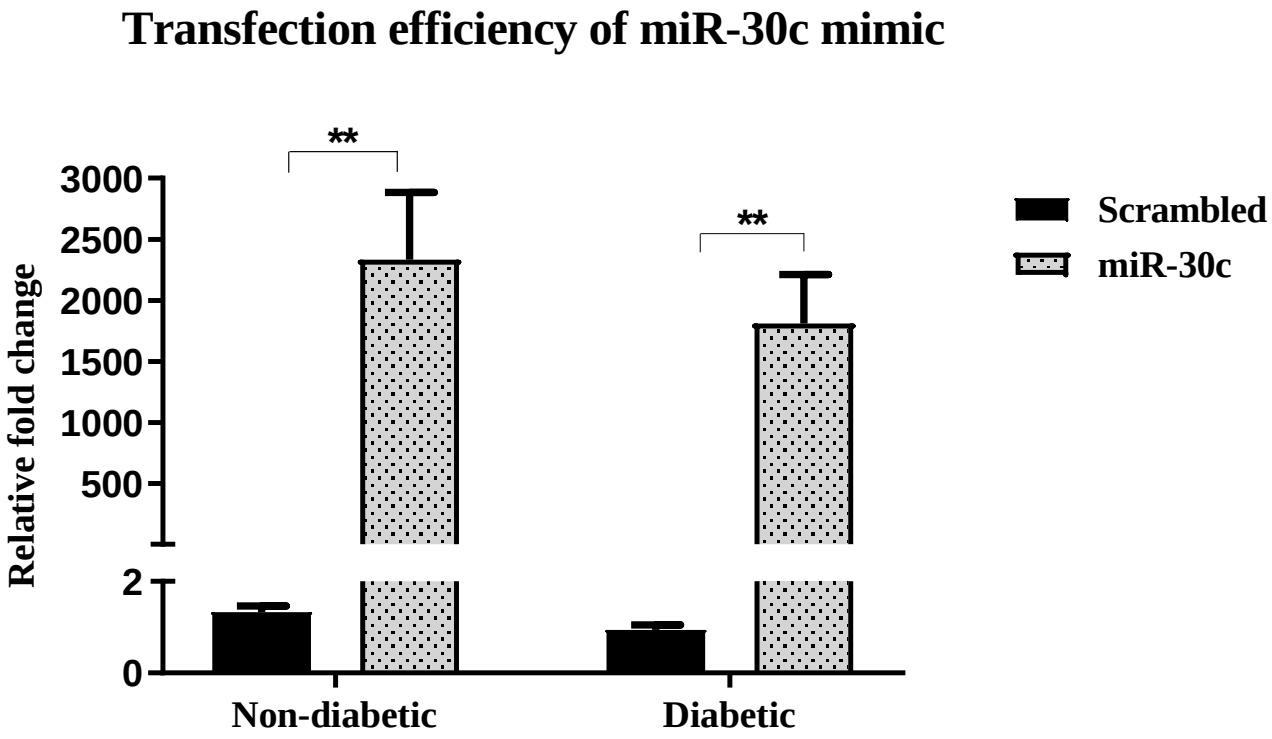

Figure 6.1. Quantitative bar graph data showing transfectional efficiency of the miR-30c mimic after its transfection into diabetic (n=4) and non-diabetic (n=4) CSCs. Performed in diabetic and non-diabetic samples to compare the stability of the mimic in both conditions. Data are means ± SEM. Significance (** = P<0.01) determined from two-tailed t-test.

6.3.2 VDAC1 was downregulated in the transfected diabetic CSCs

Western blot analyses were performed to determine the protein expression of the miR-30c target gene, VDAC1 (Fig. 6.2) and pro-apoptotic cleaved caspase-3 (Fig. 6.3) in both diabetic and non-diabetic CSCs (Fig. A8.2 in Appendix 8). A two-tailed unpaired t-test showed that miR-30c overexpression significantly reduced the expression of VDAC1 in miR-30c-transfected non-diabetic CSCs (0.75 ± 0.05, $n=4$, $P = 0.04$) and diabetic CSCs (0.71 ± 0.06, $n=4$, $P = 0.03$) compared to scrambled-transfected CSCs (Fig. 6.2). Furthermore, a one-way ANOVA showed no significant differences between repetitions in non-diabetic CSCs transfected with scrambled or miR-30 mimic ($F = 0.07$ and 1.12, respectively compared to $F_{crit} = 4.26$, $P > 0.05$), and similarly no significant differences between repititions in non-diabetic CSCs transfected with scrambled ($P > 0.05$, $F = 0.37$, $F_{crit} = 4.26$). However, there was a significant difference observed between repititions in the diabetic CSCs transfected with miR-30c mimic ($P < 0.05$, $F = 6.37$, $F_{crit} = 4.26$).

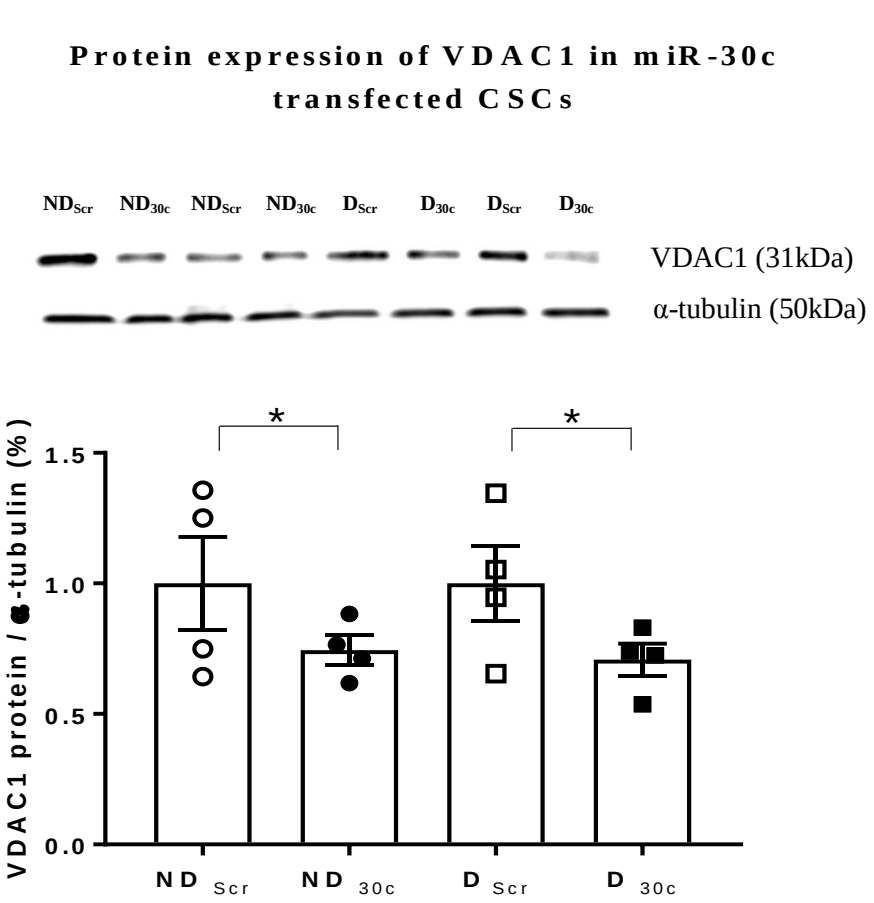

Figure 6.2. Representative immunoblots and quantitative data showing the protein expression of VDAC1 in non-diabetic (ND, n=4) and diabetic (D, n=4) CSCs transfected with either miR-30c mimic (30c) or scrambled control (Scr). Samples transfected with miR-30c mimic (ND_{30c} or D_{30c}) were normalized to either ND_{Scr} or D_{Scr}, respectively, and blots repeated three times. Data are means ± SEM. Significance (* = $P<0.05$) was determined by a two-tailed t-test.

6.3.3 Caspase-3 was downregulated in the transfected diabetic CSCs

The western blot analyses for cleaved caspase-3 expression exhibited a similar trend to VDAC1 expression in response to miR-30c overexpression in the diabetic CSCs (Fig. 6.3). The two-tailed unpaired t-test showed a significant reduction in the expression of cleaved caspase-3 in miR-30c-transfected diabetic CSCs (0.64 ± 0.10, $n=4$, $P = 0.04$) compared to scrambled-transfected diabetic CSCs (1.00 ± 0.14, $n=4$). However, despite significantly reducing VDAC1 expression, miR-30c transfection did not produce a similar reduction in cleaved caspase-3 expression in miR-30c-transfected non-diabetic CSCs (0.81 ± 0.17, $n=4$, $P=0.40$) compared to scrambled-transfected non-diabetic CSCs (1.00 ± 0.14, $n=4$) (Fig. 6.3). A one-way ANOVA showed no significant difference between repetitions in non-diabetic CSCs transfected with scrambled ($P > 0.05$, $F = 0.89$, $Fcrit = 4.26$), however there was a substantially significant difference in non-diabetic CSCs transfected with the miR-30 mimic ($P < 0.05$, $F = 8.27$, $Fcrit = 4.26$) which may have contributed to the non-significant t-test. There was no significant differences between repititions in the diabetic CSCs transfected with scrambled or miR-30c mimic ($F = 0.08$ and 1.82, respectively compared to $Fcrit = 4.26$, $P < 0.05$).

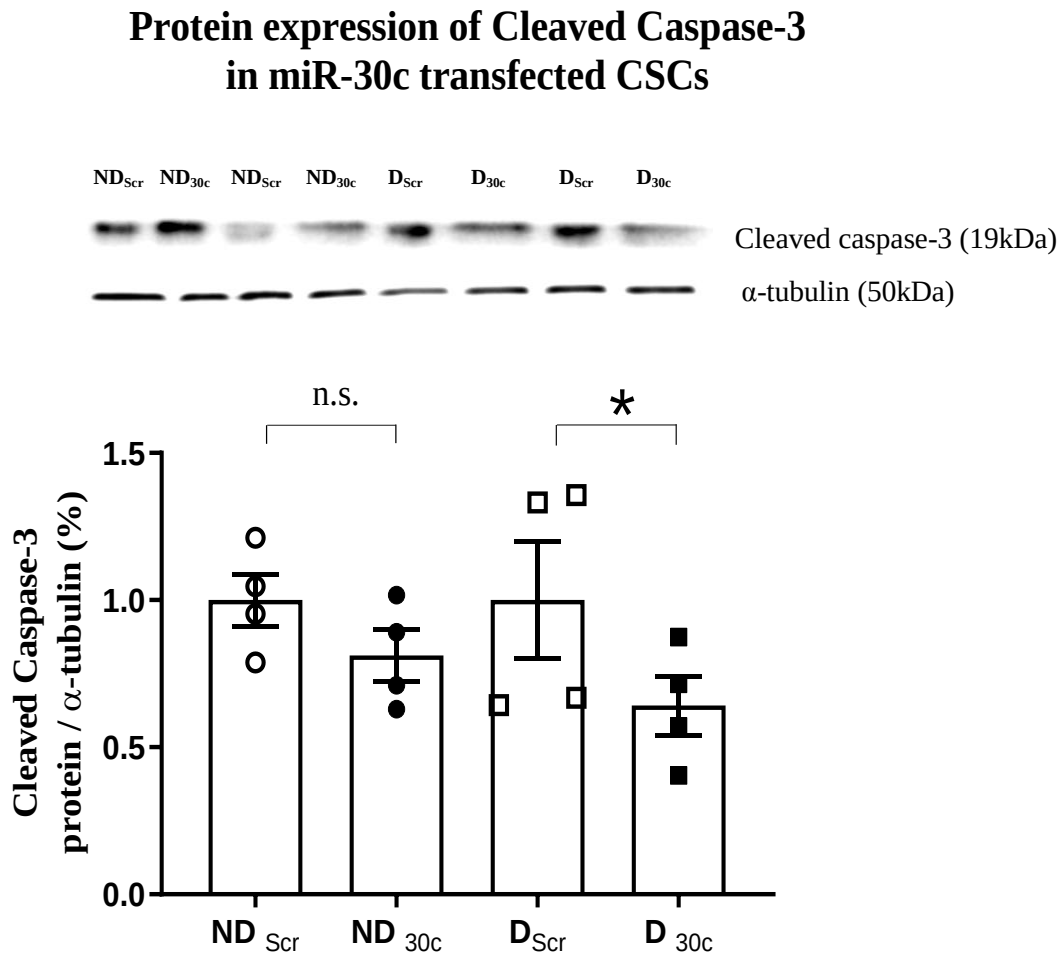

Figure 6.3. Representative immunoblots and quantiative data showing protein expression of Cleaved Caspase-3 in non-diabetic (ND, n=4) and diabetic (D, n=4) CSCs transfected with either miR-30c mimic (30c) or scrambled control (Scr). Samples transfected with miR-30c mimic (ND_{30c} or D_{30c}) were noramlized to either ND_{Scr} or D_{Scr} respectively, and blots repeated three times. Data are means ± SEM. Significance (* = $P<0.05$) determined by a two-tailed t-test. n.s. = non-significant.

As with the western blot analysis, the two-tailed unpaired t-test showed a significant reduction in the relative caspase 3/7 activity in the diabetic CSCs (0.62 ± 0.07, $n=4$, $P < 0.001$) that were transfected with the miR-30c precursor mimic compared to the scrambled control (1.00 ± 0.07, $n=4$) (Fig. 6.4). In the non-diabetic CSCs, although there was a reduction in caspase 3/7 activity in the CSCs transfected with the miR-30c precursor mimic (0.81 ± 0.10, $n=4$, this was not statistically significant ($P > 0.05$) (Fig. 6.4). A one-way ANOVA showed no significant differences between repititions in the non-diabetic CSCs transfected with scrambled or miR-30c mimic ($F = 0.92$ and 2.94, respectively compared to $Fcrit = 4.26$, $P > 0.05$), and similarly no significant differences between repititions in the diabetic CSCs transfected with scrambled or miR-30c mimic ($F = 2.50$ and 2.95, respectively compared to $Fcrit = 4.26$, $P > 0.05$). This data further supported the effect of miR-30c on caspase expression in the diabetic CSCs.

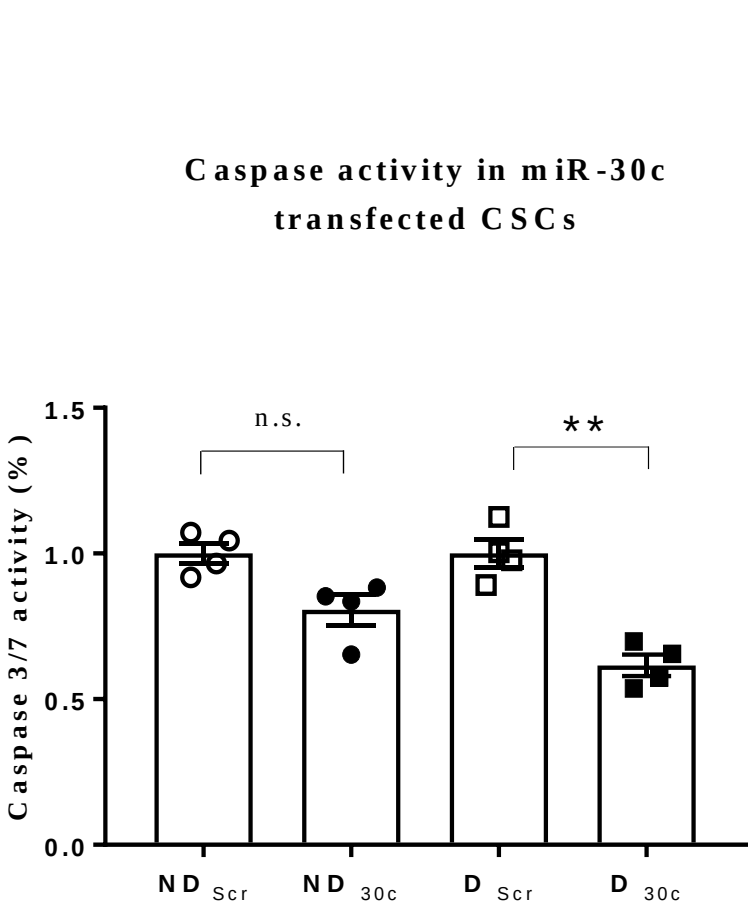

Figure 6.4. Quantitative data showing caspase 3/7 activity in total protein transfected from non-diabetic (ND) (n=4) and diabetic (D) CSCs (n=4) transfected with either miR-30c (30c) or scrambled control (Scr). Samples transfected with miR-30c mimic (ND_{30c} or D_{30c}) were normalized to either ND_{Scr} or D_{Scr}, respectively, and the assay was repeated three times. Data are means ± SEM. Significance (** = $P<0.01$) determined by a two-tailed t-test. n.s. = non-significant.

6.3.4 MiR-30c does not regulate CSC proliferation

The q-PCR to determine differential expression of proliferation markers (Ki-67 and Topo-2α) showed no statistically significant differences ($P > 0.05$) between diabetic or non-diabetic CSCs transfected with the miR-30c precursor mimic. Although not significant, a small increase in Ki-67 expression was found in miR-30c-transfected diabetic CSCs (1.12 ± 0.23, $n=4$, $P=0.62$) compared to scrambled-transfected diabetic CSCs (1.00 ± 0.03, $n=4$). There was also similar increase in Ki-67 expression in the non-diabetic CSCs (1.28 ± 0.34, $n=4$, $P=0.66$) compared to scrambled-transfected non-diabetic CSCs (1.11 ± 0.20, $n=4$) (Fig. 6.5). There was no substantial difference in Topo-2α expression in miR-30c-transfected diabetic (1.03 ± 0.09, $n=4$, $P=0.99$) and non-diabetic (1.07 ± 0.14, $n=4$, $P=0.79$) CSCs compared to the scrambled-transfected control (Fig. 6.5). Taken together, these results suggest that miR-30c does not play any role in CSC proliferation.

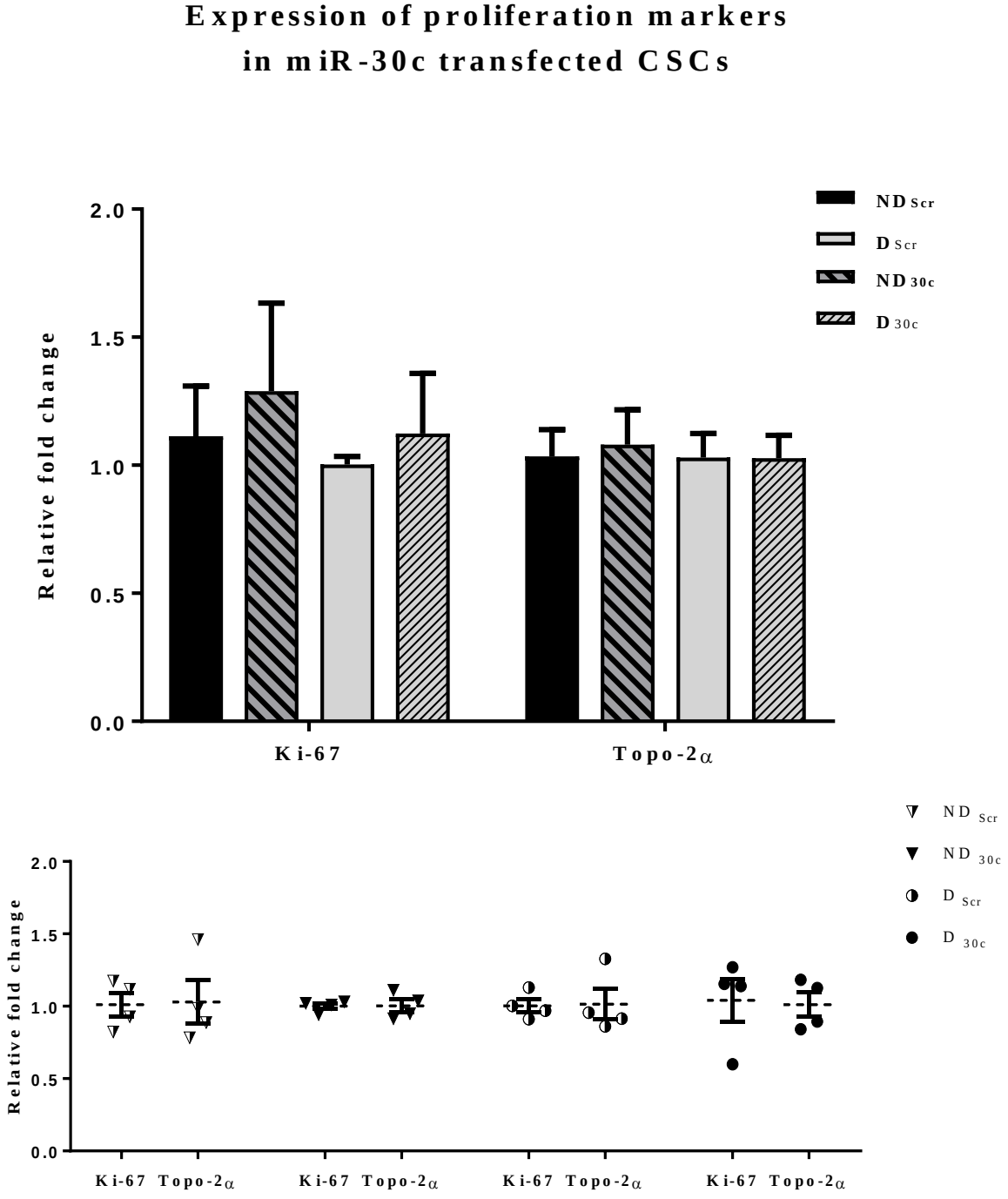

Figure 6.5. Quantitative data (bar graph and representative scatter plot) showing no significant change in expression of Ki-67 and TOP2A proliferation markers in non-diabetic (n=4) and diabetic CSCs (n=4) transfected with either miR-30c (ND_{30c}, D_{30c}) or scrambled control (ND_{Scr}, D_{Scr}). Data are means ± SEM. Statistical significance ($P<0.05$) was determined by a two-tailed t-test.

6.4 Discussion

6.4.1 Summary of results

The findings of this chapter have shown the first pieces of evidence that miR-30c has a functional role in diabetic CSCs. This was determined from a series of mechanistic experiments in which diabetic and non-diabetic CSCs were initially transfected with a miR-30c precursor mimic and compared to a scrambled control. Western blot analyses revealed VDAC1 total protein to be significantly downregulated in miR-30c-transfected diabetic and non-diabetic CSCs compared to the control. Due to the fact that VDAC1 is a pro-apoptotic gene, this finding was further supported by a downregulation in Cleaved caspase-3 total protein, as well as a reduction in caspase 3/7 activity in miR-30c-transfected diabetic CSCs. These results suggest that overexpression of miR-30c has a role in reducing the apoptosis of diabetic CSCs, which may be mediated by the targeted-inhibition of the VDAC1 gene. My results also showed that miR-30c is not involved in regulating CSC proliferation as there were no significant differences in the expression of proliferation markers, Ki-67 and Topo-2α in the transfected CSCs.

6.4.2 MiR-30c overexpression in diabetic and non-diabetic CSCs

The initial q-PCR results showed a significantly large increase in the expression of miR-30c in CSCs transfected with the miR-30c precursor mimic compared to scrambled controls. This result therefore validated the transfection procedure used for overexpressing miR-30c in the CSCs. Moreover, it confirmed that the concentration of the mimic used (10 μM) was appropriate to establish the overexpression of miR-30c in mouse CSCs. This correlates with the work of other studies that have used miR-30c precursor mimics for transfection experiments (Kong *et al*., 2014). Interestingly, the relative miR-30c expression in the miR-30c-transfected CSCs was also lower in the diabetic CSCs than the non-diabetic CSCs. This

therefore indirectly supports the original Nanostring microarray data which showed reduced expression of miR-30c in the diabetic CSCs compared to the non-diabetic CSCs.

6.4.3 MiR-30c downregulates VDAC1 in diabetic and non-diabetic CSCs

In both diabetic and non-diabetic conditions, VDAC1 total protein expression was significantly reduced in the CSCs transfected with the miR-30c precursor mimic compared to the scrambled controls. This result supported the results of the luciferase assay, indicating VDAC1 as a direct target of miR-30c. It also strengthens the mass spectrometry and western blot data (Chapter 5, section 5.3.1 and 5.3.3) suggesting that miR-30c regulates the translation of VDAC1. VDAC1 triggers apoptosis by causing the release of cyctochrome C in the mitochondria and subsequent accumulation of ROS (Baumgartner *et al*., 2009). Based on my results, I can infer that if miR-30c downregulates VDAC1 expression, it may also limit apoptosis in the CSCs, providing the first indications that miR-30c has a pathophysiological role in the CSCs.

The majority of the research conducted on VDAC1 as a viable miRNA target has been associated with neuronal development. Chaudhuri *et al*. showed that miR-7, which has been found to be protective in cellular models of Parkinson's disease, also reduces neurodegeneration by targeting VDAC1 in human neuroblastoma cells. The overexpression of miR-7 in these cells also caused a reduction in cytochrome C release and ROS generation, which is consistent with the apoptotic function of VDAC1 (Chaudhuri *et al*., 2016). In another study, Roshan *et al*. showed that the brain-specific miR-29a targets VDAC1 in the hippocampus and cerebellum of mice. Knocking down miR-29a in mouse brains causes a large increase in cell death that has been attributed to the elevated levels of VDAC1 (Roshan *et al*., 2014). These studies support the notion that the apoptotic function of VDAC1 can be regulated by miRNAs.

6.4.4 MiR-30c inhibits apoptosis in diabetic CSCs by downregulating VDAC1

Transfection of the CSCs with the miR-30c precursor mimic significantly reduced the expression of cleaved caspase-3 in diabetic CSCs. This reduced caspase-3 expression also correlated with the reduction of VDAC1 previously observed in the miR-30c-transfected diabetic CSCs. The relative difference in caspase-3 expression between the CSCs transfected with miR-30c and scrambled controls was less in the non-diabetic CSCs than in the diabetic CSCs. This may be due to the VDAC1 channel being more active in the diabetic state, although further experiments are required to confirm this notion. The caspase 3/7 assay exhibited a similar trend to the western blots for cleaved caspase-3 in terms of the ability of miR-30c to regulate apoptosis. There was a significant reduction in caspase 3/7 activity in diabetic CSCs transfected with the miR-30c precursor mimic compared to the scrambled controls. Cleaved caspase-3 protein and caspase 3/7 activity were also reduced in the miR-30c-transfected non-diabetic CSCs, although in both cases the data was not significant. These findings strongly suggest that not only does miR-30c reduce the apoptosis of diabetic CSCs, but that the mechanism behind it involves the targeted inhibition of VDAC1.

The effect of miR-30c on apoptosis has previously been investigated in other cell lines showing differential regulation depending on the cell type. For instance, Du and co-workers added cisplatin to the renal tubular cell lines, HK-2 and NRK-52E. They observed a subsequent reduction in miR-30c expression in response to the drug. Manipulating the expression of miR-30c in these cells using miR-30c precursor mimics and inhibitors caused a miR-30c-dependent change in apoptosis. The mechanism behind this was attributed to the targeted-inhibition of the pro-apoptotic genes, HSPA5 and BNIP3L. The expression of both target genes were reduced after miR-30c overexpression, while the expression of the genes were increased after knocking down miR-30c in the cells (Du *et al.*, 2017). This suggested that miR-30c is able to regulate renal tubular cell apoptosis; a finding that could potentially be used in the treatment of cisplatin-induced nephrotoxicity. However, despite a clear indication

that miR-30c regulates apoptosis in many cell lines, contradicting evidence has been noted in several cancer studies. Knock down of miR-30c in a human ovarian cancer cell line (A2780) suppressed cisplatin-induced apoptosis, while miR-30c was also found to induce apoptosis in a human myeloma cell line (H929) (Han *et al*., 2017; Zhao *et al*., 2014). These results support the reputation of miR-30c as a tumour suppressor, however there is no clear understanding as to why cancer reverses its effect on apoptosis.

Although the role of miR-30c has not yet been characterized within CSCs, seminal evidence indicate that miR-30c may have a pro-survival effect in the heart. In a recent study, Liu and co-authors showed an increase in apoptosis after knocking down miR-30c in myocardial P19 cells. In contrast, miR-30c overexpression caused a subsequent increase in the proportion of P19 cells despite using the same serum starvation treatment to stimulate apoptosis (Liu *et al*., 2016). This indicates that miR-30c can also inhibit other proteins in myocardial cells that regulate apoptosis.

6.4.5 MiR-30c does not regulate CSC proliferation

Several studies have suggested a regulatory role of miR-30c in cell proliferation. These studies have shown that miR-30c promotes the proliferation of myocardial cells in *in vivo* rat models of MI and heart failure, indicating the potential of miR-30c to prevent cardiac dysfunction (Gambacciani *et al*., 2013; Duisters *et al*., 2009). This was supported by Liu and co-authors who showed that miR-30c overexpression in myocardial P19 cells increased cell growth, whereas downregulation of miR-30c had the opposite effect. The authors also discovered that an elevated proportion of miR-30c-overexpressing cells were in the S phase of the cell cycle, indicating that miR-30c is involved in promoting cell cycle progression. (Liu *et al*., 2016). Similar effects were documented in other stem cell subtypes. For instance,

overexpressing mouse neural stem cells (NSC) with miR-30c was found to promote proliferation and neural sphere formation (Sun *et al*., 2016; Chao *et al*., 2015).

However, in contrast with these findings, the results of my study failed to show any significant change in the expression of proliferation markers, Ki-67 and Topo-2α after miR-30c overexpression in both diabetic and non-diabetic CSCs. This may be due to the difference in stem cell type (NSCs vs CSCs) as miRNAs have been found to have opposing effects on proliferation in other stem cells. This is evident for miR-378 which promotes proliferation when overexpressed in mesenchymal cells, but suppresses proliferation when overexpressed in NSCs (Huang *et al*., 2015; Xing *et al*., 2014). Furthermore, other studies have not yet shown miR-30c to regulate the proliferation of primary mouse CSCs. This is an important distinction as primary cells can differ genetically and phenotypically to cell lines derived from a homogenous tissue source (Unger *et al*., 2002).

6.4.6 The effect of diabetes on miR-30c apoptotic function

Diabetes is commonly known to promote apoptosis of pancreatic β-cells, leading to the development of insulin deficiency (Lee and Parvaiz, 2006). However, it also promotes the apoptosis of CSCs and cardiomyocytes, triggering the development of DCM (Ouyang *et al*., 2014). My results suggested that miR-30c may inhibit the apoptosis of diabetic CSCs by targeting VDAC1. This indicates that genetic manipulation of miR-30c may be a viable strategy to regulate CSC survival in the diabetic heart. It was also noted that miR-30c did not cause a significant change in the apoptosis of non-diabetic CSCs. The reason for this may be that there is a greater proportion of VDAC1 channels in the diabetic CSCs as observed from the western blot in Chapter 5, section 5.3.3. This would mean that miR-30c may have a greater impact on the functionality of VDAC1 in the diabetic state, as the inhibition of more channels would exponentially reduce the release of cytochrome C and ROS and hence

apoptosis. Another theory is that hyperglycemia may increase the opening of the VDAC1 channel in the diabetic CSCs. There have indeed been reports indicating that the high glucose treatment of endothelial cells *ex vivo* increases the opening time of the mitochondrial permeability transition pore, which comprises the VDAC1 channel (Detaille *et al*., 2005). The opening time of the mitochondrial permeability transition pore is directly correlated with the apoptotic potential of the channel (Pangare and Makino, 2012).

6.4.7 Summary

In this chapter, I have shown that miR-30c overexpression reduces apoptosis in diabetic mouse CSCs by downregulating VDAC1. This answers my second overall objective that certain miRNAs can exhibit a pathophysiological role that relates to their differential expression in diabetic CSCs. It also suggests that the genetic modification of miR-30c may be a potential therapeutic strategy to improve diabetic CSC survival. However, these results need to be replicated in the human CSCs to understand the clinical translation of these findings. This notion will be the focus of the following chapter.

CHAPTER 7: TRANSLATION INTO HUMAN CSCS

7.1 Introduction

Thus far I have shown that diabetes alters the expression of miR-329, -376c, -495 and -30c (candidate miRNAs) in CSCs in mice. I have also demonstrated the functional consequences for miR-30c dysregulation in diabetes, suggesting that miR-30c could be a potential target to improve the functional efficacy of diabetic CSCs. The next important question is whether this altered expression in mice can be translated to human CSCs. In this chapter, I will therefore describe how the expression of the candidate miRNAs were determined in human CSCs. I will describe the differences in the isolation procedure of the CSCs from human heart tissue, followed by FACS characterization and qPCR analysis to determine miRNA expression in the human CSCs.

7.1.1 Aims and objectives

The aim for this chapter is to determine the expression of miR-329, -376c, -495 and -30c in diabetic and non-diabetic human CSCs, and observe whether these results correlate with their expression in the mouse CSCs.

7.1.2 Comparisons between mouse and human CSCs

As in the mouse heart, a population of resident CSCs also exists in the human heart with self-renewing capabilities (Yadav and Mishra., 2018). Studies have indicated that human CSCs are functionally identical to those found in mice in that they have the potential to differentiate into adult cardiomyocytes (Ching *et al*., 2011; Bearzi *et al*., 2007; Oh *et al*., 2003). This

function can also contribute towards the regeneration of myocardial tissue. In response to myocardial injury, the CSCs migrate to the damaged site where they promote tissue repair by replacing the dead cardiomyocytes (Bearzi *et al*., 2007). Unlike the Sca-1^+ CSCs that were characterized in mice, the primary marker for identifying human CSCs was originally c-kit until one study disproved this marker as being purely specific for CSCs (Sultana *et al*., 2015). More recently, human CSCs have been found to express high levels of the MSC surface markers such as CD105, CD90, CD29, CD73 and CD71. This may be due to the fact that the CSCs exhibit a mesenchymal cell-like phenotype, despite being specifically programmed to differentiate into cells of cardiovascular lineage (Tateishi *et al*., 2007). Stromal cells that are phenotypically similar to Sca-1 were also found to express CD105 and CD90 in the human heart (Ryzhov *et al*., 2012). For this reason, the identity of human CSCs in this project was determined using specific antibodies that bind to the CD105 and CD90 antigen. There has not been much documented on the difference in CSC growth between human and mouse origins. However, previous experiments in the Katare lab have revealed a similar morphology and growth rate for the human and mouse CSCs (Katare *et al*., 2013).

7.1.3 Therapeutic implications of miRNA expression in human CSCs

A variety of different miRNA subtypes have been identified within human CSCs. These miRNAs target the genes within signaling pathways that regulate CSC proliferation, differentiation and survival. Genetic manipulation of such miRNAs may therefore have therapeutic implications in regenerating cardiac tissue in response to ischemic injury. My results have thus far shown that diabetes induces alterations in the expression profiles of the candidate miRNAs in mouse CSCs. Furthermore, miR-329, -376c and -495 are known to be functionally conserved across mouse and human species (Wang *et al*., 2017; Clark and Naya, 2015; Piriyapongsa *et al*., 2014). It is therefore plausible that the altered expression pattern of

the candidate miRNAs may be similar in diabetic human CSCs; and if so, it would take us one step closer to understanding the therapeutic potential of the candidate miRNAs in a clinical setting. The aim of this Chapter was therefore to replicate the altered expression of miR-329, -376c, -495 and -30c in diabetic human CSCs.

7.2 Methods

7.2.1 Collection of human heart tissue

Right atrial appendage (RAA) biopsies were obtained from six patients (three diabetic, three non-diabetic) undergoing on-pump coronary artery bypass surgery at the Dunedin Hospital. Full written and verbal consent was given by the patients to donate the RAA tissue for research purposes. The age of the patients was between 54 and 75 years old (patient information described in Table A10 in Appendix 10). The biopsies were collected from the hospital in vials containing sterile Krebs Ringer HEPES buffer solution (KRH) (Table A1.1 in Appendix 1) and kept at 4 °*C*. The samples were then taken to the Katare laboratory for processing. The RAA biopsies were 100-300 mg in weight and 1-2 inches in length.

7.2.2 Isolation procedure for human CSCs

Once the RAA biopsies were collected, they were cut into small pieces with surgical scissors after trimming away any epicardial fat tissue. To keep the tissues fresh as well as to increase the viability of the cells, all human CSC samples were processed within 1 hour of tissue collection. The same isolation procedure that was used to isolate mouse CSCs in Chapter 2, section 2.3.1 was also used to isolate the human CSCs from the RAA tissue. After digesting the CSCs chemically with the collagenase solution and mechanically with repeat-pipetting, the cell suspension was centrifuged at 1400 rpm for 5 minutes and re-suspended in 1 mL

DMEM/F12 media in T25 flasks. The human CSCs were passaged to P5 in T75 flasks. One T75 flask was then split into two T25 flasks at P6. The T25 flasks was frozen, until re-initiated for FACS (described below). The other T75 flask was plated into three wells of a six-well plate and grown to confluency, after which the total RNA was extracted from each well for q-PCR.

7.2.3 Flow cytometry protocol

FACS was performed to characterize the isolated human CSCs. Using the protocol from Chapter 2, section 2.4, three human diabetic and three human non-diabetic CSC samples were re-initiated at P6 and grown until confluent. CD105 and CD90 MSC markers were used as the primary expression markers to validate the cells as CSCs. The common HSC marker, CD34 was also included to eliminate circulating stem cells from the cell population. Circulating stem cells are those which migrate to the heart and are functionally different to the resident stem cells (Dominici *et al*., 2006). Fluorophore-conjugated anti-human monoclonal antibodies (eBiosciences, USA) specific for CD105, CD90 and CD34 were diluted to 1:50 concentration with FACS buffer, as indicated in Table A1.2 in Appendix 1. The CSCs were trypsinized and prepared (1×10^6 cells/mL) as described in Chapter 2, section 2.4.1. Following acquisition, the FACS data was analysed using FlowJo 10.0 software to determine the proportions of CD105, CD90 and CD34 in the stained and unstained samples. The CSC samples were quantified ($2.8 - 4.2 \times 10^6$ cells/mL) using a hemacytometer and further analysed to determine the proportion of cells that stained positive for both CD105 and CD90 within the CD34 negative cell population.

7.2.4 q-PCR protocol

A q-PCR was performed to determine the expression of the miRNAs in the diabetic (n=3) and non-diabetic CSCs (n=3) using the protocol described in Chapter 2, section 2.6. After quantifying total RNA from each sample, the qPCR was performed in triplicate using miRNA-specific R.T and PCR primers for miR-329, -376c, -495 and -30c. The raw PCR data was then analysed by determining the mean fold change of the miRNA expression in the diabetic CSCs (using the $2^{\Delta\Delta Cq}$ method) after normalising the data to the non-diabetic CSCs. The q-PCR was repeated three times using the same samples and a two-tailed t-test was used to determine the statistical significance ($P < 0.05$ or $P < 0.01$) of the mean fold changes between diabetic and non-diabetic CSCs. A one-way ANOVA and Kruskal Wallis H t-test were performed to determine the consistency of the results between the repetitions.

7.3 Results

7.3.1 Human CSCs exhibited similar morphology to mouse CSCs

The human CSCs exhibited the same elongated, spindle shaped morphology as the mouse CSCs. However, they grow faster as they took only 2-3 days to reach P1 after their initial isolation compared to the mouse CSCs which took one week to reach the P1 stage. There was no observable change in the growth rate of the diabetic and non-diabetic human CSCs. Moreover, the number of human CSCs in each sample were similar to the mouse CSCs once confluency was achieved.

7.3.2 Human CSCs exhibited MSC markers

The FACS data showed that both diabetic (98 ± 1%) and non-diabetic CSCs (98 ± 2%) expressed a very high level of CD105. CD90 was moderately expressed in both diabetic (64 ±

10%) and non-diabetic CSCs (67 ± 8%). Moreover, further analysis showed that CSCs positive for both CD90 and CD105 were highly expressed in the diabetic population (80 ± 10%), as well as the non-diabetic (80 ± 9%) population (Figs. 7.1 and 7.2). Finally, the CD34 expression was extremely low with only 11 ± 7% in the diabetic CSCs and 14 ± 8% in the non-diabetic CSCs, confirming that the majority of cells isolated from the heart tissue were resident CSCs. The high expression of CD105, along with the low expression of CD34 in the cell population is strongly indicative of a CSC phenotype.

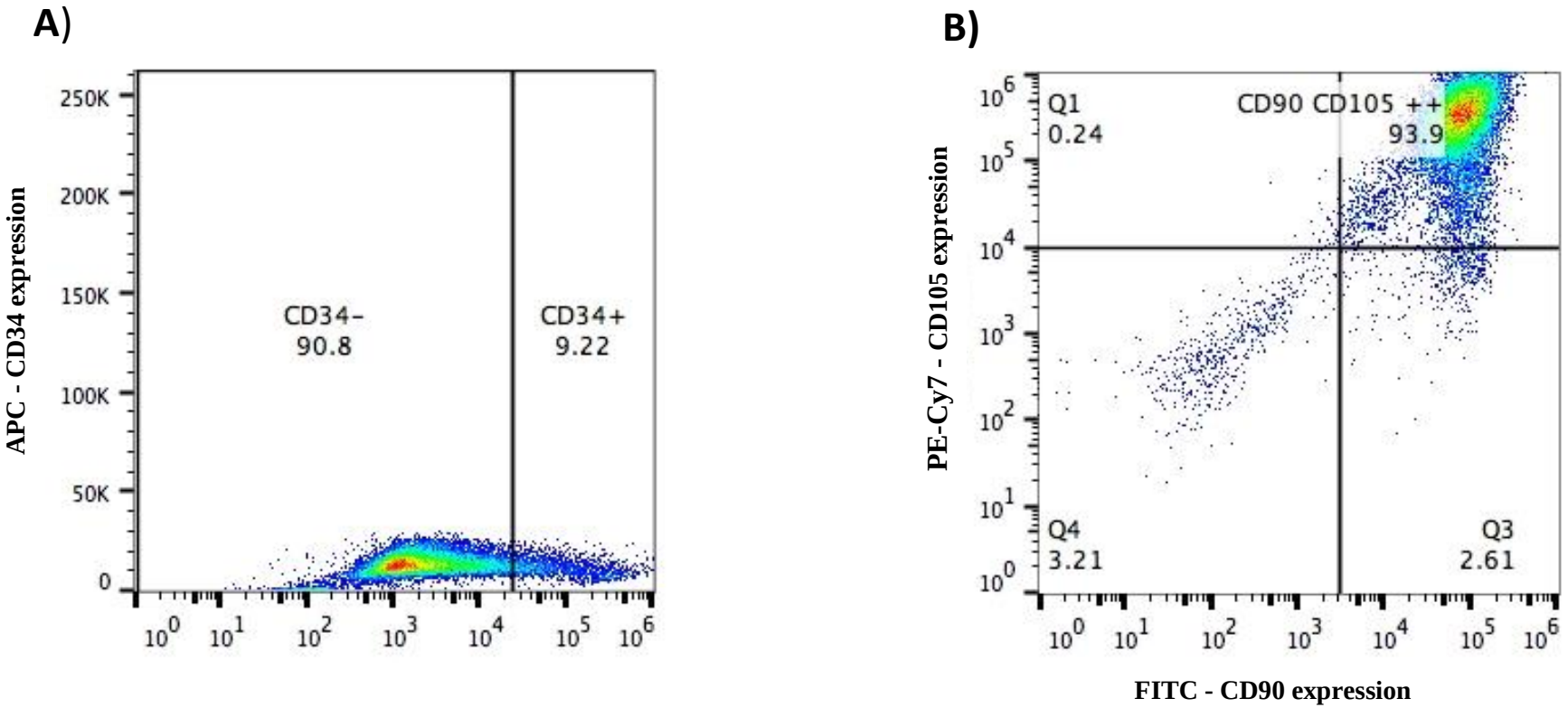

Figure 7.1. Flow cytometric scatter data showing the expression of CD105 and CD90 MSC markers (conjugated to PE-Cy7 and FITC fluorophores, respectively) among CD34$^-$ CSCs in one representative human non-diabetic CSC sample. CD34 (conjugated to APC fluorophore) was included to exclude the circulating stem cells. The expression of each marker is presented as a percentage within the CSC population of each sample. The proportion of CSCs that express CD34 is shown on the left panel (A), while the proportion of CSCs that express both CD105 and CD90 is shown on the upper right quadrant of the right panel (B).

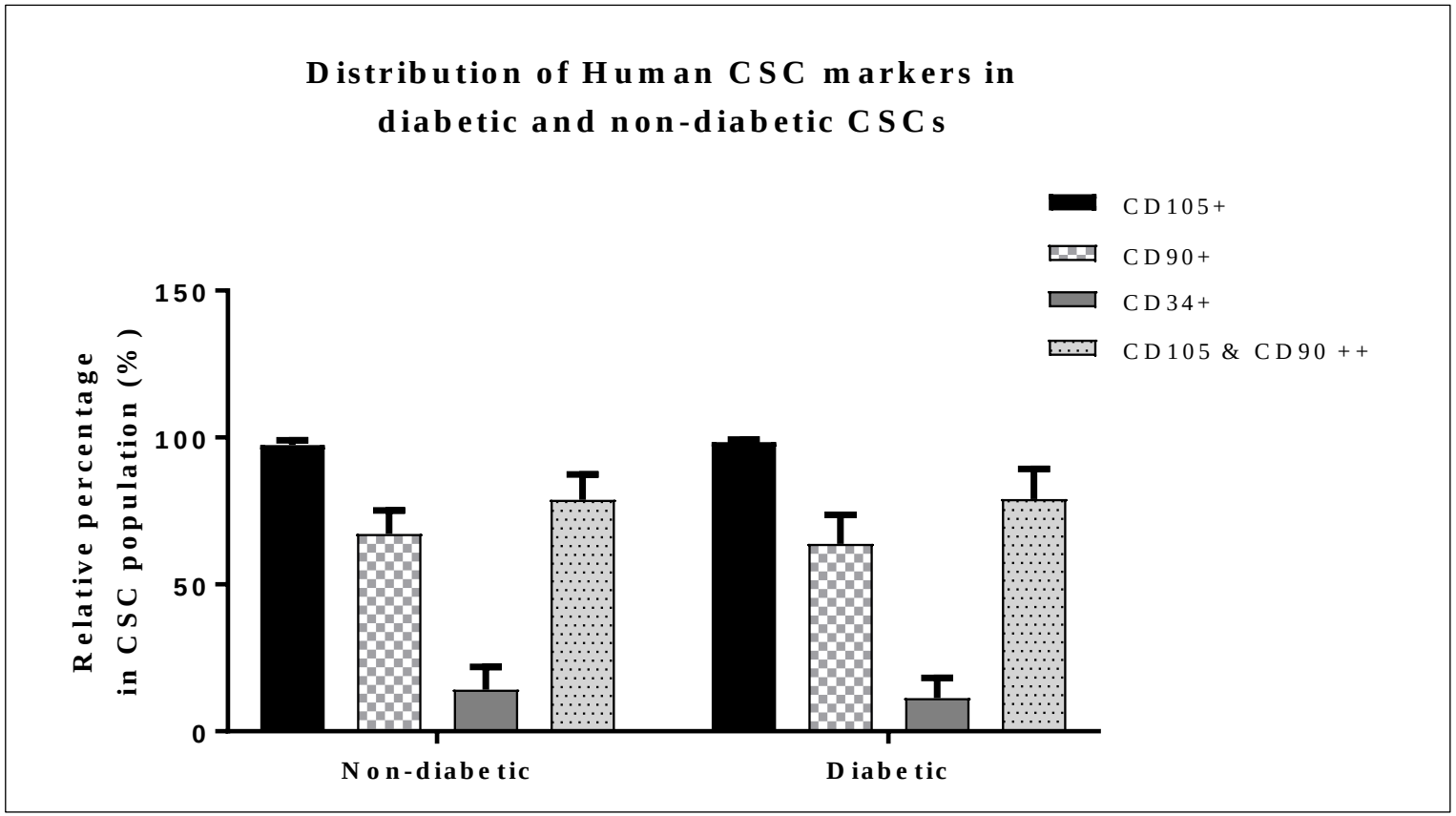

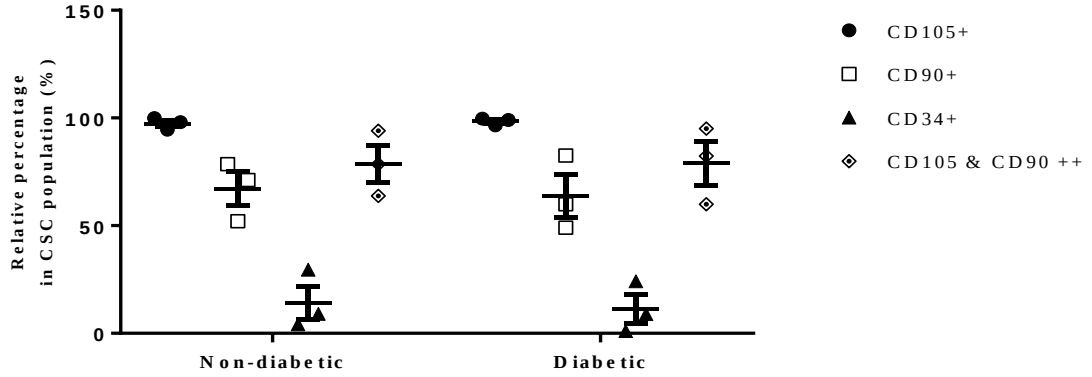

Figure 7.2. Quantitative bar graph and scatter plot showing the relative distribution of CD105, CD90 human CSC markers, as well as the CD34 marker (negative control) in human diabetic (n=3) and non-diabetic CSCs (n=3). The proportion of CSCs expressing both CD105 and CD90 are also shown in the graph. Data are means ± SEM.

7.3.3 Diabetes induced similar alterations to target miRNAs in human CSCs

After analysing the q-PCR data with a two-tailed unpaired t-test, the results showed a significant alteration in the expression of miR-376c, -495 and -30c in diabetic CSCs compared to the non-diabetic CSCs, while miR-329 expression remained unaltered (Fig. 7.3). MiR-376c (1.65 ± 0.03 in diabetic vs. 1.00 ± 0.03 in non-diabetic, $P < 0.05$) and -495 (1.43 ± 0.19 in diabetic vs. 1.01 ± 0.03 in non-diabetic, $P < 0.05$) expression was upregulated in the diabetic CSCs compared to their expression in the non-diabetic CSCs. MiR-329 exhibited a similar level of expression in both diabetic (1.07 ± 0.23) and non-diabetic CSCs (1.00 ± 0.04). Similar to its expression in mouse CSCs, miR-30c was significantly downregulated in the diabetic CSCs (0.84 ± 0.03) compared to the non-diabetic CSCs (1.00 ± 0.03). The mean fold change of miR-30c was also statistically more significant among the four miRNAs.

A one-way ANOVA showed no significant differences between the repetitions of each q-PCR for miR-329, miR-376c, miR-495 and miR-30c expression in either non-diabetic ($F = 1.25$, 0.07, 0.47 and 0.03, respectively compared to $F_{crit} = 5.14$, $P > 0.05$) or diabetic groups ($F =$ 1.16, 1.51, 1.07 and 1.70, respectively compared to $F_{crit} = 5.14$, $P > 0.05$). This consistency was also confirmed by the Kruskal Wallis H test which showed no significant differences between the repetitions for miR-329, miR-376c, miR-495 and miR-30c expression in either non-diabetic ($H = 1.87$, 0.09, 0.27 and 0.09, respectively compared to $H_{crit} = 5.99$) and diabetic groups ($H = 4.22$, 2.76, 1.69 and 1.16, respectively compared to $H_{crit} = 5.99$).

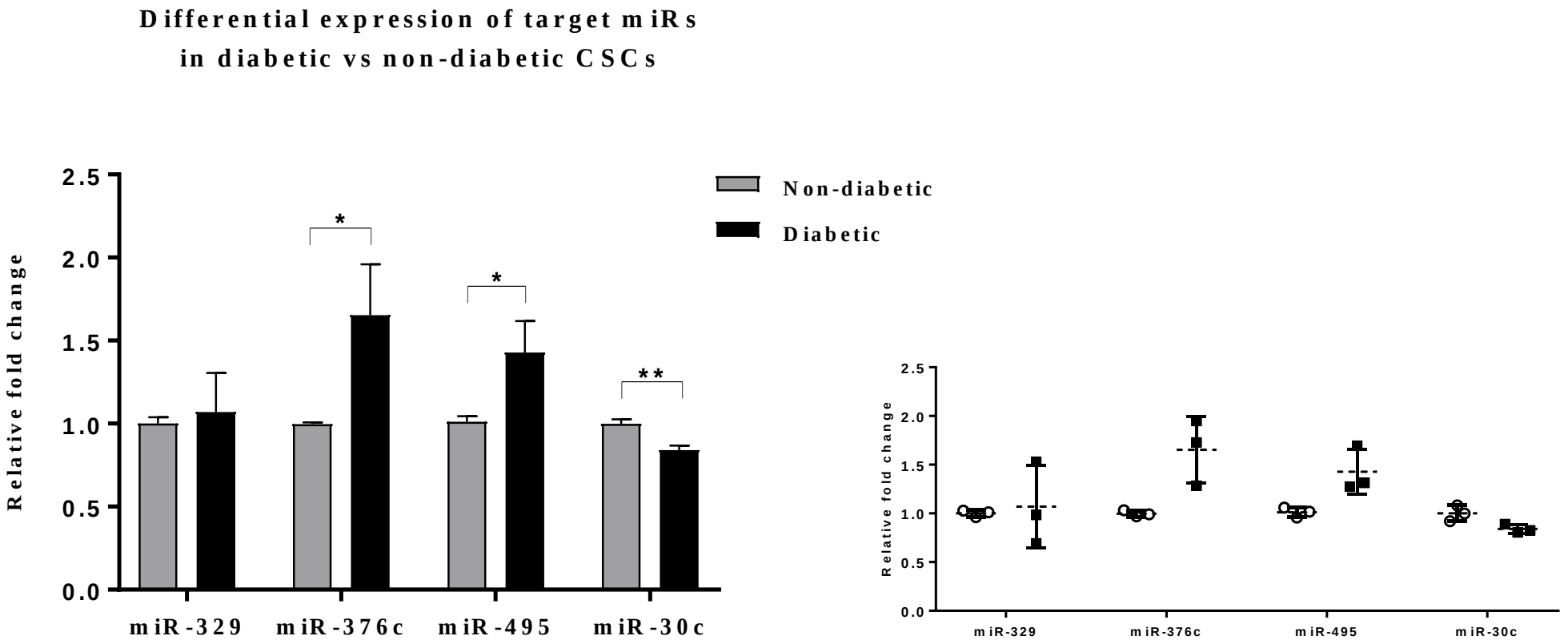

Figure 7.3. Quantitative data depicting the significantly altered expression of miRs -329, -376c, -495 and -30c in human diabetic (n=3) and non-diabetic CSCs (n=3). The q-PCR was performed three times using the same samples and a mean fold change was subsequently calculated for each miRNA. Data are means ± SEM. A two-tailed t-test was performed to determine significant data (* = $P<0.05$ or ** = $P<0.01$).

7.4 Discussion

7.4.1 Summary of results

In this chapter, I examined the differential expression of the candidate miRNAs (miR-329, -376c, -495 and -30c) in diabetic human CSCs. Using FACS, I first showed that the human CSCs that were used in these experiments were pure and expressed high levels of the well-accepted MSC markers. I then demonstrated that the expression profiles of three out of the four candidate miRNAs were altered in the diabetic human CSCs. While more experiments are required with a larger number of samples, the results from this chapter indicate the translational potential of my mouse CSC data. These results also provide a solid foundation for future studies to determine the functional implications for miRNAs in diabetic CSCs. Moreover, they indicate whether miR-30c may be a potential target in a clinical setting.

7.4.2 Human CSC validation

The diabetic and non-diabetic human CSC populations contained a very high proportion of cells positive for both CD105 and CD90 markers, as well as a very low proportion of cells positive for the CD34 marker. The relative distribution of these markers suggest that the population of cells isolated from the RAA tissue are mainly resident CSCs. The expression of individual markers within the diabetic and non-diabetic CSCs were also consistent with other studies that have used CD105 and CD90 to characterise human CSCs and CPCs (Gambini *et al*., 2011; Mishra *et al*., 2011; Tateishi *et al*., 2007). For instance, Gambini *et al*. found a similar distribution of high CD105 (98%) expression in human CPCs (Gambini *et al*., 2011), while Tateishi *et al*. found that mouse CPCs also exhibited a moderate expression (68%) of CD90 (Tateishi *et al*., 2007). These studies correlated with the relative distribution of the markers in this study, as CD105 was expressed in 98% of CSCs in both diabetic and non-diabetic CSC populations, while CD90 was expressed in moderate proportions of 64% and

67% in the diabetic and non-diabetic CSC population, respectively. Other studies reported an absence of the CD34 marker in human CSCs, which correlated with the extremely low proportions of CD34 in the diabetic and non-diabetic CSCs (Oh *et al*., 2003). Nonetheless, the presence of a CD34 positive population in my cell preparation is inevitable as the heart tissue was donated from patients who previously had ischemic heart disease, and it is well known that circulating stem cells migrate to the site of injury (Xu and Li, 2014; Rennert *et al*., 2013).

7.4.3 Differential miRNA expression in human CSCs

The q-PCR results showed that the expression profiles of miR-376c, -495 and -30c were significantly altered in the diabetic human CSCs. Notably, the expression patterns of these miRNAs were also similar to their differential expression in the diabetic mouse CSCs, as observed from the original Nanostring microarray and subsequent q-PCR analysis in Chapter 4, section 4.3.1 and 4.3.3. This indicates that diabetes affects the expression of the candidate miRNAs in a similar way in both human and mouse CSCs. Interestingly, among the three differentially expressed miRNAs, miR-376c was the most substantially upregulated in the diabetic CSCs, while miR-30c was the only miRNA that was downregulated. Unlike the other miRNAs, miR-329 showed no significant change in expression in the diabetic human CSCs. This greatly contrasted with the significant and substantial upregulation that was observed for this miRNA in the diabetic mouse CSCs from both the Nanostring microarray and subsequent q-PCR. Although, there is no other evidence for its role in CSCs, miR-329 is known to inhibit cell proliferation in other human cell types, as indicated by the targeted inhibition of cell cycle promoters such as E2F1 (Xiao *et al*., 2013). This supports the upregulation of this miRNA in the diabetic mouse CSCs, but not the unaltered expression in the diabetic human CSCs. Due to the extremely limited amount of literature concerning the expression of miR-329 in human cells, the reason for this contrasting result remains unclear. A possible explanation could be

due to the lack of glucose control in diabetic mice. The diabetic mice used in this study had a consistently elevated glucose concentration, while all the diabetic human participants involved were on glucose-lowering drugs. However, more studies need to be performed to validate this theory.

As previously stated, an upregulated miRNA expression in the diabetic CSCs suggests that it may possess a pathological function. As such, miR-495 is known to target genes that inhibit the cell cycle, as well as inhibiting the differentiation of human ESCs and MSCs (Lee *et al*., 2014; Yang *et al*., 2013; Chen *et al*., 2013). Despite the fact that there is no evidence for such a role in CSCs, the successful translation of an upregulated expression profile from mouse to human CSCs in the diabetic condition suggests that miR-495 may also target human genes that promote CSC function. The functional nature of miR-376c remains unclear as it has been shown to promote the proliferation of human trophoblasts and neural differentiation of human pluripotent stem cells (Liu *et al*., 2014; Fu *et al*., 2013). Although this suggests a beneficial role for this miRNA, it contradicts the impact of the upregulated expression of miR-376c observed in the human CSCs in this study. Furthermore, the cell-cycle promoter, CDK6 was found as a target for miR-376c in the mouse CSCs, providing further evidence for a role in reducing CSC proliferation.

Among the three miRNAs that were previously upregulated in the diabetic mouse CSCs, miR-495 was the only one that was suggested to exhibit this upregulation in diabetic human CSCs. Evidently, it is clear that more expression studies must be performed to validate the upregulated expression of miR-376c, and the unaltered expression of miR-329 in the diabetic human CSCs.

7.4.4 Functional and therapeutic implications for miR-30c in human CSCs

MiR-30c was significantly reduced in the diabetic human CSCs; a finding which correlated with the changes observed in the diabetic mouse CSCs. This indicates that miR-30c has functional and therapeutic implications in the diabetic heart. As the pathophysiological role of miR-30c has already been characterized in the mouse CSCs, its translated expression profile indicates that it may exhibit the same role in the human CSCs. MiR-30c may therefore promote the survival of human CSCs by directly inhibiting pro-apoptotic genes such as VDAC1. This has therapeutic implications in reducing the effect of diabetes on the heart by preventing CSC apoptosis, leading to an enhanced cardiomyocyte replacement after injury. Myocardial cell death also plays a pivotal role in the development of DCM, leading to MI, arrhythmias and endothelial dysfunction (Cai and Kang, 2003). A strategy involving genetic manipulation of miR-30c may therefore prevent or limit this pathological development for such patients. Moreover, the potential of stem cell transplantation yields many more therapeutic opportunities. Cardiosphere derived stem cells have been shown to increase functional cardiomyocytes and reduce scarring after transplantation in the infarcted heart (Makkar *et al*., 2012). The overexpression of miR-30c in transplanted CSCs may therefore increase their ability to improve cardiac function by promoting CSC survival in the heart.

Altogether, the results from this chapter provide the first evidence that the expression of miR-495, -376c and -30c are not only altered in diabetic mouse CSCs, but also in diabetic human CSCs. Importantly, this indicates that miR-30c may exhibit the same pathophysiological role in human CSCs that was discovered in the mouse CSCs in the diabetic condition. In the next chapter, I will discuss my findings from all previous chapters, and determine whether I have answered the objectives of this thesis.

CHAPTER 8: SUMMARY AND CONCLUSIONS

8.1 Summary and interpretation of results

In this final chapter, I will provide a complete summary of my project and discuss whether the aims and hypothesis were addressed. I will also outline the primary limitations and challenges that I faced throughout the project, as well as ways that they could have been overcome. Finally, I will discuss future work and experiments that could be implemented to advance our understanding of how miRNAs can affect CSC function.

8.1.1 Summary of mouse CSC study

In the mouse study, I first established a culture of diabetic (n=6) and non-diabetic mouse CSCs (n=6) that formed the framework for the functional experiments involving miRNAs. I isolated the CSCs from diabetic db/db mouse heart tissue and confirmed their identity by performing a MACS purification technique (targeting the Sca-1 marker); which was later analysed by FACS. Once enough of the CSCs were grown *in vitro*, I performed a Nanostring microarray using RNA extracted from the diabetic and non-diabetic CSC samples to determine the differential expression of miRNAs between the two conditions. I found that out of 598 randomly selected miRNAs, 16 miRNAs exhibited a significantly altered expression profile in the diabetic CSCs. Furthermore, seven of these 16 miRNAs were predicted to target genes that are involved in regulating stem cell self-renewal. The altered expression of four of these seven miRNAs (miR-329, -495, -376c and -30c) were then validated by q-PCR at the molecular level. The GSK3-β and MEF2C genes were predicted to be targets for these miRNAs based on bioinformatic prediction tools and relevant literature. However, preliminary western blot analysis showed no change in their expression between the diabetic and non-diabetic CSCs.

Mass spectrometry was thus implemented to produce more reliable targets for the miRNAs using protein derived from the diabetic (n=5) and non-diabetic CSCs (n=5). The mass spectrometry analysis revealed VDAC1 to be a target for miR-30c, and CDK6 to be a target for miR-329, -495, and -376c. Western blot analyses then showed VDAC1 to be significantly upregulated and CDK6 to be significantly downregulated in the diabetic CSCs, validating the differential expression of the candidate miRNAs. VDAC1 was confirmed as a direct target for miR-30c by performing a luciferase assay. Diabetic (n=4) and non-diabetic CSCs (n=4) were then transfected with a miR-30c precursor mimic to determine the functional characteristics of the miRNA. Western blot analyses showed that the presence of the miR-30c precursor mimic caused direct downregulation of VDAC1 in the transfected diabetic and non-diabetic CSCs compared to control. Additional western blots revealed that cleaved Caspase-3 was also downregulated in diabetic CSCs transfected with the miR-30c precursor mimic compared to control; a finding which was observed to directly correlate with the downregulated VDAC1 in the same condition. This indicated that miR-30c exhibits an anti-apoptotic role in the diabetic mouse CSCs by inhibiting VDAC1 (Fig. 8.1). A Caspase 3/7 assay also supported this conclusion as there was a significant reduction in caspase 3/7 activity in protein derived from diabetic CSCs transfected with the miR-30c precursor mimic compared to control.

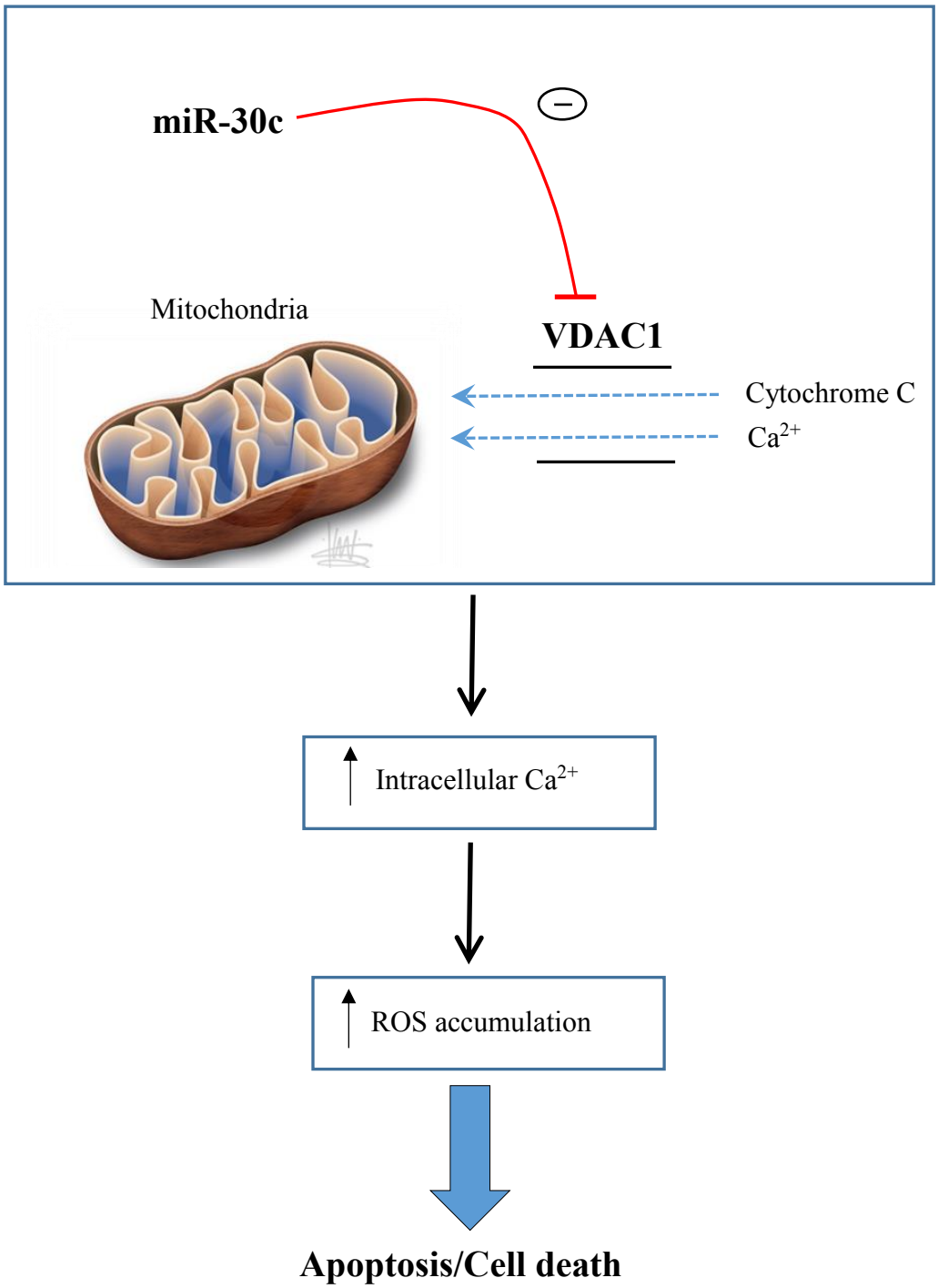

Figure 8.1. A flow chart diagram depicting the potential molecular pathway of miR-30c reducing apoptosis. My findings suggest that miR-30c inhibits the expression of pro-apoptotic VDAC1 in the mitochondrial membrane of CSCs, and in doing so prevents the facilitated transport of apoptotic molecules such as cytochrome C. This also inhibits the entry of calcium ions (Ca^{2+}) into the mitochondria, thereby preventing the accumulation of ROS in the cell. Ultimately, this means that miR-30c may promote the survival of CSCs by targeting the VDAC1 protein.

8.1.2 Summary of human CSC study

The human CSC study was performed to determine if the altered expression of miR-329, -495, -376c and -30c observed in diabetic mouse CSCs can be translated to human diabetic CSCs with the aim to demonstrate the possible clinical implication of the target miRNAs. I isolated human CSCs from RAA biopsies collected from patients undergoing coronary artery bypass surgery. The diabetic (n=3) and non-diabetic human CSCs (n=3) were grown *in vitro* to expand the cell population. Their identity was then confirmed from FACS by targeting the CD105 and CD90 markers. A q-PCR provided evidence to suggest that diabetes affected the expression profiles of miR-376c, -495 and -30c in the human CSCs in a similar manner to how they were affected in the mouse CSCs. MiR-329 was the only miRNA that could not be translated from mouse to human CSCs. This indicated that miR-376c, -495 and -30c had pathophysiological roles in diabetic human CSCs. Moreover, the anti-apoptotic role of miR-30c that was suggested in the diabetic mouse CSCs may also be present in the diabetic human CSCs. This is because the reduced expression of miR-30c that was observed in diabetic human CSCs aligns with previous studies from the Katare laboratory that have demonstrated that diabetes increases apoptosis in human CSCs (Fomison-Nurse *et al*., 2018; Katare *et al*., 2013).

8.2 Addressing aims and hypothesis of project

The first aim for this project was to determine whether diabetes affects the expression of miRNAs within mouse and human CSCs. I have addressed this aim by giving preliminary evidence that miR-329, -495, -376c and -30c exhibit significantly altered expression profiles in the diabetic mouse CSCs. I also showed that this change in expression translated to human CSCs for miR-495, -376c and -30c. This indicates that diabetes may effect the expression of these miRNAs in both mouse and human CSCs.

The second aim was to demonstrate the pathophysiological role of the differentially expressed miRNAs in the diabetic CSCs. From the four miRNAs that were altered in the mouse study, I chose to focus on the role of miR-30c. This was due to the relative lack of understanding of the functional characteristics of miR-30c, as well as the extent to which miR-30c impacted its predicted target gene, compared to the other miRNAs. I addressed this aim by providing evidence to suggest that miR-30c promotes the survival of CSCs in the diabetic condition by regulating the pro-apoptotic VDAC1 gene. This indicates that miR-30c may have a pathophysiological role in the diabetic CSCs, and also provides more evidence for a therapeutic application in CSC transplantation. Altogether, I have addressed both objectives of my PhD thesis.

8.3 Limitations

8.3.1 Markers for CSC identification

There are a number of limitations of this project, as listed below. Firstly, although specific markers were used such as Sca-1, CD105 and CD90 for the identification of mouse and human CSCs, there is no guarantee that these markers do not also bind to other cells besides CSCs. This is because unlike other stem cell subtypes, CSCs have not been characterized to the extent to which a specific marker has been identified purely for CSC identification. Nevertheless, the rationale for using these markers was based on previous published studies in which a similar population of resident stem cells was identified in the heart. Even so, the FACS data in both mouse and human CSCs did not show that the markers were bound to 100% of the cells tested for. This indicates that there were some cells in the population that could not be considered CSCs based on the method used to characterise them as such. Although the percentage of these cells was small, they may have affected the changes observed in the downstream functional results. One possible method for overcoming this in a

future study is to use FACS to purify the CD34 negative population consisting of CSCs positive for both CD90 and CD105, although, as discussed earlier, the CSCs are more effective as a heterogenous population than a specific single cell population (Li *et al*., 2010).

8.3.2 Simulating diabetes *in vitro*

The growth conditions of the CSCs may have also been a limiting factor. The cells were grown *in vitro* using DMEM/F12 media. This media contains a fixed 17.5 mM concentration of glucose. This is much higher than the normal physiological concentration for blood glucose in humans (4-6 mM), as well as the normal concentration for people with diabetes (7-10 mM) (American Diabetes Association, 2006). It is also higher than the normal physiological blood glucose levels for non-diabetic mice (2.8-5.6 mM). It is however, roughly equivalent to the normal concentration of the diabetic mice (>16.7 mM) (King *et al*., 2012). Therefore, although it can be presumed that the DMEM/F12 media was beneficial to simulate diabetic conditions for the diabetic mouse CSCs, it may not be suitable for culturing non-diabetic mouse or human CSCs. Due to the complexity of such diseases, it is very difficult to simulate diabetic conditions *in vitro*. For this reason, the glucose levels may not be the only parameter that should be regulated during the growth of the CSCs. Diabetes is also known to promote insulin deficiency, as well as the build-up of oxidative stress, leading to cell death (Ouyang *et al*., 2014; Lee and Parvaiz, 2006). To better simulate diabetic conditions, the growth conditions should therefore exhibit insulin deficiency and a hypoxic microenvironment. Furthermore, although the diabetic mice were confirmed as hyperglycemic, the impact of obesity as a complication of type-2 diabetes was not measured. The fact that these parameters were not accounted for during the culturing of diabetic CSCs may therefore reflect the fact that the statistical significant results purely indicate that effects are unlikely to have occurred

by chance, and do not necessarily confirm biological significance. More reliable techniques need to be optimized to better simulate the pathological nature of diabetes *in vitro*.

Other limitations arose from comparing the diabetic mouse and human CSCs. The type-2 diabetic patients that donated heart tissue were treated with glucose-lowering drugs, while the diabetic mice did not undergo such treatment. The effects of these drugs have not been measured; however there is a possibility that they may influence molecular events within the diabetic CSCs. Moreover, the age of the mice may be a limiting factor when making comparisons to humans. In the study, 12 week old mice were used which is equivalent to a 30 year old human (Jackson *et al*., 2017). However, the diabetic and non-diabetic patients were considerably older than this (54-75 years old), which may have affected the results. Finally, due to the association between obesity and type-2 diabetes, the weights of the human patients were recorded. Unlike the mice, the type-2 diabetic patients were not consistently heavier than the non-diabetic patients (Appendix 10), suggesting a discrepancy in the nature of the diabetic condition between humans and mice. However, this may also indicate that diabetes was a greater contributing factor than weight with regards to the differential miRNA expression that I observed in the human CSCs.

8.3.3 Bioinformatic analyses

Another limiting factor was the method used for the identification of miRNA target genes. Although bioinformatic analyses is accepted in the field, the miRNA-target prediction databases associated with this method (eg. TargetScan, miRanda) are often not experimentally validated, therefore showing low precision and sensitivity (Witkos *et al*., 2011; Alexiou *et al*., 2009). This was addressed in Chapter 5 by implementing mass spectrometry to identify more reliable targets in the experimental samples.

Bioinformatic pathways were also used to predict that 7 out of the 16 significantly regulated miRNAs were associated with regulating stem cell proliferation and self-renewal. However, if the bioinformatic pathways were unreliable, this may suggest that the other 9 miRNAs may also be involved in regulating stem cell proliferation or apoptosis.

8.3.4 Low sample size

Finally, there were instances where a larger sample size may have increased the statistical power of some of the findings in my project. This was particularly notable in two experiments. In the caspase 3/7 assay in Chapter 6, section 6.3.3, total protein derived from non-diabetic CSCs transfected with miR-30c precursor mimic was found to exhibit reduced caspase activity compared to the non-diabetic control. This change was not significant; however the P value was extremely close to being so at 0.06. A large number of samples may have reduced this P value to significant levels. Also, in the q-PCR performed in Chapter 7, section 3.3, the expression profiles of all four miRNAs were able to be translated from mouse to human CSCs in the diabetic condition, except for miR-329. However, due to time constraints and other difficulties in obtaining the RAA biopsies, only three diabetic and three non-diabetic samples were used in my project. A larger sample size may have impacted these results such that the change in expression of miR-329 may have translated better from diabetic mouse to human CSCs. Although the data was statistically significant, a larger sample size may have also reduced the variability in miR-376c and miR-495 expression between the repetitions of the q-PCR.

8.3.5 Passaged and cryopreserved CSCs

There is evidence to suggest that primary cells that are passaged and/or cryopreserved exhibit substantial changes in their morphology, gene expression and differentiation potential (Nam *et al*., 2014). Although passaging and cryopreservation can be used as tools to generate cell numbers and store these cells, respectively, they may therefore also have led to a change in the functional nature of the CSCs.

One example of the effect of passaging may be the inconsistent VDAC1 expression observed in the study. In Chapter 5, I showed that the expression of VDAC1 was substantially and significantly increased in the diabetic CSCs. However, despite not being the main focus, this increased expression was not found in the CSCs transfected with the scrambled mimic during the transfection experiment in Chapter 6. This change in expression may be due to the effects of passaging or cryopreservation. Passaging may also be a contributing factor for the lack of consistency in miRNA expression in the human study. If the human CSCs were processed at the same passage, there may be less variation in miR-376c expression between each q-PCR repetition. Therefore, reducing the number of passages and freeze-thaw cycles, and keeping these parameters consistent may have increased the reliability of my results.

8.3.6 Luciferase assay

The luciferase assay performed in the study has a number of limitations. Firstly, a larger sample size may have altered the suggested outcome that VDAC1 is a direct target for miR-30c. Also, neither the 3'UTR construct of VDAC1 or the Lipofectamine transfection reagent were tested for their individual effects alongside the co-transfected data set. They could have acted as important negative controls for the experiment.

8.3.7 Consequences of mimic overexpression

Although the study was focused on demonstrating the possible role of miR-30c in CSCs, physiological conditions are not easily attained. For this reason, the substantial increase in miR-30c expression as a result of transfecting the CSCs with the miR-30c precursor mimic may have consequences when considered in a clinical setting. However, more experiments are needed to understand the specific concentration of miR-30c mimic required to induce the molecular changes, while limiting any harmful side-effects as a result of the overexpression.

8.3.8 Increased scar formation

Sca-1 has been identified as a suitable marker for the identification of CSC. However, studies have shown that Sca-1^+ cells may differentiate into adipocytes or fibroblasts upon myocardial degeneration (Paylor *et al*., 2013). This can therefore lead to scar formation and other cardiomyopathies when these cells are transplated into tissue. This may therefore be a potential side-effect of transplanting Sca-1^+ CSCs into the human heart, and one that must be carefully addressed and remedied before considering a clinical application of miR-30c within the Sca-1^+ CSCs. However, it is possible that the cells can be genetically engineered with a cocktail of miRNAs which have the potential to reduce fibrotic differentiation. Future studies could focus on using the miRNA cocktail to improve the efficacy of stem cells.

8.4 Future work

8.4.1 Understanding mode of inhibition of miR-30c

My findings suggest that VDAC1 may be a functional target for miR-30c. It would be interesting to further understand the mode of inhibitory action associated with this interaction. As previously stated, miRNAs can either bind to the mRNA of the target gene, causing its

degradation; or alternatively, they can repress the translation of the mRNA into protein. The western blots in Chapter 5, section 5.3.3 and Chapter 6, section 6.3 indicated that miR-30c causes translational repression of the VDAC1 total protein. However, whether miR-30c also degrades the mRNA of VDAC1 has yet to be determined. A q-PCR can be performed using RNA extracted from diabetic and non-diabetic CSCs transfected with a miR-30c precursor mimic to determine the expression of the VDAC1 mRNA. This would provide an indication as to whether the mRNA of VDAC1 is repressed in the presence of the miR-30c precursor mimic. If the mRNA is repressed, it would suggest that a proportion of miR-30c binds to the VDAC1 mRNA to confer its inhibitory action.

8.4.2 Effect of miR-30c on VDAC1 in human CSCs

My findings suggest that miR-30c was similarly dysregulated in mouse and human CSCs. The suggested molecular mechanism associated with this dysregulation involves inhibition of pro-apoptotic VDAC1 and caspase-3. However, this mechanism has not yet been investigated in the human CSCs. Therefore, the next step is to determine if VDAC1 and caspase-3 proteins are similarly reduced in human CSCs transfected with the miR-30c mimic. Western blot and q-PCR analysis may be performed to demonstrate this, and the results of these studies can be compared to the mouse data. Furthermore, apoptosis functional assays may be performed to confirm the suggested role of miR-30c in regulating the apoptosis of CSCs in mice and human tissue.

8.4.3 Loss of function experiments

Loss of function (‘silencing’) experiments may also strengthen the findings of my thesis. In this context, an anti-miRNA specific for miR-30c may be transfected into the CSCs to inhibit

the expression of any existing miR-30c. As my results suggest, I would expect to observe an increased expression of VDAC1 in mouse CSCs transfected with the anti-miRNA for miR-30c. These experiments, in combination with the results of my thesis, may provide much stronger evidence to suggest that VDAC1 is not only inhibited by miR-30c, but that this interaction is directly linked to a potential role of miR-30c in regulating apoptosis.

8.4.4 Determining whether miR-30c can regulate CSC membrane potential

While my study has suggested the pro-apoptotic role of VDAC1, this gene is also known to regulate mitochondrial membrane potential. Therefore, a secondary role of miR-30c may be to regulate mitochondrial membrane potential of CSCs. In support of this, studies have shown diabetes to adversely affect mitochondrial membrane potential in a number of different tissues (Sivitz and Yorek, 2010; Widlansky *et al*., 2010). The mitochondrial membrane potential can be measured by performing a cobalt-calcein assay in the diabetic and non-diabetic CSCs transfected with the miR-30c precursor mimic. The calcein dye passively diffuses into the mitochondria, allowing the CSCs to be fluorescently labelled. The opening of the mitochondrial permeability transition pore (mPTP) leads to the exit of calcein and entry of cobalt ions into the mitochondrial compartment, manifesting as a reduction of fluorescence intensity (Lee *et al*., 2013). The loss of fluorescence is also proportional to the membrane potential of the cell. Opening of the mPTP is also associated with the onset of apoptosis. Determining the membrane potential would therefore directly parallel the results of this thesis, and improve our understanding of the pathophysiological role of miR-30c within the CSCs. It would also be interesting to determine whether diabetes affects the ability of miR-30c to regulate membrane potential of CSCs, and if it does so in a similar manner as the ability of miR-30c to regulate apoptosis.

Although from the MS results, GSK3-β was not found to be a target for miR-30c, the phosphorylation and subsequent inactivation of this gene is also known to induce opening of the mPTP and therefore membrane potential (Juhaszova *et al*., 2004). This indicates that there are other genes which may be involved in regulating the mPTP, but may not be direct targets of miR-30c. Therefore future experiments must be performed to uncover the complex molecular pathways leading to this function.

8.4.5 Functional studies on other candidate miRNAs

In this project, I have shown that diabetes causes dysregulation of miR-329, -376c, -495 and -30c in CSCs. Moreover, while my project focused on demonstrating the functional significance of only miR-30c, it would be interesting to perform similar experiments on other dysregulated miRNAs. Thus far, the general function of these miRNAs seems to involve the regulation of cell proliferation. Proliferation assays could therefore be performed on CSCs transfected with corresponding mimics to provide new insights into their anti-proliferative role in the CSCs. Moreover, because the target protein that was identified for these miRNAs was the cell-cycle regulator, CDK6, western blots could be performed on the transfected cells to determine the involvement of CDK6 in regulating proliferation. This would provide a better understanding of the roles of miR-329, -376c and -495 in mouse CSCs, and might also reveal the therapeutic potential of miR-376c and miR-495 in human CSCs. Finally, it would be interesting to determine if using precursor mimics or anti-miRNAs to overexpress or knockdown the miRNAs, respectively, will provide novel information on the synergistic effects of the combined therapy.

8.4.6 Testing the functional efficacy of miR-30c in an *in vivo* mouse model of myocardial infarction

All the results presented in my thesis were using an *in vitro* model. While these results provided the first pieces of evidence for the ability of diabetes to induce dysregulation of miRNA expression in mouse and human CSCs, as well as laying down the foundation for a potential therapeutic role of miR-30c, it is also important to test the beneficial effects of miR-30c expression in an *in vivo* model. Stem cell therapy plays a major role in improving the functional recovery of patients after a MI, whereby millions of cells are lost due to apoptotic cell death. Therefore, a mouse model of MI can also be used to demonstrate the anti-apoptotic function of miR-30c *in vivo*. Genetically engineered diabetic and non-diabetic CSCs that overexpress miR-30c can thus be injected along the border zone of the left ventricle after MI is induced. Alterations in cardiac function as a result of either miR-30c overexpression can then be observed and compared to the sham (placebo surgery) control. The parameters measured may include the functional recovery of the heart using echocardiography, or angiogenesis by performing histological analyses. This would provide a greater indication of the benefits of miR-30c in an animal model, as well as insight into its therapeutic application in treating the infarcted heart.

8.5 Concluding remarks

Diabetes is a growing epidemic that greatly reduces quality of life and damages different tissues, including the heart. It is therefore imperative to research and develop new ways of treating this disease. In this thesis, I have shown evidence to suggest that miR-30c may have an anti-apoptotic role in diabetic mouse CSCs. In particular, I have shown that miR-30c may be genetically manipulated *in vitro* to improve CSC survival, which indicates its therapeutic potential in CSC transplantation. This is an important step to understanding how miRNAs can

enhance stem cell therapy and therefore have a beneficial impact on human health, especially in pathologies such as diabetes. I have also shown that miR-495, -376c and -30c are differentially expressed in diabetic CSCs. These miRNAs may be further investigated to determine whether they have potential role within diabetic CSCs, which may lead to a therapeutic application in treating diabetic heart disease.

REFERENCES

Abu-Hamad, S., Arbel, N., Calo, D. *et al*. (2009). The VDAC1 N-terminus is essential both for apoptosis and the protective effect of anti-apoptotic proteins. *Journal of Cell Science*, vol. 122, pp. 1906-1916.

Agarwal, V., Bell, G.W., Nam, J. and Bartel, D.P. (2015). Predicting effective microRNA target sites in mammalian mRNAs. *eLIFE*, vol. 4, e05005.

Ahmed, M., Muhammed, S.J., Kessler, B. and Salehi, A. (2010). Mitochondrial proteome analysis reveals altered expression of voltage dependent anion channels in pancreatic β-cells exposed to high glucose. *Islets*, vol. 2, no. 5, pp. 283-292.

Alexiou, P., maragkakis, M., Papadopoulos, G.L., Reczko, M. and Hatzigeorgiou, A.G. (2009). Lost in translation: an assessment and perspective for computational microRNA target identification. *Bioinformatics*, vol. 25, no. 23, pp. 3049-3055.

Almalki, S.G. and Agrawal, D.K. (2016). Key transcription factors in the differentiation of mesenchymal stem cells. *Differentiation*, vol. 92, no. 1-2, pp. 41-51.

Amado, L. C. *et al*. (2005). Cardiac repair with intramyocardial injection of allogeneic mesenchymal stem cells after myocardial infarction. *Proceedings of the National Academy of Sciences of the United States of America*, vol. 102, pp. 11474–11479.

American Diabetes Association. (2006). Standards of medical care in diabetes. *Diabetes Care*, vol. 29(suppl 1): s4-s42.

Ardelean, F.A. (2017). Case study using analysis of variance to determine groups' variations. *MATEC Web of Conferences*, vol. 126, DOI: 10.1051.

Asahara, T., Kalka, C. and Isner, J.M. (2000). Stem cell therapy and gene transfer for regeneration. *Gene Therapy*, vol. 7, pp. 451-7.

Assmann, T.S., Recamonde-Mendoza, M., de Souza, B.M. and Crispim, D. (2017). MicroRNA expression profiles and type 1 diabetes mellitus: systematic review and bioinformatics analysis. *Endocrine Connections*, doi:10.1530/EC-17-0248.

Bakhach, J. (2009). The cryopreservation of composite tissues. *Organogenesis*, vol. 5, no. 3, pp. 119-126.

Balsam, L. B. *et al*. (2004). Haematopoietic stem cells adopt mature haematopoietic fates in ischaemic myocardium. *Nature*, vol. 428, pp. 668–673.

Bargaje, R., Gupta, S., Sarkeshik, A. *et al*. (2012). Identification of novel targets for miR-29a using miRNA proteomics. *PLOS ONE*, vol. 7, no. 8: e43243.

Baumgartner, H.K., Gerasimenko, J.V., Thorne, C. *et al*. (2009). Calcium elevation in mitochondria is the main Ca2 + requirement for mitochondria; permeability transition pore (mPTP) opening. *Journal of Biological Chemistry*, vol. 284, pp. 20796-20803.

Bearzi, C., Rota, M., Hosoda, T. *et al*. (2007). Human cardiac stem cells. *Proceedings of the National Academy of Sciences of the United States of America*, vol. 104, no. 35, pp. 14068-14073.

Beitzinger, M., Peters, L., Zhu, J.Y., Kremmer, E. and Meister, G. (2007). Identification of human microRNA targets from isolated argonaute protein complexes. *RNA Biology*, vol. 4, pp. 76-84.

Berlo, J.H., Kanisicak, O. and Maillet, M. *et al*. (2014). C-kit+ cells minimally contribute cardiomyocytes to the heart. *Nature*, vol. 509, no. 7500, pp. 337-341.

Betel, D., Wilson, M., Gabow, A., Marks, D.S. and Sander, C. (2008). The microRNA.org resource: targets and expression. *Nucleic Acids Research*, vol. 36, D149-D153.

Bi, W., Drake, C.J. and Schwarzz, J.J. (1999). The transcription factor MEF2C-null mouse exhibits complex vascular malformations and reduced cardiac expression of angiopoietin 1 and VEGF. *Developmental Biology*, vol. 211, no. 2, pp. 255-67.

Biemann, K. (1963). Mass spectrometry. *Annual Review of Biochemistry*, vol. 32, no. 1, pp. 755-780.

Blurton-Jones, M., Kitazawa, M., Martinez-Coria, H. *et al*. (2009). Neural stem cells improve cognition via BDNF in a transgenic model of Alzheimer disease. *Proceedings of the National Academy of Sciences of the United States of America*, vol. 106, pp. 13594-13599.

Boudina, S. and Abel. E.D. (2010). Diabetic cardiomyopathy, causes and effects. *Reviews in Endocrine and Metabolic Disorders*, vol. 11, pp. 31-39.

Brezden, C.B. and Rauth, A.M. (1996). Differential cell death in immortalized and non-immortalized cells at confluency. *Oncogene*, vol. 12, no. 1, pp. 201-206.

Burile, A.P., Messina, E., Giacomella, A. and Marbán, E. (2007). Endogenous cardiac stem cells. *Progress in Cardiovascular diseases*, vol. 50, no. 1, pp. 31-48.

Burke, S.J., Batdorf, H.M., Burk, D.H. *et al*. (2017). *Db/db* mice exhibit features of human type 2 diabetes that are not present in weight-matched C57BL/6J mice fed a western diet. *Journal of Diabetes Research*, vol. 2017, 8503754.

Cai, J., Yi, F.F., Yang, X.C. *et al*. (2007). Transplantation of embryonic stem cell-derived cardiomyocytes improves cardiac function in infarcted rat hearts. *Cytotherapy*, vol. 9, pp. 283-291.

Cai, L. and Kang, Y.J. (2003). Cell death and diabetic cardiomyopathy. *Cardiovascular Toxicology*, vol. 3, no. 3, pp. 219-228.

Caplan, A. I. & Dennis, J. E. (2006). Mesenchymal stem cells as trophic mediators. *Journal of Cellular Biochemistry*, Vol. 98, pp. 1076–1084.

Care, A., Catalucci, D., Felicetti, F. *et al*. (2007). MicroRNA-133 controls cardiac hypertrophy. *Nature Medicine*, vol. 13, no. 5, pp. 613 – 618.

Carlson, S., Trial, J., Soeller, C. and Entman, M.L. (2011). Cardiac mesenchymal stem cells contribute to scar formation after myocardial infarction. *Cardiovascular Research*, vol. 91, no. 1, pp. 99-107.

Caspi, O., Huber, I., Kehat, I., *et al*. (2007). Transplantation of human embryonic stem cell-derived cardiomyocytes improves myocardial performance in infarcted rat hearts. *Journal of American College of Cardiology*, vol. 50, pp. 1884-93.

Cha, M.J., Choi, E., Lee, S., Song, B.W., Yoon, C., Hwang, K.C. (2016). The microRNA-dependent cell fate of multipotent stromal cells differentiating to endothelial cells. *Experimental Cell Research*, vol. 341, no. 2, pp. 139-146.

Chao, C., Kan, D., Lu, K. and Chien, C. (2015). The role of microRNA-30c in the self-renewal and differentiation of C6 glioma cells. *Stem Cell Research*, vol. 9, no. 2, pp. 211-223.

Chaudhuri, A.D., Choi, D.C., Kabaria, S., Tran, A. and Junn, E. (2016). MicroRNA-7 regulated the function of mitochondrial permeability transition pore by targeting VDAC1. *Journal of Biological Chemistry*, DOI 10.1074.

Chen, H., Charlat, O., Tartaglia, L.A. (1996). Evidence that the diabetes gene encodes the leptin receptor : identification of a mutation in the leptin receptor gene in db/db mice. *Cell*, vol. 84, no. 3, pp. 491-495.

Chen, H., Gao, W., Yang, Y. *et al*. (2014). Inhibition of VDAC1 prevents Ca^{2+}-mediated oxidative stress and apoptosis induced by 5-aminolevulinic acid mediated sonodynamic therapy in THP-1 macrophages. *Apoptosis*, vol. 19, pp. 1712-1726.

Chen, J., Mandel, E.M., Thompson, J.M. *et al*. (2006). The role of microRNA-1 and microRNA-133 in skeletal muscle proliferation and differentiation, *Nature Genetics*, vol. 38, pp. 228-233.

Chen, S., Chen, H., Chen, S. *et al*. (2013). MicroRNA-495 inhibits proliferation of gliobastoma multiforme cells by downregulating cyclin-dependent kinase 6. *World Journal of Surgical Oncology*, vol. 11, no. 87, pp. 1-8.

Cheng, Y., Ji, R., Yue, J. *et al*. (2007). MicroRNAs are aberrantly expressed in hypertrophic heart. *The American Journal of Pathology*, vol. 170, no. 6, pp. 1831-1840.

Chiong, M., Wang, Z.V., Pedrozo, Z. *et al*. (2011). Cardiomyocyte death: mechanisms and translational implications. *Cell Death Discovery*, vol. 2, no. 12, pp. e244.

Chong, J.J.H., Chandrakanthan, V., Xaymardan, M. *et al*. (2011). Adult cardiac-resident MSC-like stem cells with a proepicardial origin. *Cell Stem Cell*, vol. 9, no. 6, pp. 527-540.

Chu, H., Chen, X., wang, H. *et al*. (2013). MiR-495 regulates proliferation and migration in NSCLC by targeting MTA3. *Tumor Biology*, vol. 35, pp. 3487-3494.

Ciaraldi, T.P., Oh, D.K., Christiansen, L. *et al*. (2006). Tissue-specific expression and regulation of GSK-3 in human skeletal muscle and adipose tissue. *American Journal of Physiology-Endocrinology and Metabolism*, vol. 291, no. 5, E891-E898.

Clark, A.L. and Naya, F.J. (2015). MicroRNAs in the myocyte enhancer factor 2 (MEF2)-regulated Gtl2-Dio3 noncoding RNA locus promote cardiomyocyte proliferation by targeting the transcriptional coactivator Cited2. *Journal of Biological Chemistry*, vol. 290, pp. 23162-23172.

Congdon, M.L. (1957). Bone marrow transplantation in animals exposed to whole body irradiation. *Journal of Cellular Comparative Physiology*, vol. 50, pp. 103-8.

Coombs, N.J., Gough, A.C., Primrose, J.N. (1999). Optimisation of DNA and RNA extraction from archival formalin – fixed tissue, *Nucleic Acids Research*, vol. 27, no. 16, pp. e12-i-23-iii.

Copelan, E.A. (2006). Hematopoietic stem-cell transplantation. *New England Journal of Medicine*, vol. 354, pp. 1813-1826.

Count, M. (2018). Http://www.mirbase.org/.

Crippa, S., Cassano, M., Messina, G. *et al*. (2011). MiR669a and miR669q prevent skeletal muscle differentiation in postnatal cardiac progenitors. *Journal of Cell Biology*, vol. 193, no. 7, pp. 1197-1212.

Cummings, B.S., Wills, L.P. and Schnellmann, R.G. (2012). Measurement of cell death in mammalian cells, *Current Protocols in Pharmacology*, Chapter 12, Unit 12.8, DOI: 10.1002.

Cyganek, L., Chen, S., Borchert, T. and Guan, K. (2013). Cardiac progenitor cells and their therapeutic application for cardiac repair. *Clinical and Experimental Cardiology*, ISSN: 2155-9880.

David, R., Brenner, C., Stieber, J. *et al*. (2008). Mesp1 drives vertebrate cardiovascular differentiation through Dkk-1-mediated blockade of Wnt-signalling. *Nature Cell Biology*, vol. 10: pp. 338-345.

Detaille, D., Guigas, B. Chauvin, C. *et al*. (2005). Metformin prevents high-glucose-induced endothelial cell death through a mitochondrial permeability transition-dependent process. *Diabetes*, vol. 54, pp. 2179-2187.

~~Diehl, J.A., Cheng, M., Roussel, M.F. and Sherr, C.J. (1998). Glycogen synthase kinase-3beta regulates cyclin D1 proteolysis and subcellular localization. *Genes and Development*, vol. 12, no. 22, pp. 3499-511.~~

Dominici, M., Le Blanc, K., Mueller, I. *et al*. (2006). Minimal criteria for defining multipotent mesenchymal stromal cells. The international society for cellular therapy position statement. *Cytotherapy*, vol. 8, pp. 315-317.

Du, B., Dai, X., Li, S. *et al*. (2017). MiR-30c regulates cisplatin-induced apoptosis of renal tubular epithelial cells by targeting Bnip3L and Hspa5. *Cell Death and Disease*, vol. 8, no. 8, e2987.

Duisters, R.F., Tijsen, A.J., Schroen, B. *et al*. (2009). MiR-133 and miR-30 regulate myocardial matrix remodeling. *Circulation Research*, vol. 104, pp. 170-178.

Eldar-Finkelman, H., Schreyer, S.A., Shinohara, M.M., LeBoeuf, R.C. and Krebs, E.G. (1999). Increased glycogen synthase kinase-3 activity in diabetes- and obesity-prone C57BL/6J mice. *Diabetes*, vol. 48, no. 8, pp. 1662-1666.

Esfandiari, F., Fathi, A., Gourabi, H. *et al*. (2012). Glycogen synthase kinase-3 inhibition promotes proliferation and neuronal differentiation of human-induced pluripotent stem cell-derived neural progenitors. *Stem Cells and Development*, vol. 21, no. 17, pp. 3233-3243.

Everaert, B.R., Boulet, G.A., Timmermans, J. and Vrints, C.J. (2011). Importance of suitable reference gene selection for quantitative real-time PCR: special reference to mouse myocardial infarction studies. *PLOS ONE*, vol. 6, no. 8, DOI: e23793.

Falanga, V. (2012). Stem cells in tissue repair and regeneration. *Journal of Investigative Dermatology*, vol. 132, no. 6, pp. 1538-1541.

Feng, B., Chen, S. and Chiu, J. *et al*. (2008). Regulation of cardiomyocyte hypertrophy in diabetes at the transcriptional level. *American Journal of Physiology-Endocrinology and Metabolism*, vol. 294, no. 6, pp. E1119-E1126.

Feng, B., Chen, S., George, B., Feng, Q. and Chakrabarti, S. (2010). MiR133a regulates cardiomyocyte hypertrophy in diabetes. *Diabetes/Metabolism Research and Reviews*, vol. 26, no. 1, pp. 40– 49.

Ferraro, F., Celso, C.L. and Scadden, D. (2010). Adult stem cells and their niches. *Advances in Experimental Medicine and Biology*, vol. 695, pp. 155-158.

Fiordaliso, F., Leri, A., Cesselli, D. *et al*. (2001). Hyperglycemia activates p53 and p53-regulated genes leading to myocyte cell death. *Diabetes*, vol. 50, pp. 2363-2375.

Fomison-Nurse, I., Saw, E.E.L., Gandhi, S. *et al*. (2018). Diabetes induces the activation of pro-ageing miR-34a in the heart, but has differential effects on cardiomyocytes and cardiac progenitor cells. *Cell Death and Differentiation*, vol. 25, pp. 1336-1349.

Friedman, R.C., Farh, K.K., Burge, C.B. and Bartel, D.P. (2009). Most mammalian mRNAs are conserved targets of microRNAs. *Genome Research*, vol. 19, no. 1, pp. 92-105.

Fu, G., Ye, G., Nadeem, L. *et al*. (2013). MicroRNA-376c impairs transforming growth factor-β and nodal signaling to promote trophoblast cell proliferation and invasion. *Hypertension*, vol. 61. Pp. 864-872.

Galimov, A., Merry, T.L., Luca, E. *et al*. (2016). MicroRNA-29a in adult muscle stem cells controls skeletal muscle regeneration during injury and exercise downstream of fibroblast growth factor-2. *Stem Cells*, vol. 34, no. 3, pp. 768-780.

Gambacciani, C., Kusmic, C., Chiavacci, E. *et al*. (2013). MiR-29a and miR-30c negatively regulate DNMT 3a in cardiac ischemic tissues: implications for cardiac remodelling. *microRNA Diagnostics and Therapeutics*, vol. 1, pp. 35-45.

Gambini, E., Pompilio, G., Biondi, A. *et al*. (2011). C-kit^{+} cardiac progenitors exhibit mesenchymal markers and preferential cardiovascular commitment. *Cardiovascular Research*, vol. 89, no. 2, pp. 362-373.

Gangaraju, V.K. and Lin, H. (2009). MicroRNAs: key regulators of stem cells. *Nature Reviews Molecular Cell Biology*, vol. 10, pp. 116–125.

Geiss, G.k., Bumgarner, R. Birditt, B. *et al*. (2008). Direct multiplexed measurement of gene expression with color-coded probe pairs. *Nature Biotechnology*, vol. 26, pp. 317-325.

Gepstein, L. (2002). Derivation and potential applications of human embryonic stem cells. *Circulation Research*, vol. 91, pp. 866-76.

Glass, C.E., Singal, P.K., and Singla, D.K. (2010). Stem cells in the diabetic infarcted heart. *Heart Failure Reviews*, vol. 15, pp. 581-88.

González-González, M., Vázquez-Villegas, P., García-Salinas, C. and Rito-Palomares, M. (2011). Current strategies and challenges for the purification of stem cells. *Journal of Chemical Technology and Biotechnology*, vol. 87, no. 1, pp. 2-10.

Goradel, N.H., Hour, F.G. and Negahdari, B. et al. (2017). Stem cell therapy: a new therapeutic option for cardiovascular diseases. *Journal of Cellular Biochemistry*, vol. 119, no. 1, pp. 95-104.

Gospodarowicz, D. and Moran, J.S. (1976). Growth factors in mammalian cell culture. *Annual Review of Biochemistry*, vol. 45, no. 1, pp. 531-558.

Govindarajan, R., Duraiyan, J., Kaliyappan, K. and Palanisamy, M. (2012). Microarray and its applications. *Journal of Pharmacy and Bioallied Sciences*, vol. 4, Suppl 2, pp. S310-S312.

Gundry, R.L., White, M.Y., Murray, C.I. *et al*. (2010). Preparation of proteins and peptides for mass spectrometry analysis in a bottom-up proteomics workflow. *Current Protocols in Molecular Biology*, vol. 90, no. 1, Unit 10.25, DOI: 10.1002.

Gunsilius, E., Gastl, G., and Petzer, A.L. (2001). Hematopoietic stem cells. *Biomedicine and Pharmacotherapy*, vol. 55, pp. 186-94.

Haffner, A.M., Lehto, S., Rönnemaa, T., Pyörälä, K. and Laakso, M. (1998). Mortality from coronary heart disease in subjects with type 2 diabetes and in nondiabetic subjects with and without prior myocardial infarction. *New England Journal of Medicine*, vol. 339, pp. 229-234.

Hammond, S.M. (2015). An overview of microRNAs. *Advanced Drug Delivery Reviews*, vol. 87, pp. 3-14.

Han, J., Lee, K., Yeom, H. *et al*. (2006). Molecular basis for the recognition of primary microRNAs by the DRosha-DGCR8 complex. *Cell*, vol. 125, no. 5, pp. 887-901.

Han, X., Zhen, S., Ye, Z. *et al*. (2017). A feedback loop between miR-30a/c-5p and DNMT1 mediates cisplatin resistance in ovarian cancer cells. *Cellular Physiology and Biochemistry*, vol. 41, pp. 973-986.

Hardt, E.E. and Sadoshima, J. (2002). Glycogen synthase kinase-3beta: A novel regulator of cardiac hypertrophy and development. *Circulation Research*, vol. 90, no. 10, pp. 1055-63.

Hayat, S.A., Patel, B., Khattar, R.S. and Malik, R.A. (2004). Diabetic Cardiomyopathy: mechanisms, diagnosis and treatment. *Clinical Science*, vol. 107, pp. 539-557.

Holden, J.A. (1999). DNA Topoisomerase II-alpha as a marker of cell proliferation in endocrine and other neoplasms. *Endocrine Pathology*, vol. 10, no. 2, pp. 97-102.

Hosoda, T., Iguchi, N., Cho, Y. *et al*. (2017). The proliferative potential of human cardiac stem cells was unaffected after a long-term cryopreservation of tissue blocks. *Annals of Translational Medicine*, vol. 5, no. 3, pp. 1-7.

Hosoda, T., Zheng, H., Cabral-Da-Silva, M. *et al*. (2011). Human cardiac stem cell differentiation is regulated by a mircrine mechanism. *Circulation*, vol. 123, pp. 1287-1296.

Hu, S., Huang, M., Nguyen, P.K. *et al*. (2011). Novel microRNA prosurvival cocktail for improving engraftment and function of cardiac progenitor cell transplantation. *Circulation*, vol. 124, pp. S27–S34.

Hu, S., Yan, G., He, W. *et al*. (2014). The influence of disease and age on human cardiac stem cells. *Annals of Clinical Biochemistry*, vol. 51, no. 5, pp. 582-590.

Hu, Z., Klein, J.D., Mitch, W.E., Zhang, L., Martinez, I. and Wang, X.H. (2014). MicroRNA-29 induces cellular senescence in aging muscle through multiple signaling pathways. *Aging*, vol. 6, no. 3, pp. 160-175.

Huang, Y., Liu, X. and Wang, Y. (2015). MicroRNA-378 regulates neural stem cell proliferation and differentiation in vitro by modulating tailless expression. *Biochemical and Biophysical Research Communications*, vol. 466, no. 2, pp. 214-220.

Huggett, J., Dheha, K., Bustin, S. and Zumla, A. Real-time RT-PCR normalisation; strategies and considerations, *Genes and Immunity*, vol. 6, pp. 279-84.

Imaisumi, T., Aratani, S., Nakajima, T. (2002). Retinoic acid-inducible gene-1 is induced in endothelial cells by LPS and regulates expression of COX-2. *Biochemical and Biophysical Research Communications*, vol. 292, no. 1, pp. 274-279.

Irani, S. and Hussain, M.M. (2015). Role of microRNA-30c in lipid metabolism, adipogenesis, cardiac remodeling and cancer. *Current Opinion in Lipidology*, vol. 26, no. 2, pp. 139-46.

Ivey, K.N., Muth, A., Arnold, J. *et al*. (2008). MicroRNA regulation of cell lineages in mouse and human embryonic stem cells. *Cell Stem Cell*, vol. 2, pp. 219–229.

Jackson, R., Mount, S., Ye, B. *et al*. (2017). Isolation of human explant derived cardiac stem cells from cryopreserved heart tissue. *PLOS ONE*, vol. 12, no. 4, pp. 1-14.

Jackson, S.J., Andrews, N., Ball, D. *et al*. (2017). Does age matter? The impact of rodent age on study outcomes. *Lab Animal*, vol. 51, no. 2, pp. 160-169.

Jacobsohn, D.A. and Vogelsang, G.B. (2007). Acute graft versus host disease. *Orphanet Journal of Rare Diseases*, vol. 2, no. 35, DOI: 10.1186.

James, P., Quadroni, M., Carafoli, E. and Gonnet, G. (1993). Protein identification by mass profile fingerprinting. *Biochemical and Biophysical Research Communications*, vol. 195, no. 1, pp. 58-64.

Jia, W., Eneh, J.O., Ratnaparkhe, S. (2011). MicroRNA-30c-2 expressed in ovarian cancer cells suppresses growth factor-induces cellular proliferation and downregulates the oncogene BCL9. *Molecular Cancer Research*, vol. 9, no. 12, pp. 1732-1745.

Jin, Y., Peng, D., Shen, Y. *et al*. (2013). MicroRNA-376c inhibits cell proliferation and invasion in osteosarcoma by targeting to transforming growth factor-alpha. *DNA Cell Biology*, vol. 32, no. 6, pp. 302-309.

Juhaszova, M., Zorov, D.B., Kim, S. *et al*. (2004). Glycogen synthase kinase-3β mediates convergence of protection signalling to inhibit the mitochondrial permeability transition pore. *Journal of Clinical Investigation*, vol. 113, no. 11, pp. 1535-1549.

Kang, H., Kim, C., Lee, H. *et al*. (2016). Downregulation of microRNA-362-3p and microRNA-329 promotes tumor progression in human breast cancer. *Cell Death and Differentiation*, vol. 23, pp. 484-495.

Kang, J., Kim, W., Lee, S. *et al*. (2017). TFAP2C promotes lung tumorigenesis and aggressiveness through miR-183- and miR-33a-mediated cell cycle regulation. *Oncogene*, vol. 36, pp. 1585-1596.

Karanes, C., Nelson, G.O., Chitphakdithai, P. *et al*. (2008). Twenty years of unrelated donor hematopoietic cell transplantation for adult recipients facilitated by the national marrow donor program. *Biology of Blood and Marrow Transplantation*, vol. 14, pp. 8-15.

Karbiener, M., Neuhold, C., Opriessnig, P. *et al*. (2011). MicroRNA promotes human adipocyte differentiation and co-represses *PAI-1* and *ALK2*. *RNA Biology*, vol. 8, no. 5, pp. 850-860.

Katare, R., Caporali, A., Zentilin, L. *et al*. (2011). Intravenous gene therapy with PIM-1 via a cardiotropic viral vector halts the progression of diabetic cardiomyopathy through promotion of prosurvival signalling. *Circulation Research*, vol. 108, no. 10, pp. 1238-1251.

Katare, R., Oikawa, A., Cesselli, D. *et al*. (2013). Boosting the pentose phosphate pathway restores cardiac progenitor cell availability in diabetes. *Cardiovascular Research*, vol. 97, no. 1, pp. 55-65.

Katare, R., Riu, F., Mitchell, K. *et al*. (2011). Transplantation of human pericyte progenitor cells improves the repair of infarcted heart through activation of an angiogenic program involving micro-RNA-132. *Circulation Research*, vol. 109, pp. 894-906.

Kehat, I., Kenyagin-Karsenti, D., Snir, M., *et al*. (2001). Human embryonic stem cells can differentiate into myocytes with structural and functional properties of cardiomyocytes. *Journal of Clinical Investigation*, vol. 108, pp. 407-14.

Kiger, A.A., Jones, D.L., Schulz, C., Rogers, M.B., Fuller, M.T. (2001). Stem cell self-renewal specified by JAK-STAT activation in response to a support cell cue. *Science*, vol. 294, pp. 2542-2545.

Kim, S.U. and Vellis, J. (2009). Stem cell-based cell therapy in neurological diseases: A review. *Journal of Neuroscience Research*, vol. 87, pp. 2183-2200.

Kim, S.W., Kim, H.W., Huang, W. *et al*. (2013). Cardiac stem cells with electrical stimulation improve ischaemic heart function through regulation of connective tissue growth factor and miR-378. *Cardiovascular Research*, vol. 100, pp. 241-251.

King, A.J.F. (2012). The used of animal models in diabetes research. *British Journal of Pharmacology*, vol. 133, no.3, pp. 877-894.

Kobayashi, K., Forte, T.M. and Taniguchi, S. *et al*. (2000). The *db/db* mouse, a model for diabetic dyslipidemia: molecular characterization and effects of western diet feeding. *Metabolism*, vol. 49, no. 1, pp. 22-31.

Kong, X., Xu, X., Yan, Y. *et al*. (2014). Estrogen regulates the tumour suppressor miRNA-30c and its target gene, MTA-1 in endometrial cancer. *PLOS ONE*, vol. 9, no. 3, e90810.

Krijnen, P.A.J., Simsek, S. and Niessen, H.W.M. (2009). Apoptosis in diabetes. *Apoptosis*, vol. 14, no. 12, pp. 1387-1388.

Kureel, J., John, A.A., Prakash, R. and Singh, D. (2018). MiR-376c inhibits osteoblastogenesis by targeting Wnt3 and ARF-GEF-1-facilitated augmentation of beta-catenin transactivation. *Journal of Cellular Biochemistry*, vol. 119, no. 4, pp. 3293-3303.

Kushner, J.A., Ciemerych, M.A., Sicinska, E. *et al*. (2005). Cyclins D2 and D1 are essential for postnatal pancreatic beta-cell growth. *Molecular and Cellular Biology*, vol. 25, no. 9, pp. 3752-3762.

Ladstein, R.G., Bachmann, I.M., Straume, O. and Akslen, L.A. (2010). Ki-67 expression is superior to mitotic count and novel proliferation markers PHH3, MCM4 and mitosin as a prognostic factor in thick cutaneous melanoma. *BMC Cancer*, vol. 10, no. 140, DOI: 10.1186.

Laflamme, M. A. and Murry, C.E. (2011). Heart regeneration. *Nature*, vol. 473, no. 7347, pp. 326-335.

Lagos-Quintana, M., Rauhut, R., Yalcin, A. *et al*. (2002). Identification of tissue-specific microRNAs from mouse. *Current Biology*, vol. 12, pp. 735-739.

Laurenti, E., Frelin, C., Xie, S. *et al*. (2015). CDK6 levels regulate quiescence exit in human hematopoietic stem cells. *Cell Stem Cell*, vol. 16, no. 3, pp. 302-313.

Lee, J., Choi, S., Baek, M. *et al*. (2013). $CoCl_2$ induces apoptosis through the mitochondria- and death receptor-mediated pathway in the mouse embryonic stem cells. *Molecular and Cellular Biochemistry*, vol. 379, no. 1-2, pp. 133-140.

Lee, S.C. and Pervaiz, S. (2007). Apoptosis in the pathophysiology of diabetes mellitus. *European Journal of Endocrinology*, vol. 149, pp. 99-102.

Lee, S., Yoon, D.S., Paik, S., Lee, K., Jang, Y. and Lee, J.W. (2014). MicroRNA-495 inhibits chondrogenic differentiation in human mesenchymal stem cells by targeting Sox9. *Stem Cells and Development*, vol. 23, no. 15, pp. 1798-1808.

Leri, A., Kajstura, J, and Anversa, P. (2005). Cardiac stem cells and mechanisms of myocardial regeneration. *Physiological Reviews*, vol. 85, pp. 1373-1416.

Leri, A., Rota, M., Hosoda, T., Goichberg, P. and Anversa, P. (2014). Cardiac stem cell niches. *Stem Cell Research*, vol. 13, no. 3, part B, pp. 631-646.

Letonja, M. and Petrovič. (2014). Is diabetic cardiomyopathy a specific entity? *World Journal of Cardiology*, vol. 6, pp. 8-13.

Li, C., Wu, X., Tong, J. *et al*. (2015). Comparative analysis of human mesenchymal stem cell from bone marrow and adipose tissue under xeno-free conditions for cell therapy. *Stem cell Research and Therapy*, vol. 5, no. 55, pp. 1-13.

Li, H., Radford, J.C., Ragusa, M.J. *et al*. (2008). Transcription factor MEF2C influences neural stem/progenitor cell differentiation and maturation *in vivo*. *Proceedings of the National Academy of Sciences of the United States of America*, vol. 105, no. 27, pp. 9397-9402.

Li, L. and Xie, T. (2005). Stem cell niche: structure and function. *Annual Review of Cell and Developmental Biology*, vol. 21, pp. 605-631.

Li, L., Zhang, S., Zhang, Y., Yu, B., Xu, Y. and Guan, Z. (2009). Paracrine action mediate the antifibrotic effect of transplanted mesenchymal stem cells in a rat model of global heart failure. *Molecular Biology Reports*, vol. 36, pp. 725-731.

Lis, S., Sun, L., Yang, L. *et al*. (2017). Young bone-marrow Sca-1^{+} stem cells rejuvenate the aged heart and improve function after injury through PDGFRβ-Akt pathway. *Scientific Reports*, vol. 7, Article number: 41756.

Li, S., Tang, P. and Lin, W. (2007). Intronic microRNA: discovery and biological implications. *DNA and Cell Biology* vol. 26, no. 4, pp. 195-207.

Li, T., Cheng, K., Lee, S. *et al*. (2010). Cardiospheres recapitulate a niche-like microenvironment rich in stem ness and cell-matrix interactions, rationalizing their enhanced functional potency for myocardial repair. *Stem Cells*, vol. 28, no. 11, pp. 2088-2098.

Li, X., Song, Y., Liu, D. *et al*. (2017). MiR-495 promotes senescence of mesenchymal stem cells by targeting Bmi-1. *Cellular Physiology and Biochemistry*, vol. 42, no. 2, pp. 780-796.

Li, Z., McKercher, S.R., Cui, J. *et al*. (2008). MEF2C as a neurogenic and anti-apoptotic transcription factor in murine embryonic stem cells. *Journal of Neuroscience*, vol. 28, no. 26, pp. 6557-6568.

Liang, W., Mason, A. and Lam, J. (2013). Western blot evaluation of siRNA delivery by pH-responsive peptides. *Methods in Molecular Biology*, vol. 986, pp. 73-87.

Lim, L.P., Lau, N.C., Garrett-Engele, P. *et al*. (2005). Microarray analysis shows that some microarrays downregulate large numbers of target mRNAs. *Nature*, vol. 433, pp. 769-773.

Ling, L., Gu, S., Cheng, Y. and Ding, L. (2017). bFGF promotes Sca-1^{+} cardiac stem cell migration through activation of the PI3K/Akt pathway. *Molecular Medicine Reports*, vol. 17, no. 2, pp. 2349-2356.

Liu, C., Calin, G.A., Volinia, S. and Croce, C.M. (2008). MicroRNA expression profiling using microarrays. *Nature Protocols*, vol. 3, pp. 563-578.

Liu, J., van Mil, A., Vrijsen, K. *et al*. (2011). MicroRNA-155 prevents necrotic cell death in human cardiomyocyte progenitor cells via targeting RIP1. *Journal of Cellular Molecular Medicine*, vol. 15, pp. 1474-82.

Liu, J., Wang, Y., Du, W., Yu, B. (2013). Sca-1 positive cardiac stem cell migration in a cardiac infarction model. *Inflammation*, vol. 36, no. 3, pp. 738-749.

Liu, J., Wang, L., Su, Z. *et al*. (2014). A reciprocal antagonism between miR-376c and TGF-β signalling regulates neural differentiation of human pluripotent stem cells, *The FASEB Journal*, vol. 28, no. 11, pp. 4642-4656.

Liu, J.F., Wang, B.W., Hung, H.F., Chang, H. and Shyu, K.G. (2008). Human mesenchymal stem cells improve myocardial performance in splenectomised rat model of chronic myocardial infarction. *Journal of Formosan Medical Association*, vol. 107, pp. 165-174.

Liu, X., Li, M., Peng, Y. *et al*. (2016). miR-30c regulates proliferation, apoptosis and differentiation via the Shh signalling pathway in P19 cells. *Experimental and Molecular Medicine*, vol. 48, no. 7, pp. 1-10.

Llorens, F., Hummel, M., Pantano, L. *et al*. (2013). Microarray and deep sequencing cross-platform analysis of the mirRNome and isomiR variation in response to epidermal growth factor. *BMC Genomics*, vol. 14, no. 371, DOI: 10.1186.

Lorenz, E., Uphoff, D., Reid, T.R., and Shelton, E. (1951). Modification of irradiation injury in mice and guinea pigs by bone marrow injections. *Journal of the National Cancer Institute*, vol. 12, pp. 197-201.

Ma, X., Zhu, Y., Huang, Y., Tegeler, T., Gao, S. and Zhang, J. (2015). Quantitative proteomic approach for microRNA target prediction based on $^{18}O/^{16}O$ labelling. *Cancer Informatics*, vol. 14, pp. 163-73.

Macfarland, T.W., Yates, J.M. (2016). Kruskal-Wallis H-test for one-way analysis of variance (ANOVA) by ranks. In: Introduction to nonparametric statistics for the biological sciences using R, R. Springer, Switzerland, pp. 177-211.

Mahony, D., Parry, D.A. and Lees, E. (1998). Active cdk6 complexes are predominantly nucleur and represent only a minority of the cdk6 in T cells. *Oncogene*, vol. 16, pp. 603-611.

Majno, G. and Joris, I. (1995). Apoptosis, oncosis, and necrosis: An overview of cell death. *American Journal of Pathology*, vol. 146, pp. 3-15.

Makkar, R.R., Smith, R.R., Cheng, K. *et al*. (2012). Intracoronary cardiosphere-derived cells for heart regeneration after myocardial infarction (CADUCEUS): a prospective randomised phase 1 trial. *The Lancet*, vol. 379, vol. 9819, pp. 895-904.

Malkov, V.A., Serikawa, K.A., Balantac *et al*. (2009). Multiplexed measurements of gene signatures in different analytes using the Nanostring nCounter assay system. *BMC Research Notes*, vol. 2, no. 1, pp. 80.

Mao, H.Z., Roussos, E.T. and Peterfy, M. (2006). Genetic analysis of the diabetes-prone C57BLKS/J mouse strain reveals genetic contribution from multiple strains. *Biochimica et Biophysica Acta – Molecular Basis of Disease*, vol. 1762, no. 4, pp. 440-446.

Matsuoka, S., Ebihara, Y., Xu, M. *et al*. (2001). CD34 expression on long-term repopulating hematopoietic stem cells changes during developmental stages. *Blood*, vol. 97, pp. 419-425.

Matsuura, K., Nagai, T., Nishigaki, N. *et al*. (2014). Adult cardiac Sca-1-positive cells differentiate into beating cardiomyocytes. *Journal of Biological Chemistry*, vol. 279, pp. 11384-11391.

McCulloch, E.A. and Till, J.E. (2005). Perspectives on the properties of stem cells. *Nature Medicine*, vol. 11, no.10, pp. 1026–1028.

Mendis, S., Thygesen, K., Kuulasmaa, K. *et al*. (2010). World health organization definition of myocardial infarction: 2008-09 revision. *International Journal of Epidemiology*, vol. 40, no. 1, pp. 139-146.

Meirelles, L.S., Chagastelles, P.C. and Nardi, N.B. (2006). Mesenchymal stem cells reside in virtually all post-natal organs and tissues. *Journal of Cell Science*, vol. 119, pp. 2204-2213.

Menard, C., Hagege, A.A., Agbulut, O. *et al*. (2005). Transplantation of cardiac-committed mouse embryonic stem cells to infarcted sheep myocardium: a preclinical study. *The Lancet*, vol. 366, pp. 1005-1012.

Messina, E., De Angelis, L., Frati, G. *et al*. (2004). Isolation and expansion of adult cardiac stem cells from human murine heart. *Cellular Biology*, vol. 95, no. 9, pp. 911-921.

Meyerson, M., and Harlow, E. (1994). Identification of G_1 kinase activity for ck6, a novel cyclin D partner. *Molecular and Cellular Biology*, vol. 14, no. 3, pp. 2077-2086.

Mielcarek, M., Martin, P.J., Leisenring, W. *et al*. (2003). Graft-versus-host disease after nonmyeloablative versus conventional hematopoietic stem cell transplantation. *Blood*, vol. 102, no. 2, pp. 756-762.

Mil, A.V., Vrijsen, K.R., Goumans, M.J., Metz, C.H., Doevendans, P.A. and Sluijter, J.P. (2013). MicroRNA-1 enhances the angiogenic differentiation of human cardiomyocyte progenitor cells. *Journal of Molecular Medicine*, vol. 91, pp. 1001-1012.

Mimeault, M. and Batra, S.K. (2008). Recent progress on tissue-resident adult stem cell biology and their therapeutic implications. *Stem Cell Review*, vol. 4, no. 1, pp. 27-49.

Min, H. and Yoon, S. (2010). Got target?: computational methods for microRNA target prediction and their extension. *Experimental and Molecular Medicine*, vol. 42, no. 4, pp. 233-244.

Min, I.M., Pietramaggiori, G., Kim, F.S., Passegué, E., Stevenson, K.E. and Wagers, A.J. (2008). The transcription factor EGR1 controls both the proliferation and localization of hematopoietic stem cells. *Cell Stem Cell*, vol. 2, no. 4, pp. 380-391.

Mishra, R., Vijayan, K., Colletti, E.J. *et al*. (2011). Characterization and functionality of cardiac progenitor cells in congenital heart patients. *Circulation*, vol. 123, no. 4, pp. 364-373.

Miyahara, Y. *et al*. (2006). Monolayered mesenchymal stem cells repair scarred myocardium after myocardial infarction. *Nature* Medicine, vol. 12, pp. 459–465.

Monsanto, M.M., White, K.S., Wang, B.J. (2017). Concurrent isolation of 3 distinct cardiac stem cell populations from a single human heart biopsy. *Circulation Research*, vol. 121, pp. 113-124.

Moore, A., Shindikar, A., Fomison-Nurse, I. *et al*. (2014). Rapid onset of cardiomyopathy in STZ-induced female diabetic mice involves the downregulation of pro-survival Pim-1. *Cardiovascular Diabetology*, vol. 167, no. 3, pp. 1076-1078.

Morey, J.S., Ryan, J.C. and Van Dolah, F.M. (2006). Microarray validation: factors influencing correlation between oligonucleotide microarrays and real-time PCR. *Biological Procedures Online*, vol. 8, pp. 175-193.

Murry, C. E. *et al*. (2004). Haematopoietic stem cells do not transdifferentiate into cardiac myocytes in myocardial infarcts. *Nature*, vol. 428, pp. 664–668.

Nadal-Ginard, B., Ellison, G.M. and Torella, D. (2014). The cardiac stem cell compartment is indispensable for myocardial cell homeostasis, repair and regeneration in the adult. *Stem Cell Research*, vol. 13, no. 3, part B, pp. 615-630.

Nagasawa, M., Gelfand, E.W. and Lucas, J.L. (2001). Accumulation of high levels of the p53 and p130 growth-suppressing proteins in cell lines stably over-expressing cyclin-dependent kinase 6 (cdk6). *Oncogene*, vol. 20, pp. 2889-2899.

Nagaya, N., Kangawa, K., Itoh, T. *et al*. (2005). Transplantation of mesenchymal stem cells improves cardiac function in a rat model of dilated cardiomyopathy. *Circulation*, vol. 112, pp. 1128-1135.

Nam, B.M., Kim, B.Y., Jo, Y.H. *et al*. (2013). Effect of cryopreservation and cell passage number on cell preparations destined for autologous chondrocyte transplantation. *Transplantation Proceedings*, vol. 46, no. 4, pp. 1145-1149.

Nguyen, V.T., Morange, M., Bensaude, O. (1988). Firefly luciferase luminescence assays using scintillation counters for quantitation in transfected mammalian cells. *Analytical Biochemistry*, vol. 171, no. 2, pp. 404-408.

Nussbaum, J., Minami, E., Laflamme, M.A. *et al*. (2007). Transpantation of undifferentiated murine embryonic stem cells in the heart: teratoma formation and immune response. *The FASEB Journal*, vol. 21, pp. 1345-1357.

O'Brien, M.A., Daily, W.J., Hesselberth, P.E. *et al*. (2005). Homogenous, bioluminescent protease assays: caspase-3 as a model. *Journal of Biomolecular Screening*, vol. 10, no. 2, pp. 137-148.

Oh, H., Bradfute, S.B., Gallardo, T.D. *et al*. (2003). Cardiac progenitor cells from adult myocardium: Homing, differentiation, and fusion after infarction. *Proceedings of the National Academy of Sciences of the United States of America*, vol. 100, no. 21, pp. 12313-12318.

Oh, H., Chi, X., Bradfute, S.B. *et al*. (2004). Cardiac muscle plasticity in adult and embryo by heart-derived progenitor cells. *Annals of the New York Academy of Sciences*, vol. 1015, pp. 182-9.

Oh, M., Rhee, S., Moon, J.H. *et al*. (2017). Literature-based condition-specific miRNA-mRNA target prediction. *PLOS ONE*, vol. 12, no. 3, e0174999.

Oliveira, A.C., Bovolenta, L.A., Nachtigall, P.G. *et al*. (2017). Combining results from distinct microRNA target prediction tools enhances the performance of analyses. *Frontiers in Genetics*, vol. 8, no. 59, DOI: 10.3389.

Ou, M., Zhang, X., Dai, Y. *et al*. (2014). Identification of potential microRNA-target pairs associated with osteopetrosis by deep sequencing, iTRAQ proteomics and bioinformatics. *European Journal of Human Genetics*, vol. 22, no. 5, pp. 625-632.

Ouyang, C., You, J. and Xie, Z. (2013). The interplay between autophagy and apoptosis in the diabetic heart. *Journal of Molecular and Cellular Cardiology*, vol. 71, pp. 71-80.

Oyeleye, O.O., Ogundeji, S.T., Ola, S.I. and Omitogun, O.G. (2016). Basics of animal cell culture: Foundation for modern science. *Biotechnology and Molecular Biology*, vol. 11, no. 2, pp. 6-16.

Pangare, M. and Makino, A. (2012). Mitochondrial function in vascular endothelial cell in diabetes. *Journal of Smooth Muscle Research*, vol. 48, pp. 1-26.

Paraskevopoulou, M.D., Georgakilas, G., Kostoulas, N. *et al*. (2013). DIANA-microT web server v5.0: service integration into mRNA functional analysis workflows. *Nucleic Acids Research*, W169-73.

Parcher, J.F., Wang, M., Chittiboyina, A.G. and Khan, I.A. (2018). In-source collision-induced dissociation (IS-CID): Applications, issues and structure elucidation with single-stage mass analyzers. *Drug Testing and Analysis*, vol. 10, no. 1, pp. 28-36.

Park, J.R., Kreissman, S.G., London, W.B. *et al*. (2017). A phase III randomized clinical trial (RCT) of tandem myeloblative autologous stem cell transplant (ASCT) using peripheral blood

stem cell (PBSC) as consolidation therapy for high-risk neuoblastoma (HR-NB): a children's oncology group (COG) study. *Journal of Clinical Oncology*, vol. 34, no. 18, DOI: 10.1200.

Paylor, B., Fernandes, J., McManus, B. and Rossi, F. (2013). Tissue-resident Sca1+ PDGFRα+ mesenchymal progenitors are the cellular source of fibrofatty infiltration in arrhythmogenic cardiomyopathy. *F1000Research*, DOI: 12688.

Pinzón, N., Li, B., Martinez, L. *et al*. (2017). MicroRNA target prediction programs predict many false positives. *Genome Research*, vol. 27, pp. 234-245.

Piriya pongsa, J., Bootchai, C., Ngamphiw, C. and Tongsima, S. (2014). MicroPIR2: a comprehensive database for human-mouse comparative study of microRNA-promoter interactions. *Database (Oxford)*, bau115, DOI: 1093.

Pittenger, M.F., Mackay, A.M., Beck, S.C. *et al*. (1999). Multilineage potential of adult human mesenchymal stem cells. *Science*, vol. 284, pp. 143-147.

Potdar, P.D. and Sutar, J.P. (2010). Establishment and molecular characterization of mesenchymal stem cell lines derived from human visceral and subcutaneous adipose tissues. *Journal of Stem Cells and Regenerative Medicine*, vol. 6, no. 1, pp. 26-35.

Promega. (2018). https://worldwide.promega.com/-/media/files/resources/protocols/technical-bulletins/101/caspase-glo-3-7-assay-protocol.pdf?la=en.

Purvis, N., Bahn, A. and Katare, R. (2015). The role of microRNAs in cardiac stem cells. *Stem Cells International*, DOI: 10.1155, Article ID: 194894.

Putnam, D., Namasivayam, V. and Burns, M.A. (2003). Cell affinity separations using magnetically stabilized fluidized beds: Erythrocyte subpopulation fractionation utilizing a lectin-magnetite support. *Biotechnology and Bioengineeering*, vol. 81, no. 6, pp. 650-665.

Rahimi, G., Jafari, N., Khodabaksh, M., Shirzad, Z. and Dogaheh, H.P. (2014). Upregulation of microRNA processing enzymes drosha and dicer in gestational diabetes mellitus. *Journal of Gynecological Endocrinology*, vol. 31, no. 2, pp. 156-159.

Raut, S.K., Kumar, A., Singh, G.B. *et al*. (2015). MiR-30c mediates upregulation of cdc42 and pak1 in diabetic cardiomyopathy. *Cardiovascular Therapeutics*, vol. 33, no. 3, pp. 89-97.

Raut, S.K., Singh, G.B., Rastogi, B. *et al*. (2016). MiR-30c and miR-181a synergistically modulate p53-p21 pathway in diabetes induced cardiac hypertrophy. *Molecular and Cellular Biochemistry*, no. 417, no. 1-2, pp. 191-203.

Raveh-Amit, H., Berzsenyi, S., Vas, V., Ye, D. and Dinnyes, A. (2013). Tissue resident stem cells: till death do us part. *Biogerontology*, vol. 14, no. 6, pp. 573-590.

Rawal, S., Manning, P. and Katare, R. (2014). Cardiovascular microRNAs: asmodulators and diagnostic biomarkers of diabetic heart disease. *Cardiovascular Diabetology*, vol. 13, article 44.

Rawal, S., Munasinghe, P.E., Shindikar, A. *et al*. (2017). Down-regulation of proangiogenic microRNA-126 and microRNA-132 are early modulators of diabetic cardiac microangiopathy. *Cardiovascular Research*, vol. 113, no. 1, pp. 90-101.

Rawal, S., Ram, T., Coffey, S. *et al*. (2016). Differential expression pattern of cardiovascular microRNAs in the human type-2 diabetic heart with normal ejection fraction. *International Journal of Cardiology*, vol. 202, pp. 40-43.

Rennert, R.C., Sorkin, M., Garg, R.K. and Gurtner, G.C. (2013). Stem cell recruitment after injury: lessons for regenerative medicine. *Regenerative Medicine*, vol. 7, no. 6, pp. 833-850.

Rippon, H.J. and Bishop, A.E. (2004). Embryonic stem cells. *Cell Proliferation*, vol. 37, pp. 23-34.

Roda, B., Lanzoni, G., Alviano, F. *et al*. (2009). A novel stem cell tag-less sorting method. *Stem Cell Reviews and Reports*, vol. 5, no. 4, pp. 420-427.

Rodier, F., Coppé, J.P., Patil, C.K. *et al*. (2009). Persistent DNA damage signalling triggers senescence-associated inflammatory cytokine secretion. *Nature Cell Biology*, vol. 11, no. 8, pp. 973-979.

Rodier, F., Muñoz, D.P., Teachenor, R. *et al*. (2011). DNA-SCARS: distinct nuclear structures that sustain damage-induced senescence growth arrest and inflammatory cytokine secretion. *Journal of Cell Science*, vol. 124, pt 1, pp. 68-81.

Rodrigues, M.F., Sedassari, B.T., Esteves, C.M. *et al*. (2017). Embryonic stem cells markers oct4 and nanog correlate with perineural invasion in human salivary gland mucoepidermoid carcinoma. *Journal of Oral Pathology and Medicine*, vol. 46, no. 2, pp. 112-120.

Roshan, R., Shridhar, S., Sarangdhar, M.A. *et al*. (2014). Brain-specific knockdown of miR-29 results in neuronal cell death and ataxia in mice. *RNA*, vol. 20, pp. 1287-1297.

Rostovtseva, T.K., Kazemi, N., Weinrich, M. and Bezrukov, S.M. (2006). Voltage gating of VDAC is regulated by nonlamellar lipids of mitochondrial membranes. *Journal of Biological Chemistry*, vol. 281, pp. 37496-37506.

Rota, M., LeCapitaine, N., Hosoda, T. *et al*. (2006). Diabetes promotes cardiac stem cell aging and heart failure, which are prevented by deletion of the p66shc gene. *Circulation Research*, vol. 99, no. 1, pp. 42-52.

Ruby, J.G., Jan, C.H. and Bartel, D.P. (2007). Intronic microRNA precursors that bypass drosha processing. *Nature*, vol. 448, pp. 83–86.

Ryzhov, S., Goldstein, A.E., Novitskiy, S.V. *et al*. (2012). Role of A-2B adenosine receptors in regulation of paracrine functions of stem cell antigen 1-positive cardiac stromal cells. *Journal of Pharmacology and Experimental Therapeutics*, vol. 341, no. 3, pp. 764-774.

Salabei, J.K., Lorkiewicz, P.K., Mehra, P. *et al*. (2016). Type 2 Diabetes dysregulates glucose metabolism in cardiac progenitor cells. *Journal of Biological Chemistry*, vol. 291, no. 26, pp. 13634-13648.

Sapan, C.V., Lundblad, R.L. and Price, N.C. (2010). Colorimetric protein assay techniques. *Biotechnology and Applied Biochemistry*, vol. 29, no. 2, pp. 99-108.

Santini, M.P., Forte, E., Harvey, R.P. and Kovacic, J.C. (2016). Developmental origin and lineage plasticity of endogenous cardiac stem cells. *Development*, vol. 143, pp. 1242-1258.

Sasaki, K., Donthamsetty, R., Heldak, M., Cho, Y., Scott, B.T. and Makino, A. (2012). VDAC: old protein with new roles in diabetes. *American Journal of Physiology-Cell Physiology*, vol. 303, no. 10, pp. C1055-C1060.

Scadden, D.T. (2006). The stem-cell niche as an entity of action. *Nature*, vol. 441, pp. 1075-79.

Scheicher, R., Hoelbl-Kovacic, A., Bellutti, F. *et al*. (2015). CDK6 as a key regulator of hematopoietic and leukemic stem cell activation. *Blood*, vol. 125, no. 1, pp. 90-101.

Schmittgen, T.D. and Livak, K.J. (2008). Analyzing real-time PCR data by the comparative C_T method. *Nature Protocols*, vol. 3, pp. 1101-1108.

Schuleri, K.H., Feigenbaum, G.S., Centola, M. *et al*. (2009). Autologous mesenchymal stem cells produce reverse remodelling in chronic ischaemic cardiomyopathy. *European Heart Journal*, vol. 30, pp. 2722-2732.

Schwartz, A., Marti, G.E., Poon, R. *et al*. (1998). Standardizing flow cytometry: a classification system of fluorescence standards used for flow cytometry. *Cytometry*, vol. 33, pp. 106-114.

Segers, V.F.M. and Lee, R.T. (2008). Stem-cell therapy for cardiac disease. *Nature*, vol. 451, pp. 937-942.

Shantikumar, S., Caporali, A. and Emanueli, C. (2012). Role of microRNAs in diabetes and its cardiovascular complications. *Cardiovascular Research*, vol. 93, no. 4, pp. 583-593.

Shi-Wen, X., Leask, A., and Abraham. (2008). Regulation and function of connective tissue growth factor/CCN2 in tissue repair, scarring and fibrosis. *Cytokine and Growth Factor Reviews*, vol. 19, pp. 133-144.

Shoshan-Barmatz, V., Zakar, M., Rosenthal, K. and Abu-Hamad, S. (2009). Key regions of VDAC1 functioning in apoptosis induction and regulation by hexokinase. *Biochimica et Biophysica Acta – Bioenergentics*, vol. 1787, no. 5, pp. 421-430.

Sivitz, W.I. and Yorek, M.A. (2010). Mitochondrial dysfunction in diabetes: From molecular mechanisms to functional significance and therapeutic opportunities. *Antioxidants and Redox Signaling*, vol. 12, no. 4, pp. 537-577.

Sluijter, J.P.G., van Mil, A., van Vliet. *et al*. (2010). MicroRNA-1 and -499 regulate differentiation and proliferation in human-derived cardiomyocyte progenitor cells. *Arteriosclerosis, Thrombosis, and Vascular Biology*, vol. 30, no. 4, pp. 859-868.

Soh, J., Iqbal, J., Queiroz, J., Fernandez-Hernando, C. and Hussain, M.M. (2013). MicroRNA-30c reduces hyperlipidemia and atherosclerosis by decreasing lipid synthesis and lipoprotein secretion. *Nature Medicine*, vol. 19, no. 7, pp. 892-900.

Stem cell timeline. (2015). *Heart Views*, vol. 16, no. 2, pp. 72-73.

Stocker, R. and Keaney, J.F. (2003). Role of oxidative modifications in atherosclerosis. *Physiological Reviews*, vol. 84, pp. 1381-1478.

Sultana, N., Zhang, L., Yan, J. *et al*. (2015). Resident c-kit(+) cells in the heart are not cardiac stem cells. *Nature Communications*, vol. 6, DOI: 10.1038.

Sun, F., Fu, H., Liu, Q. *et al*. (2008). Downregulation of CCND1 and CDK6 by miR-34a induces cell cycle arrest. *FEBS Letters*, vol. 582, no. 10, pp. 1564-1568.

Sun, T., Li, W. and Ling, S. (2016). MiR-30c and semaphoring 3A determine adult neurogenesis by regulating proliferation and differentiation of stem cells in the subventricular zones of mouse. *Cell Proliferation*, vol. 49, no. 3, pp. 270-280.

Takai, H., Smogorzewska, A. and de Lange, T. (2003). DNA damage foci at dysfunctional telomeres. *Current Biology*, vol. 13, no. 17, pp. 1549-56.

Takaya, T., Ono, K., Kawamura, T. *et al*. (2009). MicroRNA-1 and microRNA-133 in spontaneous myocardial differentiation of mouse embryonic stem cells. *Circulation Journal*, vol. 73, pp. 1492-1497.

Takamiya, M., Haider, K.H. and Ashraf, M. (2011). Identification and characterization of a novel multipotent sub-population of sca-1+ cardiac progenitor cells for myocardial regeneration. *PLOS ONE*, vol. 6, no. 9, pp. 1-11.

Tanic, M., Yanowsky, K., Rodriguez-Antona, C. *et al*. (2012). Deregulated miRNAs in hereditary breast cancer revealed a role for miR-30c in regulating KRAS oncogene. *PLOS ONE*, vol 7. No. 6, DOI: 10.1371.

Tasat, D.R., Mancuso, R., O'Connor, S., Molinari, B. (2003). Age-dependent change in reactive oxygen species and nitric oxide generation by rat alveolar macrophages. *Aging Cell*, vol. 2, pp. 159-164.

Tateishi, K., Ashihara, E., Honsho, S. *et al*. (2007). Human cardiac stem cells exhibit mesenchymal features and are maintained through Akt/GSK3beta signaling. *Biochemical and Biophysical Research Communications*, vol. 352, no. 3, pp. 635-41.

Thiel, A., Scheffold, A. and Radbruch, A. (1998). Immunomagnetic cell sorting – pushing the limits. *Immunotechnology*, vol. 4, no. 2, pp. 89-96.

Thompson, J.A., Itskovitz-Eldor, J., Shapiro, S.S., Waknitz, M.A. *et al*. (1998). Embryonic stem cell lines derived from human blastocysts. *Science*, vol. 282, pp. 1145-1147.

Trauger, S.A., Webb, W. and Siuzdak, G. (2002). Peptide and protein analysis with mass spectrometry. *Spectroscopy*, vol. 16, no. 1, pp. 15-28.

Tripathi, B.K. and Srivastava, A.K. (2006). Diabetes mellitus: complications and therapeutics. *Medical Science Monitor*, vol. 12, no. 7, RA130-147.

Turinetto, V., Vitale, E. and Giachino, C. (2016). Senescence in human mesenchymal stem cells: functional changes and implications in stem cell-based therapy. *International Journal of Molecular Sciences*, vol. 17, no. 7, pp. 1-18.

Ullah, I., Subbarao, R.B. and Rho, G.J. (2015). Human mesenchymal stem cells – current trends and future prospective. *Bioscience Reports*, vol. 35, no. 2, e00191.

Unger, R.E., Krump-Konvalinkova, V., Peters, K. Kirkpatrick, C.J. (2002). *In vitro* expression of the endothelial phenotype: comparative study of primary isolated cells and cell line, including the novel cell line HPMEC-ST1.6R. *Microvascular Research*, vol. 64, no. 3, pp. 384-397.

Urbanek, K., Torella, D., Sheikh, F. *et al*. (2005). Myocardial regeneration by activation of multipotent cardiac stem cells in ischemic heart failure. *Proceedings of the National Academy of Sciences of the United States of America*, vol. 102, no. 19, pp. 8692-8697.

Valente, M., Nascimento, D.S., Cumano, A. and Pinto-do-Ó, P. (2014). Sca1+ cardiac progenitor cells and heart-making: a critical synopsis. *Stem cells and Development*, vol. 23, no. 19, pp. 2263-2273.

Van belle, T.L., Coppieters, K.T. and Von Herrath, M.G. (2011). Type 1 diabetes: etiology, immunology, and therapeutic strategies. *Physiological Reviews*, vol. 91, pp. 79-118.

Veldman-Jones, M.H., Brant, R., Rooney, C. *et al*. (2015). Evaluating robustness and sensitivity of the nanostring technologies nCounter platform to enable multiplexed gene expression analysis of clinical samples. *Cancer Research*, vol. 75, no. 13, DOI: 10.1158.

Vicinanza, C., Aquila, L., Scalise, M. *et al*. (2017). Adult cardiac stem cells are multipotent and robustly myogenic: c-kit expression is necessary but not sufficient for their identification. *Cell Death and Differentiation*, vol. 24, pp. 2101-2116.

Vlachos, S., Kostoulas, N., Vergoulis, T. *et al*. (2012). DIANA miRPath v.2.0: investigating the combinatorial effect of microRNAs in the pathways. *Nucleic Acids Research*, W498-504.

Wahid, F., Shehzad, A., Khan, T. and Kim, Y.Y. (2010). MicroRNAs: synthesis, mechanism, function, and recent clinical trials. *Biochimica et Biophysica Acta – Molecular Cell Research*, vol. 1803, no. 11, pp. 1231-1243.

Wang, H., Chen, H., Feng, B. *et al*. (2014). Isolation and characterization of a Sca-1^+ /$CD31^-$ progenitor cell lineage derived from mouse heart tissue. *BMC Biotechnology*, vol. 14, no. 75, DOI: 10.1186.

Wang, J., Chen, J. and Sen, S. (2016). MicroRNA as biomarkers and diagnostics. *Journal of Cellular Physiology*, vol. 231, no. 1, pp. 25-30.

Wang, L., Min, L., Guo, Q. *et al*. (2017). Profiling microRNA from brain by microarray in a transgenic mouse model of Alzheimer's disease. *BioMed Research International*, DOI: 10.115, Article ID: 8030369.

Wang, P., Luo, Y., Duan, H., Xing, S., Zhang, J., Lu, D., Feng, J., Yang, D., Song, L. and Yan, X. (2013). MicroRNA 329 suppresses angiogenesis by targeting CD146. *Molecular and Cellular Biology*, vol. 33, no. 18, pp. 3689-3699.

Wang, X., Hu, Q., Nakamura, Y. *et al*. (2009). The role of the Sca-1^+ /$CD31^-$ cardiac progenitor cell population in postinfarction left ventricular remodelling. *Stem Cells*, vol. 24, no. 7, pp. 1779-1788.

Wang, X., Lu, X., Zhang, T. *et al*. (2016). MiR-329 restricts tumor growth by targeting grb2 in pancreatic cancer. *Oncotarget*, vol. 7, no. 16, pp. 21441-21453.

Welton, S.M., Bastiaansen, A.J., de Jong, R. *et al*. (2014). Inhibition of 14q32 microRNAs miR-329, miR-487b, miR-494 and miR-495 increases neovascularization and blood flow recovery after ischemia. *Circulation Research*, vol. 121, no. 8, pp. 1-16.

Widlansky, M.E., Wang, J., Shenouda, S.M. *et al*. (2010). Altered mitochondrial membrane potential, mass, and morphology in the mononuclear cells of humans with type 2 diabetes. *Translational Research*, vol. 156, no. 1, pp. 15-25.

Wiese, S., Reidegeld, K.A., Meyer, H.E. and Warscheid, B. (2007). Protein labelling by iTRAQ: A new tool for quantitative mass spectrometry in proteome research. *Proteomics*, vol. 7, pp. 340-350.

Wilker, P.R., Kohyama, M., Sandau, M.M. (2008). Transcription factor Mef2c is required for B cell proliferation and survival after antigen receptor stimulation. *Nature Immunology*, vol. 9, pp. 603-612.

Winter, J., Jung, S., Keller, S., Gregory, R.I. and Diederichs, S. (2009). Many roads to maturity: microRNA biogenesis pathways and their regulation. *Nature Cell Biology*, vol. 11, pp. 228–234.

Wiśniewski, J.R., Zougman, A., Nagaraj, N. and Mann, M. (2009). Universal sample preparation method for proteome analysis. *Nature Methods*, vol. 6, no. 5, pp. 359-62.

Witkos, T.M., Koscianska, E. and Krzyzosiak, W.J. (2011). Practical aspects of microRNA target prediction. *Current Molecular Medicine*, vol. 11, no. 2, pp. 93-109.

Wong, N. and Wang, X. (2015). MiRDB: an online resource for microRNA target prediction and functional annotations. *Nucleic Acids Research*, vol. 43, D146-D152.

World health organization. (2018). Http://www.who.int/features/factfiles/noncommunicable_diseases/en/.

World health organization. (2018). Http://www.who.int/news-room/fact-sheets/detail/cardiovascular-diseases-(cvds).

Wu, J., Qian, J., Li, C. *et al*. (2010). MiR-129 regulates cell proliferation by downregulating Cdk6 expression. *Cell Cycle*, vol. 1, no. 9, pp. 1809-1818.

Wysocki, V.H., Resing, K.A., Zhang, Q., Cheng, G. (2005). Mass spectrometry of peptides and proteins. *Methods*, vol. 35, no. 3, pp. 211-222.

Xiao, B., Tan, L., He, B., Liu, Z. and Xu, R. (2013). MiRNA-329 targeting E2F1 inhibits cell proliferation in glioma cells. *Journal of Translational Medicine*, vol. 11, no. 172, pp. 1-10.

Xiao, J., Liang, D., Zhang, H. (2012). MicroRNA-204 is required for differentiation of human-derived cardiomyocyte progenitor cells. *Journal of Molecular and Cellular Cardiology*, vol. 53, pp. 751-759.

Xiao, J., Pan, Y., Li, X.H. *et al*. (2016). Cardiac progenitor cell-derived exosomes prevent cardiomyocytes apoptosis through exosomal miR-21 by targeting PDCD4. *Cell Death and Disease*, vol. 7, pp. e2277.

Xing, Y., Hou, J., Guo, T. *et al*. (2014). MicroRNA-378 promotes mesenchymal stem cell survival and vascularization under hypoxic-ischemic conditions *in vitro*, *Stem Cell Research and Therapy*, vol. 5, no. 6: 130.

Xu, L. and Li, G. (2014). Circulating mesenchymal stem cells and their clinical implications. *Journal of Orthopaedic Translation*, vol. 2, no. 1, pp. 1-7.

Yadav, S.K. and Mishra, P.K. (2018). Isolation, characterization and differentiation of mouse cardiac progenitor cells. *Methods in Molecular Biology*, vol. 1842, pp. 183-191.

Yamamoto, H., Quinn, G., Asari, A. *et al*. (2003). Differentiation of embryonic stem cells into hepatocytes: biological functions and therapeutic application. *Hepatology*, vol. 37, no. 5, pp. 983-93.

Yang, H., Li, Q., Zhao, W., Yuan, D., Zhao, H. and Zhou, Y. (2014). MiR-329 suppresses the growth and motility of neuroblastoma by targeting KDM1A. *FEBS Letters*, vol. 588, pp. 192-7.

Ye, H., Ling, S., Castillo, A.C. *et al*. (2013). Nebivolol induces distinct changes in profibrosis microRNA expression compared with atenolol, in salt-sensitive hypertensive rats. *Hypertension*, vol. 61, pp. 1008-1013.

Yuan, S.H., Martin, J., Elia, J. (2011). Cell-surface marker signatures for the isolation of neural stem cells, glia and neurons derived from human pluripotent stem cells. *PLOS ONE*, vol. 6, no. 3, pp. 1-16.

Zampetaki, A., Kiechl, S., Drozdov, I. (2010). Plasma microRNA profiling reveals loss of endothelial miR-126 and other microRNAs in type 2 diabetes. *Circulation Research*, vol. 107, no. 6, pp. 810-817.

Zannad, F., Agrinier, N. and Alla, F. (2009). Heart failure burden and therapy. *EP Europace*, vol. 11, no. suppl_5, pp. v1-v9.

Zhang, F. and Guo, F. (2018). Effect of transplantation of cardiac stem cells overexpressing integrin-linked kinase on cardiac function of rats with acute myocardial infarction. *Experimental and Therapeutic Medicine*, vol. 16, no. 2, pp. 746-750.

Zhao, J., Lin, J., Zhu, D. *et al*. (2014). MiR-30-5p functions as a tumor suppressor and novel therapeutic tool by targeting the oncogenic Wnt/β-Catenin/BCL9 pathway. *Therapeutics, Targets and Chemical Biology*, vol. 74, no. 6, DOI: 10.1158.

Zhu, B. and Murthy, S.K. (2014). Stem cell separation technologies. *Current Opinion in Chemical Engineering*, vol. 2, no. 1, pp. 3-7

APPENDICES

APPENDIX 1: LIST OF REAGENTS

Table A1.1 List of buffers used and their composition

No.	Solution	Reagents
1	Phosphate Buffer Saline (PBS)	10 mM Sodium Phosphate Monobasic 1.8 mM Potassium Phosphate Dibasic 137 mM Sodium Chloride 2.7 mM Potassium Chloride
2	Hank's Balanced Salt Solution (HBSS)	1.26 mM Calcium Chloride Dihydrate 0.49 mM Magnesium Chloride Hexahydrate 0.41 mM Magnesium Sulphate Heptahydrate 5.3 mM Potassium Chloride 0.22 mM Potassium Phosphate 4.17 mM Sodium Bicarbonate 138 mM Sodium Chloride 0.34 mM Sodium Phosphate Dibasic 5.55 D-Glucose
3	Kreb's Ringer Hienslet Buffer (KRH)	116 mM Sodium Chloride 4 mM Potassium Chloride 1 mM Magnesium Chloride 1.8 mM Calcium Chloride 25 mM Glucose 10 nM HEPES Acid (adjusted to pH 7.4)
4	Collagenase type II and IV	0.02g/mL collagenase type II and IV (1357 Unit)
5	SDS-Page gel solution	12% Resolving gel (per gel): 5.3 mL dH_2O 4 mL Lower Tris (adjusted to pH 8.8) 160 µL 10% SDS 6.4 mL 30% Acrylamide/Bis-acrylamide 160 µL 10% Ammonium persulfate 10 µL TEMED 4% Stacking gel (per gel): 4.2 mL dH_2O 1.75 mL Upper Tris (adjusted to pH 6.8) 70 µL 10% SDS 0.931 mL 30% Acrylamide/Bis-acrylamide 70 µL 10% Ammonium persulfate 7 µL TEMED
6	TBS-T	0.05% TBS-T in dH_2O: 8g Sodium Chloride 0.2g Potassium Chloride 3g Tris 1L dH_2O 80 mL Tween20
7	FACS buffer	3 mM HEPES in HBSS buffer 1% Fetal Bovine Serum
8	Loading buffer	2X Loading buffer: 4.165 mL Upper Tris 10 mL 20% SDS 20 mL 50% glycerol 5 mL 30% mercaptoethanol 500 µL EDTA (200mM)

		10.38 mL dH_2O 0.05% bromophenol blue
9	RIPA lysis buffer	50 mM Tris-HCl: 0.6057g Tris 100 mL dH_2O (adjusted tp pH 7.4) 8.766g Sodium Chloride 0.0292g EDTA 1mL SDS (0.1% normally, 0.02% for MS) 1mL Triton x100

Table A1.2 List of antibodies used

No.	Type of antibody	Name of antibody	Species raised in	Dilution	Manufacturer
1	Monoclonal	Anti-Sca-1-FITC	Mouse	1:100	Miltenyl Biotenic
2	Polyclonal	Anti-VDAC1	Rabbit	1:1000	abcam
3	Monoclonal	Anti-CDK6	Mouse	1:1000	Cell Signaling Technology
4	Polyclonal	Anti-α-tubulin	Rabbit	1:1000	abcam
5	Secondary	Anti-mouse IgG	Goat	1:3000	ThermoFisher
6	Secondary	Anti-rabbit IgG	Mouse	1:3000	ThermoFisher
7	Monoclonal	Anti-CD34-APC	Human	1:50	eBiosciences
8	Monoclonal	Anti-CD90-FITC	Human	1:50	eBiosciences
9	Monoclonal	Anti-CD105-PE-Cy7	Human	1:50	eBiosciences

APPENDIX 2: FLUOROPHORES AND TUBE DESIGN FOR FLOW CYTOMETRY

Fluorophore	Emission wavelength	Excitation wavelength	Channel in flow cytometer	Conjugated antibody
APC	660	640 (red)	FL6	CD34
PE-Cy7	774	496, 565 (blue)	FL5	CD105, Sca-1
PI	620	488 (blue)	FL3	
FITC	525	488 (blue)	FL1	CD90

Table A2.1 Fluorophores and their conjugated antibodies that were used in FACS experiments. APC = Allophycocyanin, PE-Cy7 = Phycoerythrin–Cyanin 7, PI = Propidium Iodide, FITC = Fluorescein isothiocyanate.

Tube number	Solution/sample	Compensation	Beads/PI
1	FITC-CD90	Yes	Beads
2	PE-Cy7-CD105/Sca-1	Yes	Beads
3	APC-CD34	Yes	Beads
4	PI-Live	Yes	PI
5	PI-Dead	Yes	PI
6	Unstained CSC sample	No	-
7	Stained CSC sample	No	PI

Table A2.2 Tube set up for FACS experiment. The table shows the antibody (with conjugated fluorophore) solutions, as well as the CSC samples included in the reaction. It also shows whether the samples were used for compensation, and whether they were stained with the AbC Capture beads or PI.

APPENDIX 3: RNA AND PROTEIN QUANTIFICATION

I extracted RNA from the diabetic and non-diabetic CSCs in order to measure the transfectional efficiency of the miR-30c precursor mimic. The concentrations and purity of this RNA is shown below.

Sample	Concentration (ng/µL)	Purity (260/280)
Non-diabetic #1 scr A	14.76	1.768
Non-diabetic #1 scr B	14.44	1.799
Non-diabetic #1 scr C	7.41	1.860
Non-diabetic #1 30c A	11.38	2.030
Non-diabetic #1 30c B	9.42	1.845
Non-diabetic #1 30c C	8.37	1.847
Non-diabetic #2 scr A	5.96	2.050
Non-diabetic #2 scr B	12.58	1.767
Non-diabetic #2 scr C	9.38	1.894
Non-diabetic #2 30c A	8.09	2.100
Non-diabetic #2 30c B	8.25	2.095
Non-diabetic #2 30c C	6.54	2.083
Non-diabetic #3 scr A	7.52	1.928
Non-diabetic #3 scr B	8.98	1.923
Non-diabetic #3 scr C	34.85	1.820
Non-diabetic #3 30c A	11.41	1.821
Non-diabetic #3 30c B	9.26	1.792
Non-diabetic #3 30c C	11.30	1.893
Non-diabetic #4 scr A	12.42	1.997
Non-diabetic #4 scr B	14.54	1.812
Non-diabetic #4 scr C	15.86	2.026
Non-diabetic #4 30c A	22.11	1.849
Non-diabetic #4 30c B	26.15	1.971
Non-diabetic #4 30c C	20.20	1.860
Diabetic #1 scr A	13.65	1.940
Diabetic #1 scr B	9.22	2.089
Diabetic #1 scr C	9.73	2.084
Diabetic #1 30c A	9.23	2.084
Diabetic #1 30c B	14.90	2.117
Diabetic #1 30c C	11.19	1.912
Diabetic #2 scr A	8.84	1.860
Diabetic #2 scr B	14.50	1.989
Diabetic #2 scr C	15.34	1.921
Diabetic #2 30c A	14.34	2.008
Diabetic #2 30c B	15.97	1.978
Diabetic #2 30c C	13.08	1.875
Diabetic #3 scr A	7.07	2.032

Diabetic #3 scr B	11.59	1.884
Diabetic #3 scr C	10.27	2.038
Diabetic #3 30c A	9.25	2.035
Diabetic #3 30c B	10.07	1.856
Diabetic #3 30c C	10.10	1.925
Diabetic #4 scr A	5.24	2.068
Diabetic #4 scr B	5.58	2.073
Diabetic #4 scr C	4.83	1.881
Diabetic #4 30c A	7.91	1.878
Diabetic #4 30c B	9.51	2.102
Diabetic #4 30c C	10.54	1.869

Table A3.1 The table shows concentrations (ng/µL) of total RNA extracted from diabetic (n=4) and non-diabetic CSCs (n=4), transfected with either miR-30c precursor mimic (30c) or scrambled mimic (scr). Each transfected sample was extracted in triplicate (A, B and C) and analysed by a Nanodrop Spectrophotometer. The purity of the RNA is also shown by the standard 260/280 absorbance

I quantified total protein extracted from the diabetic (n=4) and non-diabetic CSCs (n=4) using the Bradford method. The optical density of each protein sample was first calculated by comparing their absorbance with the BSA reference standard curve. The following figure shows the reference standard curve, along with graph equation that can be used to calculate the optical density (x in the equation) of the protein samples, as well as the R-squared (line of best fit) measure of statistical regression. In this case, an R-squared value of 0.9604 (~1.0) indicates that there is little variation between the variables, and thus the standard curve is reliable.

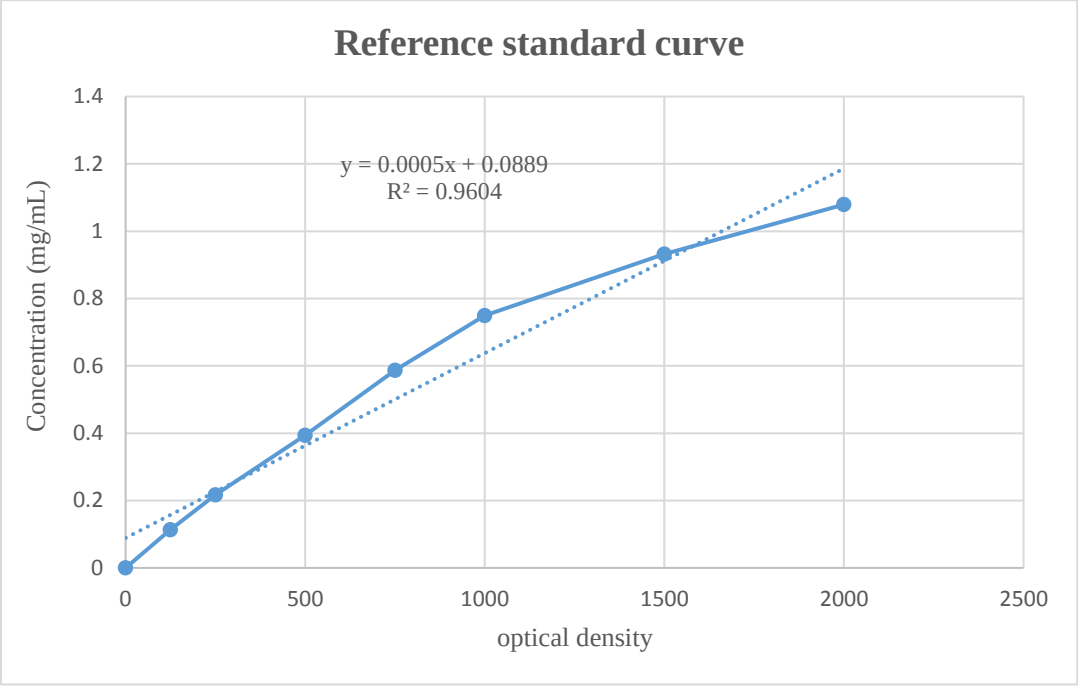

Figure A3. Reference standard curve graph for Bradford method of protein quantification. The graph shows a standard curve of BSA concentration relative to optical density, which can be used to determine the optical density (x) of the protein samples. The R-squared value is also included to show the statistical regression of the standard curve.

The optical density of each protein sample can then be used to calculate the protein concentrations as shown in example below.

Sample (5x dilution)	Optical density	Concentration in assay (mg/mL)	Concentration (mg/mL)
Non-diabetic #1 scr	0.34	0.52	2.59
Non-diabetic #1 30c	0.50	0.83	4.15
Non-diabetic #2 scr	0.62	1.06	5.41
Non-diabetic #2 30c	0.53	0.89	4.45
Non-diabetic #3 scr	0.49	0.83	4.15
Non-diabetic #3 30c	0.31	0.48	2.39
Non-diabetic #4 scr	0.30	0.44	2.21
Non-diabetic #4 30c	0.46	0.76	3.82
Diabetic #1 scr	0.31	0.48	2.38
Diabetic #1 30c	0.37	0.59	2.95
Diabetic #2 scr	0.52	0.89	4.43
Diabetic #2 30c	0.45	0.76	3.79
Diabetic #3 scr	0.42	0.68	3.42
Diabetic #3 30c	0.41	0.65	3.23
Diabetic #4 scr	0.60	1.03	5.18
Diabetic #4 30c	0.38	0.93	4.66

Table A3.2 The table shows how the protein concentration was calculated from the optical density of each diabetic (n=4) and non-diabetic sample (n=4) transfected with either miR-30c precursor mimic (30c) or scrambled mimic (scr). The samples used in the Bradford assay were diluted (1 in 5) to obtain working solutions. Using the graph equation of the reference standard curve, the concentration of protein in the assay, as well as the concentration of the sample can be calculated.

APPENDIX 4: PONCEAU STAIN IMAGE

Figure A4. Ponceau stain of total protein derived from non-diabetic (n=4) and diabetic (n=4) mouse CSCs. The blot was performed to determine CDK6 expression in the non-diabetic and diabetic CSCs. The image was taken using the Syngene PXi gel imaging system (Atkinson, USA) and the proteins bands can be seen in each lane of the membrane.

APPENDIX 5: COUNTING CSCS USING HEMOCYTOMETER

In this project, a hemocytometer was used to count the CSCs. The following procedure was used to determine the appropriate number of CSCs to seed into flasks, as well as for experiments that required a cell count (eg. MACS purification).

The CSCs were trypsinized and pelleted, before re-suspension in 1 mL DMEM/F21 media.. After gently mixing the cell suspension, 10 µL of the cell suspension was added onto the hemocytometer grid, as well as an additional 10 µL to the opposite grid. A flat cover slip was placed on top of both grids (without air bubbles) and the cells visualized under a light microscope. The CSCs were counted in each of the four corner squares, as well as in the centre square of the grid, and divided by five. The cell counts from each grid were averaged to give the number of CSCs (x 10^4/mL) in each sample. This was used to calculate the volume of cell suspension required by dividing the desired cell number by the CSC count, as shown in the table below.

Eg. After the diabetic and non-diabetic CSCs were cultured to P3 in T75 flasks, the CSCs were counted to achieve the desired number for MACS purification (1 x 10^7).

Sample	**CSC count (per mL)**	**Number of CSCs needed for MACS**	**Volume of cell suspension required (mL)**
Diabetic #1	1.9 x 10^7	1 x 10^7	526
Diabetic #2	2.4 x 10^7	1 x 10^7	417
Diabetic #3	1.3 x 10^7	1 x 10^7	769
Diabetic #4	2.8 x 10^7	1 x 10^7	357
Non-diabetic #1	1.5 x 10^7	1 x 10^7	667
Non-diabetic #2	2.6 x 10^7	1 x 10^7	385
Non-diabetic #3	1.9 x 10^7	1 x 10^7	526
Non-diabetic #4	1.4 x 10^7	1 x 10^7	714

Table A5. Volumes of diabetic and non-diabetic CSC cell suspensions required from MACS purification based on cell count.

APPENDIX 6: IMAGE OF CSCS AFTER 10 WEEKS

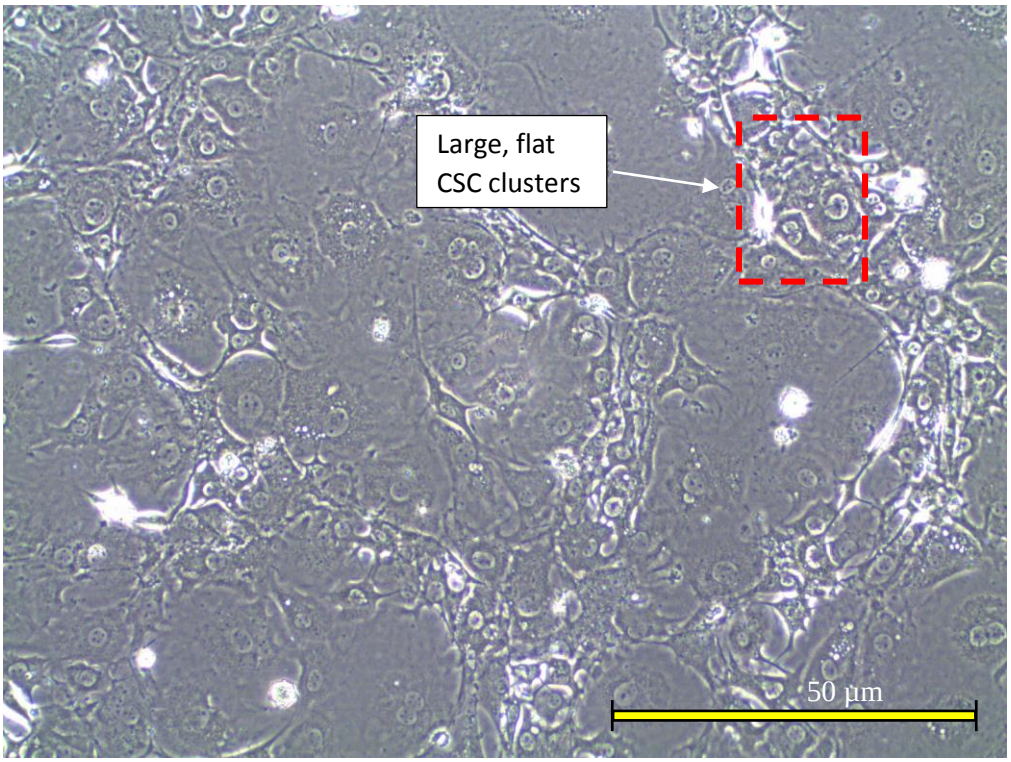

Figure A6. Phase contrast image taken from observing purified CSCs under a light microscope. The cells are shown at 10 weeks following initial isolation from diabetic mouse heart tissue. Cells appear similar to senescent cell morphology, with large, flat clusters of cells (dotted red square) along the surface of the flask (Scale bar = 50 µm, 10x magnification).

APPENDIX 7: SEQUENCES FOR PRIMERS

Primer name	**Sequence of primer**	
	Forward primer (5' – 3')	**Reverse primer (5' – 3')**
Ki-67 (Mouse)	CCTTTGCTGTCCCCGAAGA	GGCTTCTCATCTGTTGCTTCCT
Topo-2α (Mouse)	CTCCACGAGAAACAGAGCCA	ACCGGTAGTGGAGGTGGAAG
MiR-30c precursor mimic (Mouse)	ACCAUGUUGUAGUGUGUGUAAACAUCCUACACUCUCAGCUGUGAGCUCAAGGUGGCUGGGAGAGGGUUGUUUACUCCUUCUGCCAUCGGA	

Table A7. Sequences of proliferation primers (Ki-67, Topo-2α) used in the q-PCR to determine the proliferation of miR-30c-transfected diabetic and non-diabetic CSCs, as well as the sequence of the miR-30c precursor mimic used for all transfection experiments.

APPENDIX 8: ADDITIONAL IMMUNOBLOTS

A8.1) Non-transfected western blots for VDAC1 and CDK6:

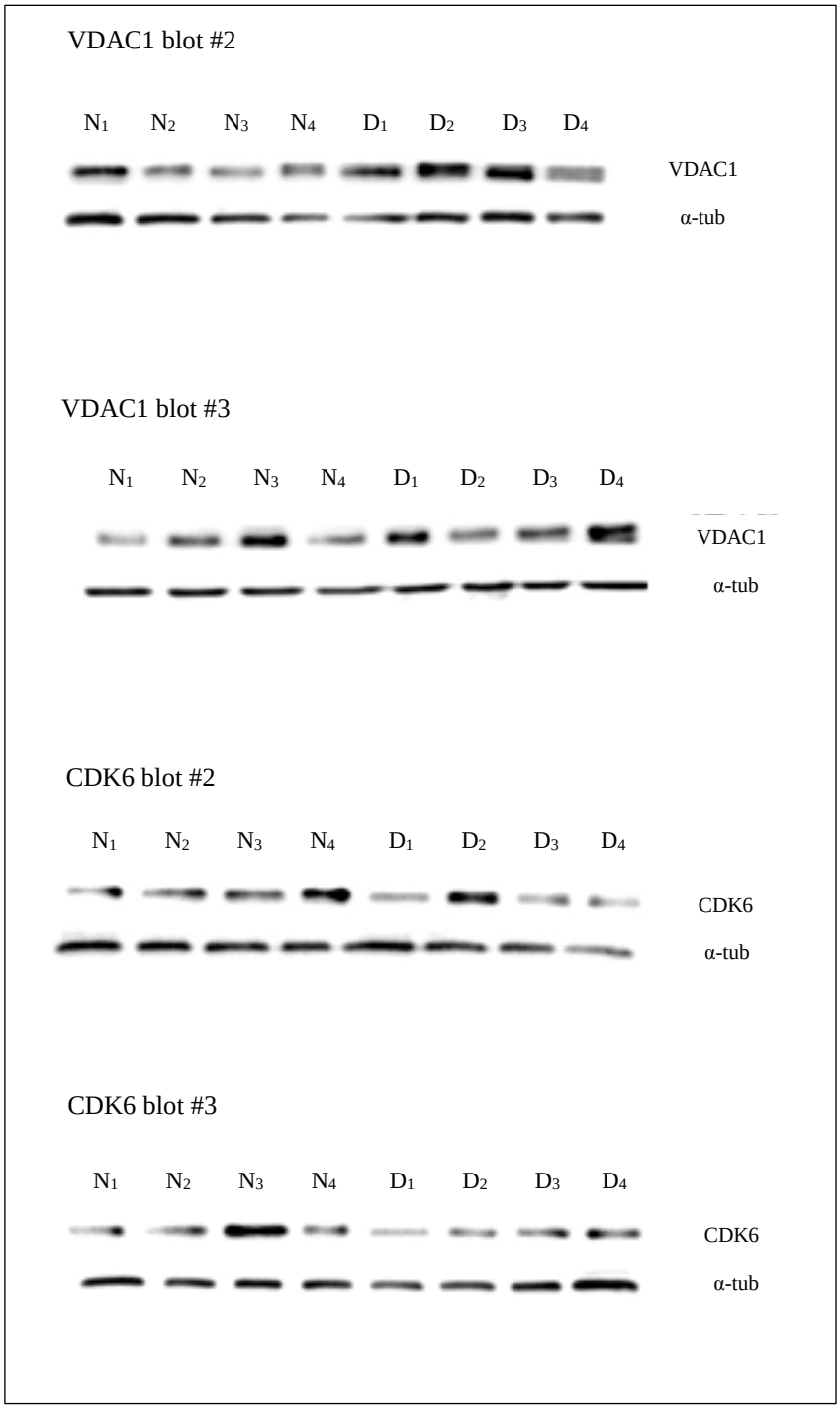

A8.2) Transfected western blots for VDAC1 and cleaved caspase-3:

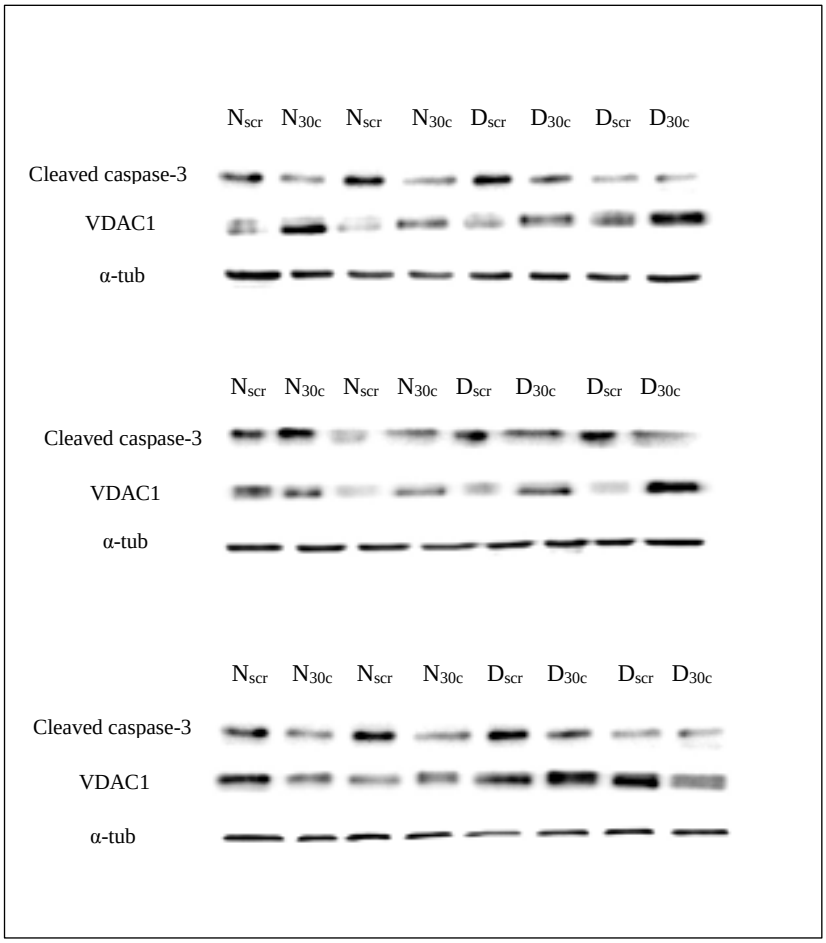

Figure A8. Additional immunoblots for determining expression of VDAC1, CDK6 and cleaved caspase-3 in transfected (A8.2) and non-transfected (A8.1) diabetic (n=4) and non-diabetic CSCs (n=4). N = Non-diabetic, D = Diabetic, N_{scr} = Non-diabetic transfected with scrambled mimic, N_{30c} = Non-diabetic transfected with miR-30c mimic, D_{scr} = Diabetic transfected with scrambled mimic, D_{30c} = Diabetic transfected with miR-30c mimic.

APPENDIX 9: SUPPLEMENTARY DATA FOR TRANSFECTION PROCEDURE

To measure the transfectional efficiency of the miR-30c precursor mimic, 6 x 10^5 diabetic (n=4) and non-diabetic CSCs (n=4) were initially seeded into 12-well plates in triplicate. Meanwhile, 1x 10^6 CSCs from the same samples were seeded into T25 flasks for western blot analysis. The reagents used in the transfection experiment are shown in the table below.

Flask/Plate	**Number of CSCs seeded**	**miR-30c precursor mimic (µL)**	**Scrambled mimic (µL)**	**RNAiMAX lipofectamine reagent (µL)**	**DMEM/F12 (µL)**
12-well plate (per well)	6 x 10^5	4	4	12	400
T25 flask	1x 10^6	14	14	42	1,400

Table A9. Table showing the volumes of miR-30c/scrambled mimic, lipofectamine reagent, and DMEM/F12 required for transfecting CSCs depending on the number of CSCs required for each flask/plate. Numbers are shown for either one well of the 12-well plate or one T25 flask.

APPENDIX 10: HUMAN PATIENT INFORMATION

Case No.	Date collected	Sex	Type	Age (years)	Weight (kg)
293	26/02/15	Male	Diabetic-type 2	54	132
290	19/02/15	Male	Non-diabetic	58	106
322	28/04/15	Male	Diabetic-type 2	59	101
284	29/01/15	Male	Non-diabetic	61	115
308	26/03/15	Male	Non-diabetic	64	87
326	21/04/15	Male	Diabetic-type 2	75	81

Table A10. Patient information for three type-2 diabetic and three non-diabetic human patients. This includes the date collected, sex and age of the patients

APPENDIX 11: Top 40 significantly upregulated and top 40 significantly downregulated MS peptides

Peptide/gene name	Fold change	Significance (P value)
Downregulated		
Signal transducer and activator 1 (STAT1)	0.375819	2.75E-12
UDP-N-acetylhexosamine pyrophosphorylase (UAP1)	0.207817	2.35E-09
Cyclin-dependent kinase 6 (CDK6)	0.439827	4.40E-07
Translationally-controlled tumor protein (TPT1)	0.753579	3.92E-05
Rab3 GTPase-activating protein catalytic subunit (RAB3GAP1)	0.544419	0.00012
Heparin Binding Growth Factor (HDGF)	0.654617	0.00012
1-Phosphatidylinositol-4,5-bisphosphate phosphodiesterase beta-3 (PLCB3)	0.598453	0.00017
GRIP And Coiled-Coil Domain-Containing Protein 2 (GCC2)	0.53808	0.00055
Crk-like protein (CRKL)	0.670665	0.00021
Nexilin (NEXN)	0.663014	0.0007
UMP-CMP kinase (CMPK1)	0.776847	0.00088
Vamp6/Vps39-like protein (VPS39)	0.476113	0.00098
SAP Domain Containing Ribonucleoprotein (SARNP)	0.595147	0.00143
Mannosidase Alpha Class 1A Member 1 (MAN1A1)	0.607646	0.00776
Guanylate cyclase soluble subunit beta-1 (GUCY1B1)	0.62574	0.01368
40S ribosomal protein S7 (RPS7)	0.695617	0.01734
Protein disulfide-isomerase (P4HB)	0.632183	0.01768
Family With Sequence Similarity 129 Member A (FAM129A)	0.883568	0.0178
Constitutive coactivator of PPAR-gamma-like protein 1 (FAM120A)	0.736727	0.01813
Metaxin 2 (MTX2)	0.690314	0.01845
Erythrocyte Membrane Protein Band 4.1 Like 2 (EPB41L2)	0.688939	0.01846
RAB11-binding protein (RELCH)	0.631278	0.01951
Tripeptidyl-peptidase 1 (TPP1)	0.801314	0.01975
Integrin Linked Kinase (ILK)	0.74826	0.02101
Guanine nucleotide-binding protein Gq (GNAQ)	0.746936	0.02103
Uveal autoantigen with coiled-coil domains and ankyrin repeats (UACA)	0.602769	0.02138
Sorting nexin 7 (SNX7)	0.841615	0.02145
Glutathione reductase (GSR)	0.6343	0.02157
Pirin (PIR)	0.657804	0.02172
Ubiquitin carboxyl-terminal hydrolase 14 (USP14)	0.888771	0.02186
Flotillin-2 (FLOT2)	0.77797	0.02326
V-type proton ATPase subunit D (ATP6V1D)	0.792766	0.02369
Eukaryotic translation initiation factor 2 subunit 1 (EIF2S1)	0.849724	0.03291
Dehydrogenase/reductase (SDR family) X-linked protein (DHRSX)	0.724815	0.03292
Milk fat globule-EGF factor 8 protein (MFGE8)	0.571682	0.03295
WD Repeat Domain 11 (WDR11)	0.68289	0.03341

Vacuolar protein sorting-associated protein 26A (VPS26A)	0.710931	0.03354
Phosphoribosyl Pyrophosphate Synthetase Associated Protein 1 (PRPSAP1)	0.721211	0.03624
ATPase H+ Transporting V0 Subunit A2 (ATP6V0A2)	0.741759	0.0369
Copper transport protein (ATOX1)	0.911446	0.03914
Upregulated		
Cartilage-associated protein precursor (CRTAP)	1.778638	8.88E-09
Myosin-10 (MYO10)	1.707861	2.45E-06
Spectrin alpha chain, non-erythrocytic 1 (SPTAN1)	1.62398	6.24E-06
Dihydrolipoyllysine-residue succinyltransferase component of 2-oxoglutarate dehydrogenase complex (DIST)	1.864016	0.00014
26S proteasome non-ATPase regulatory subunit 13 (PSMD13)	1.789953	0.00024
Transmembrane and TPR repeat-containing protein 3 (TMTC3)	1.867017	0.00036
Pyruvate carboxylase (PCX)	2.582412	0.00038
NAD-dependent protein deacetylase sirtuin-2 (SIRT2)	1.506322	0.00107
Rab GTPase-binding effector protein 2 (RABEP2)	1.993037	0.00163
NAD(P)H dehydrogenase [quinone] 1 (NQO1)	2.117885	0.00188
Peptidyl-prolyl cis-trans isomerase A (PPIA)	2.129923	0.00193
Voltage-dependent anion-selective channel protein 1 (VDAC1)	1.668126	0.00214
Lysosome-associated membrane glycoprotein 1 (LAMP1)	2.234822	0.00385
RNA polymerase II-associated protein 1 (RPAP1)	1.982721	0.00613
Collagen alpha-2(I) chain precursor (COL1A2)	1.31064	0.00729
Nuclear pore complex protein Nup153 (NUP153)	1.713274	0.01164
Adenosine deaminase (ADA)	1.292302	0.00041
DnaJ homolog subfamily B member 11 precursor (DNAJB11)	1.356682	0.00053
Dihydropyrimidinase-related protein 3 CRMP4b (DPYSL3)	1.392175	0.00054
Sterol-4-alpha-carboxylate 3-dehydrogenase, decarboxylating (NSDHL)	1.397111	0.00075
Importin subunit alpha-4 (KPNA3)	1.138781	0.0008
Tubulin beta-6 chain (TUBB6)	1.31872	0.00091
Peptidyl-prolyl cis-trans isomerase B precursor (PPIB)	1.240009	0.00105
Actin, cytoplasmic 1 (ACTB)	1.582567	0.00118
Aspartate aminotransferase, cytoplasmic (GOT1)	1.337512	0.00136
Carboxypeptidase E precursor (CPE)	1.614357	0.00146
Cathepsin D precursor (CTSD)	1.29219	0.00151
Cytoplasmic dynein 1 light intermediate chain 1 (DYNC1LI1)	1.254479	0.00178
AP-3 complex subunit mu-1 (AP1M1)	1.549883	0.00201
Aspartate aminotransferase, mitochondrial (GOT2)	1.234478	0.00216
Protein ERGIC-53 precursor (LMAN1)	1.638345	0.00249
Ubiquitin-40S ribosomal protein S27a precursor (RPS27A)	1.239542	0.00262
Tricarboxylate transport protein, mitochondrial (SLC25A1)	1.244248	0.00341
Target of Myb protein 1 (TOM1)	1.204444	0.00856
Amine oxidase [flavin-containing] B (MAOB)	1.240643	0.00994
Collagen alpha-1(I) chain preproprotein (COL1A1)	1.137343	0.01514
Filamin-C isoform 2 (FLNC)	1.154882	0.01587
26S protease regulatory subunit 10B (PSMC6)	1.803936	0.01715
Prostaglandin reductase 1 (PTGR1)	1.265975	0.01813
Annexin A1 (ANXA1)	1.141198	0.01956
Acyl-coenzyme A thioesterase 9 (ACOT9)	1.143652	0.02172

Signal transducing adapter molecule 2 (STAM2)	1.40476	0.02202
Proteasome subunit beta type-5 (PSMB5)	1.142082	0.02283
COP9 signalosome complex subunit 5 (COPS5)	1.261288	0.02389
Elongation factor 1-beta (EEF1B)	1.152118	0.02649
Muscleblind-like protein 2 (MBNL2)	1.691183	0.02738
Secretory carrier-associated membrane protein 1 (SCAMP1)	1.248962	0.02804
Cytosolic non-specific dipeptidase (CNDP2)	1.225636	0.02967
Voltage-dependent anion-selective channel protein 2 (VDAC2)	1.204845	0.03108
Vacuolar protein sorting-associated protein 35 (VPS35)	1.091945	0.03126
Actin, aortic smooth muscle (ACTA2)	1.412265	0.03331
Cytochrome b5 (CYB5A)	1.227659	0.03435
Proteasome subunit beta type-6 precursor (PSMB6)	1.149633	0.03725
Elongation factor 1-gamma (EEF1G)	1.145832	0.03845
Coronin-1C (CORO1C)	1.207869	0.03855
Proteasome subunit alpha type-7 (PSMA7)	1.192553	0.03971

Table A11. Table showing the top 40 peptides that were upregulated and top 40 peptides that were downregulated from mass spectrometry. Potential gene targets were selected from this group on the basis of statistical significance and fold change.